On the non-thermal physics of magnetic fields and cosmic rays in galactic ecosystems

Thesis by
Sam Bharat Vijay Karthikeyan Ponnada

In Partial Fulfillment of the Requirements for the
Degree of
Doctor of Philosophy in Astrophysics

CALIFORNIA INSTITUTE OF TECHNOLOGY
Pasadena, California

2026
Defended July 2nd, 2025

Sam Bharat Vijay Karthikeyan Ponnada
ORCID: 0000-0002-7484-2695

ACKNOWLEDGEMENTS

At risk of being long-winded, I will try to be as exhaustive as possible in my acknowledgements of all those who have supported me in my journey to and through this endeavour, in what will be a futile attempt to reach full completeness. The old adage states it takes a village to raise a child, and analogously I believe it takes a few villages for one to obtain a PhD!

First, I cannot fully express my gratitude and thanks to my advisor, Prof. Phil Hopkins. I still vividly recall the first time I came across one of Phil's papers as an undergraduate student, eager to tackle the 40+ page behemoth it was, to present at a journal club during a summer research assistant-ship. Funnily enough, it was a work that I cite quite often in this thesis, "But what about...: cosmic rays, magnetic fields..." Little did I know then that would lay the foundation for five years of my own research and academic development, and that it would be facilitated by Phil himself! And what an irreplaceable opportunity it has been to do so – I am incredibly indebted to Phil for his patient, kind, supportive, and invaluable guidance over the course of my graduate studies. I have learned a lot from him about all things astrophysical and more, and he has taught me to read and think more critically, hone my arguments, and build my physical intuition, whether through my direct interactions with him, or via diffusion down a cartoonishly steep pressure gradient in knowledge, which I will aspire to level throughout my time as an astrophysicist. I hope to be even a fraction of the shining example that he has set for me.

I also extend my thanks to several professors who have advised, taught, and/or mentored me throughout time as a research trainee at Caltech. I would like to thank the members of my candidacy and thesis committees for providing useful feedback at various stages of my PhD — Profs. Vikram Ravi, Chuck Steidel, Paul Bellan, Elias Most, Jim Fuller, and Chris Martin. In particular, I would like to thank Vikram for always providing me advice in a kind and constructive manner, giving me useful high-level career and research "meta-game" guidance, and generally always being such an enthusiastic and supportive mentor to consult. I also thank Prof. Bellan in particular for an edifying graduate course series on fundamental plasma physics, as well as Prof. Mansi Kasliwal, whose High Energy Astrophysics class during my Zoom year was a highlight. The many staff in Cahill and PMA who facilitated various logistics during my PhD — JoAnn Boyd, Gita Patel, Stephanie Cha-Ramos, Dr. Nam Ung, and Mika Walton — my immense thanks to you all.

I am also very thankful for the mentorship and collaboration of Dr. Cameron Hummels, Dr. Iryna Butsky, and Prof. Gina Panopoulou, with whom I worked on several varied topics during my PhD and learned immensely from. These thanks extend to the broader Hopkins research group, including (but not limited to) Dr. Nadine Soliman, soon-to-be-Dr. Isabel Sands, soon-to-be-Dr. Emily Silich, and Dr. Raphael Skalidis, among others, for their support, camaraderie, and intellectually stimulating discussions. And more broadly, to the FIRE collaboration I am a part of, specifically to Profs. Dusan Keres, Claude-Andre Faucher-Giguere, Eliot Quataert, Sarah Wellons, and Rachel Cochrane, as well as Dr. Chris Hayward for providing valuable feedback on my manuscripts, and to friendly, supportive, and kind co-members of the FIRE data team: Dr. Kung-Yi Su, Dr. Jenna Samuel, and Dr. Pratik Gandhi for their camaraderie through the various data management tribulations we navigated together.

There are also many people from my time as an undergraduate at the University of Iowa and the University of Edinburgh for whom I am deeply grateful — Profs. Philip Kaaret, Hai Fu, Sadegh Khochfar (Edinburgh), Mary Hall Reno, Robert Mutel, Steve Spangler, and Paul Kleiber. Without kind and supportive research mentorship early in my studies from Profs. Kaaret, Fu, and Khochfar, I would never have been in the fortunate position to pursue graduate studies in astrophysics at Caltech. The wonderful foundational (astro)-physics courses taught by Profs. Reno, Mutel, Spangler, Fu, and Kleiber stick with me through this day and deepened my love for physics and for learning about the natural world. I cannot thank them all enough, and I will aspire to inspire future students through mentorship and teaching as they influenced me. I also thank the denizens of 316 Van Allen Hall — Clare Dietz, Hailey Moore, Hannah Gulick, Genna Crom, and Danny Tallon, among many others, who were exceptional classmates in virtually all of my major college classes, and made those four years of learning physics and astronomy very memorable. I also thank the other amazing friends I had the luck of meeting in college, Zoe Swinton, Nadav Kohen, Dr. Akanksha Chilukuri, Michelle Kumar, Ellen Harper, Oliver Baldwin, and Olivier Adams, who have all supported me in my personal and academic journeys and helped me to believe in my ability to accomplish my goals. I would here like to acknowledge that this thesis is also dedicated to the memory of my late college classmate, roommate, and friend, Calvin Whitaker, with whom I shared so much joy in tackling physics and mathematics — your bright light shines on in my memory and I shall carry your passion for learning with me forever.

In college, I also benefited greatly through my interactions with the very kind and supportive staff at the Iowa Center for Research by Undergraduates (ICRU), Melinda Licht and Dr. Bob Kirby, for helping me achieve my goals of exploring new research directions abroad in Scotland and always being helpful mentors to talk to. Without both procedural and financial support from ICRU, I would not have been able to pursue a summer research assistant-ship in Edinburgh to explore theoretical and computational astrophysics with Prof. Khochfar, which led me to my research directions today.

I have been incredibly fortunate to have several teachers from earlier on in my education in Montego Bay, New York, and Iowa who had a profound impact upon me and enabled my journey to this point — specifically I would like to thank Mrs. Nadine Williams (Montego Bay Preparatory School), Mrs. Brenna Leighton (Woodmere Middle School), Mr. Richard Peters (Clear Lake High School), Mr. Richard Strike (Cedar Falls High School), Mrs. Diane Flaherty (Cedar Falls High School) and Mr. Kenton Swartley (Cedar Falls High School). I would not be here without the strong foundations you all and many other teachers helped me to develop.

Next, I would like to thank my delightful friends I have been so, so fortunate to meet during my time at Caltech. I have been so blessed to have been surrounded by so many magnificent scientists and people who have taught me so much about all matters, academic and not, and shaped me into the person I am today. I would not have been able to forge these unparalleled bonds without the passion and commitment we all share towards advancing our ideals of a better world, which was cemented in the form of our fledgling labor union. My dear friends whose friendship I will cherish lifelong, *thank you*. In no particular order, soon-to-be Drs. Abdullah Farooq, Nadia Suryawinata, Rahma Elsiesy, Natasha Reich, Jasmine Emtage, Dee Dunne, Jakob Faber, Rohan Shenoy, Simona Miller, Jack Wilding, Jessica Jacobs-Li, Marina Lecouche, and Quinn Morgan, as well as Drs. Aditi Narayanan, Tom Naragon, Ranjani Murali, Kriti Sharma, Ryan Rubenzahl, James Williams, Varun Wadia, Alex VW, Ashay Patel, Michael Greklek-McKeon, Pat Meyers, Sean Pike, Peishi Cheng, and Sophie Hourihane, among others. I had to break the sentence there, but thank you also to Tej Bhakta, Kavitha Iyengar and Piril Nergis. I am truly, truly blessed to have so many people to thank. The past few years would not been have nearly as bearable, let alone fun, without my chosen family and compatriots. I am so, so, incredibly thankful for the culture of community and care that my labor union, C/GPU (UAW Local 2478) has built, consolidating what was an enormous

undertaking overcome through the unflinching labor of love of these same friends and many others. I look forward to it lasting the test of time and to fighting for a better world together with you in solidarity, forever.

The past few years also would not have been the same without the close-knit Astrograd community at Caltech. I am very grateful for all of the various Astrograds I had the privilege of interacting with as TAs, peers, and friends during my time here, and for my cohort especially, particularly Dr. Ivey Davis and Dr. Jean Somalwar — I hope we finally write that omnibus paper/textbook/treatise some day. The camaraderie our cohort shared in many late nights poring over first-year problem sets and adjusting to PhD life in the middle of a pandemic was quite central to me getting through that first year. I am also deeply grateful for all the support and close friendship of older Astrograds who have now moved on to bigger and brighter things: Prof. Mia de los Reyes, Drs. Sarah Blunt, Nitika Yadlapalli, and Evan Nunez-Cravin, among many others. And this gratitude extends double to my roommates, soon-to-be-Drs. Dee Dunne and Jakob Faber, for so much support particularly in this last very taxing and emotional year, as well as to soon-to-be-Dr. Harshda Saxena for our cathartic chai chats.

Friends who have been there since virtually the start of this journey ten years ago in high school, Anj Droe, Merlin MacGilivray, Aditi Rao, Nic Gasser, Mariam Rawwas, Hexiang Zhang, and Mary Anton — thank you. Sincerely, you all got me through what was personally a very turbulent time in high school and I wouldn't be here to be writing this thesis if not for you.

I wholeheartedly thank my kind, supportive, and positive partner, Kiran Grewal, for being by my side through what has been quite a stressful past year for many reasons, only one of which has been finishing this PhD!

The various sweet pets who have provided companionship and comfort over the course of my PhD — my cat Cannoli, who's been raised in a house of astronomers, as well as my sister's cat Luna and Kiran's cat Nugget all deserve thanks. Their purrs shared many secrets about astronomy as well as much needed solace.

In these trying times of late, I would like to explicitly thank the National Science Foundation and NASA, and public support for basic science which has made my research possible. It is my sincere hope that these institutions weather current and future storms and enable future generations of scientists to uncover the mysteries of our Universe and find solutions to the pressing problems we face in our future. I

commit to doing everything in my power to ensure that we do.

Last but far from least, I would like to thank my family. My dear older sister, Sri Ponnada, has always been an inspiration and critical support in my life. Needless to say, I would not be here without you — you traversed so many difficult paths to make it all the more easy for me. Your support during my often abrupt and chaotic visits for conferences and/or research travel is so appreciated, and I am so thankful for it. I also would like to thank my mother, Dr. Vara Ponnada, who made innumerable sacrifices through thick and thin in order for me to be in this position today, and always instilled in me to approach my studies and mission with diligence, care, and grace. Your love has always helped me through the toughest of challenges, and I owe this PhD and much more to you both that I cannot briefly express in words.

I acknowledge the past and present Gabrielino-Tongva people and their unceded Indigenous lands upon which this research was conducted at the California Institute of Technology. This thesis is dedicated to all those who aim to build and fight for a world free of dispossession, exploitation, and oppression. I dedicate this work to all scientists heretofore and hereafter who advance science as a truly democratic tradition, a science for the people.

This thesis is the iterative result of many who have come before me and contributed knowledge within the millennia-old tradition of astronomy and astrophysics, the oldest of the sciences, as I merely peer over the shoulders of many towering giants.

> If you wish to make an apple pie
> from scratch, you must first invent
> the Universe.
>
> ---
>
> *Carl Sagan*
> *Cosmos*

ABSTRACT

The role of the non-thermal components of galaxies, magnetic fields (**B**) and relativistic charged particles, known as cosmic rays (or CRs), is one of the most uncertain aspects of our understanding of galaxy formation and evolution. While magnetic fields and cosmic rays have long been known to be important components of our own Galaxy, the Milky Way, their part in shaping galactic ecosystems remains elusive. This owes partly to fundamentally indirect observations of physical quantities relevant to **B** and CRs which are fraught with questionable assumptions to make any physical inference, and partly due to the difficulty in modeling them theoretically.

It has only become possible in the past decade to fully model **B** and CRs dynamically in simulations of galaxy formation within a cosmological context, all while maintaining high hydrodynamic resolution and evolving the relatively well-constrained physics of star formation and stellar feedback to produce realistic bulk- and spatially-resolved galaxy properties without calibration. In this thesis, I use state-of-the-art simulations which explicitly evolve **B** and CRs in concert with these explicit treatments of star formation and stellar feedback in a cosmological context towards two ends. One is to better understand where our observational assumptions oft used in our indirect constraints may go awry and to develop more physical estimators of **B** and CRs. In Chapters 2 and 3, I explore this avenue using by generating a host of synthetic observations. The second is to hold the well-constrained (to within an order-of-magnitude) physics fixed, and explore much more widely uncertain physics, namely that of cosmic ray transport, to constrain via emergent observables. In Chapters 4 and 5, I generate synthetic observational predictions across the electromagnetic spectrum for simulations with orders-of-magnitude variation in cosmic ray transport and compare to observations.

In Chapter 6, I develop a novel analytic framework to survey the vastly uncertain CR transport parameter space, and explore implications for arbitrarily complex injections of cosmic rays from episodic black hole accretion or star formation, and outline a sub-grid model to incorporate CRs in large volume cosmological simulations which otherwise would suffer from additional computational overhead or artefacts arising from time-independent modeling assumptions. Finally, I conclude summarizing the constraints these various studies provide on galactic **B** and CRs, and the outlook for future simulations and observational comparisons.

PUBLISHED CONTENT AND CONTRIBUTIONS

Ponnada, Sam B., Rachel K. Cochrane, et al. (Feb. 2025). "Hooks, lines, and sinkers: How active galactic nucleus feedback and cosmic-ray transport shape the far-infrared–radio correlation of galaxies." en. In: *The Astrophysical Journal* 980.1. Publisher: The American Astronomical Society, p. 135. ISSN: 0004-637X. DOI: 10.3847/1538-4357/ada280.

Ponnada, Sam B., Iryna S. Butsky, et al. (May 2024). "Synchrotron signatures of cosmic ray transport physics in galaxies." In: *Monthly Notices of the Royal Astronomical Society* 530. Publisher: OUP ADS Bibcode: 2024MNRAS.530L...1P, pp. L1–L6. ISSN: 0035-8711. DOI: 10.1093/mnrasl/slae017.

Ponnada, Sam B., Georgia V. Panopoulou, Iryna S. Butsky, Philip F. Hopkins, Raphael Skalidis, et al. (Feb. 2024). "Synchrotron emission on FIRE: equipartition estimators of magnetic fields in simulated galaxies with spectrally resolved cosmic rays." In: *Monthly Notices of the Royal Astronomical Society* 527.4, pp. 11707–11718. DOI: 10.1093/mnras/stad3978.

Ponnada, Sam B., Georgia V. Panopoulou, Iryna S. Butsky, Philip F. Hopkins, Sarah R. Loebman, et al. (Nov. 2022). "Magnetic fields on FIRE: Comparing B-fields in the multiphase ISM and CGM of simulated L* galaxies to observations." In: *Monthly Notices of the Royal Astronomical Society* 516. ADS Bibcode: 2022MNRAS.516.4417P, pp. 4417–4431. ISSN: 0035-8711. DOI: 10.1093/mnras/stac2448.

Sam Ponnada is the leading author on all four of these published manuscripts. Sam was involved in the conception of each project, led the development of analysis pipelines and (semi-)analytical models, and led subsequent science analysis and preparation of manuscripts.

TABLE OF CONTENTS

LIST OF ILLUSTRATIONS

LIST OF TABLES

Chapter 1

INTRODUCTION

Magnetic fields and cosmic rays in the context of cosmological galaxy formation The small-scale interactions between relativistic charged particles, or cosmic rays (CRs), and magnetic fields (**B**) on *solar-system scales* may have profound impacts on the evolution of *entire galaxies*, and yet the details of their micro-physically interlaced nature which give rise to macroscopic effects remain largely unknown. The role of these coupled non-thermal physics in shaping galactic ecosystems is a primary mystery in modern astrophysics — to quote the Astro2020 Decadal Survey, ***'the impact of cosmic rays is one of the largest uncertainties in understanding feedback in galaxy formation'*** (National Academies of Sciences, Engineering, and Medicine, 2023). This is the central question I will explore in this thesis.

Galactic magnetic fields are grown from primordial fields seeded by currents generated by density gradients and/or instabilities in the hot, ionized plasma characterizing the early Universe (Biermann, 1950). While the exact nature of these battery mechanisms remains an open question (Soliman, Hopkins, and Squire, 2025), these fields on large scales characteristic of cosmic structure formation are frozen into the ionized plasma in an ideal magnetohydrodynamic fashion and then amplified via dynamo processes associated with gas accretion-driven turbulence, energetic stellar and black hole feedback, and large scale differential motions (Beck, Beck, and Rainer, 2000; Schober, Schleicher, et al., 2015; Martin-Alvarez, Devriendt, et al., 2018; Pakmor, Bieri, et al., 2024; Soliman, Hopkins, and Squire, 2025). This gives rise to **B** in the interstellar medium (ISM) of galaxies with magnetic energy density (u_B) in near equipartition with those of the turbulence, starlight, and gas thermal motions (Boulares and Cox, 1990; Beck, 2015a).

Cosmic rays have also been of notable interest in galaxy formation for several decades (Fermi, 1949), with the cosmic-ray energy density (e_{CR}) in the Milky Way's ISM also being in rough equipartition with the other aforementioned pressure terms. It is now established that the bulk of CRs in the Milky Way and other star-forming galaxies (a.k.a L^* galaxies, at the break of the galaxy luminosity function in the local Universe; Schechter, 1976) can be explained by acceleration at shocks associated with supernovae at the end of stellar life cycles (Bell, 1978; Bell, 2004), with roughly

$\sim$ 10% of the supernova kinetic energy being converted into CRs via diffusive shock acceleration, with the ensuing injection spectrum primarily dominated by CR protons at ~GeV kinetic energies (Yuan, Liu, and Bi, 2012; Caprioli, 2012).

The role of these two 'non-thermal' components of galaxies has been long studied analytically for their potential role in regulating the growth of galaxies over cosmological time (Parker, 1958; Ipavich, 1975). However, cosmological galaxy formation is notoriously non-linear owing to feedback from stars and black holes, and the nature of CR propagation in magnetized plasma is inherently non-linear, as CRs can exchange energy with the thermal gas and vice-versa. These effects can be difficult to capture with traditional 'pen-and-paper' calculations, and so progress in our understanding of galaxy formation, let alone the role of magnetic fields and cosmic-rays, was limited by construction.

In decades since these classic works, algorithmic and computational advances have pushed our theoretical understanding of these non-thermal components of galaxies further. Recent works utilizing magnetohydrodynamic simulations have found that magnetic fields may be vital to promoting thermal instability in the circum-galactic medium (CGM) (Ji, Oh, and McCourt, 2018; van de Voort et al., 2021), along with many studies of varied analytic and numerical approaches predicting that the ~1-10 GeV CR protons which dominate the overall CR energy budget are of significant importance in the circum-galactic medium (CGM) as well (Booth et al., 2013; Salem and Bryan, 2014; Simpson et al., 2016; Salem, Bryan, and Corlies, 2016; Butsky and Quinn, 2018; Buck et al., 2020; Hopkins, Chan, Garrison-Kimmel, et al., 2020). If CRs are able to enter the galactic halo (but not escape too quickly; Hopkins, Chan, Squire, et al., 2021), these works with varied implementations of stellar feedback and numerical schemes find that CRs are capable of establishing large scale pressure gradients, subsequently driving coherent outflows (Hopkins, Chan, Ji, et al., 2021; Armillotta, Ostriker, and Jiang, 2022), and modifying the thermal instability (Butsky, Fielding, et al., 2020). A characteristic example of this *qualitatively different physical behavior* is illustrated in Figure 1.1, where the structure of outflows in the CGM around a Milky-Way-like galaxy simulated with cosmic ray-magnetohydrodynamics (CR-MHD) is juxtaposed to the same identical initial conditions run without CRs, with all other physics held invariant.

Meanwhile, on the observational front, absorption line spectroscopy surveys targeting halos around low redshift galaxies ($z \lesssim 0.35$, i.e., relatively local Universe or recent cosmic time $t \gtrsim 10$ Gyr since the Big Bang), both actively star-forming

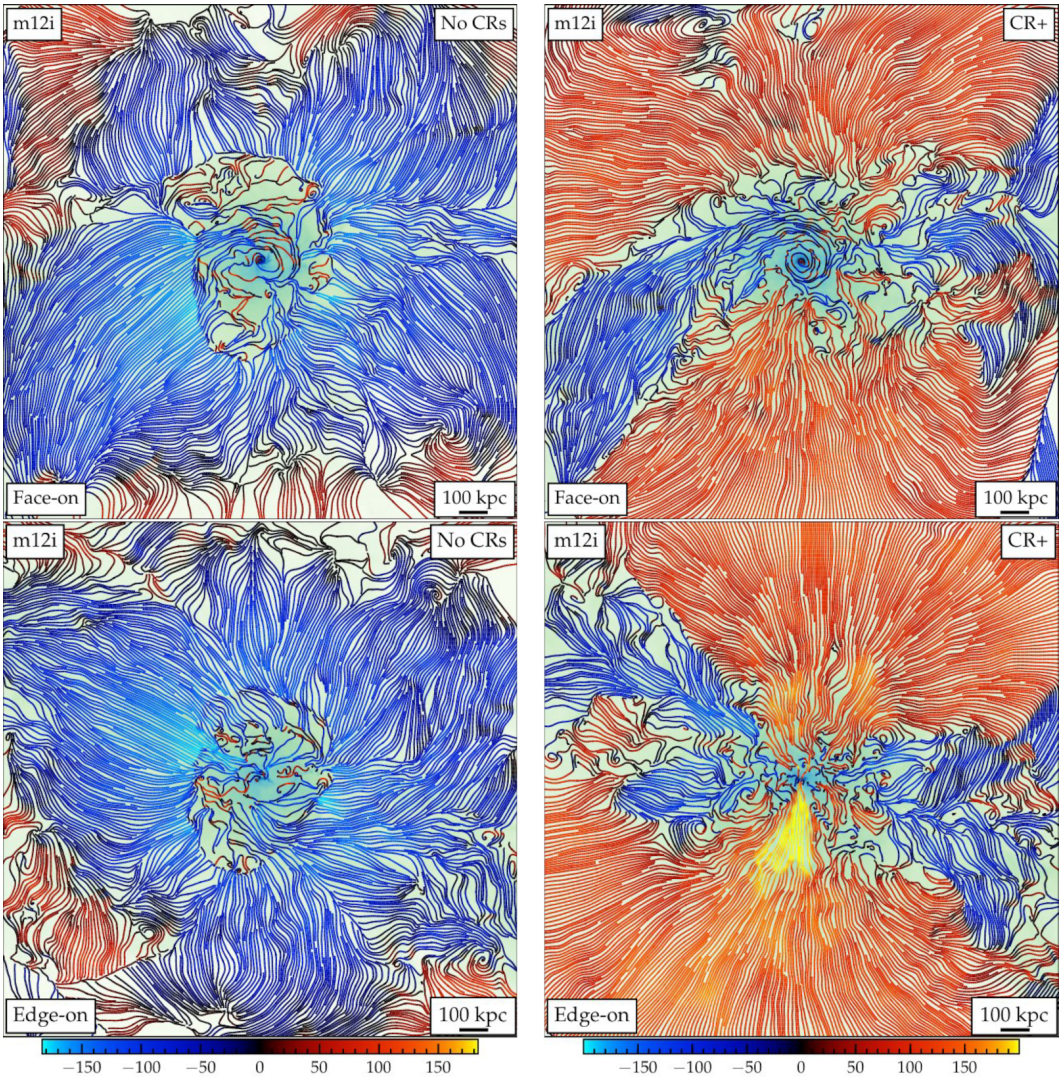

Figure 1.1: *Gas flow structure out to a Mpc in a cosmological zoom-in simulation of a Milky-Way-like galaxy with and without a cosmic-ray dominated halo*. A 2D slice of the same cosmological initial condition is shown run without CRs on the left and with CRs on the right, with streamlines velocity flow structure colored by radial velocity in km s^{-1}. If CRs efficiently escape the disk of the galaxy, they can establish large scale non-thermal pressure gradients which accelerate outflows out to very large scales ($\gtrsim$Mpc), fundamentally altering CGM gas phase structure and kinematics. Figure taken from (Hopkins, Chan, Ji, et al., 2021) with permission from the author.

and "quenched," have found that "cool" CGM gas (T $\sim 10^4$ K) is relatively ubiquitous (Tumlinson, Peeples, and Werk, 2017). Not only that, but the densities of this observed cool gas are inferred to be orders-of-magnitude lower than what would be naively expected for the cool clouds to be in thermal pressure equilibrium with the hot, virialized phase (Werk et al., 2014). This implies the existence of non-negligible non-thermal pressure support which would allow the gas to cool isochorically, rather than along a two-phase equilibrium condition, which would demand it become denser as it cools. Naturally, this raises two questions. One is the question of what the source of non-thermal pressure support may be in galactic halos, be it turbulence, magnetic pressure, or cosmic rays. The second is the puzzle of why this cool gas is not precipitating onto the ISM of these galaxies and collapsing into young stars, as the observed presence of cool gas around even "red and dead," quenched galaxies indicates there are large reservoirs of fuel for fresh star formation. Magnetic fields and cosmic rays may be part and parcel of the answers to both of these fundamental questions regarding galaxy formation and evolution.

The "state-of-the-art": phenomenological cosmic ray transport

Many of the recent works which have begun to establish the importance of these coupled non-thermal physics have relied on simple treatments of CR transport in simulations of galaxy formation with otherwise physical treatments of known behaviors of cosmological structure formation or idealized setups, ideal MHD, gas cooling, thermal/radiative/kinetic feedback from stars. This is due to the complex nature of CR transport — physically, after being injected into the ISM, rather than freely escaping galaxies at close to the speed of light, CRs 'stream' along the local magnetic field on gyrating orbits. These fields can be advected with gas motions as the field lines are frozen into the plasma, as well as being topologically complex in their own right. As the CRs stream along the local $\mathbf{B}$ (with local direction $\hat{\mathbf{b}}$, they can be deflected, or 'scattered' in their pitch angle ($\mu \equiv \hat{\mathbf{v}}_{\rm CR}\cdot\hat{\mathbf{b}}$ in the CR rest-frame by $\delta\mathbf{B}$ fluctuations on the gyro-resonant scale, with $r_{\rm gyro} \equiv p_{\rm CR}/Z_{\rm CR}e\mathbf{B}$ where $p_{\rm CR}$ is the CR momentum and $Z_{\rm CR}e$ is the charge carried by the CR (Zweibel, 2013). The gyro-radii of interest are much smaller than typically relevant scales for galaxy formation — for instance, **the typical gyro-radius in ~1-10μG ISM B is ~0.1-1 AU for ~GeV CRs** of dynamical importance; ~2 dex below the magnetohydrodynamic (MHD) fast-mode dissipation scale and ~**5-8 dex below resolved parsec-kiloparsec scales in most modern observations and simulations**. Averaged over large spatial and temporal scales, this pitch-angle scattering leads to "streaming-" or "diffusion-like"

behavior.

So, the most-widely incorporated ‘state-of-the-art’ in the field has been to utilize two-fluid approximations, evolving CRs as a "single-bin" relativistic fluid, modeling the peak of the CR energy distribution at ∼GeV (or equivalently a constant CR spectrum, integrated over all CR energies) with simplistic treatments for CR transport characterized by spatially and temporally constant "diffusion" or "streaming" speeds (see Hanasz, Strong, and Girichidis, 2021; Ruszkowski and Pfrommer, 2023, for recent reviews). These are chosen utilizing empirical constraints on the local ISM-averaged diffusion/streaming speeds, which are ‘fit’ for utilizing steady-state CR propagation models from local ISM measurements of CR spectra, the ratios of primary CRs (produced at injection) to secondary CRs (produced via spallation reactions of CRs with ambient ISM/CGM gas along their scrambled travel paths), and matter to anti-matter ratios (Cummings et al., 2016; Bisschoff, Potgieter, and Aslam, 2019; Di Mauro, Korsmeier, and Cuoco, 2024). While steady-state models of this sort inform us regarding the volumetrically-averaged scattering properties of CRs in local ISM-like conditions, it remains unclear how the scattering properties (and thus emergent transport and dynamical properties of CRs) would vary in the vast physical dynamical range of plasma conditions characterizing the multi-phase ISM and CGM (Wolfire et al., 1995; Tumlinson, Peeples, and Werk, 2017), across redshift, or across different galaxy types. And of course by construction of being time-steady models fit to singular observations, do not inform us regarding the dynamical effects CRs may have had over their lifetimes.

In order to determine the plausible effects CRs *may* have, studies discussed above utilizing CR-MHD simulations of galaxy formation have utilized this phenomenological approach, invoking empirically-motivated priors on this spatially/temporally constant transport parametrization based on local observations and calibrating a posteriori to emergent observables associated with ∼ GeV CRs like γ-ray emission (Chan, Kereš, Hopkins, et al., 2019; Werhahn, Pfrommer, Girichidis, and Winner, 2021). Nonetheless, this choice of the effective diffusion coefficient or streaming speed, ultimately, presents the most significant uncertainty in answering the question of how important CRs may be to galaxy formation as a whole.

In short, despite knowing that **B** and CRs are important in ISM physics, their potentially outsized significance to galactic ecosystems through CGM non-thermal pressure support, which can *significantly alter gas phase structure and kinematics* (Butsky and Quinn, 2018; Ji, Chan, et al., 2020; Butsky, Werk, et al., 2022) remains

orders-of-magnitude uncertain (Zweibel, 2013; Butsky, Nakum, et al., 2023), even across the most extensively studied "first-principles" plasma physics theories of CR propagation (Hopkins, Chan, Squire, et al., 2021; Hopkins, Squire, Chan, et al., 2021). Particularly pressing is our lack of understanding of the strength and geometry of **B** in different galaxies, and how often CRs scatter off δ**B** fluctuations on gyro-resonant scales, which are very small compared to galactic length scales.

When measurement eludes us, phenomenology avails us!

Exacerbating these immense uncertainties regarding the non-thermal components of galaxies is a dearth of theoretical and observational constraints. Indeed, the only physical context in which we have *directly* measured data on interstellar **B** or CRs is in the local ISM of our own Milky-Way (Gurnett et al., 2013)! A few of these indirect methods are summarized below.

In the cool, neutral ISM (CNM), the hyper-fine 21 cm transition of neutral hydrogen and transitions of diatomic and molecular species can undergo Zeeman splitting for typical $\gtrsim$1-10 μG field strengths, which results in a frequency shift between left- and right-circular polarizations of light (Draine, 2011). The systematic shift in the difference of these polarized spectra is proportional to the strength and direction of the magnetic field component along the line of sight ($B_{||}$; Crutcher 2012). As this method is sensitive to reversals, it uniquely probes the regular (ordered and coherent) field component within a single system giving rise to a line component, however it becomes "indirect" when one considers a given system is seen in projection, and so while the measurement of $B_{||}$ is robust, its connection to other key quantities like the three-dimensional gas density or thermal pressure become fraught, and thus so do the inference of the plasma β.

In the warm, ionized phase of the ISM (WIM), the field can be measured through the joint use of rotation and dispersion measures (RMs and DMs), which arise due to the phase differences of left- and right-circularly polarized light waves in a magnetized plasma and the frequency-dependent dispersive delay in wave group velocities in ionized plasmas, respectively. When measuring RMs and DMs towards background polarized light sources like pulsars (Simard-Normandin and Kronberg, 1980; Han, Manchester, Lyne, et al., 2006; Manchester et al., 2005; Sobey et al., 2019) or fast radio bursts (FRBs; Lan and Prochaska 2020; Prochaska et al. 2019; Connor and Ravi 2022), these tracers give an estimate for $B_{||}$ averaged along large distances in the ISM and CGM, assuming that the thermal electron density and **B** are

uncorrelated (Seta and Federrath, 2021). Again, with RM/DM being an projected quantity averaged over large length scales, it becomes unclear how it maps to the true underlying magnitude of **B** or its associated pressure in the volumes they sample integrated along a line-of-sight.

Another common technique to measure **B** and e_{CR} is to use the non-thermal emission arising from gyrating cosmic rays (synchrotron emission), primarily observed at radio frequencies, to characterize the relevant energy densities; however, this is subject to several assumptions - the primary assumption being that of energy equipartition between **B** and CRs, which may or may not hold in different ISM/CGM phases and on different scales. There are auxiliary assumptions as well regarding the spatial invariance of the spectral shape and ratio of CRe (which dominate the emission) to the CR protons, which may be fraught due to the highly variant loss terms, and further assumptions about the size of the emitting regions (Beck and Krause, 2005).

Hence, our observational probes remain indirect and/or strictly degenerate with other astrophysical quantities, or marred by projection effects, which then require simplifying assumptions to “measure" the non-thermal components. These simplifications, however, *may not hold in the dynamic, multi-phase ISM and cosmologically complex CGM*, as explored in this thesis. Progressing in understanding these non-thermal physics requires a multi-tracer theoretical approach emphasizing observational comparisons.

The phenomenological approach for CR transport commonly used, in conjunction with cosmological zoom-in simulations of realistic Milky-Way-like galaxies with explicit treatments of star formation and stellar feedback, gas cooling, and CR-MHD provides a useful testbed for these methods. Chapters 2 and 3 primarily explore this question of how well our indirect observational tracers recover the ‘true’ reference properties to *understand how to extract physical information regarding **B** and CRs from indirect tracers* from simulations which reproduce the set of relatively well-constrained observables of galaxies (e.g., galaxy stellar masses, metallicities, morphologies, gas thermo-chemical properties, multi-wavelength spectral energy distributions) (Hopkins, Chan, Garrison-Kimmel, et al., 2020; Hopkins, Wetzel, Wheeler, et al., 2023).

But what about physically-motivated models of CR transport?

Empirically-motivated treatments of CR transport are far from ideal to advance the ultimate goal of a "first-principles" picture of the role of non-thermal physics

in cosmological galaxy formation, but the large dynamic range of relevant length- and time-scales prohibits directly simulating the scattering and emergent transport of CRs in idealized simulations of galaxies, let alone fully dynamical CR-MHD, cosmological zoom-in simulations. Despite this, significant progress has been made to explore well-known models via sub-grid treatments.

For different micro-physically motivated models of CR transport, the local pitch-angle scattering rate and thus the emergent CR diffusivity $\kappa_{\parallel}$ and/or streaming speed v_{st} can vary significantly with plasma properties. Notably, two main pictures of micro-physical transport prevail: those of self-confinement (SC; Skilling, 1975) and extrinsic turbulence (ET; (Jokipii, 1966)). In SC models, magnetic fluctuations at the gyro-resonant scale are driven by Alfvén waves excited by the CRs themselves as they stream down their pressure gradients. The balance of the growth and damping of these waves then sets $\kappa_{\parallel}$ and v_{st}, and model variations within this class are defined by uncertainties in the dominant wave damping mechanism on these relevant scales. In the ET picture (Jokipii, 1966), $\delta\mathbf{B}$ are extrapolated from turbulent power spectra from the driving scale (on order of $\sim$ 100 pc) down to the very small ($\sim$ AU) gyro-resonant scales and subject to uncertainties in the primary damping modes and anisotropy of these extrinsic turbulent structures.

While it has been shown that the most commonly assumed scalings in these model classes fail to reproduce the observed γ-ray, e_{CR}, and CR spectra constraints (Hopkins, Squire, Chan, et al., 2021; Hopkins, Squire, Butsky, and Ji, 2022; Kempski and Quataert, 2022), there still exist ad-hoc variations within these general model classes which may be plausible given a yet undetermined physical mechanism with provides additional source/damping terms. This model degeneracy, then, motivates generating new observational constraints which can help to delineate between model classes. This is what we aim to do in Chapters 3 and 4 by holding relatively well-constrained physics invariable and exploring *orders-of-magnitude locally variable CR transport*, modeling emergent properties from end-to-end, and making testable predictions.

Non-thermal physics in galaxies beyond the Milky-Way mass scale and at earlier epochs

In the past decade, much of the work regarding CR feedback and magnetic fields has focused on L^* and at relatively low-z. This is in part owing to where there exist the bulk of our observational constraints, as again our only "direct" measurements

relating to **B** and CRs probe the very local ISM, and where contributions of CRs from approximately steady-state star formation, for empirically-motivated transport speeds, would be able to establish significant pressure gradients in the CGM (Hopkins, Chan, Garrison-Kimmel, et al., 2020). However, evidence is emerging that supermassive black holes at the centers of massive galaxies might primarily quench star formation via CR feedback.

Recent simulations have pushed the edge of 'sub-grid' modeling of AGN feedback to *parsec* scales from the black hole, allowing *explicit* modeling of the emergent feedback modes on galactic scales (Anglés-Alcázar, Quataert, et al., 2021; Wellons et al., 2023). These works have surfaced a new paradigm wherein **CRs from AGN could be central to ceasing star formation in massive galaxies** ($M_{\rm DM\,halo} \gtrsim 10^{12}$ $M_\odot$) and maintaining their quiescence to reproduce observables (Byrne et al., 2024) via *preventative* feedback, suppressing cooling flows Su, Bryan, Hayward, et al., 2024, where other feedback compositions (thermal-, magnetic-, kinetic-dominated) may fail (Su, Hopkins, Bryan, et al., 2021).

However, injection of CRs from episodic AGN accretion may not resemble the relatively steady-state injection of CRs which well characterize low-z L^* galaxies. Moreover, due to potentially long transport times of CRs out to large scales, the CR pressure in the halo may not itself have established a steady-state, as many analytic treatments commonly assume (Quataert, Thompson, and Jiang, 2022). Indeed, preliminary work analyzing the CGM properties of massive galaxies show CR pressure profiles out to large radii that deviate considerably from the steady-state, continuous injection profiles (Goyal et al., in prep.) that well characterize the emergent profiles in fully dynamical CR-MHD simulations of L^* galaxies at low-z.

In the final chapter of this thesis, Chapter 6, we present as-of-now unpublished work which develops semi-analytic and numerical frameworks for exploring time-dependent CR winds and their potential ensuing effects on galaxy formation, which is of importance for CRs injected from any time-variable source (AGN and/or bursty star formation) and at high-z where the conditions in galactic halos may be well out of steady-state.

Chapter 2

MAGNETIC FIELDS ON FIRE: COMPARING B-FIELDS IN THE MULTIPHASE ISM AND CGM OF SIMULATED L_* GALAXIES TO OBSERVATIONS

Ponnada, Sam B. et al. (Nov. 2022). "Magnetic fields on FIRE: Comparing B-fields in the multiphase ISM and CGM of simulated L* galaxies to observations." In: *Monthly Notices of the Royal Astronomical Society* 516. ADS Bibcode: 2022MNRAS.516.4417P, pp. 4417–4431. ISSN: 0035-8711. DOI: 10.1093/mnras/stac2448.

2.1 Chapter Abstract

The physics of magnetic fields (**B**) and cosmic rays (CRs) have recently been included in simulations of galaxy formation. However, significant uncertainties remain in how these components affect galaxy evolution. To understand their common observational tracers, we analyze the magnetic fields in a set of high-resolution, magneto-hydrodynamic, cosmological simulations of Milky-Way-like galaxies from the FIRE-2 project. We compare mock observables of magnetic field tracers for simulations with and without CRs to observations of Zeeman splitting and rotation/dispersion measures. We find reasonable agreement between simulations and observations in both the neutral and the ionised interstellar medium (ISM). We find that the simulated galaxies with CRs show weaker ISM |**B**| fields on average compared to their magnetic-field-only counterparts. This is a manifestation of the effects of CRs in the diffuse, low density inner circum-galactic medium (CGM). We find that equipartition between magnetic and cosmic ray energy densities may be valid at large (> 1 kpc) scales for typical ISM densities of Milky-Way-like galaxies, but not in their halos. Within the ISM, the magnetic fields in our simulated galaxies follow a power-law scaling with gas density. The scaling extends down to neutral hydrogen number densities < 300 cm^{-3}, in contrast to observationally-derived models, but consistent with the observational measurements. Finally, we generate synthetic rotation measure (RM) profiles for projections of the simulated galaxies and compare to observational constraints in the CGM. While consistent with upper limits, improved data are needed to detect the predicted CGM RMs at 10-200 kpc and better constrain theoretical predictions.

2.2 Introduction

Magnetic fields are of considerable importance in galaxies, as they are a substantial source of pressure support in the interstellar medium (ISM) and circumgalactic medium (CGM) (Beck, 2015a). They are capable of significantly influencing the dynamics of both fully-ionised gas and star-forming molecular clouds, thereby modulating star formation rates (for a review, see Krumholz and Federrath, 2019). Magnetic fields also determine the propagation of cosmic rays (CRs) throughout the ISM and into the CGM (Fermi, 1949; Kulsrud and Pearce, 1969; Desiati and Zweibel, 2014; Shukurov et al., 2017). Despite their well established physical significance, magnetic fields and their connection to galaxy evolution have yet to be fully understood, with progress limited by the ability to accurately characterize magnetic field strengths and topologies. Obtaining accurate measurements of the magnetic field strength and geometry in and around galaxies has implications for many open questions, including their origins and amplification, as well their role in providing non-thermal pressure support and influencing the physical state of the ISM and CGM (Butsky, Zrake, et al., 2017; Ji, Oh, and McCourt, 2018; Hopkins, Wetzel, Kereš, et al., 2018; Rodrigues et al., 2019; Ntormousi et al., 2020; Pakmor, Van De Voort, et al., 2020).

Obtaining reliable observational measurements of the field strengths and topologies remains difficult. Most observable tracers of the magnetic field are indirect and rely on certain assumptions: most notably, that of equipartition between CR and magnetic energy densities. Assuming equipartition/minimum-energy was first employed to determine field strengths in the jet of M87 by Burbidge (1956), and has been utilized to determine galactic field strengths (Beck, Beck, and Rainer, 2000; Fletcher et al., 2011; Chyzy et al., 2011; Beck, 2015a). These estimates utilize the total synchrotron intensity to give information about the magnetic field in the plane of the sky, perpendicular to our line-of-sight ($B_\perp$), which is used to infer the total magnetic field strength (B_{tot}). As Beck (2015a) delineates, this method of estimating magnetic field strengths is not without caveats; variation of B along the line-of-sight (LOS) or within the telescope beam (Beck, Shukurov, et al., 2003), energy losses of CR electrons (Beck and Krause, 2005), and invalidity of equipartition on small scales can all lead to overestimating or underestimating the true field strength (Stepanov et al., 2014).

Other observational measurements of magnetic field strengths are sensitive to the field component parallel to the LOS ($B_\parallel$) convolved with various LOS plasma

properties, and uncertain ISM phase structure. These include measurements from Zeeman splitting of spectral lines, which probes the cold, atomic ISM (e.g., Crutcher et al., 2010; Crutcher, 2012) as well as the use of the ratio of the rotation measure (RM) and dispersion measure (DM) towards background sources like pulsars or fast radio bursts (FRBs) (Han, Manchester, and Qiao, 1999; Lan and Prochaska, 2020; Seta and Federrath, 2021), which probe the highly-ionized phases. Both Zeeman splitting and RM/DM are sensitive to the direction of the magnetic field along the LOS, and measure the magnitude of the regular (ordered and coherent) field component, weighted differently by properties like gas density. It is worth noting that inferring magnetic field strengths from RM/DM relies on the assumption that the thermal electron density and magnetic field strength are uncorrelated (Beck, 2015a; Seta and Federrath, 2021).

A common thread amongst measurements of magnetic fields in galaxies is reliance on several simplifying assumptions which may or may not hold in the multiphase ISM and CGM. This provides motivation for exploring the validity of these assumptions from a theoretical perspective, along with the relative paucity of forward modeled predictions for RM/DM and Zeeman inferred measurements of magnetic fields, especially in cosmological simulations of galaxy formation with amplification from primordial fields. Furthermore, CRs have only recently been included in simulations of galaxy formation, allowing for physics prescriptions which can notably change properties of the ISM and CGM, as well as the potential to forward model synchrotron emissivities (Pakmor, Pfrommer, et al., 2016; Hopkins, Chan, Garrison-Kimmel, et al., 2020; Werhahn, Pfrommer, and Girichidis, 2021; Pfrommer et al., 2022).

It is only recently that simulations of galaxy formation that included magnetic fields have been capable of following the evolution of galaxies over cosmic time while resolving the ISM (for example, Marinacci, Pakmor, and Springel, 2014; Pakmor, Marinacci, and Springel, 2014; Rieder and Teyssier, 2017; Hopkins, Wetzel, Kereš, et al., 2018). Previously, galaxy-scale simulations that included magnetic field information were often limited to mostly idealized, non-cosmological simulations (Wang and Abel, 2009; Pakmor and Springel, 2013; Su, Hopkins, Hayward, et al., 2017; Butsky, Zrake, et al., 2017; Steinwandel, Beck, et al., 2019; Steinwandel, Dolag, Lesch, Moster, et al., 2020; Steinwandel, Dolag, Lesch, and Burkert, 2022). Within state-of-the-art simulations, models for feedback and their numerical implementations vary considerably. It has been shown that including essential physics

such as gas cooling, star formation, and feedback from stars results in different magnetic field saturation strengths and morphologies (Rieder and Teyssier, 2017; Su, Hayward, et al., 2018).

Previous work which analyzed magnetic fields includes Hopkins, Chan, Garrison-Kimmel, et al. (2020), who used a set of simulations with magnetic fields and magnetic fields including CRs (which are also analyzed in this chapter) to demonstrate that magnetic pressure appears to be generally sub-dominant to thermal pressure ($\beta = P_{thermal}/P_{magnetic} >> 1$), especially in the CGM, though this chapter did not closely analyze the magnetic field strengths in the dense ISM, where conditions can be markedly different. They also found that field morphology is tangled on all scales, and found hints of observationally relevant trends with regards to clumping factors, equipartition, and halo gas distributions, but they did not perform a detailed comparison of the magnetic fields with observations.

Cosmic rays have been found to have little impact on the magnetic field structure and strength in the CGM, however, they have been shown to significantly influence on the dynamics and phase structure of gas in the disk-halo interface, which is the region within 10 kpc vertically from the disk plane (Ji, Chan, et al., 2020; Chan, Kereš, Gurvich, et al., 2022). The resulting impact on the recycling of outflows, i.e. fountain flows, may be of considerable importance to the amplification of magnetic fields (Su, Hopkins, Hayward, et al., 2017; Anglés-Alcázar, Faucher-Giguère, et al., 2017; Martin-Alvarez, Devriendt, et al., 2018). But again, these analyses were not focused on observational comparison.

Despite efforts in understanding the physical implications of magnetic fields and CRs on galactic properties, specifically in the CGM, there have been few forward-modeled observations from idealized and cosmological simulations with explicit treatment of magnetic fields and/or CRs (e.g., Pakmor, Guillet, et al., 2018; van de Voort et al., 2021; Werhahn, Pfrommer, and Girichidis, 2021; Pfrommer et al., 2022), and little focus on magnetic fields in the ISM of simulated galaxies (though, see Guszejnov et al., 2020; Pakmor, Van De Voort, et al., 2020; Rappaz, Schober, and Girichidis, 2022).

In this chapter, we present analyses of six cosmological 'zoom-in' simulations from the Feedback in Realistic Environments Project (FIRE-2[1]), described in Section 2.3. We aim to compare synthetic observational tracers of magnetic fields to observed quantities in both the ISM and CGM of L_* galaxies. This is done for two different

[1] https://fire.northwestern.edu/

physical models, one including cosmic rays and one without, and we discuss how the inclusion of CRs impacts the magnetic fields and their observational tracers in Section 2.4. We also investigate the degree to which the simulated galaxies' magnetic fields and tracers match observations. In Section 2.5, we compare our results in context of other relevant work, and in Section 2.6, we summarize our results and discuss future work on probing galactic magnetic fields through synthetic observations.

2.3 Simulations and Methods

We refer the reader to Hopkins, Chan, Garrison-Kimmel, et al. (2020) and references therein for extensive details on the simulations. Here we summarize the most relevant information, and list the fundamental properties of each simulation in Table 2.1. The simulations analyzed here are part of the second iteration of the FIRE project, FIRE-2 (see Hopkins, Wetzel, Kereš, et al., 2018), and so include the physics of gas cooling, explicit treatment of stellar feedback (stellar winds, radiation, and SNe), with the set analyzed in this study including magnetic fields, cosmic rays, and fully anisotropic conduction and viscosity. These simulations are fully cosmological, with adaptive treatment of hydrodynamics and gravity in gas cells, and constant softening parameters for stellar and dark matter particles. The equations of ideal magneto-hydrodynamics (MHD) are solved, and simulations with cosmic rays include an ultra-relativistic fluid ($\gamma = 4/3$) treatment of CRs with injection from SNe and fully anisotropic streaming, advective and diffusive terms, loss terms, and gas coupling. The injection of CRs from SNe is done by assuming 10 percent of the fiducial SNe energy of 10^{51} erg goes to CRs and is coupled to gas adjacent to the SNe site. Since it is thought that CRs with energies of $\sim$ 1 GeV dominate the CR energy density in L_* galaxies, the CR energy density is evolved for CR energies only around this value (Boulares and Cox, 1990). In this study, the simulations with cosmic rays assume a constant effective diffusion coefficient κ = 3e29 cm^2 s^{-1}, which is observationally motivated (Chan, Kereš, Hopkins, et al., 2019).

We focus only on the most massive galaxy in each of three zoom-in volumes, galaxies roughly akin in mass and size to the Milky-Way, which are named m12i, m12f, and m12m (see Table 2.1). Note that while the runs analyzed in this study are not publicly available, snapshots of the FIRE-2 simulations with the fiducial treatment of feedback physics are publicly available[2] (Wetzel et al., 2022). Some important systematic trends are notable between the simulations modeling MHD

[2] http://flathub.flatironinstitute.org/fire

Simulation	M_{halo}^{vir} [$M_\odot$]	M_*^{MHD} [$M_\odot$]	M_*^{CR} [$M_\odot$]	$< \|\mathbf{B}\| >_{disk}^{MHD}$ [μG]	$< \|\mathbf{B}\| >_{disk}^{CR}$ [μG]	$< \|\mathbf{B}\| >_{inner\ CGM}^{CR}$ [μG]	$< \|\mathbf{B}\| >_{outer\ CGM}^{CR}$ [μG]	Description
m12i	1.2e12	7e10	3e10	7.93	3.99	0.025	0.012	Late forming MW-mass halo with a massive disc
m12f	1.6e12	8e10	4e10	5.36	4.64	0.024	0.011	MW-like disk with a LMC-like satellite merger
m12m	1.5e12	1e11	3e10	10.65	1.78	0.012	0.008	Earlier forming halo with strong bar at lower redshift

Table 2.1: Simulation properties for the simulations analyzed in this study, from Hopkins, Chan, Garrison-Kimmel, et al. (2020). The columns show the halo's virial mass at $z = 0$ following (Bryan and Norman, 1998), the galaxy's stellar mass in the MHD+ and CR+ simulations at $z = 0$, the galaxy's average magnetic field strength in the disk at $z = 0$ (defined as the mass-averaged magnetic field strength in all gas cells in the disk), the mass-averaged magnetic field strength in all gas cells in the inner CGM (50 kpc < r < 100 kpc), the mass-averaged magnetic field strength in all gas cells in the outer CGM (100 kpc < r < 240 kpc), and a short description of each galaxy. We show only the CR+ $< |\mathbf{B}| >_{CGM}^{CR}$ as at large radii from the galaxy, $< |\mathbf{B}| >$ is nearly identical between MHD+ and CR+ simulations (Fig 2.9).

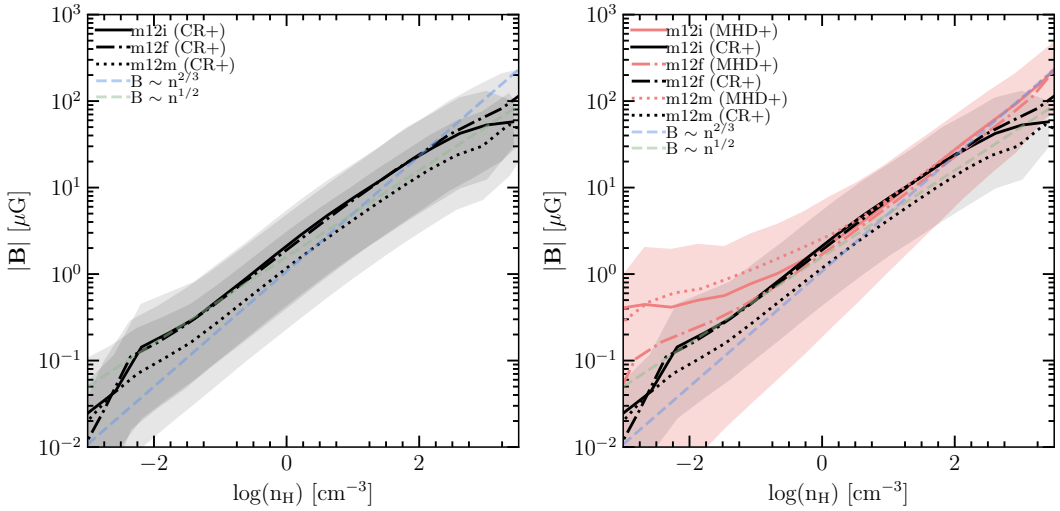

Figure 2.1: *Mean $|\boldsymbol{B}|$ vs. gas number density, n_H, for all gas cells in the galactic disk*. **Left**: Mean $|\mathbf{B}|$ at each n_H bin for each of the three CR+ simulations (black lines as described in legend). The shaded regions represent the 5-95 percentile range. Scaling relations expected for isotropic flux freezing, with and without spherical geometry of $|\mathbf{B}| \sim n_H^{2/3}$ and $n_H^{1/2}$ are also shown (blue and green dashed lines, respectively). **Right**: Mean $|\mathbf{B}|$ at each n_H bin for m12i (MHD+) in coral, and the same for the CR+ run in black. Owing to second-order dynamical effects in the "inner CGM," CR+ simulations exhibit suppressed magnetic field strengths at low gas densities ($n_H < 0.1$ cm^{-3}). All of our simulations show roughly the same power-law scaling relation in $|\mathbf{B}|$ vs. n_H, consistent with that of isotropic flux-freezing, with subtle normalization differences due to galaxy-galaxy variation.

and those modeling MHD including cosmic rays (hereafter denoted MHD+ and CR+, respectively). One of these systematic trends is that the CR+ galaxies are ∼ 2-3 times lower in stellar mass than their MHD+ counterparts. The reason for the systematically lower stellar masses in the CR+ galaxies is explained in Hopkins, Chan, Garrison-Kimmel, et al. (2020), Ji, Chan, et al. (2020), and Ji, Kereš, et al. (2021) as CR pressure support in the CGM preventing gas for star formation from precipitating onto the disk at redshift $z \lesssim$ 1-2. Correspondingly, the CR+ simulations also tend to have systematically lower ISM gas masses, gas densities, and star-formation rates (SFRs), as well as lower (∼ 20 percent) neutral hydrogen velocity dispersions in the inner disk, ± 250 pc vertically from the disk mid-plane (Chan, Kereš, Gurvich, et al., 2022).

When we calculate line-of-sight integrated quantities, we project the galaxy face-on or edge-on using the angular momentum vector of the stars to define the direction perpendicular to the galactic disk, which we use as the z component. Every particle position and vector field in the simulation is transformed accordingly, and this is the coordinate frame in which we define spatial regions below. We integrate gas quantities using the method of Hopkins, Hernquist, et al. (2005) along a set of lines of sight (LOSs) which uniformly sample the desired area. The sampling is done by dividing the area of interest into a two-dimensional, 700 × 700 image, with little to no difference in the results when increasing the image resolution. The required magnetic fields and gas quantities such as temperature and ionization state are calculated self-consistently in-code (Hopkins, 2015; Hopkins, Wetzel, Kereš, et al., 2018; Hopkins, Chan, Garrison-Kimmel, et al., 2020).

For ISM quantities, we restrict LOS integrations to gas within a cylindrical region of 14 kpc to account for the extent of our galaxies' gas disks (Bellardini et al., 2021) and height $|z| < 1$ kpc, though none of our results are especially sensitive to the exact threshold. If we restrict to "Solar Circle" radii, we only include cells with galactocentric radii, R, that satisfy: $7\,\mathrm{k}pc < R < 9\,\mathrm{k}pc$. Furthermore, since the Milky-Way pulsar observations we compare to (2.4) sample typical distances to sources between $\sim 0.1-4$ kpc, we divide the ISM integration into "slabs" uniformly sampling varying depths in log(distance) over this range; we agglomerate a collection of sightlines through the disk with slabs of thickness in z of 0.1, 0.2, 0.5, 1, 2, and 4 kpc. This is equivalent to placing sources and observers randomly in order to sample a similar distance distribution to the observations. For CGM quantities, we integrate sightlines through a sphere of physical radius r = 245 kpc, corresponding

to a projected radius of 200 kpc centered on the galaxy. We define the physical radius to be $r = \sqrt{x^2 + y^2 + z^2}$, while the projected galactocentric radius is $R = \sqrt{x^2 + y^2}$ for a face-on projection and $R = \sqrt{x^2 + z^2}$ for an edge-on projection (where x, y, z are all centered on the galaxy center).

2.4 Results

Magnetic Fields vs. Gas Density in the ISM

We first investigate the relation between the magnetic field, **B**, and gas density, n_H, in the simulations, within the ISM. Throughout this chapter, we often refer to the magnetic field in the simulation as the "true" magnetic field to distinguish from observationally-derived magnetic field measures. We select all gas cells in the disks, i.e. cells with z coordinate $|z| < 1$ kpc and galactocentric radius $R = \sqrt{x^2 + y^2} < 14$ kpc, where x, y refer to the coordinates of the cell in the simulation volume.

The relation of $|\mathbf{B}|$ with n_H for the different MHD+ and CR+ simulations is shown in Figure 2.1. In our simulations, $|\mathbf{B}| \sim n_H^{\alpha}$ for typical ISM gas densities ($n_H \gtrsim 1\ cm^{-3}$), where α is a power-law fit to the mean and ranges around $\sim$ 0.5-0.6. In a simplistic case where the exponent α is set by the collapse of gas in the absence of magnetic flux diffusion (flux freezing), α is related to the geometry of the collapse. The value of α can range from 0, if gas collapses along magnetic field lines, to 1, if the collapse is perpendicular to field lines, while the case of isotropic collapse gives an exponent of $\alpha = 2/3$ (Crutcher et al., 2010; Crutcher, 2012; Tritsis et al., 2015). Our simulations exhibit a scatter in the slope of the relation consistent with the resulting trend from isotropic flux freezing, $|\mathbf{B}| \sim n_H^{2/3}$ (or $|\mathbf{B}| \sim n_H^{1/2}$ in the case where the assumption of spherical cloud geometry is invalid. $|\mathbf{B}| \sim n_H^{1/2}$ is preferred where the cloud geometry is more slab-like or filamentary, with field lines perpendicular to the slab, or at an angle relative to the primary axis of the filament, which collapses radially (see Tritsis et al., 2015, for a detailed discussion).

At lower densities, $n_H \ll 1 cm^{-3}$, we find different behaviors for the MHD+ and CR+ simulations. While the mean values of $|\mathbf{B}|$ in the MHD+ and CR+ relations mostly agree at typical ISM densities (the mean ISM number density for these simulated galaxies is $\sim$ a few cm^{-3}, with a standard deviation of $\sim$ 100 cm^{-3}), there is a substantial offset (of a factor of 2-10) in the very diffuse gas, at number densities less than 0.01 cm^{-3}. For m12i and m12m, shown in the right panel of Figure 2.1, the CR+ simulations exhibit suppressed mean $|\mathbf{B}|$ values compared to the MHD+ simulations. For m12f, however, there is no significant offset. When comparing

among the CR+ runs, we find only modest galaxy-to-galaxy differences in their |**B**| — n_H relations. While m12i (CR+) and m12f (CR+) exhibit very similar trends in |**B**| vs. n_H, we find that m12m (CR+) has a mean |**B**| systematically lower at a given gas density at $n_H > 1\ cm^{-3}$ by a factor[3] of ~ 2. The origin of these galaxy-to-galaxy variations may arise in the specific merger histories of the galaxies, as m12m has a considerably different merger history than m12i and m12f, with m12m (CR+) also exhibiting the largest difference in stellar mass from its MHD+ counterpart, or due to its different gas and stellar mass profiles and morphology (see Hopkins, Chan, Garrison-Kimmel, et al., 2020), but we are unable to identify any single variable that explains the more systematic offset in this galaxy. Investigating this is beyond the scope of the present work, however, for our purposes, these observed variations can serve as rough guide for "systematic" uncertainties present in our derived |**B**| vs. n_H relations.

From our comparison between the CR+ and MHD+ simulations, it is clear that at typical ISM densities in the warm ionised medium (WIM), warm neutral medium (WNM), cold neutral medium (CNM), and molecular phase, cosmic rays do not alter typical magnetic field strengths *at a given gas density*, though m12m CR+ exhibits systematically lower field strengths, this owing more to galaxy-galaxy variation than to cosmic ray effects. While CRs and magnetic fields are known to influence each other via plasma instabilities (e.g. Bell, 2004), these effects are well below our resolution scale ($\sim$ 66 pc at n_H of 1 cm^{-3}, see Hopkins, Wetzel, Kereš, et al. (2018)), and have very little effect on galaxy-scale magnetic fields. Thus, while they may influence the "average" magnetic field strength within a galaxy, it would be indirectly, through changing the overall mass budget at different gas densities or in different phases, moving along the same |**B**| — n_H relation.

We have demonstrated that in some cases, CRs do appear to indirectly lower magnetic fields in the lowest-density gas. We have confirmed that this offset is not a result of the overall mass offset between CR+ and MHD+ simulations, by comparing the "m11" simulations (order of magnitude lower-mass halos) run with MHD+, which do not exhibit such an offset in field strength at a given gas density. Moreover, inspection shows that the offset seen in Fig. 2.1 (right) is not coming from supernova bubbles (the HIM), nor from any particular position within the disk midplane (measuring these trends just at the solar circle versus averaged over the whole disk shows the same effect). And we show below that in the outer CGM (far from the galaxy),

[3]While this offset at higher gas densities is noteworthy, we are cautious about how much to interpret this, given that it is much smaller than the instrinsic scatter in |**B**| at a given number density.

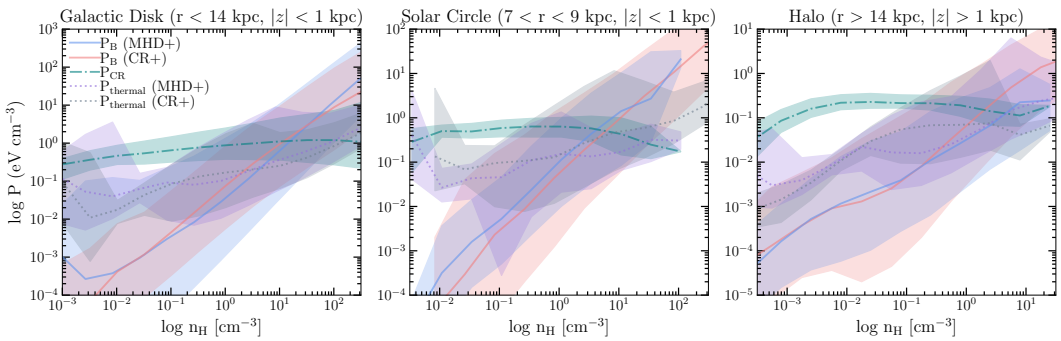

Figure 2.2: *Pressure budget as a function of gas density, for various regions in the simulations of m12i.* Here, we show magnetic pressure, P_B, with blue and coral solid lines (for MHD+ and CR+, respectively), thermal pressure, $P_{thermal}$, with purple and gray dotted lines (MHD+ and CR+, respectively) and CR pressure, P_{CR}, with teal dash-dotted line for the CR+ run. The lines represent the means for each density bin and shaded regions show 5-95 percentile intervals (approximate 2σ). **Left:** galactic disk, **center**: approximate solar circle, **right**: halo/CGM. In the galactic disk, cosmic rays are in pressure equilibrium with magnetic energies at typical ISM densities ($n_H \sim$ 1-10 cm^{-3}), indicating that equipartition assumptions may hold. In the halo, however, magnetic fields are subdominant to cosmic rays in the diffuse phase which fills the CGM volume, and not in equilibrium with thermal pressure.

magnetic field strengths are roughly the same in the MHD+ and CR+ simulations. The systematic difference appears to manifest primarily in the "inner CGM" or "disk-halo interface" — tenuous gas between the midplane and ∼a few kpc above the disk. In Section 2.5, we discuss how this is not a direct effect of including CR physics, but rather a second-order effect of the dynamical influence of CRs in this region.

Pressure budget of the ISM and CGM

In this section, we examine the density dependence of energy densities in the simulations, allowing us to see in which regions of parameter space the magnetic pressure can dominate. Notably, in our CR+ simulations, the cosmic ray energy density ($e_{\rm CR}$) at 1 GeV is evolved self-consistently, allowing us to examine whether commonly adopted assumptions about equipartition between magnetic and CR energy densities hold in these simulations.

In Figure 2.2, we present the magnetic, thermal, and CR pressures (defined as $P_B \equiv |B|^2/8\pi$, $P_{thermal} \equiv n_H k_B T$, $P_{CR} \equiv (\gamma_{CR} - 1)\, e_{CR}$), respectively) as a function of n_H for different regions of m12i. Note that P_B is also equivalent to u_B, the magnetic energy density. At densities of around 1-10 cm^{-3}, the magnetic energy density is

in approximate equipartition with that of CRs, especially in the "Solar circle" (Fig. 2.2, middle). This is in agreement with observational constraints in the Solar neighborhood (Strong, Moskalenko, and Reimer, 2000; Beck, 2001). Equipartition between these various pressures does not hold generally; in our simulations, we see that the CR pressure dominates in the low density ($n_H < 1$ cm^{-3}) gas. This can be understood by the fact that CRs are able to diffuse across field lines, and are thus more weakly functions of the gas density compared to magnetic and thermal pressures. Furthermore, the exact n_H at which the magnetic and CR pressures are equal varies with distance from the galactic center, comparing the "Solar circle" and halo regions to the whole disk. Notably, when considering all cells in the galactic disk of m12i (CR+), we find that a mean $\log_{10}(\frac{P_B}{P_{CR}})$ of $\sim$ -1, with a standard deviation ~ 1.

In the halo, however, magnetic fields do not reach equipartition strengths except at higher densities than the majority of gas in the CGM. Thus, in CR-pressure dominated haloes like those of the FIRE galaxies (see also Ji, Chan, et al. (2020)) one would overestimate the magnetic field strength when using the common assumption of equipartition applied to observations. In our simulations, the CR energy density is much larger than the magnetic energy density in the halo. For a constant diffusivity (as these simulations assume), the CR energy density decreases as $\sim r^{-1}$ far from the galaxy, while for an isothermal halo with flux freezing, $|\mathbf{B}| \sim r^{-4/3}$, falls more rapidly (Ji, Chan, et al., 2020). But we caution that this is of course sensitive to the assumptions of how CRs propagate - the diffusivity may not be constant in nature, and many models that fit the MW solar system constraints equally well can produce a more-rapidly declining P_{CR} with radius (see Hopkins, Squire, Chan, et al. (2021)).

Furthermore, in the halo, it appears that magnetic fields are in near-equipartition with the thermal pressure at densities of 1-10 cm^{-3}, but for diffuse halo gas which fills most of the volume, the magnetic fields are subdominant to thermal pressure. This is consistent with previous studies which found plasma $\beta >> 1$ in halo gas (Su, Hayward, et al., 2018; Butsky, Fielding, et al., 2020; Ji, Chan, et al., 2020), but is in contrast to results found by Pakmor, Van De Voort, et al. (2020), which may have more to do with the differing feedback models and numerical implementations, as we discuss further in Section 2.5. The relation between thermal and magnetic energy densities in our simulations is in contrast to models which predict fields at equipartition pressure with thermal pressure terms, thought to aid in accretion of cool CGM gas (Pakmor, Pfrommer, et al., 2016; Butsky and Quinn, 2018; Prochaska

et al., 2019). At high gas densities ($>\sim 50\,\mathrm{cm}^{-3}$), magnetic pressures dominate over thermal pressures, but perhaps not over the turbulent/dispersion pressure, which was explored in the ISM of FIRE-2 simulations by Gurvich et al. (2020).

Equipartition between cosmic rays and magnetic fields is an assumption whose validity may be scale-dependent due to the propagation of cosmic-rays in the ISM from their injection sites at SNe (Beck, 2015a; Seta and Beck, 2019). In Figure 2.3, we examine the scale-dependence of equipartition between cosmic rays and magnetic fields in the ISM and disk-halo interface (the very inner CGM) of m12i (CR+) by visualizing the ratio of mass-weighted projections of the magnetic and cosmic ray pressures ($\frac{\int P_{\rm B} d\ell}{\int P_{\rm CR} d\ell}$). These projections are computed using the routine for line-of-sight integrated quantities described in Section 2.3, where for the face-on projection we utilize the same convention described therein, and for the edge-on visualization we integrate the line of sight along ± 14 kpc from the galactic center.

We find that in the ISM, equipartition is valid on large (> 1 kpc) scales, consistent with observational constraints (Stepanov et al., 2014) and recent theoretical work using idealized simulations of magnetized disks (Rappaz, Schober, and Girichidis, 2022). However, this equipartition is not universal, and regions where equipartition holds are primarily cospatial with the density distribution in spiral structures, with large-scale cavities where the ratio of pressures is as low as 10^{-3}. On small scales, pressure ratios as high as 10^3 are apparent, coincident with dense molecular complexes along the line of sight.

Magnetic fields in the cold, neutral/molecular ISM: comparison to Zeeman Splitting

In this Section, we compare the magnetic field amplitude in our simulations to observations of cold neutral and molecular gas in the Milky Way.

Line of Sight Magnetic Field Strength vs. H I Column Density

The most comprehensive compilation of observations of magnetic field strengths in the cold phases of the ISM has been presented by Crutcher et al. (2010). These estimates rely on observations of the Zeeman effect, which can be used to probe the line-of-sight component of the magnetic field towards diffuse HI clouds and giant molecular clouds (GMCs).

To directly compare with these observations, we integrate the line-of-sight (parallel) component of the magnetic field in the simulations, $B_{\parallel}$, weighted by the cold,

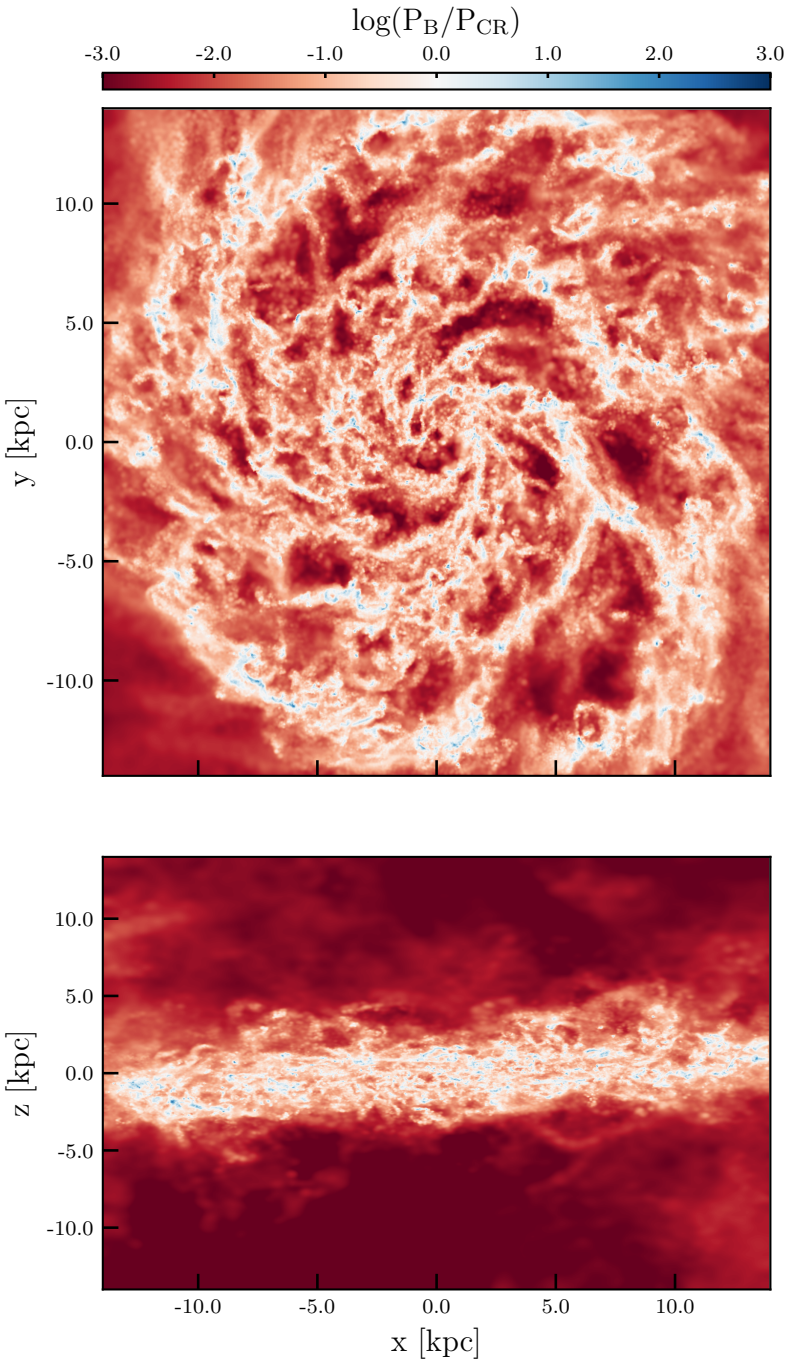

Figure 2.3: *Logarithm of the ratio between magnetic and cosmic ray pressures in m12i (CR+)* ($\frac{\int P_B d\ell}{\int P_{CR} d\ell}$), for a face-on projection in the top panel and edge-on projection in the bottom panel. We see that equipartition (white regions) holds on large (> 1 kpc) scales in the galactic disk, cospatially with spiral structure, however with large deviations in inter-arm regions (dark red pockets). On small scales, equipartition does not hold in regions of high magnetic energy density within dense, molecular gas (small, blue regions).

neutral hydrogen mass, to obtain a "Zeeman-inferred" magnetic field. Specifically, we construct sightlines through a face-on projection of the disk, and use the routine described in Section 2.3 of Hopkins, Hernquist, et al. (2005) to calculate the Zeeman-inferred magnetic field as:

$$B_{\parallel,\,\mathrm{Zeeman-inferred}} = \frac{\int_L n_{\mathrm{HI,cold}}\, B_\parallel \, d\ell}{\int_L n_{\mathrm{HI,cold}}\, d\ell}, \tag{2.1}$$

where the integration is performed along, ℓ, the path length through the disk. The cold fraction observed in Zeeman absorption is estimated as $n_{\mathrm{HI,cold}} \sim n_{\mathrm{H}}\, e^{-T/50\,K}$ following Crutcher et al., but our results are insensitive to this threshold temperature for any values between T = 50 − 500 K as for these cutoff temperatures, the sightlines are still effectively weighted by the dense gas along the line of sight.

Figure 2.4 shows the relation between $B_{\parallel,\,\mathrm{Zeeman-inferred}}$ and column density (N_{HI}) for the CR+ simulations as well as the observational data. Here, the N_{HI} of interest is the same cold, neutral-hydrogen column density, $\int n_{\mathrm{HI,\,cold}}\, d\ell$. The variables required to compute these line-of-sight values are self-consistently calculated in the simulation and require no further modeling. We have compared a set of sightlines computed using the same method uniformly sampling the entire galactic disc, versus those only sampling the solar circle (7-9 kpc), and find that the results at a given N_{HI} are nearly identical.

We find that there is reasonable agreement between the Zeeman-inferred magnetic field and the observations across the range of column densities; i.e., the majority of the Zeeman observations lie within the scatter of the mock Zeeman measurements for both the CR+ (Fig. 2.4) and MHD+ (not shown) simulations. However, there is qualitatively poorer agreement at low N_{HI}, especially in m12m (CR+), where the mock Zeeman measurements lie below the majority of the observations. We attribute this to an overall decrease in the total magnetic field strength relative to the MHD+ simulations, which was shown in Figure 2.1, due to sightlines probing more diffuse atomic gas (see Ji, Chan, et al., 2020, who show that the CR+ simulations do feature significantly more cold atomic gas at low densities $n_{\mathrm{H}} \sim 0.1$ - 1 cm^{-3}, due to CR pressure support leading to lower thermal pressures at a given gas temperature).

It is also important to note that observations do not probe these diffuse sightlines very robustly, and the constraints in the low N_{HI} regime are mostly upper-limits.

There are some caveats to these mock observations: these are not full radiative transfer calculations of the Zeeman splitting of spectral lines in individual clouds,

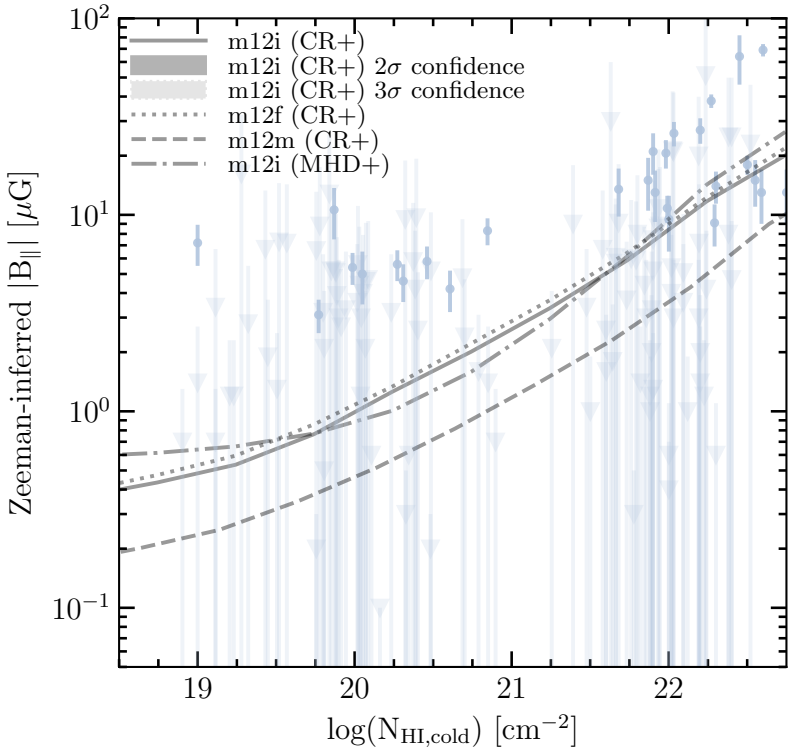

Figure 2.4: $B_{\parallel,\mathrm{Zeeman-inferred}}$ *(Equation 2.1) vs. cold neutral-hydrogen column density* for face-on projections of m12i, m12f, and m12m (CR+). The black solid line shows the median value at each column density bin for sightlines passing through the galactic disk for m12i, with the same for m12f (CR+) and m12m (CR+) shown with dotted and dashed lines. The results are unchanged if restricted to the solar circle. Shaded regions show 5-95 percentile and 1-99 percentile (approximately 2σ and 3σ confidence regions) for m12i (CR+). Light blue points show observational measurements from Crutcher (2012) and associated 1σ error-bars. Non-detections are shown as inverted triangles with $+3\sigma$ upper error-bars. Our CR+ simulations show good agreement with the observational data, however; they are slightly more discrepant at the low column density end due to sightlines probing more diffuse atomic gas, which exhibit lower field strengths compared to the MHD+ simulations.

nor is any of our simulations a perfect analog to the Milky Way. However, the comparisons shown here demonstrate that the simulated galaxies reproduce the observed Milky Way magnetic field strength - column density relation at the order-of-magnitude level.

Zeeman-Inferred Field Strengths and Gas Densities

In this section, we examine the relation between the Zeeman-inferred $|B_{\parallel}|$ and the three-dimensional gas density which is often discussed in the star formation literature

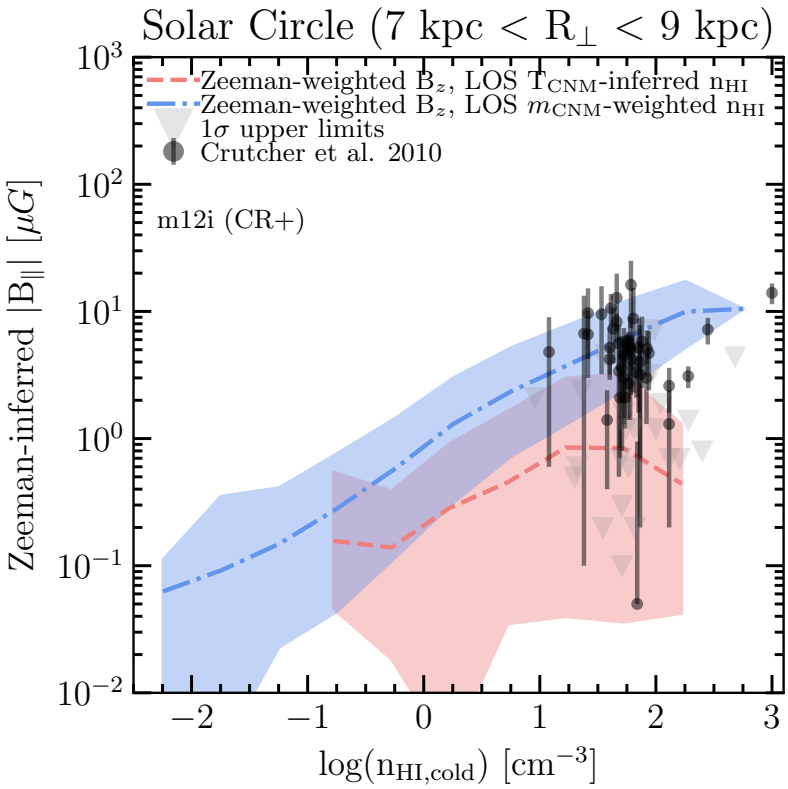

Figure 2.5: *Zeeman-inferred* $|B_{\parallel}|$ *vs. cold, neutral hydrogen number density* for m12i (CR+). Each line shows the mean Zeeman-inferred $|B_{\parallel}|$ at each number density bin. The coral line shows $|B_{\parallel}|$ vs. $n_{\mathrm{HI,T_{CNM}}}$ (Equation 2.3), which is the number density inferred from the LOS cold, neutral hydrogen weighted-temperature assuming thermal pressure equilibrium. The blue line also shows the Zeeman-inferred $|B_{\parallel}|$, but plotted against $n_{\mathrm{HI,M_{CNM}}}$ (Equation 2.2), which is the LOS cold mass-weighted density. Black points show observations from (Crutcher et al., 2010) and associated 1σ errorbars, and non-detections are shown with inverted grey triangles. Shaded regions show the 5-95 percentiles (approximately 2σ). The results are nearly identical for the MHD+ run, and for m12f and m12m (not shown). The relation between $|B_{\parallel}|$ and $n_{\mathrm{HI,M_{CNM}}}$ is broadly consistent with the purely theoretical values of $|\mathbf{B}|$ vs. n. However, when using $n_{\mathrm{HI,T_{CNM}}}$, the relation is flattened due to thermal pressure equilibrium being a poor approximation in the cold ISM, thus not faithfully tracing the "true" density.

(for a review see Crutcher, 2012). Particularly of interest are the results of Crutcher et al. (2010) examined in the previous section, now in a different observational plane which depends on methodology for determining three-dimensional cloud densities. In Figure 2.5, we study the relation between Zeeman-inferred magnetic field strength and three-dimensional gas density at the Solar circle in our simulated galaxies.

It is not usually possible to determine the mean density $n_{\mathrm{HI,cold}}$ of the individual

Zeeman absorbers from observations, and since it is well-known that the absorbers are small structures along the line-of-sight, using a quantity like $\int_L \mathrm{n}_{\mathrm{HI,\,cold}}\, d\ell / \int_L d\ell$ would severely under-estimate their typical densities. So instead, we compare two approaches. First, a root-mean-squared (rms) or cold-gas mass weighted density, similar to what one might (ideally) estimate via cold gas line emission, which appropriately weights for clumping along the line of sight:

$$\mathrm{n}_{\mathrm{HI,M_{CNM}}} = \frac{\int_L \mathrm{n}^2_{\mathrm{HI,cold}} d\ell}{\int_L \mathrm{n}_{\mathrm{HI,cold}} d\ell} \tag{2.2}$$

Second, we approximate the method from Crutcher et al. (2010) and Crutcher (2012), which assumes that the H I spin temperature $\mathrm{T}_{\mathrm{spin}}$ gives the kinetic temperature $\mathrm{T} = T_{\mathrm{spin}}$ of the gas, which itself is in thermal pressure equilibrium with a universal constant pressure, so that everywhere $\mathrm{n}_{\mathrm{HI,\,cold}} \cdot \mathrm{T} = 3000\ \mathrm{K\,cm^{-3}}$. This gives

$$\mathrm{n}_{\mathrm{HI},\,T_{\mathrm{CNM}}} = 3000\,\mathrm{K}\,cm^{-3}\,\frac{\int_L \mathrm{n}_{\mathrm{HI,\,cold}}\, d\ell}{\int_L \mathrm{n}_{\mathrm{HI,\,cold}}\,\mathrm{T}\, d\ell} \tag{2.3}$$

Figure 2.5 shows the $\mathrm{B}_{\parallel,\,\mathrm{Zeeman\text{-}inferred}}$ vs density for the two different density estimators. We see that $\mathrm{B}_{\parallel,\,\mathrm{Zeeman\text{-}inferred}}$ versus $\mathrm{n}_{\mathrm{HI},\,M_{\mathrm{CNM}}}$ gives at least a broadly similar trend to the "true" theoretical $|\mathbf{B}|$ versus $\mathrm{n_H}$ in Figure 2.1, with a differing normalization by a factor of ~ 2 owing to the geometric effect of measuring solely the line-of-sight component of the magnetic field. While $\mathrm{B}_{\parallel,\,\mathrm{Zeeman\text{-}inferred}}$ is consistent with the observed data, the relation between $\mathrm{B}_{\parallel,\,\mathrm{Zeeman\text{-}inferred}}$ and $\mathrm{n}_{\mathrm{HI},\,T_{\mathrm{CNM}}}$ is flattened significantly, and we find that this effect remains even if we isolate the sightlines with dense complexes ($\mathrm{n}_H > 300\ \mathrm{cm^{-3}}$) along the path length, or draw sightlines through those dense complexes themselves, rather than sampling sightlines through the entire disk at the Solar circle. This is because there is very little correlation, over the dynamic range here, between $\mathrm{n}_{\mathrm{HI},\,T_{\mathrm{CNM}}}$ and either $\mathrm{n}_{\mathrm{HI},\,M_{\mathrm{CNM}}}$ or the true gas density $\mathrm{n_H}$ from which the Zeeman absorption originates. The poor correlation owes to the fact that: (1) *thermal pressure equilibrium is not a particularly good approximation in the cold ISM*, where other forms of pressure (including magnetic as we show in Figure 2.2, turbulent, and cosmic ray) all dominate over thermal, and the conditions are highly dynamic (Grudić et al., 2021), and (2) even if thermal pressure equilibrium were reasonable, *there is not a single thermal pressure across all clouds in all locations in the Milky Way* (e.g. towards the galactic center, it is well-known that cloud pressures are much higher). As a result, using $\mathrm{n}_{\mathrm{HI},\,T_{\mathrm{CNM}}}$,

which not only assumes constant thermal pressure, but a *single value* of thermal pressure across all sightlines, introduces considerable scatter in the x-axis of Figure 2.5, essentially "smearing out" the correlation. Recall that our values of $|B_{\parallel}|$ are the same for all sightlines, so the effect on the normalization depends on which densities are most heavily sampled. If we sampled denser true sightlines more numerously, as in the Crutcher et al. (2010) analysis, then the normalization of this curve would be the same as their favored value.

Magnetic fields in the ionised ISM and CGM: comparison to rotation and dispersion measures

Comparison to Pulsar RMs and DMs in the Galaxy

In this Section, we compare the simulations with observational probes of the magnetic field in the ionized medium, primarily through use of Faraday rotation and dispersion measure. Faraday rotation occurs due to the the interaction of light with a magneto-ionic plasma, causing the plane of polarization to rotate as a function of the electron density and magnetic field strength. The average magnetic field along the line of sight ($|\langle B_{\parallel} \rangle|$) can be determined through the rotation measure if an independent constraint is found on the electron density, n_e, given by the dispersion of radio pulses. The dispersion measure is dependent on the thermal electron column density and we compute the DMs along the mock line-of-sight as DM = $\int \mathrm{n_e} d\ell$. The RMs are computed with the standard definition (Beck, 2015a):

$$\mathrm{RM} = \frac{e^3}{2\pi \mathrm{m_e^2 c^3}} \int_L n_e \mathbf{B} \cdot \mathbf{dl} = 0.808 \int_L n_{\mathrm{e}}(cm^{-3}) \mathbf{B}(\mu G) \cdot \mathbf{dl}(pc), \tag{2.4}$$

where e is the electron charge, m_e is the electron mass, c is the speed of light, and the integration is performed along the path-length ℓ.

To compare the synthetic measurements as expected from our MW-analogs to MW pulsar observations, we use the same line-of-sight computation routine described in Section 2.3 of dividing the galactic disk into "slabs" to determine RMs and DMs. For Zeeman splitting, it makes no difference if we integrate arbitrarily large sightlines "outside" of the disk because these have a very small probability of intercepting cold atomic H I. However, for RM/DM measurements, it is important that we sample sightlines of appropriate depths through the disk (similar to those for the actual observed Galactic pulsars), and not simply integrate all sightlines to $\pm\infty$, because then the predicted DM would be completely dominated by the cumulative contribution from halo and IGM ionized gas.

In Figure 2.6 we show the synthetic RM vs. the synthetic DM for m12i, along with MW pulsar data from the Australian Telescope National Facility (ATNF) catalogue (Manchester et al., 2005) and from the Low-Frequency Array (LOFAR) (Sobey et al., 2019). Our simulated RMs and DMs are in good agreement with the observations, with most of the observational measurements towards MW pulsars falling within 1σ of the simulation scatter and almost all within 2σ. This indicates that we find similar magnetic field strengths and geometries averaged over sightlines through the disk in the warm, ionized medium to what is seen in the Milky Way. Between the CR+ and MHD+ runs, we find negligible differences in the inferred properties of the magnetic field in the WIM, consistent with our previous results that CRs do not substantially affect the magnetic properties and observables in the ISM.

As many have noted (Simard-Normandin and Kronberg, 1980; Rand and Kulkarni, 1989; Han, Manchester, and Qiao, 1999; Han, Manchester, Lyne, et al., 2006; Sobey et al., 2019), a naive estimate of $|\langle B_{\parallel} \rangle| \sim 1.2\,|\mathrm{RM}|/\mathrm{DM}$ gives $|\langle B_{\parallel} \rangle| \sim 0.1 - 10\,\mu G$ with a median around $\sim 1\,\mu G$. Note that $|\langle B_{\parallel} \rangle|$, which is probed by $1.2\,|\mathrm{RM}|/\mathrm{DM}$, differs from $\langle |B_{\parallel}| \rangle$ in that the absolute value is taken *after* the line-of-sight averaging. This, in turn, means that $1.2\,|\mathrm{RM}|/\mathrm{DM}$ will be sensitive to reversals of the magnetic field along the line of sight, under-predicting the true magnitude of $\langle |B_{\parallel}| \rangle$ and thereby informing us about the coherence of the magnetic field along the line of sight.

In our simulated disks, we see that $1.2\,|\mathrm{RM}|/\mathrm{DM}$ under-estimates the actual average values of $\langle |\mathbf{B}| \rangle$ weighted by the thermal electron density by a factor of ~ 2.5. Note that $\langle |\mathbf{B}| \rangle$, which is the linear-weighted average of the magnitude of $\mathbf{B}$, is a factor of 1.2-2.2 smaller than the "rms" $\mathbf{B}$ often quoted in the literature, for example in Seta and Federrath (2021), and is given by $\langle \mathbf{B}^2 \rangle^{1/2}$, where the multiplicative factor depends on the clumping of the magnetic field. Along sightlines drawn through our simulated WIM, this factor appears to be ~ 1.2.

In the next section, we will explore how RMs and DMs trace magnetic fields in the CGM, and how CRs may have an impact on these observables.

RMs and DMs in the ISM and CGM to distant observers

Recently, there has been a surge of theoretical and observational interest in the properties (including magnetic fields) of the CGM, so we extend our comparison to galactocentric radii $\sim 10 - 200\,\mathrm{kpc}$. Note that we restrict to RMs and DMs here

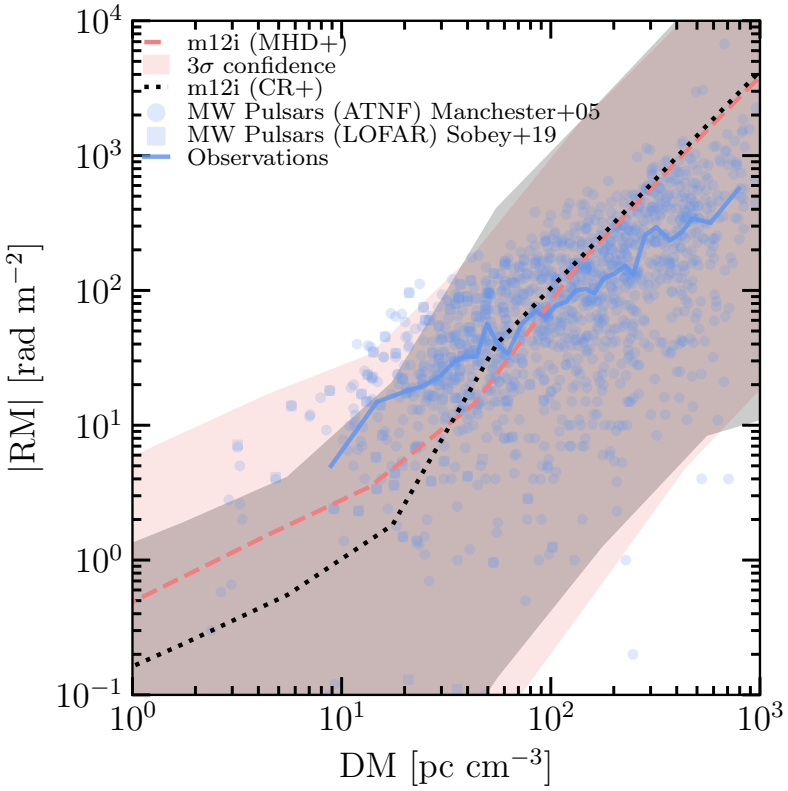

Figure 2.6: *|RM| vs. DM for sightlines through the disks* of m12i MHD+ and CR+ (coral and black, respectively). Lines indicate the mean |RM| in each DM bin and the shaded region represents 1-99 percentiles (approximate 3σ). Blue points show observations of Milky Way pulsars using LOFAR done by Sobey et al. (2019) and as queried by Seta and Federrath (2021) from the ATNF Pulsar Catalogue (Manchester et al., 2005), with the solid blue line showing the median |RM| of both sets of observations at each DM, with 30 bins of equal numbers of observations.

(as opposed to Zeeman splitting), since the CGM gas is predominantly ionized and there do not exist Zeeman splitting data for the CGM.

In Fig. 2.7 we visualize the RMs, DMs, and $B_{\parallel}$ seen in a face-on projection of the galaxy zoomed in on the central 40 kpc, while in Fig. 2.8 we present visualizations out to 200 kpc. Inspection reveals sign flips (field reversals) in RM or $B_{\parallel}$ on both large and small scales, with notable features including the spiral arms and large-scale inflows joining the disk — these features are consistent with observations, as discussed below.

Constraints on the strength and geometry of ISM magnetic fields in nearby galaxies come from intensity and RM measurements of diffuse radio emission (Beck, 2015a; Han, Han, and L., 2017). Fletcher et al. (2011) published the most detailed map

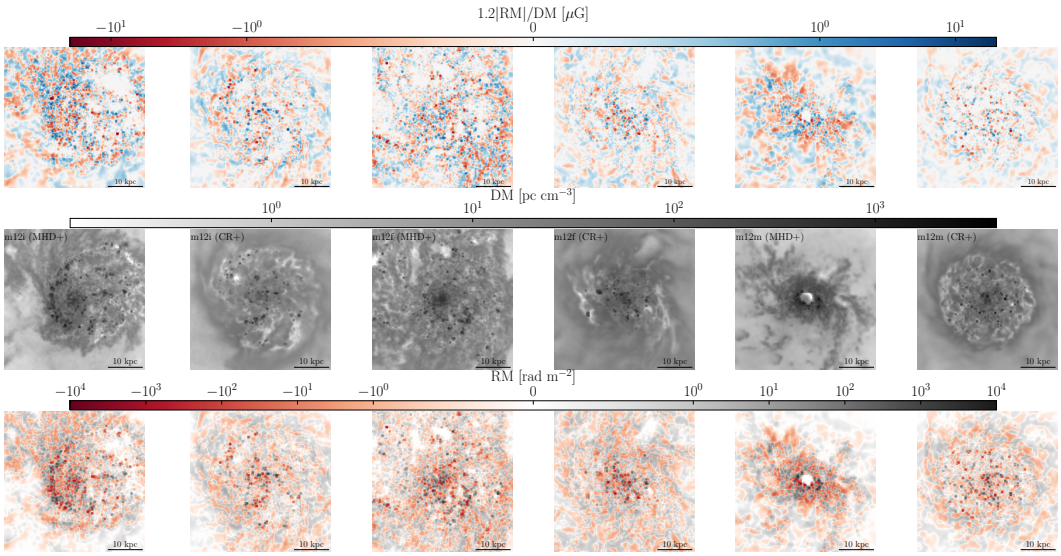

Figure 2.7: *Visualizations of various line of sight quantities within the central 40 kpc.* **Row 1:** Line-of-sight RM/DM-inferred magnetic field strength. **Row 2:** Dispersion Measures. **Row 3:** Rotation Measures, with m12i (MHD+ and CR+), m12f (MHD+ and CR+), and m12m (MHD+ and CR+) form left to right. Our simulations exhibit small-scale reversals in the sign of RMs similarly to observations, indicative of small-scale field reversals due to explicit treatment of stellar feedback and partially resolved ISM phase structure.

of RMs, towards the face-on spiral galaxy M51 by inferring RM through modeling the variation of the synchrotron polarization angle with wavelength at 3-6 cm. Qualitatively, the RM visualization is similar, with sign flips on all observed scales. This is also similar to what is inferred from modeling the spatial distribution of MW pulsar RMs and DMs, and variations in dust polarization and synchrotron to construct galactic magnetic field maps (e.g. Jansson and Farrar, 2012; Haverkorn, 2015; Han, Han, and L., 2017; Beck, Chamandy, et al., 2020). The same appears to be true in the LMC, from visual inspection (Gaensler et al., 2005).

Briefly, Fletcher et al. (2011) explicitly note that they cannot measure the shape of the distribution of RMs in M51 (as their observed RM distribution is noise-dominated), but they can estimate the intrinsic rms value of |RM| averaged over the Galactic disk (giving $\langle |\mathrm{RM}|^2 \rangle^{1/2} \sim 10\,\mathrm{rad\,m^{-2}}$, about half the measured rms before accounting for observational errors), which is similar to rms values we obtain in our simulated disks in Fig. 2.7 of around $\sim 20\,\mathrm{rad\,m^{-2}}$.

We quantify the dependence of various quantities of interest as a function of galactocentric radius in the CGM in Figure 2.9. We present cylindrically averaged radial

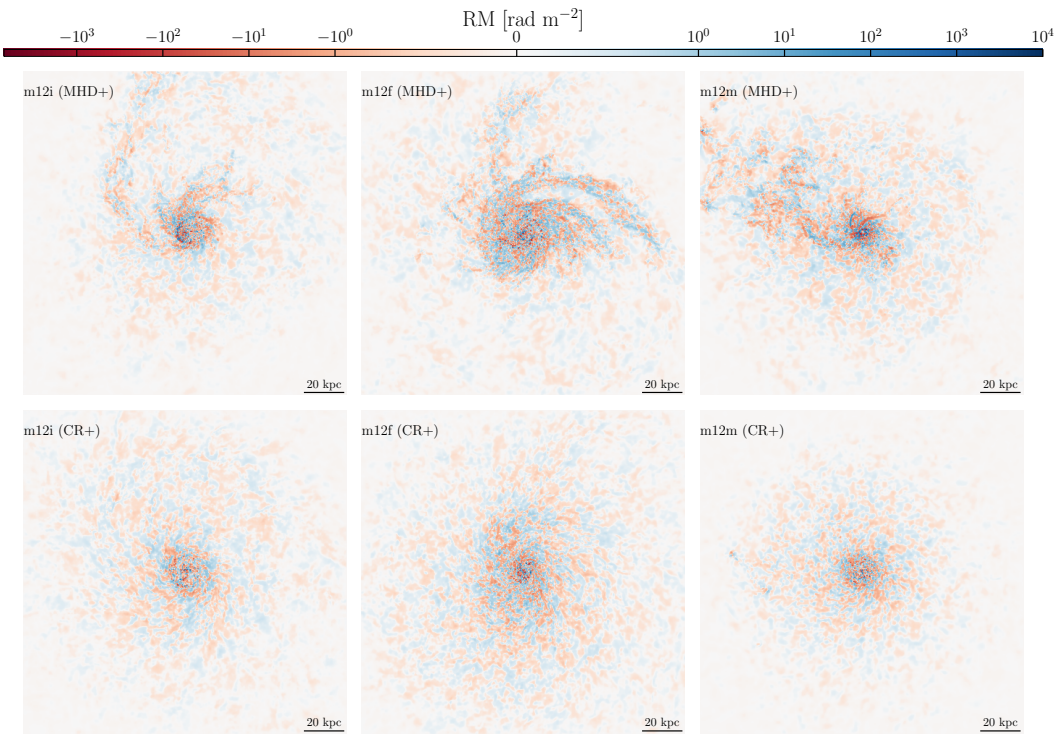

Figure 2.8: *Face-on visualizations of synthetic rotation measures out to a projected radius of 200 kpc as seen by an external observer towards an ideal background source.* **Row 1:** MHD+ simulations. **Row 2:** CR+ simulations, with m12i, m12f, m12m from left to right. Large scale gas inflows and spiral structure can be seen, as well as sign reversals in RM on both large and small scales. In m12m MHD+, an in-falling satellite galaxy and tidal tail can be observed.

profiles of RM, DM, and $\langle|\mathrm{B}|^2\rangle^{1/2}$ in the CGM. A few trends are evident. First, we see that while there is considerable detailed spatial structure in Fig. 2.8, the cylindrically-averaged median profiles (Fig. 2.9) are quasi-universal radial power-laws in impact parameter R, with median DM $\propto R^{-1}$ (expected for gas in an isothermal-sphere type profile with three-dimensional $\rho \propto r^{-2}$), $\langle|B_{\parallel}|\rangle \propto R^{-1}$ and correspondingly |RM| $\propto R^{-2}$, on average. The range of slopes for each is roughly ± 0.3. The intrinsic scatter about the trend is large, however, ~ 1 dex in $|RM|$, and subsequently similar in $1.2\,|RM|/DM$. Interestingly, the trend in $\langle|\mathrm{B}_{\parallel}|\rangle$ is a bit shallower than what we might expect for isotropic flux-freezing ($|\mathbf{B}| \propto \rho^{2/3} \propto R^{-4/3}$), closer to what we might expect for $\langle|\mathrm{B}_{\parallel}|\rangle \propto \rho^{1/2}$ in the CGM, similar to the trend seen in the ISM, in Fig. 2.5.

Second, there are some small but systematic offsets between the MHD+ and CR+ simulations. In the inner CGM approaching the disk ($r \sim 10\,\mathrm{kpc}$), $\mathrm{B}_{\parallel}$ is a factor

of 1.5-2 higher in MHD+, directly related to the offset in Fig. 2.1. Far from the disk, the DMs are a factor of 1.5-2.5 lower in MHD+: this owes to the lack of CR pressure (able to support a larger "weight" of CGM gas) and inefficient galactic outflows leading to more accretion from the CGM onto the galaxy (Ji, Chan, et al., 2020; Ji, Kereš, et al., 2021; Hopkins, Chan, Ji, et al., 2021). In contrast, within the disk, this leads to higher DMs for MHD+. Together, these mean that while typical ISM RMs are larger in the more massive, more dense MHD+ simulations, *the RM profile in the CGM is nearly identical*.

Third, we see that the inferred $\langle B_{\parallel} \rangle \sim 1.2\,|\mathrm{RM}|/\mathrm{DM}$ under-estimates the median $|B_{\parallel}|$, or $\langle |\mathbf{B}_{\parallel}| \rangle$ of gas along the LOS by a factor of $\sim 5-7$. The fields are close to isotropic in this statistical and cylindrically-averaged sense, where we are averaging multiple lines of sight along annuli at a given galactocentric radius. So, this means that $\langle |\mathbf{B}| \rangle \sim 2\langle |\mathbf{B}_{\parallel}| \rangle$, which means on average $|\mathrm{RM}|/\mathrm{DM} \sim 0.1\,\langle |\mathbf{B}| \rangle$ where the averaged terms are weighted by electron density in the same manner as RM. We have confirmed that this owes primarily to cancellation due to random field components along the LOS; crudely, this systematic offset is equivalent to the statement that the coherence length of the magnetic field is $\sim 10\%$ the size of the system contributing to RM (i.e. $\sim 20\,\mathrm{kpc}$ — comparable to the halo scale length — in the outer CGM).

While there is no observational measurement of RM from the CGM around any $\sim L_*$ galaxy, a number of studies measuring RMs from background fast radio bursts (FRBs) and other bright radio sources have placed upper limits which can be compared to the predictions of our simulations. At the radii shown in Figure 2.9, we plot the most stringent upper limits to date, specifically the upper limit towards an FRB found in Prochaska et al. (2019) and the 3σ upper limits quoted as a function of impact parameter in the FRB study of (Lan and Prochaska, 2020).[4] At even larger impact parameters $\gtrsim 500\,\mathrm{kpc}$ (not shown), Ravi et al. (2016) place a 2σ upper limit on $\langle \mathbf{B}_{\parallel} \rangle_{\mathrm{IGM}}$ of $2.1\times10^{-2}\,\mu$G, and O'Sullivan et al. (2020) measure a 2σ upper limit $|\mathrm{RM}| < 1.9\,\mathrm{rad\,m^{-2}}$ and constrain the IGM magnetic field strength to be $\langle |\mathbf{B}| \rangle_{\mathrm{IGM}} < 4\times10^{-3}\,\mu$G, both from FRB detections. We see that the simulations are easily consistent with all of these limits, but the data are not yet particularly constraining. Still, with much larger FRB samples expected in the near future from

[4]Note that while the FRBs used in Prochaska et al. (2019) and Lan and Prochaska (2020) have measured RMs, these RMs are almost certainly strongly dominated by the contribution from the FRB host galaxy, with an unknown additional contribution from the FRB source and IGM, so the authors can place only a statistical upper limit on the contribution to the measured RM from the CGM of the foreground $\sim L_*$ galaxy.

DSA-110, CHIMES, and CHORD it should be possible to improve these upper limits by an order of magnitude or more, potentially reaching detection thresholds at least in the inner CGM (Vanderlinde et al., 2019; CHIME/FRB Collaboration et al., 2018; Kocz et al., 2019; Connor and Ravi, 2022). Further observational data are needed to delineate between differing physical and numerical schemes which predict order of magnitude differences in halo field strengths from our results, discussed below (Pakmor, Van De Voort, et al., 2020).

2.5 Discussion and Conclusions

The results in this chapter have presented probes of the magnetic field as traced in different gas phases; cold, dense and neutral ISM gas ($T \sim 100$ K, $n_H \gtrsim 10$ cm^{-3}), warm ionized ISM gas ($n_H \sim 0.1$ cm^{-3}, $T \gtrsim 6000$ K), and hot, diffuse CGM gas ($T \gtrsim 10^6$ K, $n_H \sim 0.001$ cm^{-3}). Due to having resolved phase structure of the ISM in these simulations, we are able to meaningfully compare these tracers to their observational counterparts without use of additional modeling or assumptions, and are thus able to both (a) test whether observational assumptions apply in these simulations and (b) comment on how two physical models (MHD+, CR+) compare in their predictions of the observables.

We investigated how the magnetic field properties vary in two types of simulations of the same galaxies: MHD+ and CR+. We find general agreement in the scaling of the overall relation of $|\mathbf{B}|$ vs. number density in all of the simulations, but with a modest offset between the MHD+ and CR+ runs of a factor of $\sim 2-10$ primarily at very diffuse ISM densities ($n < 0.01$ cm^{-3}) which increases towards more diffuse densities and is more systematic for m12m, with an offset of a factor of ~ 2 at ($n > 1$ cm^{-3}). This difference at very diffuse ISM densities, as mentioned above, arises primarily due to differences in the "inner CGM."

The "inner CGM" is precisely where previous studies (Booth et al., 2013; Simpson et al., 2016; Girichidis, Naab, Hanasz, et al., 2018; Buck et al., 2020; Ji, Chan, et al., 2020; Ji, Kereš, et al., 2021; Hopkins, Chan, Ji, et al., 2021; Chan, Kereš, Gurvich, et al., 2022) have shown CRs can play a dramatic role influencing the dynamics of galactic fountains and outflows. Specifically, in simulations without cosmic rays, MW-mass galaxies at low redshifts have their outflows "trapped" by CGM pressure, creating high-velocity fountains with rapid recycling (Muratov et al., 2015; Anglés-Alcázar, Faucher-Giguère, et al., 2017; Gurvich et al., 2020; Stern et al., 2021; Hafen et al., 2022), while in the CR+ simulations, the added CR pressure gradient both

maintains gas acceleration and reduces the pressure barrier to outflows, allowing disk outflows to smoothly escape to the outer halo (references above). We directly confirm that, as a result, the velocity dispersion of the low-density inner-CGM gas which drives the offset of $|\mathbf{B}|$ versus $n_{\rm gas}$ is lower in the CR+ simulations by a factor of $\sim 2-3$. This, in turn, means that magnetic fields experience significantly less amplification by "turbulent" or fountain flows in this range of conditions due to recycling of outflows (Martin-Alvarez, Devriendt, et al., 2018), and greater adiabatic attenuation, since the escaping outflow will reduce the magnetic field strength of any advected fields from the disk via flux-freezing as the outflowing gas expands. This can explain some of the offset in $|\mathbf{B}|$ vs. number density between MHD+ and CR+ galaxies, but not the whole difference.

From our CR+ simulations, which self-consistently evolve the GeV CRs which dominate the CR energy budget, we are able to make predictions for the relative strengths of magnetic, thermal, and CR pressures in different gas phases. We find that in the disk, equipartition assumptions between CRs and magnetic fields (as is often assumed for estimating magnetic field strengths from observations of diffuse radio emission Chyzy et al., 2011; Beck, 2015a) may hold on large scales, and at typical ISM densities (L $>$ 1 kpc, $n_{\rm H} \sim$ 1-10 cm^{-3}); however in the CGM, this assumption breaks down. Similarly, assumptions of equipartition between thermal and magnetic pressures in the CGM appear to be invalid given the predictions of our model; however, details of this depend on how CRs are treated and their interplay with metal-enriched, actively-cooling gas (Prochaska et al., 2019; Hopkins, Butsky, Panopoulou, et al., 2022). That being said, in both the halo and the ISM, we generally see a plasma $\beta \ll 1$ in cold/neutral dense gas (reaching values as low as 5×10^{-5}), and $\beta \gg 1$ in low density, mostly-ionized gas (reaching values as high as 7×10^{8}), consistent with most previous theoretical studies (Su, Hayward, et al., 2018; Ji, Chan, et al., 2020; Butsky, Fielding, et al., 2020).

We compare ISM magnetic field values inferred from Zeeman measurements within the Galaxy for the cold, neutral medium, and find broad agreement (Figure 2.4). In detail, there are some differences between runs, primarily that the offset in magnetic field strength at lower gas densities results in CR+ simulations predicting slightly lower values of $B_{||}$ relative to the MHD+ simulations at lower column densities, which probe more of the diffuse gas. This results in slightly poorer agreement at lower column densities ($\log_{10}(N_{\rm H}) < 21$ cm^{-2}) between the existing observations of Crutcher (2012) and our simulations. While the CR+ simulations exhibit slightly

lower values of $B_{||}$ relative to the MHD+ simulations, we note that the overall qualitative agreement with the observations is not notably different between the two physical models.

The physical relations of $B_{||}$ vs. density (Figure 2.5) for both the MHD+ and CR+ simulations agree considerably well with the Solar circle diffuse H I observations of Crutcher et al. (2010). The observations of interest span higher densities (n > 300 cm^{-3}), where there is little difference in the magnetic field strength of the MHD+ and CR+ simulations.

As discussed in Section 3.3.2, the poor correlation between $n_{HI,T_{CNM}}$ and $n_{HI,M_{CNM}}$ flattens the relation between $|B_{||}|$ and n. This may explain some aspects of the Crutcher et al. (2010) analysis, which compiles Zeeman observations from three types of clouds (diffuse H I, IR dark, and dense molecular) of varying densities using three different tracers (H I, OH, CN). It is important to note that *within any one sample*: i.e. within any one "type of cloud" or within any one tracer, there is no statistically significant trend of $|B_{||}|$ with $n_{HI,T_{CNM}}$ in the Crutcher et al. (2010) data.

This leads, for example, to their conclusion that the Zeeman-inferred $|B_{||}|$ is approximately constant in diffuse gas with $n < 300\,cm^{-3}$, which are exclusively sampled by diffuse H I — it is only when the different datasets, each of which samples different median density ranges (e.g. diffuse H I at $10^1 - 10^{2.5}\,cm^{-3}$, dark clouds for $10^{3.5} - 10^{4.5}\,cm^{-3}$, dense molecular clumps at $10^{5.5} - 10^{6.5}\,cm^{-3}$) are combined that the underlying trend (quite similar to what we predict here) can be observed. Here, we show that detecting the predicted trend *within* the dynamic range of densities probed by H I Zeeman data alone (a factor of $\sim 10 - 30$ in gas density) requires a three-dimensional gas density estimator which is accurate to much better than this dynamic range (i.e. to within a factor of ~ 2 or so).

In visually examining the synthetic rotation measures for our simulated galaxies, we find variations of the sign of RM on small scales as well as large scales, with quantitative values in agreement upper limits placed in the halos of L_* galaxies by Prochaska et al. (2019) and Lan and Prochaska (2020). Zooming in on the disk, we find RM sign reversals on small scales in a manner qualitatively similar to the RM maps of M51 produced by Fletcher et al. (2011), with little to no correlation of the RMs with galactic structure, differing from work done by Pakmor, Guillet, et al. (2018), who performed a similar study of the RM by analyzing a MW-analog from the Auriga simulations. Our synthetic RMs show a less ordered, more turbulent magnetic field in better agreement with the observations, which is

primarily indicative of the effect of explicit stellar feedback and resolution of the ISM phase structure, in contrast to the sub-grid "effective equation-of-state" model used for the ISM in that work.

For the warm, ionized phase of the ISM of our simulated galaxies, we find good agreement with RMs and DMs towards Milky Way pulsars. While the mean RM/DM-inferred magnetic field strength ubiquitously under-predicts the mean "true" rms $|\mathbf{B}|$ in the disk, at the column densities of interest, it traces $B_{||}$ averaged along sightlines through the disk.

While we primarily focus the discussion of the RMs, DMs, and subsequent inferred estimates of $B_{||}$ on the halo in Figure 2.9, we find good qualitative agreement between the intrinsic dispersion of the RM as inferred from synchrotron polarization at 3 and 6 cm by Fletcher et al. (2011), with the caveat that the methodology of our synthetic RMs does not aim to faithfully reproduce that of Fletcher et al. (2011) and contains information averaged over large ($\sim$ 280 kpc deep) sightlines rather than solely arising from the disk. In the region that is primarily of interest for these synthetic background point source RMs, i.e., the halo, the MHD+ and CR+ profiles converge, independently of resolution.

Our CGM-focused results suggest that use of RMs and DMs towards point sources as measures of $B_{||}$ underestimate the "true" magnetic field strength in the halo at a given galactocentric radius by about a dex. This is consistent with work done by Seta and Federrath (2021), who found that in the presence of driven subsonic, transonic, and supersonic turbulence, the standard deviation of the average parallel component of the magnetic field is about an order of magnitude less than the true rms magnetic field strength of the box. Here, in Figure 2.9, the RM/DM estimate traces effectively the ionized-mass-weighted parallel component of the magnetic field, and $< |B|^2 >^{1/2}$ averaged over the extensive (240 kpc) lines of sight probes the root mean square magnetic field strength. This result may be of particular importance for observers looking to characterize the magnetic field strengths in the halos of galaxies towards background FRBs, implying that RM/DM estimates may be a factor of $\sim$ 10 lower than the true halo magnetic field strength. From our estimate of how well the RM/DM-inferred $B_{||}$ traces the "true" rms $\langle |\mathbf{B}|^2 \rangle^{1/2}$ we infer that the coherence length is $\sim$50% the characteristic length scale in the ISM (on order of the disk scale height), and $\sim$10-20% of the characteristic length scale in the CGM, on order the halo scale length. This result on the coherence length is similar to predictions or the large-scale coherence length towards MW pulsars from random walk models

described by Seta and Federrath (2021).

Notably, the predictions of RMs and $\langle|\mathbf{B}|^2\rangle^{1/2}$ of the Auriga cosmological zoom-in simulations presented in Pakmor, Van De Voort, et al. (2020) are a factor of ~ 10 higher than those computed from the FIRE simulations. The Auriga simulations use an effective equation-of-state model of the ISM Springel and Hernquist (2003) in contrast to the explicit treatment of feedback used in our simulations. The typical inter-cell spacing in the CGM of the halos of FIRE and Auriga are similar ($\sim$ kpc), and both are notably turbulent (see Ji, Chan, et al., 2020), however it remains unclear what dominates magnetic amplification in the halo, and whether resolving the inertial scale of turbulence in the CGM will be key to generating accurate halo magnetic fields. We note also that varying the σ_p, σ_h, and α_ψ divergence cleaning and slope-limiter terms (Hopkins and Raives, 2016, see) by factors of $\sim$5 does not affect the magnetic field properties of these simulated galaxies, indicating that the magnetic field strength is set by physical processes rather than numerics. We have shown that in our simulations with resolved ISM phase structure, the magnetic field strengths very reasonably agree with existing constraints from the Milky Way and M51, however the halo remains uncertain. Present observational constraints are unable to distinguish between these different physical models and numerical treatments, and future observations (e.g. Kocz et al., 2019) will be key for understanding CGM magnetic fields.

2.6 Summary and Future Work

In this chapter, we have analyzed the magnetic fields in the multiphase ISM and CGM in a set of high-resolution, cosmological simulations from the FIRE-2 project, run with two different physical models (MHD+, CR+). We analyze the differences between the magnetic fields in simulations run with each model, and compare forward-modeled observables tracing magnetic fields in the ISM and CGM to existing observational constraints.

In summary, our conclusions are as follows:

- Inclusion of CRs in simulations of galaxy formation does not directly affect the magnetic field strengths in the ISM at a given gas density, though there are modest differences in the lowest density gas ($n < 0.01$ cm^{-3}) due to dynamical effects of CRs in the disk-halo interface (the inner most region of the CGM). The main effect of CRs is indirect, causing the average $|B|$ in

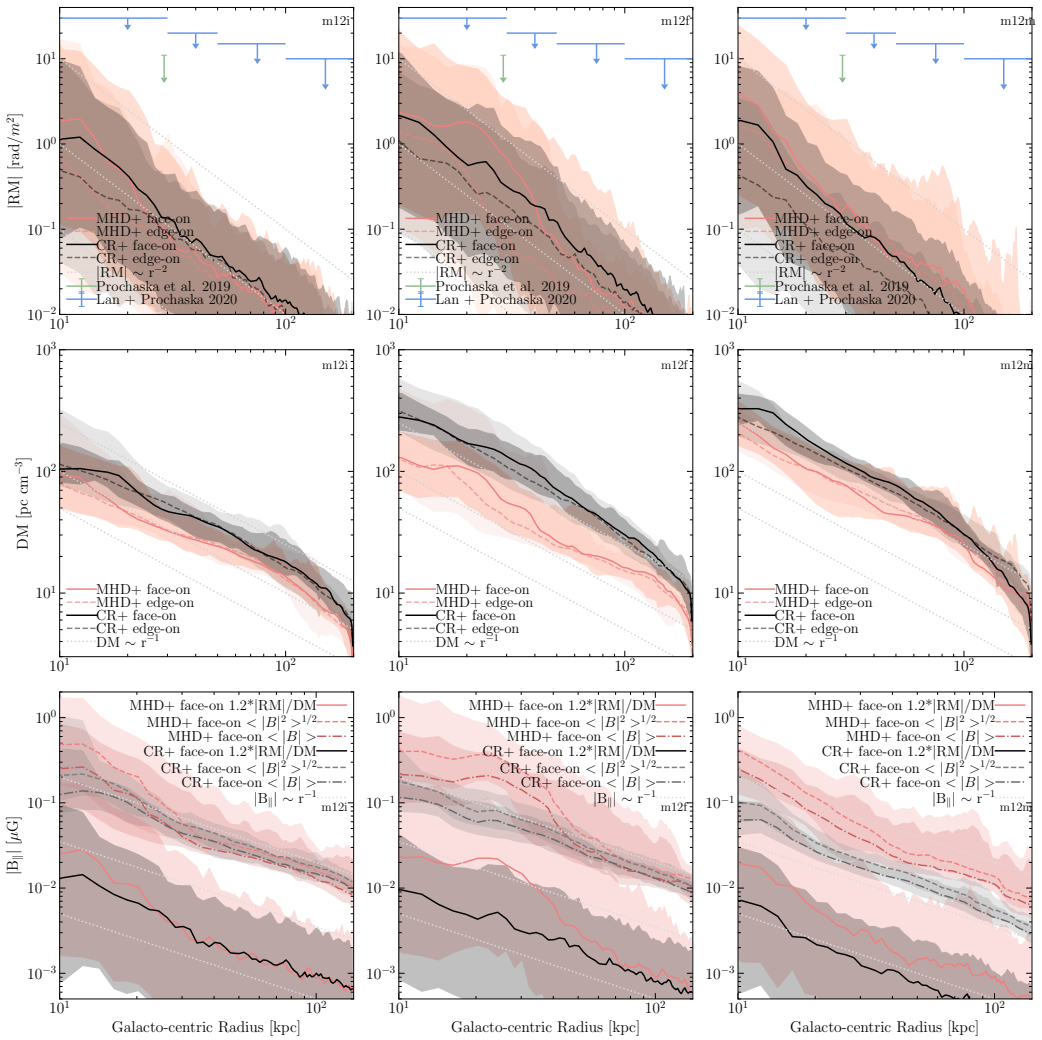

Figure 2.9: *Rotation measure (*|RM|*), dispersion measure (DM), and* $|B_{\parallel}|$ *profiles as a function of galactocentric radius (R).* **Row 1:** RM profiles with MHD+ simulations (m12i, m12f, m12m from left to right) shown in coral and CR+ simulations shown in black. Face-on and edge-on profiles are denoted by solid and dashed lines, respectively. Each line shows the median at a given radial bin. Shaded regions show 5-95 percentile intervals (approximate 2σ error-bars). The green point shows an upper-limit from the RM measured towards an FRB in the halo of a galaxy with $M_* \sim 10^{10.69}$ $M_\odot$ studied by Prochaska et al. (2019). The blue lines show 3σ upper-limits on RMs in the CGM from a sample of high-redshift radio sources studied by Lan and Prochaska (2020). Grey dotted lines show representative power-laws as a visual guide. **Row 2:** Dispersion measure (DM) profiles with the same color and line style conventions as the RM profiles. **Row 3:** Estimates of $|B_{\parallel}|$ as determined from 1.232 RM/DM shown in solid lines, and "true" $< |B| >$ and $< |B|^2 >^{1/2}$ shown with dot-dashed and dashed lines, respectively. Our RM and DM profiles are not in tension with the existing observations, which are not yet constraining. The predicted 1.2 |RM|/DM profiles are consistent with what would be expected for those of an isothermal sphere. Subtle systematic offsets between MHD+ and CR+ RM profiles exist directly due to the offset in diffuse gas near the disk at low R, and far from the disk in the DM profiles due to CR pressure support. Our $|B_{\parallel}|$ profiles indicate that RM/DM significantly under-predicts $< |B| >$ averaged over large lines of sight as well as the rms $< |B|^2 >^{1/2}$ by a factor of $\sim$ 15-20.

those galaxies' less massive, less dense disks to be lower than their MHD counterparts, moving along the same scaling relations between $|B|$ and n_H.

- Our predicted relation for $|\mathbf{B}|$ vs. three dimensional gas density n_H is consistent with that of flux freezing in spherically symmetric and non-spherical geometry ($|\mathbf{B}| \sim n_H^{2/3}$ or $|\mathbf{B}| \sim n_H^{1/2}$).

- Equipartition between magnetic, thermal, and cosmic ray pressures is achieved in our simulated galactic disks at typical ISM densities (n $\sim$ 1-10 cm^{-3}). Equipartition between magnetic and cosmic ray energy densities primarily holds on large (> 1 kpc) scales, cospatial with the spiral structure of our galactic disks, and fails in the interarm regions and on small scales in the presence of dense molecular gas.

- In the halos of our simulated galaxies, equipartition between magnetic pressures and cosmic ray pressures does not hold, and neither does equipartition between thermal and magnetic pressures ($\beta >> 1$).

- Our simulated magnetic field strengths in the cold, neutral ISM agree well with existing Zeeman observations in the Milky Way, and indicate observational estimates of the three dimensional gas density in diffuse HI from spin temperatures may be noisy due to thermal pressure equilibrium being a poor assumption in this phase of the ISM. This can act to obfuscate existing correlations between $|\mathbf{B}_{\parallel}|$ and n_H for $n_H < 300$ cm^{-3}.

- The magnetic field strengths in the warm, ionized ISM of our simulated galaxies are in agreement with observations of Milky Way pulsars and M51 as inferred through rotation measures and dispersion measures.

- Our synthetic rotation measures as a function of impact parameter are in agreement with existing constraints from FRBs probing the halos of L_* galaxies, however there is a large parameter space occupied in this plane by various physical and numerical models. Future surveys which will localize 100s of FRBs per year will be crucial to constraining current model predictions.

- In the CGM, our CR+ simulations exhibit slightly enhanced DMs relative to the MHD+ simulations in the inner CGM (R $\sim$ 50-100 kpc) due to cosmic ray pressure support.

- Our simulations' comparison of 1.2 |RM|/DM ($\langle \mathbf{B}_{\parallel} \rangle$) to the "rms" field $\langle |\mathbf{B}^2|^{1/2} \rangle$ indicates that observational estimates of magnetic fields in the halos of L_* galaxies from FRBs may under-predict the true rms field strength by a factor of 15-20, in qualitative agreement with previous works.

Our study provides motivation to more closely study the magnetic fields in these simulations (e.g., turbulent magnetic field amplification and its connection to feedback models), and to generate detailed mock observations using radiative transfer codes like `POLARIS` (Reissl, Wolf, and Brauer, 2016). This will enable detailed comparison with more indirect magnetic field tracers, such as synchrotron intensities, magnetic field morphologies inferred from polarized dust and synchrotron emission (Borlaff et al., 2021), and resolved Zeeman spectra.

We will also explore predictions for different galaxy types (e.g. dwarfs or starbursts), and redshift evolution, which may help shed light on magnetic field amplification mechanisms. It is also important to continue to explore different physics: as we noted above, our CR+ models adopt a highly simplified empirical (constant-diffusivity) assumption for CR transport, and previous work (Hopkins, Squire, Chan, et al., 2021) has shown that other observationally-allowed models with variable diffusivity can produce different results (so even if CRs are present, reality may closely resemble our MHD+ simulations, for example).

Additionally, our simulations neglect the effects of Active Galactic Nuclei (AGN), which may be an important component of the feedback budget for L_* galaxies (e.g., Wellons et al., 2023; Feldmann, Quataert, Faucher-Giguère, et al., 2023, and references therein). Further understanding of galactic magnetic fields and their tracers from a theoretical perspective may lead to insight on questions related to survival and infall of cool CGM gas, star formation efficiency in dense gas, and the ability of cosmic rays to influence galactic properties via transport along magnetic field lines.

Acknowledgements

We wish to recognize and acknowledge the past and present Gabrielino-Tongva people and their Indigenous lands upon which this research was conducted. Additionally, we thank the staff at our institutes, without whose endless efforts this work would not be possible during the ongoing pandemic. Support for SP and PFH was provided by NSF Research Grants 1911233, 20009234, 2108318, NSF CAREER grant 1455342, NASA grants 80NSSC18K0562, HST-AR-15800. GVP acknowl-

edges support by NASA through the NASA Hubble Fellowship grant #HST-HF2-51444.001-A awarded by the Space Telescope Science Institute, which is operated by the Association of Universities for Research in Astronomy, Incorporated, under NASA contract NAS5-26555. Numerical calculations were run on the Caltech compute cluster "Wheeler," allocations AST21010 and AST20016 supported by the NSF and TACC, and NASA HEC SMD-16-7592. The Flatiron Institute is supported by the Simons Foundation.

Chapter 3

SYNCHROTRON EMISSION ON FIRE: EQUIPARTITION ESTIMATORS OF MAGNETIC FIELDS IN SIMULATED GALAXIES WITH SPECTRALLY-RESOLVED COSMIC RAYS

Ponnada, Sam B. et al. (Feb. 2024). "Synchrotron emission on FIRE: equipartition estimators of magnetic fields in simulated galaxies with spectrally resolved cosmic rays." In: *Monthly Notices of the Royal Astronomical Society* 527.4, pp. 11707–11718. DOI: 10.1093/mnras/stad3978.

3.1 Chapter Abstract

Synchrotron emission is one of few observable tracers of galactic magnetic fields (**B**) and cosmic rays (CRs). Much of our understanding of **B** in galaxies comes from utilizing synchrotron observations in conjunction with several simplifying assumptions of equipartition models, however it remains unclear how well these assumptions hold, and what **B** these estimates physically represent. Using FIRE simulations which self consistently evolve CR proton, electron, and positron spectra from MeV to TeV energies, we present the first synthetic synchrotron emission predictions from simulated L_* galaxies with "live" spectrally-resolved CR-MHD. We find that synchrotron emission can be dominated by relatively cool and dense gas, resulting in equipartition estimates of **B** with fiducial assumptions underestimating the "true" **B** in the gas that contributes the most emission by factors of 2-3 due to small volume filling factors. Motivated by our results, we present an analytic framework that expands upon equipartition models for estimating **B** in a multi-phase medium. Comparing our spectrally-resolved synchrotron predictions to simpler spectral assumptions used in galaxy simulations with CRs, we find that spectral evolution can be crucial for accurate synchrotron calculations towards galactic centers, where loss terms are large.

3.2 Introduction

Magnetic fields (**B**) and relativistic charged particles (cosmic rays, hereafter CRs) are of significant importance in astrophysics. Both are known to provide a significant source of non-thermal pressure support in the interstellar medium (ISM) (Boulares and Cox, 1990), influence the physics of giant molecular clouds (for relevant reviews, see Crutcher, 2012; Beck, Chamandy, et al., 2020), and magnetic fields determine the transport of the dynamically coupled CRs through the ISM and into the CGM (Zweibel, 2013), therefore influencing the structure of galactic outflows (see Zhang, 2018; Owen et al., 2023; Ruszkowski and Pfrommer, 2023, for relevant reviews).

A major difficulty in our understanding of galactic magnetic fields, and subsequently on our understanding of CR propagation and ensuing effects, is the measurement of magnetic field strengths and geometries. A unique extragalactic probe of **B** and CRs comes from the synchrotron emission radiated by CRs as they gyrate around magnetic field lines (Ginzburg and Syrovatskii, 1965). Most estimates of magnetic field strengths in dwarf and spiral galaxies (Fitt and Alexander, 1993; Beck, Beck, and Rainer, 2000; Chyzy et al., 2011; Fletcher et al., 2011; Basu and Roy, 2013; Beck, 2015b) are derived indirectly from the intensity of this non-thermal synchrotron emission, often at radio frequencies, with the key assumption of energy equipartition between CR protons and **B**, used to resolve their formal strict degeneracy.

As discussed in Beck and Krause (2005), Stepanov et al. (2014), and Seta and Beck (2019), the energy equipartition method is motivated by the intertwined dynamics of cosmic rays and magnetic fields, in approximate pressure equilibrium in the local, warm ISM. While this technique has been applied to several radio observations of galaxies across a wide range of spatial scales (Beck, Chamandy, et al., 2020), it is not clear whether **B** and CRs are in approximate pressure equilibrium at all spatial scales, and across the large dynamic range of ISM gas densities and temperatures. Additionally, the method is subject to further assumptions regarding the spectrum, the spatial distribution of CR electrons (CRe) and protons (CRp), as well as the effective emitting volume, which are potentially order-of-magnitude uncertain given the multi-phase nature of the ISM.

Given these assumptions and caveats, it is unclear how to interpret the equipartition estimates of **B**. **B** is known to vary by orders of magnitude with gas density and with ISM phase (Crutcher, 2012; Han, Han, and L., 2017), and while equipartition-inferred estimates of **B** may inform us about some volumetric and LOS-averaged

estimator of **B**, it remains unclear how this maps to measuring **B** *within* a given ISM phase or gas density. In other words, what phase of the ISM dominates the synchrotron emission, and how well does the equipartition estimate of **B** trace it?

Exploring questions about synchrotron emission and equipartition in numerical simulations has been limited in scope by the computational complexity of self-consistently evolving **B** and CRs, in the context of the multi-phase ISM, which exhibits great spatial and temporal variation in gas properties across cosmological time. Simulations have only recently been able to evolve magnetic fields (Peng and Tom, 2009; Pakmor, Marinacci, and Springel, 2014; Marinacci, Pakmor, and Springel, 2014; Su, Hopkins, Hayward, et al., 2017; Rieder and Teyssier, 2017; Butsky, Zrake, et al., 2017; Martin-Alvarez, Devriendt, et al., 2018; Ntormousi et al., 2020) including CRs as a coupled fluid term (Booth et al., 2013; Girichidis, Naab, Walch, et al., 2016; Butsky and Quinn, 2018; Chan, Kereš, Hopkins, et al., 2019; Buck et al., 2020; Werhahn, Pfrommer, and Girichidis, 2021; Werhahn, Pfrommer, Girichidis, and Winner, 2021; Werhahn, Pfrommer, Girichidis, Puchwein, et al., 2021; Hopkins, Chan, Garrison-Kimmel, et al., 2020; Farcy et al., 2022), though it varies whether the simulations in these studies are cosmological, in addition to differences in resolution, physics prescriptions, and numerical methods. Furthermore, these simulations which incorporate a fluid treatment of CRs often take the so-called "single-bin" approximation, evolving solely the ∼1-10 GeV CR proton energy density (or a constant underlying spectrum, with transport coefficients corresponding to the 1-10 GeV CR protons) and by construction fail to capture the CRe spectra, which are required for predictive synchrotron calculations.

Recent algorithmic advances have pushed this boundary of explicitly modeling the CR spectrum (Yang and Ruszkowski, 2017; Girichidis, Pfrommer, Hanasz, et al., 2020; Ogrodnik, Hanasz, and Wóltański, 2021), allowing us to evolve the spectra of various CR species in live-kinetic magneto-hydrodynamic (MHD) simulations of galaxy formation (Hopkins, Butsky, Panopoulou, et al., 2022). Additionally, detailed study of **B** within this family of simulations (which share the same physical prescriptions, up to the novel spectral treatment of CRs) has shown that they produce realistic **B** strengths and geometries in resolved ISM phases (Ponnada, Panopoulou, Butsky, Hopkins, Loebman, et al., 2022).

In this chapter, we forward-model synchrotron emission from high-resolution simulations of galaxy formation with cosmological initial conditions. We present our methodology for computing synchrotron emission from a set of L_* galaxies from

the Feedback in Realistic Environments project (FIRE)[1] simulation suite (Hopkins, Wetzel, Kereš, et al., 2018; Hopkins, Wetzel, Wheeler, et al., 2023) in Section 3.3. In Section 3.4, we compare our results for the spectrally-resolved FIRE runs to relevant observations, and explore how equipartition estimates of magnetic field trace the underlying magnetic fields within these simulations. Through resolving multi-phase ISM structure in our simulations, we disentangle how different phases of the ISM contribute to the resulting synchrotron intensity, and physically interpret equipartition measurements of **B**, discussing how well each of the fundamental assumptions in empirical equipartition models does or does not apply. In Section 3.5, we present a toy model for understanding equipartition magnetic field estimates in the context of a multi-phase ISM motivated by our results in the prior section. Finally, we discuss our results and conclusions and summarize our findings in Section 3.6.

3.3 Methods

In this section, we will discuss the details of the simulations used in this study, and describe our methodology to compute synchrotron emissivities from the simulations in post-processing.

We investigate three zoom-in simulations of galaxies roughly similar in mass and size to the Milky Way, named `m12i`, `m12f`, and `m12m`. These simulations were shown in previous works to all produce CR spectra consistent with those local ISM (LISM) constraints (Hopkins, Butsky, Panopoulou, et al., 2022).

All three simulations here have been presented and extensively studied in Hopkins, Butsky, Panopoulou, et al. (2022) (which did not, however, model their synchrotron properties), to validate that many other properties (e.g. stellar and gas masses, sizes, kinematics, etc) are plausibly consistent with observed galaxies of similar masses. The simulations all have a Lagrangian mass resolution of 56000 $M_\odot$ for gas cells, and the typical spatial resolution ranges from $\sim 1 - 10$ pc in dense gas.

Simulations

The simulations studied here are all fully-dynamical, cosmological, magnetohydrodynamic-radiation-thermochemical-cosmic ray-gravitational star and galaxy formation simulations. This means they self-consistently follow galaxy formation from cosmological initial conditions at redshifts > 100 including both dark matter and baryons (in

[1] `https://fire.northwestern.edu/`

gas and stars), with magnetic fields grown self-consistently from arbitrarily small trace seed fields at $z \approx 100$, with phase structure and thermo-chemistry in the galaxy emerging from cooling with temperatures $T \sim 1 - 10^{10}\,\mathrm{K}$ and self-gravity, fully-coupled to multi-band (EUV/FUV/NUV/OIR/FIR) radiation transport, with star formation in the most dense gas ($\gtrsim 1000\,\mathrm{cm}^{-3}$), and those stars influencing the medium in turn via their injection of radiation, stellar mass-loss, and both Type Ia and core-collapse SNe explosions (followed self-consistently according to standard stellar evolution models). The cosmic ray physics is itself coupled directly to the dynamics, with CRs propagating along magnetic field lines according to the fully general CR transport equations, and interacting with the gas via scattering, Lorentz forces, and losses.

This means that when we model CRs, all quantities needed to compute the fully non-equilibrium CR dynamics and losses are captured in-code, except for the micro-physical CR scattering rate ν. This arises physically from CR pitch-angle scattering off magnetic field fluctuations on gyro-resonant scales — far smaller than we can possibly resolve (~ 0.1 au in the warm ISM, for $\sim$ GeV CRs). As such, the simulations must insert some assumed "sub-grid" scattering rate. We stress that the more familiar CR "diffusion coefficient" and/or "streaming speed" arise self-consistently from ν in the appropriate limits of the CR dynamics equations (for example, if the CR distribution function is sufficiently close to isotropic and in local flux steady-state, the effective parallel diffusion coefficient is simply $\kappa_{\parallel} \sim v_{\rm cr}^2/3\nu$).

As mentioned earlier, the simulations presented in Section 3.4 are the same as those presented in Hopkins, Butsky, Panopoulou, et al., 2022, and so we refer the reader for further details therein. Here, we summarize the most pertinent details. These simulations are run with GIZMO[2], in the mesh-free finite-mass mode. All simulations include MHD as treated in (Hopkins and Raives, 2016; Hopkins, 2016), and fully-anisotropic Spitzer-Braginskii conduction and viscosity (Hopkins, 2017; Su, Hopkins, Hayward, et al., 2017). These simulations were restarted at $z \approx 0.05$ from a high-resolution, cosmological, FIRE-2 'single-bin' CR-MHD simulation of the same galaxy, using the self-consistently evolved CR energy densities in each cell to populate the CR distribution function, and then run for ~500 Myr. Starting from this low redshift and evolving for this runtime are sufficient for the galaxies CR spectra to reach quasi steady-state behavior in the disk and inner CGM at $z = 0$. This is true also of secondary leptons, which reach a steady-state on their dominant

[2]GIZMO is publicly available at http://www.tapir.caltech.edu/~phopkins/Site/GIZMO.html.

loss timescale (Coulomb/ionization, diffusive, and radiative losses for ~MeV, ~GeV, and $\gtrsim$ 50 GeV leptons, respectively), which never exceed ~10 Myr in the disk and inner halo, as shown in numerical tests of (Hopkins, Butsky, Panopoulou, et al., 2022). The details of prescriptions for star formation, stellar feedback, CR-MHD spectral evolution, and coupling to gas follow those of Hopkins, Wetzel, Wheeler, et al. (2023).

Our implementation of the CR physics is described in detail in (Hopkins, Butsky, Panopoulou, et al., 2022), and self-consistently includes adiabatic, diffusive re-acceleration, gyro-resonant loss, Coulomb, ionization, hadronic and other collisional, radioactive decay, annihilation, Bremstrahhlung, inverse Compton (IC), and synchrotron loss terms. Hadronic losses are assumed to be dominated by the proton-proton interaction, with total pion loss rates following Mannheim and Schlickeiser (1994) and Guo and Oh (2008) and those of Evoli et al. (2017) for antimatter. CRs are injected via a power-law spectrum in momentum at SNe (Types Ia & II) and stellar winds (OB/WR) to neighboring gas cells with fixed fractions $\epsilon_{\rm CR}^{\rm inj}$ = 0.1 and $\epsilon_{\rm e}^{\rm inj}$ = 0.002 of the initial ejecta kinetic energy going into CRs (protons) and leptons. These injection fractions are well motivated by theoretical work on nonlinear diffusive shock acceleration and inverse modeling of observed CR spectra (Caprioli, 2012; Yuan, Liu, and Bi, 2012). Most notably, the fiducial simulations here differ in their treatment of CRs from those presented and analyzed in Hopkins, Chan, Garrison-Kimmel, et al. (2020) and Ponnada, Panopoulou, Butsky, Hopkins, Loebman, et al. (2022) by explicitly evolving each bin of the injected CR spectra, following the method of Girichidis, Pfrommer, Hanasz, et al. (2020) and Ogrodnik, Hanasz, and Wóltański (2021) as presented in Hopkins, Butsky, Panopoulou, et al. (2022). These simulations follow standard practice and assume a spatially and temporally constant scaling for the scattering rate as a function of CR rigidity $\nu \sim 10^{-9}$ (R/GV)$^{-1/2}$ s^{-1} (calibrated explicitly therein to fit all of the observations of CRs in the Milky Way from observations such as Voyager, AMS-02, Fermi, and others).

Synchrotron Forward Modeling

Our methodology to compute the synchrotron specific emissivities from our simulations follows the equations of synchrotron emission as derived in Ginzburg and Syrovatskii (1965), and summarized again in Padovani et al. (2021).

For each gas cell in our simulations, we calculate synchrotron emissivities as follows. First, we extract the internally evolved CRe and positron spectra, $j_e(E)$ and

components of the magnetic field perpendicular to the line of sight, $\mathbf{B}_\perp$.

Then, we compute the critical frequency of emission for each spectral bin of CRe,

$$\nu_c(B_\perp, E) = \frac{3eB_\perp}{4\pi m_e c}\left(\frac{E}{m_e c^2}\right)^2 \tag{3.1}$$

where $B_\perp$ is the magnetic field strength perpendicular to the line of sight, m_e is the electron mass, and c is the speed of light.

We also calculate the power emitted per unit frequency by CRe in each spectral bin from MeV to TeV energies both parallel and perpendicular to the LOS,

$$P_{\nu,\perp}(E) = \frac{\sqrt{3}e^3}{2m_e c^2} B_\perp [F(x) - G(x)], \tag{3.2}$$

$$P_{\nu,\parallel}(E) = \frac{\sqrt{3}e^3}{2m_e c^2} B_\perp [F(x) + G(x)], \tag{3.3}$$

where $B_\perp = |\mathbf{B}_\perp|$ and $x = \nu/\nu_c$.

The functions F(x) and G(x) are defined as

$$F(x) = x \int_x^\infty K_{5/3}(\xi) d\xi, \tag{3.4}$$

and

$$G(x) = x K_{2/3}(x), \tag{3.5}$$

where $K_{5/3}$ and $K_{2/3}$ are the modified Bessel functions of order 5/3 and 2/3. For each bin, we use the relevant F(x) and G(x) from pre-computed look-up tables provided by Padovani et al. (priv. comm.).

We then compute the linearly polarized specific emissivities by integrating the contributions over j_e,

$$\epsilon_{\nu,\parallel} = \int_{m_e c^2}^\infty \frac{j_e(E)}{v_e(E)} P_{\nu,\parallel}(E) dE, \tag{3.6}$$

and

$$\epsilon_{\nu,\perp} = \int_{m_e c^2}^\infty \frac{j_e(E)}{v_e(E)} P_{\nu,\perp}(E) dE, \tag{3.7}$$

where v_e is the electron velocity.

From these specific emissivities, we also compute the Stokes Q_ν and U_ν specific emissivities,

$$\epsilon_{\nu,Q} = [\epsilon_{\nu,\perp} - \epsilon_{\nu,\parallel}] \cos(2\theta), \tag{3.8}$$

and

$$\epsilon_{\nu,U} = [\epsilon_{\nu,\perp} - \epsilon_{\nu,\parallel}] \sin(2\theta), \tag{3.9}$$

where θ is the local polarisation angle given by the orientation of $\mathbf{B}_\perp$ rotated by $\pm$ 90°.

When calculating LOS-integrated quantities, we project the galaxy face-on or edge-on using the angular momentum vector of the stars to define the direction perpendicular to the galactic disk, which we define as the $\hat{z}$ direction. All cell vector fields ($\mathbf{r}$, $\mathbf{B}$, $\mathbf{v}$) are transformed accordingly. To compute the corresponding images of the specific intensity I_ν, Q_ν, and U_ν, the respective emissivity terms are integrated along the line of sight using a projection routine first described in Hopkins, Hernquist, et al. (2005). This routine appropriately computes the contribution to the emission from every gas cell along the line of sight by taking into account their spatial distribution and hydrodynamic smoothing lengths.

3.4 Results: FIRE Simulations with Resolved Cosmic Ray Spectra

Synthetic Observations

In this section, we present our synthetic observations and explore which ISM phases contribute to the resultant emission. We first show images of I_ν at λ = 6.2 cm for face-on projections of the galactic disks for the three fiducial simulations, following the procedure outlined in Section 3.3, in Figure 3.1. The images are in their fiducial high-resolution format at a scale of ∼120 pc/pix and not smoothed to an observational beam.

A few things are evident from visual inspection: first, our synthetic synchrotron images have typical values of I_ν in qualitative agreement with those observed in nearby spiral galaxies (Basu and Roy, 2013; Beck, 2015b) with spatially resolved radio continuum observations; we defer quantitative comparisons to the observations to Section 3.4. Second, the synchrotron emission is broadly coincident with the spatial distribution of neutral gas, with stronger emission coming from dense gas near the galactic center and correlated with spiral structure, and weaker emission in inter-arm regions and towards the galactic outskirts.

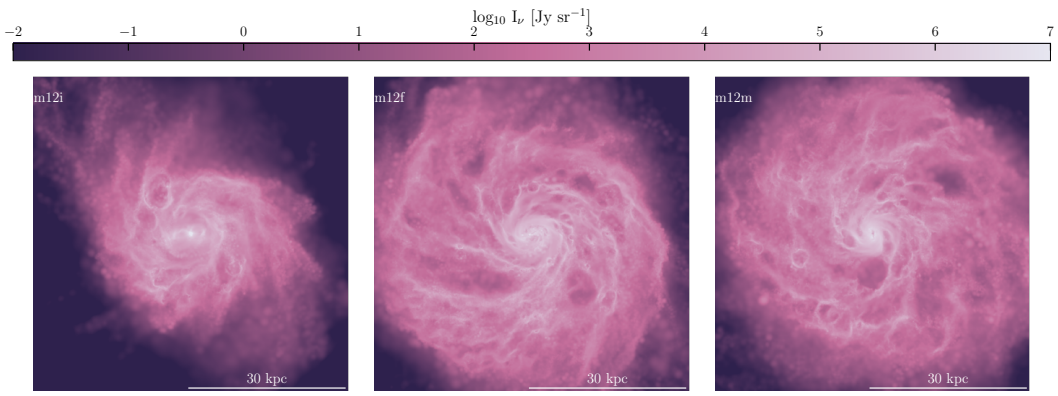

Figure 3.1: *Images of specific intensity (I_ν)* for `m12i`, `m12f`, and `m12m` at λ = 6.2 cm, with the colorbar showing $\log_{10}(I_\nu)$. All three simulations exhibit a range of I_ν values broadly consistent with radio continuum observations of nearby spiral galaxies. The synchrotron intensity closely traces the neutral gas spatial distribution, with enhanced emission coincident with spiral structure and relatively lower levels of emission in inter-arm regions.

In Figure 3.2, we present 2-D histograms of the gas density and temperature, for the gas cells producing the emission visualized in Figure 3.1, all weighted by each gas cell's contribution to the specific synchrotron intensity I_ν . In these intensity-weighted ISM phase diagrams, the bimodal nature of gas which dominates the emission becomes clear; the synchrotron emission primarily arises from the cold, neutral medium (CNM - T ∼100-300 K, n ∼3-30 cm^{-3}) and warm, neutral medium (WNM - T ∼3×10^3 -10^4 K, n ∼0.1-1 cm^{-3}). Inspecting similar intensity-weighted histograms of the gas cells' neutral hydrogen fractions confirms that this gas is primarily neutral.

This evinces a physical scenario in which relatively cool, dense gas, which comprises a small fraction of the total ISM volume, contributes significantly to synchrotron emission. While warm, more appreciably volume-filling ISM gas is synchrotron-bright as well, the emission arises largely from the denser and neutral warm gas as opposed to the more diffuse (n < 0.1 cm^{-3}), ionized warm/hot gas, which fills the majority of the ISM volume. Put more quantitatively, neutral gas with (n > 0.1 cm^{-3}, T < 10^4 K) contributes ∼80% of the emission, despite filling only ∼20% of the volume.

We note that a scenario in which CRs are not modeled self-consistently would predict a different intensity-weighted phase distribution: if one assumed a priori that e_{CR} was locally in equipartition with a self-consistently evolved B, then the

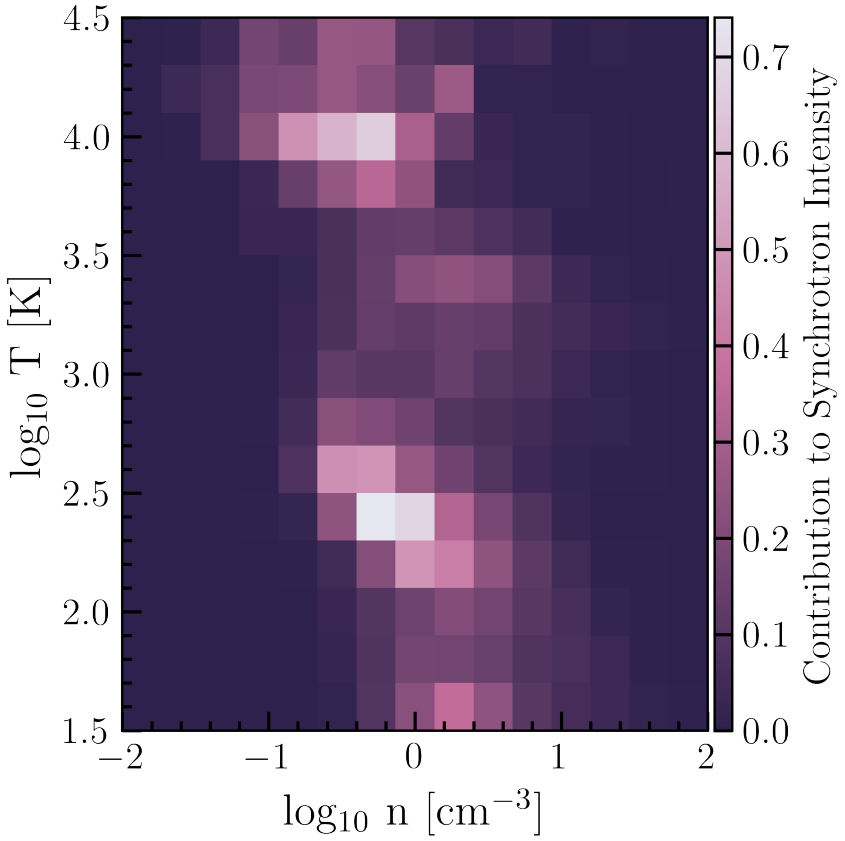

Figure 3.2: *ISM phase diagram, or 2-D histogram of temperature vs. density of gas cells*, weighted by contribution to specific synchrotron intensity for `m12f` at λ = 6.2 cm, within cylindrical R < 10 kpc. Color-bar shows the probability density. Consistent with visual inference from Figure 3.1, the synchrotron emission is largely dominated by neutral gas typical in CNM and WNM ISM conditions, rather than diffuse, volume-filling, and ionized phases.

intensity-weighted distribution would be more biased towards higher density gas as $\mathbf{B} \sim \rho^{\alpha}$, with $\alpha \sim 0.5$-0.66 (Ponnada, Panopoulou, Butsky, Hopkins, Loebman, et al., 2022). Whereas if one assumed the ISM to be a homogeneous slab with a constant volumetric B in equipartition with CRs, the distribution would then effectively look like the volume-weighted distribution and thus weighted towards the more diffuse phases of the ISM. This result subsequently has physical implications for what traditional equipartition models à la Beck and Krause (2005) and Lacki and Beck (2013) infer in the form of the "mean **B**" from synchrotron observations, which we show and discuss in Sections 3.4, 3.5, and 3.6.

Radial intensity profiles and comparisons to observations

In Figure 3.3, we compare the radial profiles of synchrotron specific intensity at observing frequencies of 0.33 GHz from our fiducial simulations to a few observed face-on spiral galaxies of roughly similar mass. We have also calculated the simulations' emission profiles at 4.8 GHz, as one of the observed galaxies, IC342, was measured at this frequency. But since the relative comparison is similar, we simply plot all systems at 0.33 GHz, shifting IC342 according to the authors' assumed spatially constant spectral index of -1. The radial profile of the non-thermal emission as plotted in Beck (2015b) for IC342 is also shown, and for the other observed galaxies, we show the radial profiles of the non-thermal emission (corrected to remove the free-free emission) out to the radii published in Basu and Roy (2013).

We find the predicted $I_{\nu,\,\nu=4.83\mathrm{GHz}}$ for our simulations generally ranging from $10^{5.5}$ to $\sim 10^{4}$ Jy/sr at the galactic center to the "Solar circle" (galacto-centric cylindrical radius R = 7-9 kpc) and $I_{\nu,\,\nu=0.33\mathrm{GHz}}$ ranging from 10^{7} to $\sim 10^{5}$ Jy/sr in Fig. 3.3. When comparing our predicted radial emission profiles to observations of nearby spiral galaxies, we see an order-of-magnitude agreement, though two of the four observed profiles (NGC5055 and NGC 6946) appear to fall more slowly at large R $\geq$ 5 kpc. We caution that none of these simulations are meant to be exact analogs of the observed galaxies, but are only order-of-magnitude similar in morphology and galaxy mass. Various galaxy-to-galaxy differences in the profiles partly reflect this set of galaxies' diversity in properties like gas surface density and star formation rate, and in Figure 3.6 we show similar specific intensity profiles normalized to the gas surface density, which are qualitatively more similar in the shape of the profiles.

Spectral variation and emission properties

Evolving the full CR spectrum is computationally expensive, and most simulations of galaxy formation including CRs utilize the 'single-bin' approximation, solely evolving the 1-10 GeV e_{CRp}. We are therefore motivated to test whether explicitly evolving CR spectra makes significant quantitative or qualitative differences in the predicted synchrotron emission.

To compare what the emission would look like for the same simulated galaxies if we did not evolve the full spectral information of CRs, we illustrate a few different spectral assumptions in Figure 3.4 starting from our fiducial simulations of `m12i` and `m12f`. First, we see that excluding emission from positrons (light-blue, dot-dashed lines) deducts minimally, contributing $\lesssim$ 10% of the emission at most radii, and

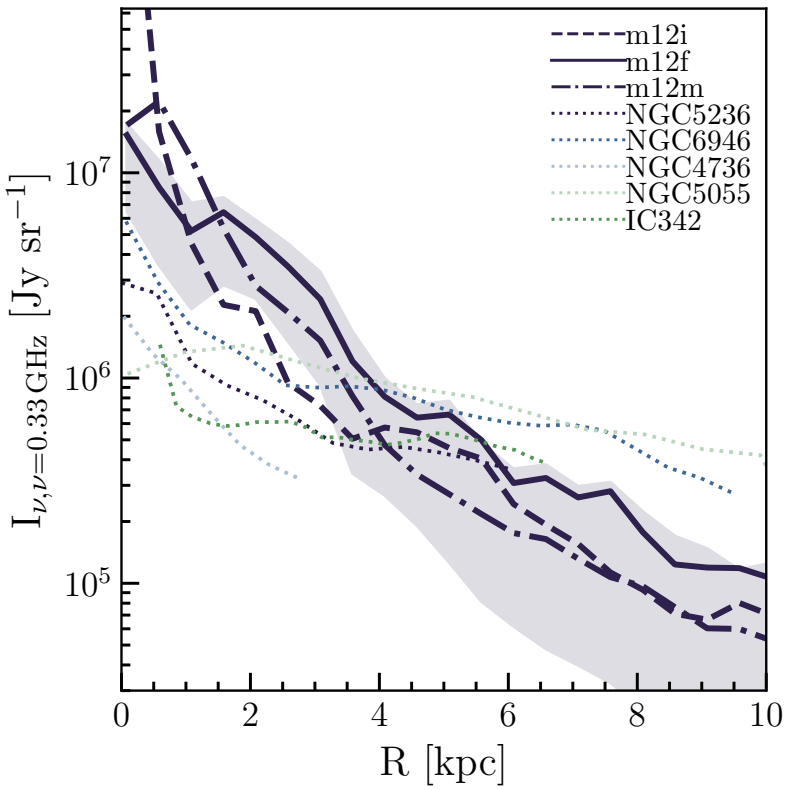

Figure 3.3: *Azimuthally averaged (mean) radial profiles of synchrotron specific intensity at 0.33 GHz* for `m12i`, `m12f`, and `m12m`, in navy dashed, solid, and dot-dashed lines. Shaded regions show the 25-75 percentile range at a given radial bin. Corresponding radial profiles of non-thermal synchrotron emission (free-free emission corrected) for nearby face-on spiral galaxies from Basu and Roy (2013) and Beck (2015b) are shown in dotted lines, with 4.83 GHz observations of IC342 scaled up by $\nu/{\nu_0}^{\alpha}$. Our synthetic synchrotron images for the fiducial model agree to within an order-of-magnitude with spatially resolved synchrotron emission from nearby spiral galaxies. Variation in the shapes of the profiles towards the galactic centers and outskirts partially arises due to differences in the gas surface density (see Figure 3.6 for corresponding plot), though the simulations appear to produce steeper radial profiles in comparison to the observed systems compared.

reaching ∼20% near the galactic center of `m12i`.

Secondly, we show the results corresponding to scaling the CR electron spectrum of Bisschoff, Potgieter, and Aslam (2019) by $e_{CRe,\ sim}$, thereby holding the shape of j_e constant (purple dotted lines), as well as scaling according to e_{CRp} in each gas cell, which additionally fixes $\mathcal{K}$ (pink dashed lines), the total energy density ratio e_{CRp}/e_{CRe} to the literature value (akin to what might be done in the "single-bin" scenario where only e_{CRp} is known). Holding the spectral shape constant with the "right" $\mathcal{K}$ shows that one would tend to over-predict the emission by up to factors of ∼6 in regions where losses at the energies of interest are strong (towards the galactic center). Additionally fixing $\mathcal{K}$, we see that evolving the CR spectral information can make a modest difference at a factor of ∼2 in I_ν for typical spiral galaxy conditions as shown in much of `m12f` and the outer radii of `m12i`, but can make large (factor of ∼10-50) differences towards the central regions of the galaxy.

We break this down in more detail, showing that these deviations owe to a radially-varying proton-to-electron ratio between the galactic center and outskirts compounding with changing spectral shape (comparing constant spectral shape and constant $\mathcal{K}$ + spectral shape lines, which differ only in normalization) to further over-predict the emission, rather than the varying proton-to-electron ratio alone (green dashed-dotted lines, constant $\mathcal{K}$, $j_{e,\ sim}$). This effect arises in `m12i` due to a quasi-starburst in the circum-nuclear region R < 3 kpc, where Σ_{gas} quickly rises from ∼30-250 $M_\odot$ pc^{-2} in comparison to lower surface densities ∼30-70 and 30-100 $M_\odot$ pc^{-2} in `m12f` and `m12m`, respectively. Correspondingly, loss terms owing to higher gas densities being correlated with higher **B**, increased radiation field intensities, etc., result in significant cooling of the CRe spectra at the energies of interest and a changing $\mathcal{K}$.

As expected, there is little difference at "Solar circle" radii, where our simulations have been shown to faithfully agree with the observed LISM spectrum (Hopkins, Butsky, Panopoulou, et al., 2022). However, these results illustrate the need to self-consistently model the CR spectral shapes and $\mathcal{K}$ to accurately predict synchrotron emission in galactic environments where loss terms become important, as simple spectral assumptions from a 'single-bin' treatment of CR protons can lead to order-of-magnitude differences in the predicted emission. These differences may also vary with frequencies different from the ∼GHz observations probed here which would probe different energy intervals of the CRe spectrum. Furthermore, evolution in $\mathcal{K}$ has implications on key assumptions invoked in equipartition estimates of **B**, as we detail in the next section.

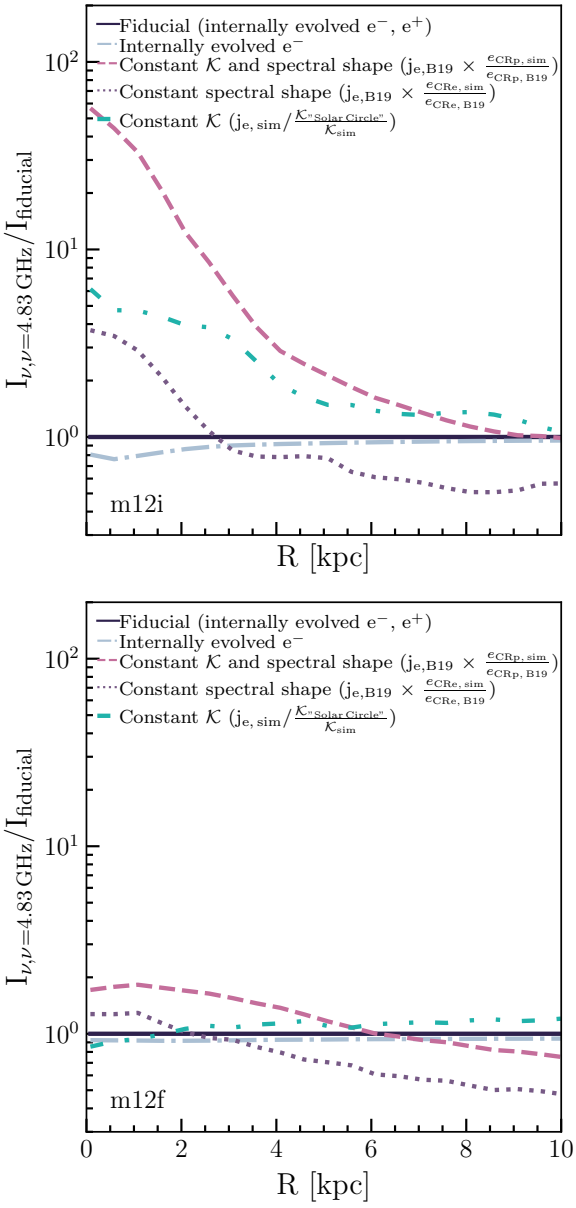

Figure 3.4: *Azimuthally averaged (mean) radial profiles of the ratio of I_ν to $I_{\nu,\,fiducial}$ under different assumptions for j_e* for `m12i` (top) and `m12f` (bottom) at 4.83 GHz. Lines show fiducial intensity using internally evolved j_e including e^+ contribution (navy solid), fiducial intensity without e^+ (light blue dot-dashed), holding spectral shape and $\mathcal{K}$ constant by re-scaling j_e of Bisschoff, Potgieter, and Aslam (2019) (B19) to internally evolved e_{CRp} (pink dashed), holding the spectral shape constant by re-scaling the fiducial spectrum by e_{CRe} (purple dotted), and holding $\mathcal{K}$ constant by re-scaling the fiducial j_e to the nominal value at that simulation's "Solar Circle" (teal). Emission from secondaries contributes fractionally to overall emission at all radii, though reaching ~20% contribution at high Σ_{gas}. As demonstrated in `m12i`, strong CRe cooling at relevant energies corresponds to over-predicting emission towards the galactic center, where Σ_{gas} is relatively higher, for constant $\mathcal{K}$ and/or spectral shape assumptions. This effect driven by variation in $\mathcal{K}$ compounding with spectral shape effects as shown by the pink line. Thus, in galactic environments where losses become important, modeling the CR spectra and $\mathcal{K}$ explicitly is necessary for predictive calculations, while in environments where cooling is relatively weak at relevant energies (galactic outskirts and much of `m12f`), spectral shape/$\mathcal{K}$ assumptions make at most factor of ~2 differences.

Equipartition magnetic field strengths: what do they really measure?

The most commonly used formalism to determine equipartition estimates of the magnetic field ($\mathbf{B_{eq}}$) from radio continuum observations of non-thermal emission from galaxies is that of Beck and Krause (2005). The equation is as follows:

$$\mathbf{B}_{\rm eq} = \{4\pi(2\alpha+1)(\mathbf{K}_0+1)I_\nu E_p^{1-2\alpha}(\nu/2c_1)^\alpha \\ /(2\alpha-1)c_2(\alpha)(f_V * L)c_4(i)\}^{1/(\alpha+3))}\} \quad (3.10)$$

where α is the synchrotron spectral index, $\mathrm{E_p}$ is the proton rest energy, and $\mathrm{c_1}$, $\mathrm{c_2}$, and $\mathrm{c_4}$ are combinations of physical constants which encapsulate dependencies on α and the inclination of the magnetic field. The equipartition formula also requires assumptions about the depth of the emitting material, L (here the implicit dependence of the volume-filling factor of emitting gas, f_V, is written explicitly), and $\mathbf{K}_0$, the ratio of number densities of CRp and CRe at energies from $\mathrm{E_p}$ up to some energy $\mathrm{E_{syn}}$ beyond which synchrotron and IC losses dominate for CR electrons[3] (Beck and Krause, 2005).

As described in the Introduction, equipartition estimation of the magnetic field is subject to a few extra assumptions beyond that of $\mathrm{e_{CR}} = \mathrm{u_B}$. The first auxiliary assumption is that of a constant ratio of the number densities of CRe and CRp, $\mathbf{K}_0 \sim$100, motivated by the injection spectrum of primary CRs from SNe via diffusive shock acceleration and measurements at the Milky Way Solar Circle (Bell, 1978; Bell, 2004; Beck and Krause, 2005). Though there have been modifications to this assumption for galaxies where the synchrotron emission is expected to have significant contribution from secondary CRe and positrons generated from the resultant pion-decays of primary CR collisional losses (Lacki and Beck, 2013), these are not generally applied to galaxies like those in Fig. 3.3. This assumption further implicitly requires that the CRp and CRe spectrum to have constant and equal power-law indices, which holds close to injection sites, but may not hold in a spatially and temporally independent manner across galaxies. It also assumes negligible contribution from positrons, and that the synchrotron is optically thin.

Secondly, CRe and positrons, which dominate the synchrotron emission at frequencies of a few GHz, and ∼1-10 GeV CR protons, which dominate overall the energy density, are assumed to have the same, spatially and temporally uniform distribution

[3]Note that $\mathbf{K}_0$ differs from $\mathcal{K}$, which is the ratio of the total CRp/CRe energy densities.

within and across each pixel, and as a function of height above the mid-plane up to some height L. These assumptions are subject to questioning on galactic scales, where the dominant energy loss terms and correspondingly the loss timescales for CRe and CR protons can differ significantly due to large local variations (along a line of sight and across an observational beam) in gas density, magnetic and radiation energy densities, and phase structure (Wolfire et al., 1995; Evans II, 1999).

Thirdly, the size of the emitting region both along the line of sight and within a given pixel or beam must be assumed. While traditional applications of the equipartition formula to galaxies have assumed path lengths of L ∼1-2 kpc for face-on observations, it remains unknown what the typical volume filling factor of synchrotron emitting gas actually is in galaxies. Implicit within this assumption is a homogeneous and volume-filling field, which given the multi-phase nature of the ISM, may not reflect the true **B** that primarily contributes to the synchrotron emission.

From the synthetic synchrotron images and radial profiles shown in the previous sections, we can now explore equipartition magnetic field strengths ($\mathbf{B}_{\mathbf{eq}}$) from the forward-modeled specific synchrotron intensity and test the several assumptions invoked.

In Figure 3.5, we show estimators of **B** weighted by $I_{\nu,\,\nu=0.33\mathrm{GHz}}$ and volume in `m12f`, and how $\mathbf{B}_{\mathbf{eq}}$ compares. We show $\mathbf{B}_{\mathbf{eq}}$ resulting from assuming α = 1, L = 1 kpc, $\mathbf{K}_0$ = 100, and f_V = 1, which are typical model assumptions in observational literature. In this case, it becomes immediately clear that Equation 3.10 *under-predicts the "true" I_ν-weighted **B** by ∼0.3-0.6 dex across all radii and e_{CR} by ∼0.3-1.0 dex for R > 4 kpc* (though interestingly, traces the volume-weighted **B** well, which we discuss in detail in Section 3.5). Examining the assumptions for $\mathbf{K}_0$ and f_V in this model, we find $\mathbf{K}_0$ varies from ∼100 ± 10 near the galactic center to ∼60 ± 10 near the "Solar circle" with the exception of `m12i`, where $\mathbf{K}_0$ rises rapidly to $\sim 10^3$ near the galactic center due to strong leptonic losses at relatively higher gas surface densities $\gtrsim$ 150 $M_\odot$ pc^{-2}. Varying the assumed value of $\mathbf{K}_0$ according to this radial variation would only affect the equipartition-inferred values at the tens of percent level ($\mathbf{B}_{\mathbf{eq}} \sim \mathbf{K}_0{}^{1/4}$), and so we find that $\mathbf{K}_0$ = 100 is a decent assumption in our simulations for most of the galaxy conditions sampled here, with the exception of the very inner (R < 2 kpc) region of `m12i`.

The assumption of the depth of the emitting material being ∼1 kpc is more suspect, however. Computing the volume filling fraction of the gas cells which contribute

to the upper 50% of I_ν within radial bins of vertical thickness 1 kpc reveals that f_V varies from ~0.05 - 0.2 over the radial range. This volume filling fraction is very similar to the ratio of the face-on scale height of emission to the path length, H_{I_ν}/L, implying that the emission is primarily arising from the mid-plane. This, in conjunction with Figure 3.2, further develops the picture of the emission primarily being dominated by the cold and warm neutral medium relatively confined to the thin disk.

When f_V is subsequently corrected to representative values ~0.05 - 0.2, the equipartition formula gives values of $\mathbf{B_{eq}}$ and e_{CR} that are closer to the "true," I_ν -weighted values of **B** (though over-predicting I_ν -weighted e_{CR} owing to deviations from physical equipartition with u_B). The I_ν -weighted **B** is generally higher (0.2-0.6 dex) than the volume-weighted **B**, while the I_ν -weighted e_{CR} and volume-weighted e_{CR} exhibit less difference. This indicates that the primary effect of correcting f_V is to correct for the higher **B** in the denser mid-plane gas, rather than to correct for e_{CR}, which more weakly scales with gas density in our simulations owing to CRs' ability to diffuse (Ponnada, Panopoulou, Butsky, Hopkins, Loebman, et al., 2022; Hopkins, Butsky, Panopoulou, et al., 2022). It is important to note that the volume filling gas at heights L ~ 1 kpc above the mid-plane at R ~ 5 kpc has typical **B** ~2-4 μG $\ll \langle \mathbf{B}_{\rm synch} \rangle$, (see Ponnada, Panopoulou, Butsky, Hopkins, Loebman, et al., 2022, for details), so the traditional estimator also severely over-estimates typical **B** in more diffuse gas above the disk, via assumptions of a homogeneous, height-independent **B**.

We emphasize that this is consistent with state-of-the-art, high-resolution radio continuum observations (Krause et al., 2018; Heesen, Krause, et al., 2018); detailed studies of nearby edge-on spiral galaxies have revealed very bright thin-disk components with scale heights ranging from 10s-100s of pc, which are $\lesssim$ the observational beam size and thus subject to large errors. The best-fit two-component models to these observations all indicate that this thin, mid-plane component almost ubiquitously dominates the overall emission, with additional extended thick-disk components with nominal scales of L ~kpc as invoked in equipartition models contributing fractionally to the overall emission. Thus, when viewed face-on, the emission largely traces the thin disk component, and so taking typical values for L associated with these extended synchrotron halos rather than the scale height of the medium which contributes most to the emission (which is still subject to a high degree of observational uncertainty), leads to vastly under-predicting the I_ν -weighted

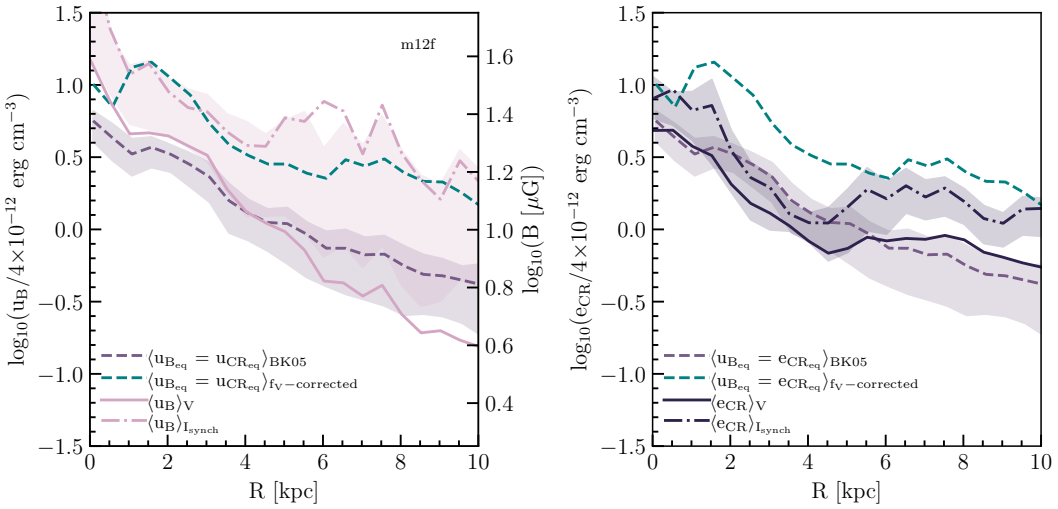

Figure 3.5: *Azimuthally averaged radial profiles of u_B (left) and e_{CR} (right) weighted by volume and I_ν in comparison to $u_{B_{eq}}$* for `m12f`. Lines represent u_B (pink), e_{CR} (navy), volume-weighted (solid) and $I_{\nu,\,\nu=0.33\mathrm{GHz}}$ -weighted (dot-dashed) averages of each quantity, within $|z| \leq 0.5$ kpc. The result of applying Equation 3.10 to the radial profile presented in Figure 3.3 is shown, with L = 1, $\mathbf{K_0}$ = 100, f_V = 1 (purple dashed) and f_V computed within each radial bin (teal dashed). Shaded regions show the approximate $\pm\ 1\sigma$ scatter (32-68 percentile) of the emission-weighted quantity and fiducial equipartition model at a given radial bin. Unilaterally, we see that without correcting for the volume-filling factor of the neutral mid-plane gas which dominates I_ν , **the equipartition formula under-predicts the "true" I_ν -weighted B by ~0.3-0.6 dex and e_{CR} by by ~0.1-0.6 dex**. Furthermore, due to the emission being dominated by mid-plane gas, the equipartition model with the right volume-filling factor is generally not representative of the volume-weighted u_B, though the fiducial model surprisingly traces the volume-weighted quantities well owing to a confluence of factors (see Section 3.5). While not shown in this figure, `m12i` and `m12m` show generally the same behavior.

.

B.

We have checked that treating edge-on synchrotron images of our simulations in an observational manner, smoothing to a representative observational beam of 10," and fitting two-component exponential disk models akin to observational studies yield similar results for thin and thick disk scale heights (~100 pc, ~1 kpc, respectively; see Figure 3.7).

3.5 A Toy Model for Estimating B from Synchrotron Emission in a Multi-Phase Medium

In this section, we present a toy model to characterize **B** in a multi-phase medium to gain intuition as to what factors cause the traditional model to deviate from the "true" values, given the understanding from the previous section that the synchrotron emission is primarily arising from neutral mid-plane gas (up to variations in the CR transport physics).

Consider the mean, volume-weighted magnetic energy density in a vertical ISM slab (at a given cylindrical radius R) of some finite height to be described by an exponential function anchored to the mean mid-plane ($|z| \leq 0.1$ kpc) value of u_B:

$$\langle u_B \rangle = \langle u_{B_0} \rangle e^{-(|z|/H_B)} \tag{3.11}$$

where the radial dependencies of $\langle u_{B_0} \rangle$ and H_B (the magnetic scale height) are implicit. Correspondingly, we can describe the volume-weighted average of the CR energy density in each slab:

$$e_{CR} = \psi * u_{B_0} \left(\frac{\langle u_B \rangle}{\langle u_{B_0} \rangle} \right)^{\beta} \tag{3.12}$$

where ψ is $\langle e_{CR_0} \rangle / \langle u_{B_0} \rangle$ and accounts for differences in the energy density at the mid-plane[4] and β accounts for differences in the vertical scale height of u_B and e_{CR} and the local inter-dependence.

Within each vertical slab, we can make the assumption that the coherence length of the magnetic field is much less than the vertical scale height or the radius, and thus construct a volume-weighted PDF of given magnetic fluctuations ($\delta_{u_B} = u_B / u_{B_0}$) describing the probability of a given unit volume having a magnetic fluctuation δ_{u_B}. We further make the ansatz that this PDF is a log-normal distribution of fluctuations in δ_{u_B}, motivated by descriptions of density fluctuations in MHD turbulence (Hopkins, 2013; Beattie et al., 2022):

$$P_V(ln\, \delta_{u_B}) = \frac{V_{tot}}{\sqrt{2\pi S_\delta}} \exp\left\{ -\frac{(ln\, \delta_{u_B} + S_\delta/2)^2}{2S_\delta} \right\} \tag{3.13}$$

where V_{tot} is the total volume within a vertical slab, S_δ describes the volume-weighted variance of $\ln(\delta_{u_B})$ arising from turbulent, multi-phase structure.

[4] For a more detailed look at ψ, which describes the volume-averaged physical "equipartition" between **B** and CRs, we present radial profiles of ψ in Figure 3.8.

With these equations in hand, we can build a model which relates the observable synchrotron intensity (averaged over some finite pixel resolution A) to the underlying volume-weighted **B**.

Starting with the same assumptions as in Beck and Krause (2005) and including spectral dependencies implicitly (α will remain a free parameter), one can work to an expression for $\langle \mathrm{I}_\nu \rangle$ given Equations 3.11 and 3.12 as follows:

$$\langle I_\nu \rangle = \frac{\int\int \psi C(\alpha) u_B^\gamma dA dz}{A} = \frac{1}{A} \int \psi C(\alpha) u_B^\gamma u_{\mathrm{B}_0}^{1-\beta} dV \tag{3.14}$$

where dV is a volume element, C(α) is a combination of physical constants with minor dependencies on the power-law index and ν[5], and $\gamma = [\frac{(\alpha+1)}{2} + \beta]$. From this expression, we can utilize the PDF given by Equation 3.13 to find a closed form expression for $\langle I_\nu \rangle$ as follows:

$$\langle I_\nu \rangle = \frac{2\psi C * H_B \exp\left\{\frac{S_\delta(\gamma-1)\gamma}{2}\right\}}{\gamma} \langle u_{\mathrm{B}_0} \rangle^{\frac{(\alpha+3)}{2}} \tag{3.15}$$

which can be re-arranged to find an expression for $\langle u_{\mathrm{B}_0} \rangle$:

$$\langle u_{\mathrm{B}_0} \rangle = \left(\frac{\gamma \langle I_\nu \rangle}{2\psi C * H_B \exp\left\{\frac{S_\delta(\gamma-1)\gamma}{2}\right\}} \right)^{2/(\alpha+3)} \tag{3.16}$$

This expression is analogous to the Beck and Krause (2005) formalism of Equation 3.10, but relaxes the assumptions of equipartition between $\mathrm{u_B}$ and $\mathrm{e_{CR}}$ and a homogeneous medium with uniform **B** and $\mathrm{e_{CR}}$; instead, we parameterize our ignorance of equipartition into a simple power-law relation between the two quantities and variations due to inhomogeneity in the ISM in the form of the volume-weighted variance in δ_{u_B} and the magnetic scale height $\mathrm{H_B}$. Our revised expression reduces to Equation 3.10 when $\mathrm{S}_\delta = 0$, $\psi = 1$, and $\beta = 1$.

Note that our Eq. 3.16 for $\langle u_{\mathrm{B}_0} \rangle = \langle u_\mathrm{B} \rangle_V$ is identical to the Beck and Krause (2005) (BK05) formula in Eq. 3.10 with the replacement $f_\mathrm{V} \rightarrow \psi\, f_\mathrm{cl}\, H_\mathrm{B}/L$ (BK05 implicitly take $f_\mathrm{V} = 1$), where $f_\mathrm{cl} \equiv \gamma^{-1} \exp\left[\gamma\,(\gamma-1)\,S_\delta/2\right]$.

[5] $C_\alpha = \frac{(2\sqrt{2\pi})^{\alpha+1} c_4^2 (4\alpha-2) c_2(\alpha)}{(\mathbf{K}_0+1)(2\alpha+1)(\frac{\nu}{2c_1})^\alpha E_P^{1-2\alpha}}$, where $\mathrm{c_1}$-$\mathrm{c_4}$ are defined in Appendix A of Beck and Krause (2005)

We have three terms here parameterizing three physical assumptions/uncertainties: (1) ψ represents the (mean) deviation from equipartition; (2) $f_{\rm cl}$ represents the "clumping factor" which can boost emission (for a given volume-weighted set of properties) owing to substructure with larger magnetic and/or CR energy density; and (3) H_B/L simply corrects the ad-hoc constant $L = 1\,$kpc to the "correct" size of the emitting disk. Observationally, of course, these are largely unknown, hence taking $f_V = 1$ in BK05. But here, we can estimate the true values in the simulations of each parameter.

The value of ψ can be directly read off from Fig. 3.5, increasing from $\sim 0.7-3$ at $R \sim 1-10\,$kpc. This radial trend is expected given the diffusive nature of CRs (see discussion of this in Hopkins, Butsky, Panopoulou, et al. 2022), since it means the CR energy density will fall less-rapidly than the gas pressure (and $u_{\rm B}$) at large galacto-centric radii. Taking $H_{\rm B}$ to be the atomic disk scale-height gives $H_{\rm B} \sim 200\,$pc, similar to canonical scale heights for the star-forming disks of the Milky Way and other observed galaxies (Kalberla and Kerp, 2009; Yim et al., 2014; Patra, 2020; Gensior et al., 2023).

Direct examination of the $e_{\rm CR}-u_{\rm B}$ correlations (shown in Hopkins, Butsky, Panopoulou, et al. 2022) gives $\beta \sim 0.2-0.3$: this arises again because the CRs are diffusive, so (especially on small scales) always form a locally-smooth distribution compared to the magnetic fields (Butsky and Quinn, 2018; Chan, Kereš, Hopkins, et al., 2019; Buck et al., 2020). And we can estimate S_δ directly from the midplane scatter in $\ln u_{\rm B}$ giving $S_\delta \sim 2-4$ — this is naturally expected from the same turbulence models which motivated our lognormal assumption in the first place, which predict $S_\delta \approx \ln[1+\mathcal{M}_c^2]$ (where $\mathcal{M}_c$ is the compressive Mach number of ISM turbulence, and $\mathcal{M}_c \sim$ a few in both observations and simulations; see Federrath et al. 2010; Hopkins 2013).

We can immediately follow the same procedure to calculate the intensity-weighted magnetic energy density,

$$\langle u_{\rm B}\rangle_{I_\nu} = (\gamma/(\gamma+1))\,\exp\left(\gamma\,S_\delta\right)\,\langle u_{B_0}\rangle,$$

as well as the volume-weighted and intensity-weighted midplane CR energy densities

$$\langle e_{\rm CR}\rangle_V = \psi\,\langle u_{\rm B_0}\rangle,$$

$$\langle e_{\rm CR}\rangle_{I_\nu} = (\gamma/(\gamma+\beta))\ \exp\left[\beta\,(\alpha+3\,\beta)\,S_\delta/2\right]\,\langle e_{\rm CR}\rangle_{\rm V}.$$

This provides a natural explanation for several phenomena we saw in Fig. 3.3. The ratio $\langle u_{\rm B}\rangle_{I_\nu}/\langle u_{\rm B}\rangle_{\rm V} \sim 30-40$ in the outer disk, arises primarily from the "clumping factor" correction. The ratio of $\langle u_{\rm B}\rangle_{\rm V} = \langle u_{\rm B_0}\rangle$ in the disk mid-plane to $\langle u_{\rm B}\rangle_{\rm BK05}$ (the standard equipartition formula) is given by $(\psi\,f_{\rm cl}\,H_B/L)^{-2/(\alpha+3)}$, which in the outer disk is ~ 0.7 (and is ~ 1.4 in the inner disk) so the BK05 formula will slightly over-estimate (under-estimate) $\langle u_{\rm B}\rangle_{\rm V}$ in the outer (inner) disk, as we see. The difference is small — i.e. BK05 appears to "correctly" obtain roughly the correct $\langle u_{\rm B}\rangle_{\rm V}$, because the corrections $f_{\rm cl}$ and $H_{\rm B}/L$ are both relatively large but tend to go in opposite directions (cancelling each other out), combined of course with the effect of the small power law $2/(\alpha+3)$ which tends to suppress any differences. In other words, the true emitting region is smaller along the line of sight than assumed by BK05, but the emission is also boosted within that region by clumping. Of course, BK05 under-estimates $\langle u_{\rm B}\rangle_{I_\nu}$ by a very large factor as predicted.

Using the same exercise/model we can compare the intensity and volume-weighted CR energy densities $\langle e_{\rm CR}\rangle_{I_\nu}$ and $\langle e_{\rm CR}\rangle_{\rm V}$. Given the small $\beta \ll 1$, we predict that although $\langle u_{\rm B}\rangle_{I_\nu} \gg \langle u_B\rangle_{\rm V}$, $\langle e_{\rm CR}\rangle_{I_\nu}$ only exceeds $\langle u_{\rm CR}\rangle_{\rm V}$ by a factor $\sim 1.5-2$. Thus for a given ψ, β and S_δ or $f_{\rm cl}$, and $H_{\rm B}$, we can quantitatively explain all of the relative values of the different estimators in Fig. 3.3.

3.6 Summary and Conclusions

In this chapter, we have presented the first end-to-end predictions of synchrotron emission from MHD galaxy formation simulations which self-consistently evolve **B** and the CR(e) spectra from Hopkins, Butsky, Panopoulou, et al. (2022). These simulations utilize a constant in space and time scaling for the CR scattering rate ν, calibrated to reproduce both Solar System CR data (e.g. Voyager, AMS-02) and resolved γ-ray observations of the MW and nearby galaxies (e.g. Fermi).

We have found that synchrotron emission in L_* galaxies arises not only from the volume-filling, warm/hot phases of the ISM, but can be dominated by cooler and denser WNM/CNM phases. This is not unexpected; the long discovered and well studied FIR-Radio correlation of galaxies (Voelk, 1985; Ivison et al., 1985; Jong et al., 1985; Helou, Soifer, and Rowan-Robinson, 1985; Condon, Anderson, and Helou, 1991) which exists also on sub-kpc resolved scales (Murphy, Braun, et al., 2006) requires a connection between the FIR emission, which arises from dust

re-radiating UV photons from star formation, and the synchrotron emission which also arises from star forming regions with high neutral gas densities and magnetic field strengths. Furthermore, recent synchrotron observations of edge-on galaxies (Krause et al., 2018; Heesen, Krause, et al., 2018) have found bright thin disk components which would be spatially coincident with thin, mostly neutral mid-plane gas, and contribute most of the emission when viewed face-on. Moreover, recent observations of structures within our Galaxy have found synchrotron emission arising from cold, neutral gas as well (Bracco, Padovani, and Soler, 2023).

While this is now known, the conventional wisdom when applying equipartition models to observations of extra-galactic non-thermal radio continuum emission has been to implicitly assume that the emission arises from a volume-filling phase of the ISM which is far more extended in the vertical direction compared to the atomic gas disk. This assumption can lead to underestimating the "true" **B** of the synchrotron-emitting dense gas, and over-estimating **B** in the volume-filling, tenuous thick disk/halo gas at ~kpc above the disk.

We have found that explicitly evolving the CR(e) spectra is important for accurate synchrotron predictions towards galactic centers, where loss terms are drastically different from typical spiral galaxy conditions. Comparing to the "single-bin" scenario shows that the resulting predicted emission changes relative to assuming a constant LISM spectrum by modest factors of ~1.5-2 in typical spiral galaxy conditions at outer radii (R > 3 kpc), but can be particularly important by a factor ~10 - 50 towards the galactic center, where loss terms can be drastically different. This is consistent with the softer CRe spectrum seen in these simulations towards the galactic center in Hopkins, Butsky, Panopoulou, et al. (2022), and highlights the varying importance of different loss rates and CR source distributions in generating predictive spectra and synchrotron images. We show that the difference in synchrotron owes primarily to variation in the p/e^- ratio compounding with changes in spectral slope, rather than e^+ contributions.

Finally, we formulate a toy model that accounts for clumping factors, a varied magnetic scale height, and deviations from equipartition in order to more robustly trace **B** weighted by different quantities. From our toy model calculations, we find that uncertainty in connecting the equipartition values to the "true" values of u_B and e_{CR} boils down to the assumption of energy equipartition and the size/volume-filling factor of the emitting regions, and less so on spectral effects. When estimating a volume-averaged mean $\langle u_B \rangle$, the fact that CRs are diffusive and so naturally form

a smoother distribution, means that there are large local violations of equipartition. But this smoothness partially cancels the "clumping factor" from in-homogeneous **B**. This leads to surprisingly reasonable values of **B**. Future high-resolution radio observations at GHz frequencies (Murphy, Bolatto, et al., 2018) may further constrain the volume filling and clumping factors of synchrotron emission, including the current observationally uncertain thin-disk scale heights.

We note that while we have only studied simulations with constant power-law scattering (or diffusivity) of CRs in this chapter, we have also studied a set of FIRE-2 simulations with varied CR transport motivated by extrinsic turbulence and self-confinement in Ponnada, Butsky, et al. (2024), though with the caveat that those are "single-bin" simulations. There, we find that the CR transport physics can drive differences in gas phase structure, morphology, and non-thermal properties, leading to markedly different synchrotron emission particularly for the self-confinement models relative to extrinsic turbulence or constant diffusivity models. Correspondingly, there are implications for what phase of the ISM dominates the emission and the distribution of gas in the disk and inner CGM, which would affect what one would infer with equipartition assumptions. In particular, in runs with self-confinement motivated CR transport, the strong trapping of CRs in regions of high e_{CR} can lead to non-linear CR-driven, magnetized winds and thus result in a more volume-filling, diffuse phase of the ISM dominating the emission, more in-line with fiducial equipartition assumptions, though those simulated galaxies differ in detail from observed star-forming L^* galaxies, as we discuss in Ponnada, Butsky, et al. (2024). In future work, we will continue to investigate how varied CR transport physics can act to vary synchrotron properties using fully cosmological, spectrally-resolved CR-MHD galaxy simulations.

Synchrotron emission has also been used to estimate physical properties of CRe like their transport length and diffusion coefficient (with an assumed streaming or advection speed), or the CRe scale height (Heesen, 2021; Heesen, De Gasperin, et al., 2023). In future work, we will explore these estimators using our simulations.

Acknowledgements

We wish to recognize and acknowledge the past and present Gabrielino-Tongva people and their Indigenous lands upon which this research was conducted. Additionally, we thank the staff at our institutes, without whose endless efforts this work would not be possible during the ongoing pandemic. We thank the anonymous ref-

eree for their helpful comments which improved the quality of this manuscript. We thank Marco Padovani for providing lookup tables for the synchrotron emissivity calculation. SP thanks Dr. Viviana Casasola for providing gas surface density data for the galaxies compared to in this study, and thanks Dr. Aritra Basu for providing FITS files of radio continuum observations for the same galaxies. Support for SP and PFH was provided by NSF Research Grants 1911233, 20009234, 2108318, NSF CAREER grant 1455342, NASA grants 80NSSC18K0562, HST-AR-15800. GVP acknowledges support by NASA through the NASA Hubble Fellowship grant #HST-HF2-51444.001-A awarded by the Space Telescope Science Institute, which is operated by the Association of Universities for Research in Astronomy, Incorporated, under NASA contract NAS5-26555. CBH is supported by NSF grant AAG-1911233 and NASA grants HST-AR-15800, HST-AR-16633, and HST-GO-16703. Numerical calculations were run on the Caltech compute cluster "Wheeler," allocation AST21010 supported by the NSF and TACC, and NASA HEC SMD-16-7592. The Flatiron Institute is supported by the Simons Foundation. CAFG was supported by NSF through grants AST-2108230 and CAREER award AST-1652522; by NASA through grants 17-ATP17-0067 and 21-ATP21-0036; by STScI through grant HST-GO-16730.016-A; by CXO through grant TM2-23005X; and by the Research Corporation for Science Advancement through a Cottrell Scholar Award. ISB was supported by the DuBridge Postdoctoral Fellowship at Caltech. DK was supported by NSF grant AST2108314. KS acknowledges support from the Black Hole Initiative at Harvard University, which is funded by grants from the John Templeton Foundation and the Gordon and Betty Moore Foundation. This work was supported by NSF grant AST-2109127.

3.7 Appendix: Auxiliary Figures

In this appendix, we provide supporting figures to the results presented and discussed in Chapter 3 regarding synchrotron emission and equipartition estimators of magnetic fields.

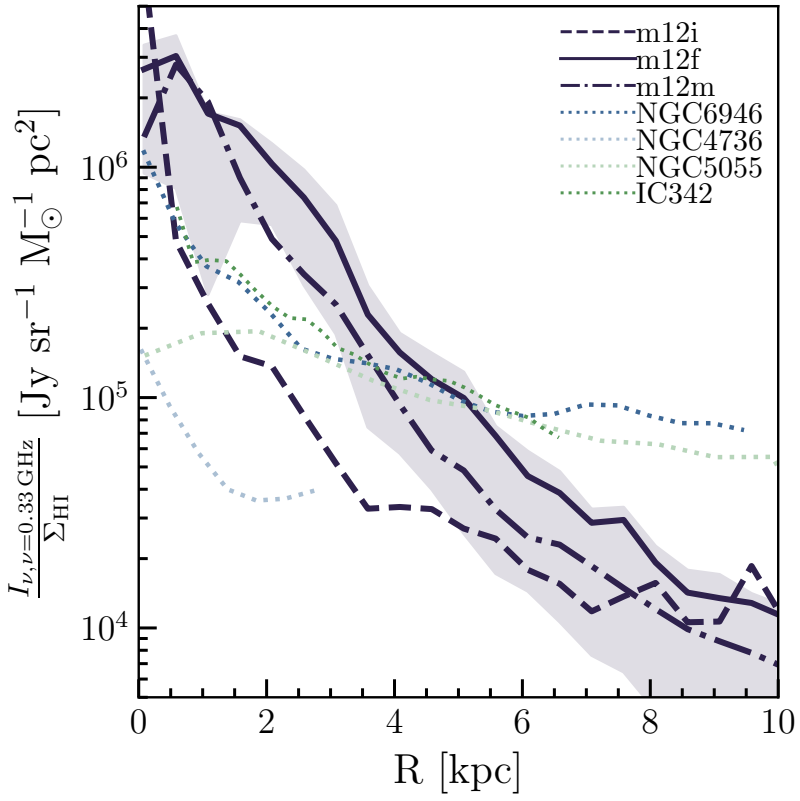

Figure 3.6: *Azimuthally averaged radial profiles of synchrotron specific intensity normalized by HI surface density* for `m12i`, `m12f`, and `m12m`, in navy dashed, solid, and dot-dashed lines. Shaded regions show the approximate ± 1σ scatter (32-68 percentile) at a given radial bin. Corresponding radial profiles for nearby spiral galaxies from Basu and Roy (2013) and Beck (2015b) are shown in dotted lines, normalized by the Σ_{HI} from (Casasola et al., 2017). Normalized in this way, the radial profiles exhibit broader similarities when compared to the specific intensity profiles shown in Figure 3.3, though the simulations' radial profiles still remain steeper than the observations compared to here.

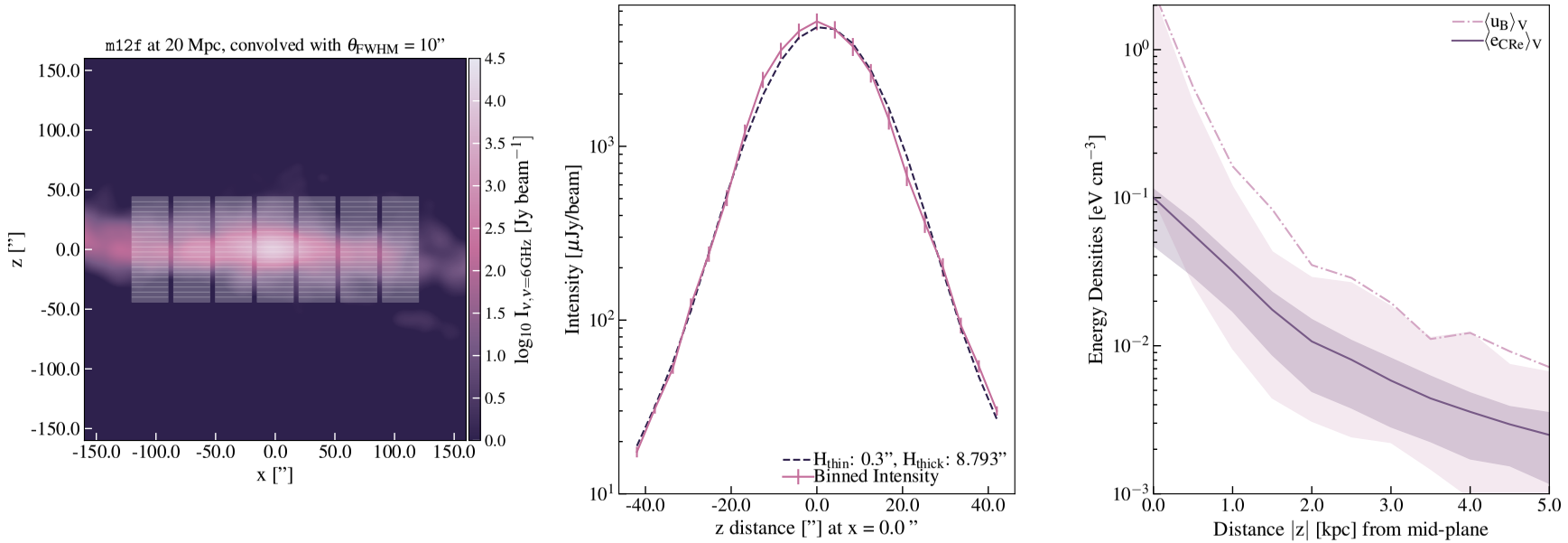

Figure 3.7: *Edge-on image analysis:* **Left:** 10" Gaussian beam-convolved image of `m12f` at 6 GHz with the observer at a distance of 20 Mpc (1" ∼100 pc) with bins overlaid akin to the method of (Krause et al., 2018). **Center**: Lines showing intensity profiles for the central strip of bins (pink solid) with best-fit two-component exponential fit overlaid (purple dashed). **Right:** Lines showing vertical profiles of volume-weighted magnetic (pink dot-dashed) and CRe (navy solid) energy densities, with shaded regions showing 25-75 percentile ranges. Our results are consistent with observational constraints estimates of thin and thick disk components of edge-on spiral galaxies, with the thin disc component with small scale height (∼120 pc when averaged across each vertical strip) dominating the emission and the thick disk component contributing little to the emission but extended out to scale heights of ∼kpc. This primarily owes to a small magnetic scale height, with u_B falling off more quickly than e_{CRe}, which owing to CRe diffusion have a flatter profile.

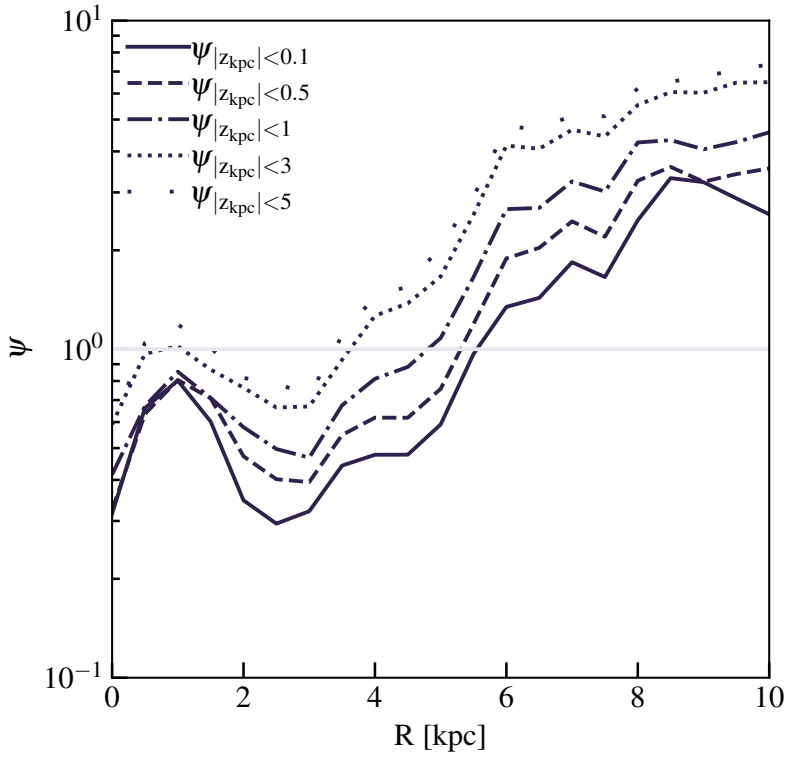

Figure 3.8: *Radial profiles of ψ (physical equipartition between **B** and CRs), or $\langle e_{CR}\rangle_V/\langle u_B\rangle_V$,* in cylindrical annuli of varying height from the mid-plane for `m12f`. For a cylindrical annulus of a given height, in the inner disk where gas densities are high, magnetic energy densities can dominate CR energy densities at the factor of $\sim$ 2 level for cylindrical heights $\leq$ 1 kpc in this volume-averaged sense, with this trend increasing as more of the dense mid-plane gas is sampled (lower heights). In the outer-disk, where gas densities are lower, CRs start to dominate the relative energy density, with the effect accentuated by sampling more "halo" gas at larger heights above the disk where e_{CR} tends to dominate u_B by factors of $\sim$ 2-4 for heights $\leq$ 1 kpc at the very outer radii (Ponnada, Panopoulou, Butsky, Hopkins, Loebman, et al., 2022).

Chapter 4

SYNCHROTRON SIGNATURES OF COSMIC RAY TRANSPORT PHYSICS IN GALAXIES

Ponnada, Sam B. et al. (May 2024). "Synchrotron signatures of cosmic ray transport physics in galaxies." In: *Monthly Notices of the Royal Astronomical Society* 530. Publisher: OUP ADS Bibcode: 2024MNRAS.530L...1P, pp. L1–L6. ISSN: 0035-8711. DOI: 10.1093/mnrasl/slae017.

4.1 Chapter Abstract

Cosmic rays (CRs) may drive outflows and alter the phase structure of the circumgalactic medium, with potentially important implications on galaxy formation. However, these effects ultimately depend on the dominant mode of transport of CRs within and around galaxies, which remains highly uncertain. To explore potential observable constraints on CR transport, we investigate a set of cosmological FIRE-2 CR-MHD simulations of L_* galaxies which evolve CRs with transport models motivated by self-confinement (SC) and extrinsic turbulence (ET) paradigms. To first order, the synchrotron properties diverge between SC and ET models due to a CR physics driven hysteresis. SC models show a higher tendency to undergo 'ejective' feedback events due to a runaway buildup of CR pressure in dense gas due to the behavior of SC transport scalings at extremal CR energy densities. The corresponding CR wind-driven hysteresis results in brighter, smoother, and more extended synchrotron emission in SC runs relative to ET and constant diffusion runs. The differences in synchrotron arise from different morphology, ISM gas and **B** properties, potentially ruling out SC as the dominant mode of CR transport in typical star-forming L_* galaxies, and indicating the prospect for non-thermal radio continuum observations to constrain CR transport physics.

4.2 Introduction

Relativistic charged particles, or cosmic rays (CRs), are ubiquitous in the Universe. Injected and accelerated at supernovae (SNe), stellar winds, and associated shocks fronts, CRs are known to be a considerable component of the Milky Way (MW) interstellar medium (ISM) (Boulares and Cox, 1990; Bell, 1978) and are observed in other L_* galaxies via their γ-ray and non-thermal synchrotron radiation (Lacki, Thompson, Quataert, et al., 2011; Tang, Wang, and Tam, 2014).

In the past decade, the importance of CRs as a source of feedback in galaxies has come to be appreciated (for recent reviews, see Owen et al., 2023; Ruszkowski and Pfrommer, 2023). A host of theoretical studies employing varied numerical and physical prescriptions have established that CRs can play an important role in driving and altering the structure of winds (Booth et al., 2013; Salem and Bryan, 2014; Girichidis, Naab, Walch, et al., 2016; Simpson et al., 2016; Pakmor, Pfrommer, et al., 2016; Bustard et al., 2020; Huang and Davis, 2022; Huang, Jiang, and Davis, 2022; Quataert, Thompson, and Jiang, 2022; Armillotta, Ostriker, and Jiang, 2022; Thomas, Pfrommer, and Pakmor, 2023; Modak et al., 2023) and providing a potentially key source of non-thermal pressure support in the circum-galactic medium (CGM) (Butsky and Quinn, 2018; Chan, Kereš, Hopkins, et al., 2019; Buck et al., 2020; Hopkins, Chan, Garrison-Kimmel, et al., 2020; Farcy et al., 2022).

These effects can manifestly change the star formation histories of L_* galaxies by preventing cool gas from precipitating onto the disk, altering the dynamics of gas in the tenuous inner CGM (Butsky, Werk, et al., 2022) or 'disk-halo interface' (Chan, Kereš, Gurvich, et al., 2022) with potential implications on the amplification of magnetic fields (Ponnada, Panopoulou, Butsky, Hopkins, Loebman, et al., 2022) as well as the phase structure and ionization state of halo gas (Salem, Bryan, and Corlies, 2016; Ji, Chan, et al., 2020; Butsky, Fielding, et al., 2020; Tsung, Oh, and Bustard, 2023).

However, a major caveat remains that all of the aforementioned effects depend sensitively on the dominant mode of transport of CRs through the ISM and into the CGM, which is highly uncertain with elusive observational constraints (Hopkins, Chan, Squire, et al., 2021). An understanding of CR transport is thus crucial to contextualize the importance of CRs for galaxy formation and evolution, as CR effects in the ISM and CGM are heavily dependent on the macroscopic transport speed, often parameterized through the diffusion coefficient κ (more specifically,

$\kappa_{\parallel}$), or streaming speed v_{st}.

The transport of CRs on ~kpc−Mpc galactic scales is fundamentally tied to the scattering of CRs on orders-of-magnitude smaller gyro-resonant scales (~ 0.1 AU for ~GeV CRs). Thus, there has been increasing theoretical interest in understanding the macro-physical transport properties of CRs motivated by models of plasma-scale CR transport (Jokipii, 1966; Skilling, 1975) and how their predicted observables compare to observations (Hopkins, Squire, Chan, et al., 2021; Hopkins, Squire, Butsky, and Ji, 2022; Kempski and Quataert, 2022; Butsky, Nakum, et al., 2023).

Despite some constraining power of existing observations, there is a dire need for further observational comparison to narrow the broad theoretical parameter space, which radio-continuum synchrotron observations may provide. In this Letter, we forward-model synchrotron emission from cosmological, zoom-in simulations of galaxy formation including CRs with different physically-motivated CR transport models from the Feedback in Realistic Environments (FIRE) suite[1] (Hopkins, Wetzel, Kereš, et al., 2018; Hopkins, Squire, Chan, et al., 2021) and explore the physical basis for corresponding observable differences which emerge owing to CR physics. In Section 4.3, we briefly describe the simulations and our methods. Then, we present our results for models with varied CR transport physics in Section 4.4. Lastly, we discuss our conclusions in Section 4.5.

4.3 Simulations and Methods

In this study, we utilize a subset of the simulations presented in (Hopkins, Chan, Squire, et al., 2021; Hopkins, Squire, Chan, et al., 2021) which evolve a 'single-bin' of 1-10 GeV CRs and utilize FIRE-2 (Hopkins, Wetzel, Kereš, et al., 2018) physics. We summarize the most pertinent aspects here, but refer the reader to the aforementioned papers for a more in-depth discussion of numerical details.

The simulations are all fully cosmological, magnetohydrodynamic (Hopkins and Raives, 2016; Hopkins, 2016) simulations of galaxy formation which include baryons and dark matter, fully anisotropic Spitzer-Braginskii conduction and viscosity (Hopkins, 2017) at a Lagrangian mass resolution of 56000 $M_{\odot}$. Prescriptions for explicit stellar feedback and gas cooling (for T ~ 10-10^{10} K) follow (Hopkins, Wetzel, Kereš, et al., 2018); stars form in dense (n > 1000 cm^{-3}), self-shielded, Jeans unstable gas with multi-band radiation, mass-loss, and explosive feedback from Types Ia and II SNe (evolved self-consistently following stellar evolution models)

[1] https://fire.northwestern.edu/

coupled to gas.

Cosmic rays are injected from SNe and OB/WR stellar winds with an energy efficiency of $\epsilon_{\rm CR} = 0.1$ of the inital ejecta kinetic energy. In these 'single-bin' simulations, we solely evolve the ~1-10 GeV CR energy density ($e_{\rm CR}$), or equivalently a constant spectral distribution, as a relativistic fluid with $\gamma_{\rm CR} = 4/3$. The CR dynamics are coupled to the gas and evolve self-consistently, with transport coupled to magnetic field lines according to the CR transport equations and loss terms (collisional, streaming) computed in-code (again, see details in Hopkins, Squire, Chan, et al., 2021).

These simulations invoke scalings for the CR scattering rate, ν, with various plasma properties motivated by micro-physical scenarios. One such model class includes "extrinsic turbulence" (ET) scenarios (Jokipii, 1966), where CRs are scattered off of gyro-resonant fluctuations in $\mathbf{B}$ on scales of order the CR gyro-radius that arise from a turbulent cascade down to those (small) scales. Model variants in this general class vary widely (as shown in Hopkins, Squire, Chan, et al. 2021) according to uncertainties in the shape of the turbulent cascade at small scales, which turbulent modes are of primary importance for scattering on these scales, the importance of certain damping terms, and geometric considerations of the (an)isotropy of said turbulent modes. But broadly speaking, the assumption for our purposes is that the scattering rate ν varies with the local Alfvén scale ($\ell_{\rm A}$) and Alfv́en Mach number ($\mathcal{M}_{\rm A}$) of turbulence on *resolved* simulation scales as $\nu \propto \mathcal{M}_{\rm A}^2/\ell_{\rm A}$. The normalization of ν for these models at ~1 GeV is fitted by Hopkins, Squire, Chan, et al. (2021) to the Voyager, AMS-02, and Fermi data.

The second primary class of models are "self-confinement" scenarios (Skilling, 1975), in which CRs excite Alfvén waves as they stream down their pressure gradients, which dominates the generation of gyro-resonant fluctuations in $\mathbf{B}$ which subsequently scatter CRs. The CR scattering is determined by the balance of the growth and damping of these gyro-resonant Alfvén waves and so model variants within this class are sensitive to the choice of Alfvén speed, assumptions regarding the wave damping and growth terms, and uncertainties in the turbulent dissipation timescales. The key scaling here for ultra-relativistic CRs is $\nu \propto (\frac{e_{\rm CR}}{e_{\rm B}})(\frac{{\rm v_A c}}{\ell_{\rm CR} r_{\rm L} \Gamma})$ in terms of the magnetic and CR energy densities $e_{\rm B}$, $e_{\rm CR}$; Alfvén speed $v_{\rm A}$; gradient scale length $\ell_{\rm CR}$; gyro radius $r_{\rm L}$; and plasma damping terms Γ. These are again re-normalized in Hopkins, Squire, Chan, et al. (2021) to fit the aforementioned ~1-10 GeV observations.

The subset of model variants from Hopkins, Squire, Chan, et al. (2021) explored here were shown to reasonably reproduce observables of γ-ray emission, effective isotropic diffusivities, and cosmic ray energy densities at the "Solar circle," though we will also describe results for simulations which were not consistent with the above constraints to illustrate qualitative differences tying the physics of the model class to the synchrotron properties.

We also compare these model variants to a FIRE-2 simulation that uses a spatially and temporally constant scattering rate (hereafter called the 'constant diffusivity' or CD run) presented in Hopkins, Chan, Garrison-Kimmel, et al. (2020), and whose magnetic field properties were detailed extensively in Ponnada, Panopoulou, Butsky, Hopkins, Loebman, et al. (2022). This run's constant parallel diffusivity is $\kappa_{\parallel} = 3 \times 10^{29}$ cm^2/s, which was chosen to be consistent with the aforementioned constraints Chan, Kereš, Hopkins, et al. (2019).

To generate our synchrotron predictions, we follow the procedure outlined in Ponnada, Panopoulou, Butsky, Hopkins, Skalidis, et al. (2024), with the caveat that as these are 'single-bin' simulations, we assume a constant CR electron (CRe) spectral shape of Bisschoff, Potgieter, and Aslam (2019) and scale the spectrum by the ratio of each gas cell's self-consistently evolved e_{CR} to the local ISM value. This is akin to assuming a constant proton-to-electron ratio as well as a constant spectral shape. Since Bisschoff, Potgieter, and Aslam (2019) provides an empirical spectrum, we are assuming that these models have been tuned to give the right spectral slope according to constraints at Milky Way Solar Circle, though see Kempski and Quataert (2022) and Hopkins, Squire, Butsky, and Ji (2022) for why this may not be physically possible in practice.

Subsequently, the following analysis cannot capture the effects of potential variation in spectral shape and proton-to-electron ratios owing to varying CRe loss terms in gas of different phases and ionization states, nor variation owing to the varied CR transport models and their coupling to gas properties. However, this provides a first look at how the emission properties differ to first-order owing to dynamical differences and corresponding effects on phase structure and gas properties owing to CR transport effects, notwithstanding the caveats mentioned above.

4.4 Synchrotron Emission and The Physics of Cosmic Ray Transport

We examine the synchrotron emission and magnetic field structure from two representative model variants in the ET and SC model classes in Figure 4.1 and charac-

terize key differences in the properties of the gas giving rise to the emission.

There appears to be a dichotomy, on average, in the physical morphologies of the galaxies in the two model classes. ET runs exhibit more typical spiral structure and SC runs have a more central bulge-dominated, lenticular-like appearance. The SC runs tend to show brighter, smoother, and more extended emission and have more ordered magnetic field structure relative to the ET runs; ET runs look qualitatively similar to the constant diffusivity run, with brighter emission coincident with the spiral arms and neutral gas structures in the galactic center. The physical differences underpinning the visual differences between the ET and SC runs become clear in the intensity weighted histograms (Figure 4.1, bottom panels). Figure 4.1 shows that the extended emission in the ET runs is primarily arising from the denser cool and warm neutral gas while the SC runs have emission mostly arising from warmer and more diffuse gas.

In Figure 4.2, we examine these differences more quantitatively with radial profiles of the forward-modeled synchrotron emission for CR physics model variants simulated in Hopkins, Squire, Chan, et al. (2021) that met their reasonable observational γ-ray and e_{CR} constraints. We see significant variation in the profiles depending on CR transport physics. We see a separation between the ET and SC model variants: SC runs typically exhibit brighter emission averaged at a given radius by a factor of $\sim$3-10 relative to ET runs, despite brighter clumped peaks in the spiral arms of ET runs. The SC runs also exhibit smoother emission that falls off more gradually with radius relative to ET and constant diffusivity runs. We stress that the correlation is *not* one-to-one; we can see many earlier (higher-redshift) snapshots where the SC models look more like ET. And some simulations with very low constant diffusivity (2 dex lower than observationally allowed) look similar to the SC runs. We discuss this below.

While the radial profiles for the SC runs appear to be qualitatively more similar to a couple of the known observational profiles in that they exhibit a shallower falloff with radius (Basu and Roy, 2013; Beck, 2015b), the apparent morphological features of the galaxies look markedly different. We defer a comprehensive observational comparison to future work using spectrally-resolved cosmological runs. The variation in the synchrotron profiles between classes of CR transport models indicate the potential for the comparison of larger samples of spatially resolved synchrotron images to model predictions to constrain deeply uncertain CR transport physics.

The shape, normalization, and scatter in the profiles is a function of the phase of the

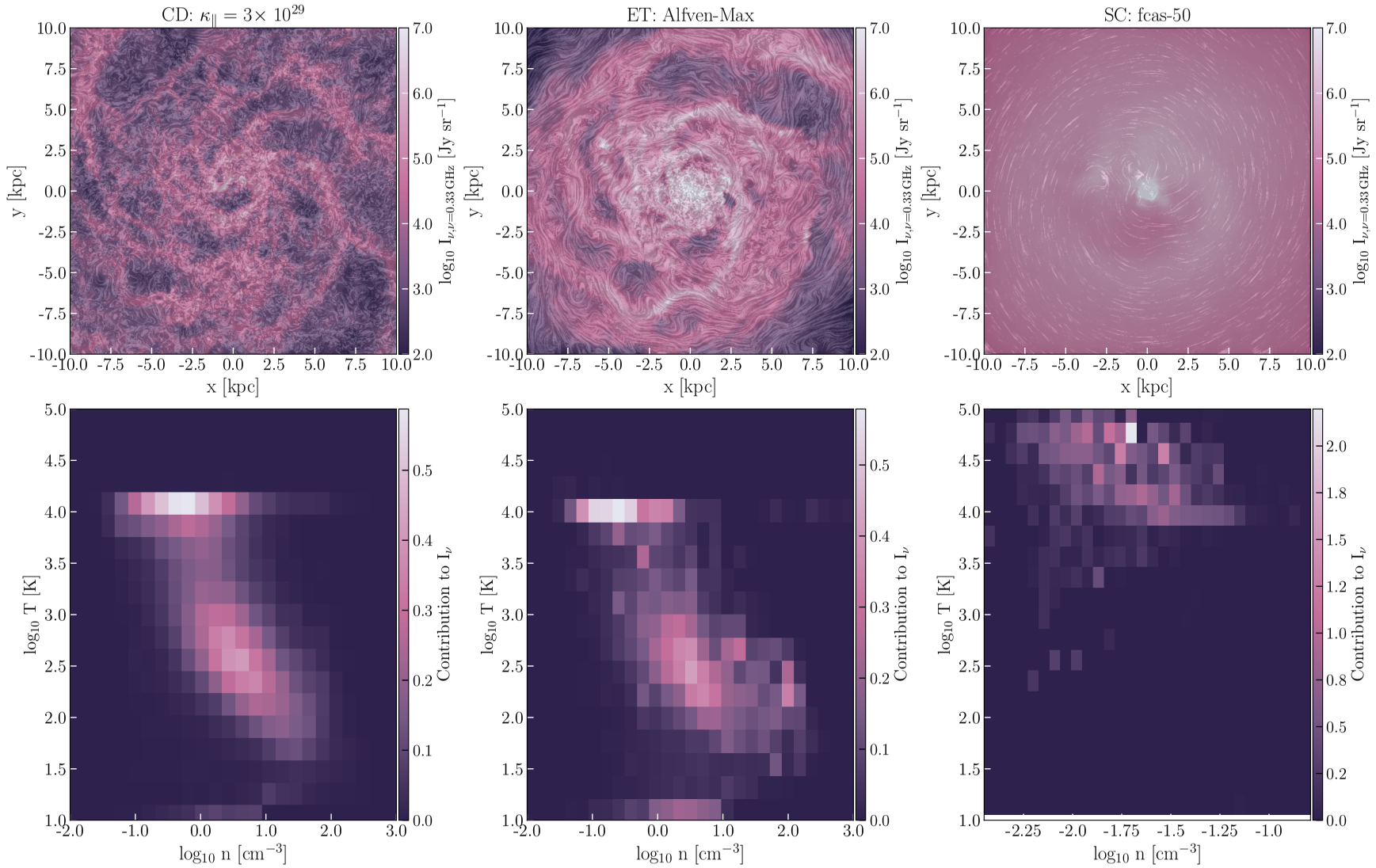

Figure 4.1: *Visualizations of the synchrotron emission at 0.33 GHz and intensity-weighted phase diagrams for FIRE-2 simulations of* `m12i` *with varied CR transport physics at z = 0.* **Row 1:** Specific intensity maps with superimposed lines showing the orientation of the mass-averaged components of the magnetic field. A model variant with spatially and temporally constant $\kappa_{\parallel} = 3 \times 10^{29}$ cm s^{-1} is shown on the left, a variant within the ET class of models ('Alfvén-Max') is shown in the middle, and a SC model ('fcas-50') on the right. CD and ET models generally exhibit more turbulent structure in the magnetic fields, weaker emission, and more variation in brightness contrast to highly ordered **B** and brighter and smoother emission in the SC models. **Row 2:** Intensity-weighted histograms for 2 < R/kpc < 10 and |z| < 3 kpc for the CD, ET and SC runs above. We exclude the central 2 kpc in order to characterize the extended emission properties rather than the bright central cores. In SC models, the synchrotron emission primarily arises from the WIM/WNM compared to the CNM/WNM dominated scenario in the CD and ET runs.

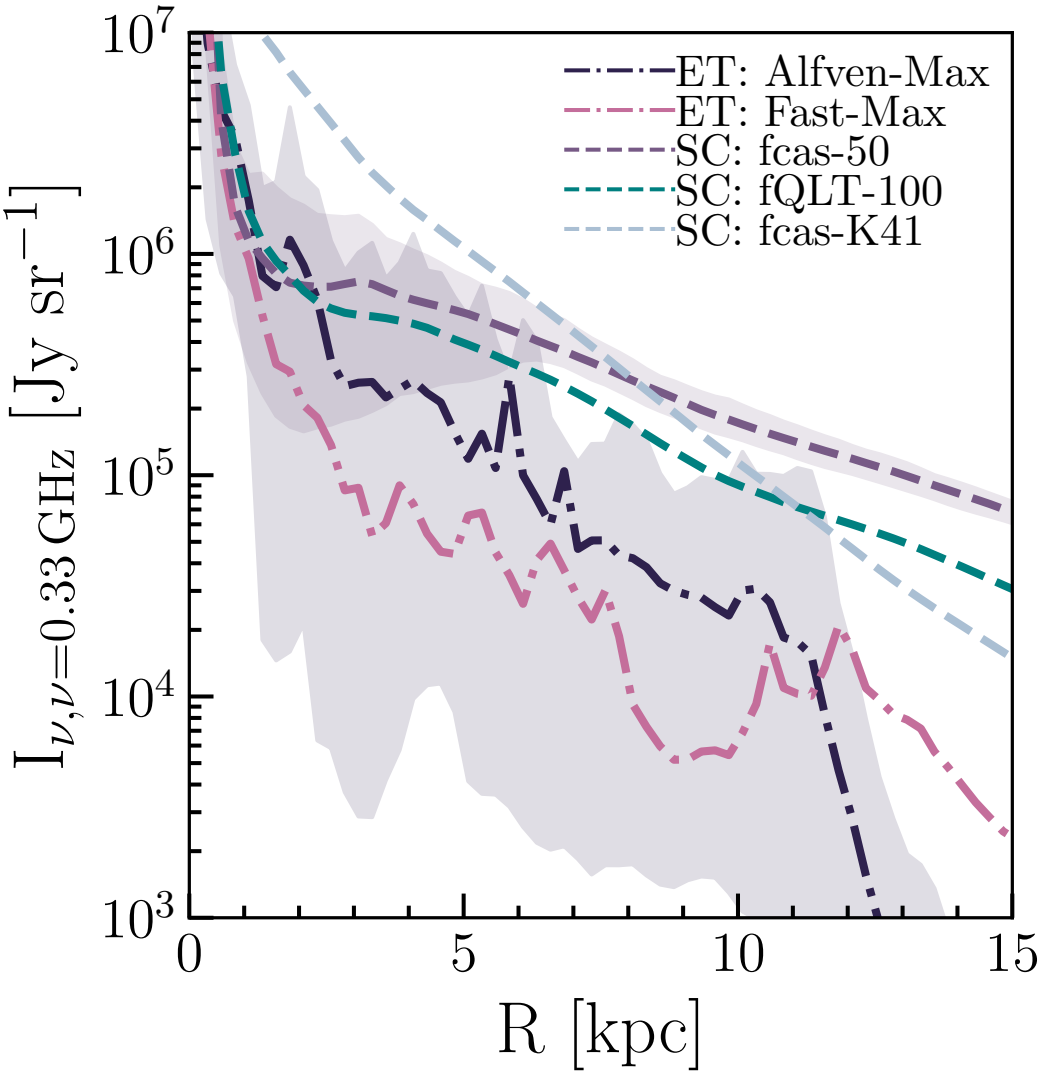

Figure 4.2: *Azimuthally averaged, face-on radial profiles of synchrotron specific intensity for FIRE-2 simulations of* `m12i` *with varied CR transport physics at* $z = 0$. Lines show simulations with ET (dot-dashed) and SC (dashed) model variants of CR transport. Shaded regions show the 5-95 percent range at a given radial bin. Our predictions show significant differences in the shape and normalization of the synchrotron emission profiles, with pathologically different behaviors exhibited between model classes. SC models tend to show brighter, smoother, and more extended profiles in comparison to ET and CD models. The difference in the profiles arises qualitative differences in the phase structure, magnetic field properties, and gas distribution modulated by a CR-physics driven hysteresis.

ISM dominating the galaxy. The smoothness of the SC profiles is induced by the emission arising mostly from the warm neutral/warm ionized media (WNM/WIM), while on the other hand, the synchrotron intensity profiles of the ET and CD runs are dominated by emission coming from the WNM and denser cold neutral medium (CNM). This key physical difference appears to be driven by differences in the CR transport physics between the SC and ET models, as we will describe in the next section.

A Cosmic Ray Physics Driven Hysteresis

The striking differences between the observables and properties of the CD, ET and SC models boil down to some crucial differences in the physics of CR transport. One of the main features of SC models is the (general) scaling of the scattering rate (see Section 4.3) as $\nu \propto e_{\rm CR}$, i.e., the effective/emergent diffusion coefficient is inversely proportional to $\rm e_{CR}$ ($\kappa_{\parallel} \propto e_{\rm CR}^{-1}$ in SC model variants, which is the defining characteristic of these types of models; for exact scalings of the models variants considered, see Hopkins, Squire, Chan, et al. 2021). This scaling is true when the linear damping term dominates the gyro-resonant Alfv́en waves, and the CR flux is in approximate local steady state. This inverse scaling of the diffusion coefficient with the CR energy density can lead to scenarios in which regions of high $\rm e_{CR}$ are prone to more efficient trapping of CRs. This trapping of CRs then leads to the limit of increasing $\rm e_{CR}$, therefore increasing ν and so on until $\nu \rightarrow \infty$, and the CRs are trapped to move strictly with Alfvén wave packets in the gas. This means a large CR pressure has built up and been "trapped" in the dense ISM gas. This build-up of CR pressure eventually blows apart ISM gas, and thus the galaxy is largely filled with warm/hot and diffuse phases, with dense, magnetized, CR-laden gas spread via these outflows into a much larger, smoother distribution. In contrast, regions of high $\rm e_{CR}$ in ET runs would rapidly diffuse/escape, and due to high $\rm e_{CR}$ compressive modes can be effectively damped, even further "de-confining" CRs locally.

This difference in the behavior of CRs especially at high $\rm e_{CR}$ seems to underpin a CR physics driven hysteresis between the SC model variants and the rest. In SC runs, at $z = 0$ we typically see a warmer and more diffuse phase structure, lower gas surface densities outside R ∼4 kpc, stronger and more ordered **B** at a given $n_{\rm gas}$ and at a given radius, and a steeper $\rm e_{CR}$ - $n_{\rm gas}$ relation. These differences primarily appear to arise after a non-linear feedback event owing to the SC-runaway in which CRs expel most of the cool and neutral gas outside of R ∼4 kpc. At the earlier snapshots this has not yet occurred; it is of course possible that no runaway occurs, but based

on the analysis of the 3 SC-motivated runs that meet constraints here, as well as 6 of the SC-motivated runs that failed to meet constraints in (Hopkins, Squire, Chan, et al., 2021), we conclude that it happens eventually than not, as we do not see *any* SC-motivated runs that do not suffer from this issue.

To see this in more detail, in Figure 4.3, we show PDFs of the vertical component of velocity ($|v_z|$) weighted by u_B and e_{CR} for two snapshots ~820 Myr apart of the SC run 'fcas-50' at displacements of 0.5-3 kpc from the disk mid-plane. The later snapshot has clear signatures of a feedback event, with the e_{CR}-weighted velocity PDF shifting to having many gas cells with $|v_z| > 100$ km/s, and the magnetic energy density-weighted PDF shifting similarly, though with lower magnitude. The presence of these e_{CR}-loaded winds corresponds directly with a transition in these SC runs from morphological spirals with relatively similar gas distributions, ISM phase structure, and magnetic field properties to the ET and CD runs.

While we show only the velocity PDFs for 'fcas-50', this general picture of e_{CR}-loaded winds, which drive substantial changes in the galaxy properties and synchrotron observables appears to emerge for the other SC models explored in this chapter as well. As further confirmation of this process, we note that we see a similar effect of CR and u_B-loaded winds from "trapped" CRs in runs not shown here but run in Hopkins, Squire, Chan, et al. (2021) where they adopted a constant but extremely large scattering rate (very low diffusivity, factors > 100 lower than the observationally-allowed values). As noted by those authors, those particular runs were strongly ruled out by CR spectra, primary-to-secondary ratios, and γ-ray emission in the Galaxy, hence our not comparing them further here. But, by definition, they produce efficient CR trapping, so it should not be surprising that they can produce a similar "blowout" event to the SC runs here. This demonstrates a new prediction for variations of CR transport models in the SC regime: if CR transport at 1-10 GeV is dominated by modulation from self-excited, gyro-resonant Alfvén waves, galaxies may be more conducive to 'ejective feedback' scenarios through CR-driven winds.

4.5 Discussion and Conclusions

In this chapter, we explore the effects of different physically-motivated models for the CR scattering rate ν which allow it to vary dynamically as function of local plasma properties, heuristically motivated by self-confinement (SC) and extrinsic turbulence (ET) models, in "single-bin" simulations (not evolving the full CR spec-

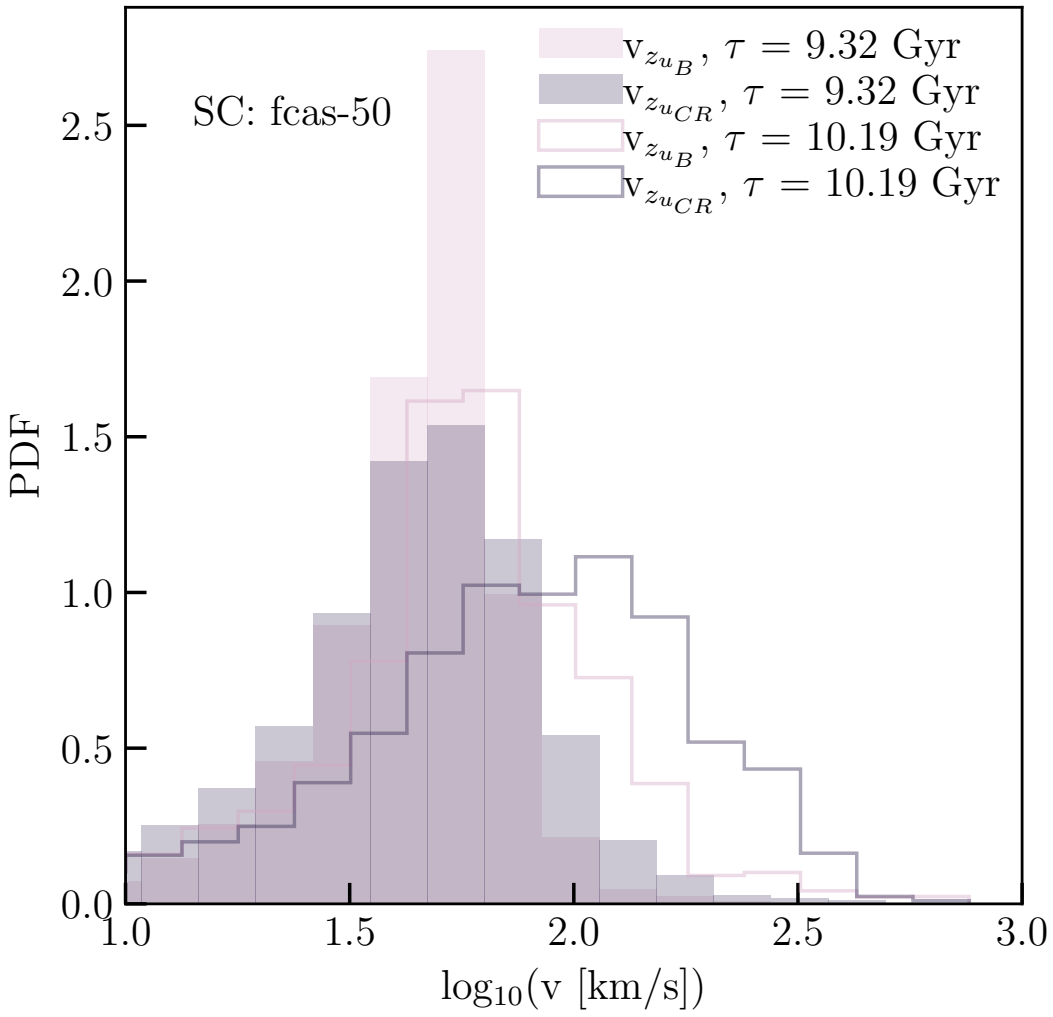

Figure 4.3: *PDFs of the gas velocity $log_{10}(|v_z|)$ weighted by u_B (pink) and e_{CR} (black)* at two snapshots 820 Myr apart (filled and unfilled) for R < 14 kpc at heights from the mid-plane of 0.5-3 kpc for a SC run ('fcas-50'). Runs with SC model variants for CR transport appear to be more likely to undergo extreme feedback scenarios in which a build-up of e_{CR} runs away until expelling highly magnetized and e_{CR}-loaded winds from the galaxy. These winds carry away cool, neutral gas and transform the phase structure and corresponding observable properties of the synchrotron emission.

trum) calibrated to give reasonable mean $\langle \nu \rangle$ at ~GeV energies in Hopkins, Squire, Chan, et al. (2021).

Simulated galaxies with SC models of CR transport tend to have brighter, more spatially extended and smoother synchrotron emission than ET and CD models. The brighter emission in the SC models corresponds with a relatively featureless, warm-hot phase dominated ISM, elevated $\mathbf{B}$-n_{gas} relation, and a more ordered and mean-field dominated $\mathbf{B}$.This apparent hysteresis seems to be CR physics driven, as SC runs have the potential for a runaway at high e_{CR} which leads to CR energy concentrating until cold and dense gas is blown out via e_{CR} and u_B loaded winds, resulting in the stark morphological and physical differences between SC and ET/CD runs.

Already, the sheer lack of detailed cold, neutral phase structure diverges from typical $\sim L_*$ spiral galaxies, which may indicate that SC is not the dominant mode of CR transport in these types of galaxies, though it may operate more so within galaxies with a lenticular-like morphology with a more featureless gas/dust distribution. Despite this, the radial intensity profiles of the SC models are characteristically less steep than those of CD/ET models, and more similar in shape to the small sample of observed radial profiles compared to in Ponnada, Panopoulou, Butsky, Hopkins, Skalidis, et al. (2024). This may also indicate that something is missing from ET models, but we have not found a way to hybridize this model class with SC scalings in a way that does not suffer the 'SC runaway' effects. It is easier in principle to reconcile the relative steepness of ET synchrotron emission profiles with physics not directly related to the CR transport scalings through slightly higher gas surface densities or magnetic field strengths. However, this work indicates the potential for differences between CR transport models to be probed in a spatially resolved manner with larger samples with future radio instruments like the DSA-2000 (Hallinan et al., 2019), ngVLA (Murphy, Bolatto, et al., 2018), and Square Kilometer Array (Dewdney et al., 2009) and with already existing and future HI 21 cm surveys (Walter et al., 2008).

We emphasize also that the differences seen in the model variations here are highly nonlinear, and do not indicate that SC models of CR transport will *always* exhibit these differences relative to ET/CD models. Rather, the predictions made here are for SC transport models which have undergone the 'SC runaway,' and simulations which have not undergone this nonlinear process (like higher redshift snapshots or those not run with the SC transport scalings fully cosmologically) do not exhibit the

same characteristic synchrotron properties. And we stress that, as shown in more detail in Hopkins, Squire, Chan, et al. (2021) and Hopkins, Squire, Butsky, and Ji (2022), qualitative and order-of-magnitude uncertainties remain in first-principles models for the CR scattering rate ν and indeed *no* first-principles model has been demonstrated to predict the correct CR spectra and primary-to-secondary ratios at ~MeV-TeV energies (Hopkins, Squire, Butsky, and Ji, 2022).

And although the differences explored here appear to be driven by the CR physics, there are several other interrelated factors that may be important. Notably, the non-linear interplay of our stellar feedback model, the coupling of CR feedback, and the physics of gas cooling altogether influence the corresponding gas properties and are not cleanly separable i.e., these are the predictions of these CR transport models *given* the FIRE-2 feedback and cooling physics and numerics. Changing the feedback and cooling prescriptions might lead to different results for the effect of the CR transport models on the synchrotron emission properties of simulated galaxies. The exact timing and prominence of these "blowout" events may also potentially depend on the gas resolution, which we will increase in future studies to $\sim$ 7000 $M_\odot$, though we have checked the same CR transport variants for an intermediate-mass simulated galaxy (`m11f` in Hopkins, Squire, Chan, et al. (2021), factor of ~2 lower in halo mass than the simulations presented here) at a higher Lagrangian mass resolution of 12000 $M_\odot$ and found similar results. The dynamical interaction of CRs again highlights the need for explicit evolution of CRs in galaxy formation simulations, as tracer particle or post-processing approaches to CR transport, for instance, popular methods like those of `GALPROP` (Strong and Moskalenko, 1998) would by construction fail to capture these important effects.

Future work will include the exploration of more FIRE-3 simulations which vary CR transport and explicitly evolve CR(e) spectra beyond the "single-bin" simulations explored in this chapter. These FIRE-3 simulations will allow for the generation of more robust synchrotron predictions (i.e., spectral variation) that may generate new predictions for conducting observational tests of CR transport models. In a similar vein, multi-wavelength analysis of varied CR transport models, for example with spatial cross-correlations, may prove fruitful in generating more predictive constraints that can be tested against observations.

Acknowledgements

We wish to recognize and acknowledge the past and present Gabrielino-Tongva people and their Indigenous lands upon which this research was conducted. Additionally, we thank the staff at our institutes, without whose endless efforts this work would not be possible during the ongoing pandemic. Support for SP and PFH was provided by NSF Research Grants 1911233, 20009234, 2108318, NSF CAREER grant 1455342, NASA grants 80NSSC18K0562, HST-AR-15800. GVP acknowledges support by NASA through the NASA Hubble Fellowship grant #HST-HF2-51444.001-A awarded by the Space Telescope Science Institute, which is operated by the Association of Universities for Research in Astronomy, Incorporated, under NASA contract NAS5-26555. CBH is supported by NSF grant AAG-1911233 and NASA grants HST-AR-15800, HST-AR-16633, and HST-GO-16703. Numerical calculations were run on the Caltech compute cluster "Wheeler," allocation AST21010 supported by the NSF and TACC, and NASA HEC SMD-16-7592. The Flatiron Institute is supported by the Simons Foundation. CAFG was supported by NSF through grants AST-2108230 and CAREER award AST-1652522; by NASA through grants 17-ATP17-0067 and 21-ATP21-0036; by STScI through grant HST-GO-16730.016-A; by CXO through grant TM2-23005X; and by the Research Corporation for Science Advancement through a Cottrell Scholar Award. ISB was supported by the DuBridge Postdoctoral Fellowship at Caltech. DK was supported by NSF grant AST2108314. KS acknowledges support from the Black Hole Initiative at Harvard University, which is funded by grants from the John Templeton Foundation and the Gordon and Betty Moore Foundation. This work was supported by NSF grant AST-2109127.

Chapter 5

HOOKS, LINES, AND SINKERS: HOW ACTIVE GALACTIC NUCLEUS FEEDBACK AND COSMIC RAY TRANSPORT SHAPE THE FAR INFRARED-RADIO CORRELATION OF GALAXIES

Ponnada, Sam B. et al. (Feb. 2025). "Hooks, lines, and sinkers: How active galactic nucleus feedback and cosmic-ray transport shape the far-infrared–radio correlation of galaxies." en. In: *The Astrophysical Journal* 980.1. Publisher: The American Astronomical Society, p. 135. ISSN: 0004-637X. DOI: 10.3847/1538-4357/ada280.

5.1 Chapter Abstract

The far-infrared (FIR) - radio correlation (FRC) is one of the most promising empirical constraints on the role of cosmic-rays (CRs) and magnetic fields (**B**) in galaxy formation and evolution. While many theories have been proposed in order to explain the emergence and maintenance of the FRC across a gamut of galaxy properties and redshift, the non-linear physics at play remain unexplored in full complexity and cosmological context. We present the first reproduction of the $z \sim 0$ FRC using detailed synthetic observations of state-of-the-art cosmological zoom-in simulations from the FIRE-3 suite with explicitly-evolved CR proton and electron (CRe) spectra, for three models for CR transport and multi-channel AGN feedback. In doing so, we generally verify the predictions of 'calorimeter' theories at high FIR luminosities ($L_{60\mu m} \gtrsim 10^{9.5}$) and at low FIR luminosities ($L_{60\mu m} \lesssim 10^{9.5}$) the so-called 'conspiracy' of increasing ultraviolet radiation escape in tandem with increasing CRe escape, and find that the global FRC is insensitive to *orders-of-magnitude* locally-variable CR transport coefficients. Importantly, the indirect effect of AGN feedback on emergent observables highlights novel interpretations of outliers in the FRC. In particular, we find that in many cases, 'radio-excess' objects can be better understood as *IR-dim* objects with longer-lived radio contributions at low z from Type Ia SNe and intermittent black hole accretion in quenching galaxies, though this is sensitive to the interplay of CR transport and AGN feedback physics. This creates characteristic evolutionary tracks leading to the $z = 0$ FRC, which shape the subsequent late-time behavior of each model.

5.2 Introduction

For over five decades, the origins of the correlation between the observed far-infrared (FIR) and radio luminosities of galaxies and its evolution with redshift has been explored with great theoretical and observational interest. First found for the cores of a few bright Seyfert galaxies (Kruit, 1971), the FIR-radio correlation (hereafter, FRC), was established to hold for larger samples of galaxies (Jong et al., 1985; Helou, Soifer, and Rowan-Robinson, 1985; Wunderlich, Klein, and Wielebinski, 1987; Condon, Anderson, and Helou, 1991; Yun, Reddy, and Condon, 2001; Bell, 2003) encompassing a broad swath of galaxy types including dwarf, irregular, and star-forming spiral galaxies.

(Helou, Soifer, and Rowan-Robinson, 1985) observed that the nonthermal radio emission in these systems was quickly determined to be too large to arise solely from un-resolved supernova remnants, indicating that the bulk of the emission must be arising from extended distributions of cosmic rays (CRs). Since the FIR emission originates from dust heated by star formation and AGN, the FRC presented the first sign of the close coupling between dust heating, CR production, and magnetic fields (**B**) with star formation across vastly differing galaxy conditions.

To explain this coupling between star-formation and thermal dust emission and the non-thermal physics of CRs and **B**, Voelk (1989) proposed that galaxies are simply cosmic ray electron (CRe) and FIR “calorimeters." This meant that CRe radiate away their energy to synchrotron and Inverse Compton (IC) losses, and all of the UV photons are reprocessed in surrounding optically-thick gas to FIR. This simplified calorimeter theory (and other similar theories, e.g. Lisenfeld, Voelk, and Xu, 1996) would neatly explain the FRC, however challenges naturally arise as not all galaxies are UV calorimeters (Bell, 2003). Indeed, the fraction of star formation that is obscured decreases with decreasing galaxy mass (Hayward et al., 2014; Whitaker et al., 2017). Nor are all galaxies expected to be CRe calorimeters as the diffusive escape timescales for CRs can be much shorter than the synchrotron loss timescales in dwarf galaxies, and not strictly *synchrotron* calorimeters in galaxies like the Milky Way (Strong, Porter, et al., 2010), though great uncertainties remain in the transport of CRs through the interstellar and circumgalactic media (ISM and CGM) (Zweibel, 2013; Hopkins, Squire, Chan, et al., 2021; Kempski and Quataert, 2022; Hopkins, Squire, Butsky, and Ji, 2022).

Due to these issues with the “calorimeter" class of models in explaining the existence of the FRC across the gamut of star-forming galaxies, Helou and Bicay (1993)

proposed an alternative non-calorimetric “conspiracy" model, in which the CRe scale height varies as a power-law function of the gas density scale height, subject to assumptions of synchrotron losses being dominant. This class of model ameliorates the issue for galaxies with low gas surface densities; however, it fails to explain the FRC in the high surface density starburst regime and neglects several potentially important CRe loss processes.

In a synthesis of these contrasting theoretical pictures, Lacki, Thompson, and Quataert (2010) explored a large set of one-zone numerical models where galaxies are represented with a self-consistent set of galaxy-averaged parameters related to the injection of photons and CRs, computing the corresponding FIR and non-thermal properties. Through this work, a more detailed understanding of the FRC's origins emerged as a combination of UV, CRe and CR *proton* calorimetry in starbursts, where rapid free-free and IC losses of CRe are balanced by the production of secondary CRe via charged pion (π^+ and π^-) decay and CRe escape is balanced by lower optical thickness to UV light.

While the approach of one-zone, “leaky-box" phenomenology presents an effective way to explore large parameter spaces, it by construction marginalizes over the highly complex and dynamic nature of the multi-phase ISM and CGM, which vary by several orders-of-magnitude in physical quantities relevant to CR(e) loss and propagation timescales; i.e., the local magnetic field properties, ionization fraction, turbulence, and gas and photon densities (Schmidt, 1959; Vallée, Vallée, and P., 1995; Crutcher et al., 2010; Ponnada, Panopoulou, Butsky, Hopkins, Loebman, et al., 2022). Moreover, these models fail to reproduce the observed spectral slopes at ~GHz frequencies for star-forming galaxies, and fail to capture how the complex, non-linear dynamics of CRs and their back-reaction on gas may impact the relevant observables.

In the past decade, numerical simulations of galaxy formation have advanced significantly, capable of simulating the physics of star formation and feedback, magneto-hydrodynamics (MHD) (Peng and Tom, 2009; Pakmor, Marinacci, and Springel, 2014; Marinacci, Pakmor, and Springel, 2014; Rieder and Teyssier, 2017; Butsky, Zrake, et al., 2017; Martin-Alvarez, Devriendt, et al., 2018; Ntormousi et al., 2020; Steinwandel, Dolag, Lesch, Moster, et al., 2020; Wibking and Krumholz, 2021; Robinson and Wadsley, 2023) in concert with CRs (Booth et al., 2013; Salem and Bryan, 2014; Girichidis, Naab, Walch, et al., 2016; Butsky and Quinn, 2018; Chan, Kereš, Hopkins, et al., 2019; Buck et al., 2020; Werhahn, Pfrommer, and Girichidis,

2021; Werhahn, Pfrommer, Girichidis, Puchwein, et al., 2021; Werhahn, Pfrommer, Girichidis, and Winner, 2021; Pfrommer et al., 2022; Farcy et al., 2022; Thomas, Pfrommer, and Pakmor, 2023), and in many cases, halo growth from cosmological initial conditions (Hopkins, Chan, Garrison-Kimmel, et al., 2020; Hopkins, Wetzel, Wheeler, et al., 2023; Rodríguez Montero et al., 2024).

Leveraging some of these advances, Werhahn, Pfrommer, and Girichidis (2021) and Pfrommer et al. (2022) utilize a set of isolated galaxy simulations with CR-MHD to explore the physics driving the linear FRC and its associated scatter, largely finding agreement with the semi-analytic one-zone models of Lacki, Thompson, and Quataert (2010). These works advance our understanding of the emergence of the FRC by self-consistently evolving galactic magnetic fields and the dynamical interplay of CRs, thereby reducing the number of free parameters in the modeling, though with some caveats. Notably, they by construction utilize a steady-state formulation to solve for the relevant CRe spectra, do not explicitly resolve the multi-phase nature of the ISM, and do not evolve galaxies' cosmological environments, which in turn influence the injection of CRs from the ISM via episodic star-formation and the ensuing transport into halos with realistic, extended gas distributions.

Evolving CR(e) spectra across several orders-of-magnitude in energy has recently become possible in galaxy formation simulations (Girichidis, Pfrommer, Hanasz, et al., 2020; Hopkins, Squire, and Butsky, 2022) including in cosmological simulations with explicitly resolved CR-MHD (Hopkins, Butsky, Panopoulou, et al., 2022; Hopkins, Wetzel, Wheeler, et al., 2023). These self-consistent simulations are capable of capturing the full dynamical, non-linear, and non-equilibrium physics of CRs which may be crucial for determining the details of the intensity and spatial distributions of synchrotron-emitting gas (Ponnada, Panopoulou, Butsky, Hopkins, Skalidis, et al., 2024).

Furthermore, the role of AGN feedback (even via strictly *indirect* effects) in shaping the emergence of the FRC has remained largely unexplored in the literature. As the physics of black hole accretion and subsequent energy injection is far below modern simulation resolution limits, there are varied "sub-grid" prescriptions for AGN feedback in different cosmological simulation suites (Schaye et al., 2015; Pillepich et al., 2018), with the corresponding physical interpretation of the resolved-scale observables, which are typically $\gtrsim$ kpc, remaining unclear.

Advances of late have pushed this 'sub-grid' boundary for AGN energy and momentum injection much further inwards, down to $\sim pc$ scales, *explicitly* evolving

the known (but largely unconstrained) channels of feedback from AGN (radiative, mechanical, and non-thermal, relativistic jets) and their subsequent physical interactions with the multi-phase ISM/CGM and stellar feedback effects upon injection from a sub-grid accretion kernel scale (Su, Hopkins, Bryan, et al., 2021; Su, Bryan, Hayward, et al., 2024; Wellons et al., 2023; Hopkins, Wetzel, Wheeler, et al., 2023), with BH fueling physics therein motivated by more idealized, but hyper-refined simulations down to far smaller scales (Anglés-Alcázar, Quataert, et al., 2021).

The goals of this paper are to model in full cosmological complexity the emergence of the FRC across a large dynamic range in galaxy properties and characterize its evolution with redshift to the well-studied $z = 0$ FRC. For the first time, we also aim to gain a better physical understanding of outliers in the FRC in the context of AGN feedback and varied CR transport. To this end, we utilize a large sample of novel zoom-in, dynamical CR-MHD simulations from the latest version of the Feedback in Realistic Environments project (FIRE)[1] simulation suite (Hopkins, Wetzel, Wheeler, et al., 2023) which crucially evolve CR and CRe dynamics within a self-consistent cosmological framework while resolving multi-phase ISM/CGM structure.

We describe our simulations, present our sample selection, and detail our post-processing methodology to generate radio continuum and multi-band UV-IR imaging in Section 5.3. In Section 5.4, we present our results and compare to the relevant observations of the FRC, and explore the origins of the FRC and its scatter in different physical regimes. With the breadth of physics probed by our simulation sample, we describe potential physical mechanisms giving rise to the $z \sim 0$ FRC's properties as galaxies evolve with redshift, and the emergence of interesting outliers. Finally, we discuss our results and conclusions and summarize our findings in Section 5.5.

5.3 Methodology

Simulations

Our sample of FIRE-3 simulations contains galaxies with $z = 0$ dark matter halo masses $M_{\rm halo}^{z=0} = 3 \times 10^{10}$ - 10^{13} $M_\odot$ which were run with physics variations explored herein. In previous works utilizing FIRE simulations, these halo masses are commonly referred to as `m11`, `m12`, and `m13`, and we use the same naming convention here. These halo mass grouping correspond to $M_{\rm halo}^{z=0} \sim 3 \times 10^{10}$– 7×10^{11} $M_\odot$, 7×10^{11} - 1.5×10^{12} $M_\odot$, and 5×10^{12} - 10^{13} $M_\odot$, respectively. The baryonic

[1] https://fire.northwestern.edu/

mass resolution for the `m11's` ranges from m_b = 2000-10000 $M_\odot$ depending on the individual M_{halo} at $z = 0$, while is fixed at 6×10^4 $M_\odot$ for `m12's` and 3×10^5 $M_\odot$ for `m13's`, respectively.

These are all fully-dynamical, cosmological zoom-in, magnetohydrodynamic galaxy formation simulations capable of evolving radiation and feedback from star formation and evolution, in addition to detailed thermo-chemical properties of gas with "live" CR spectra. These simulations are run with the `GIZMO`[2] code, in the mesh-free finite-mass mode. All simulations include MHD as treated in Hopkins and Raives (2016) and Hopkins (2016), and fully-anisotropic Spitzer-Braginskii conduction and viscosity (Hopkins, 2017; Su, Hopkins, Hayward, et al., 2017).

Galaxy formation from cosmological initial conditions at redshifts $z \gtrsim 100$ including both dark matter and baryons (in gas and stars) occurs self-consistently, with magnetic fields amplified from arbitrarily small trace seed fields at $z \approx 100$, and phase structure and thermo-chemistry in galaxies naturally emerging from cooling with temperatures $T \sim 1 - 10^{10}$ K and self-gravity. Star formation occurs in self-gravitating, Jeans unstable gas with converging flows (or diverging slowly compared to the free-fall/star-formation timescale) on resolved scales. Those stars then influence the medium in turn via their injection of radiation fully-coupled to multi-band (EUV/FUV/NUV/OIR/FIR) radiation transport, stellar mass-loss, and both Type Ia and core-collapse SNe explosions (determined consonantly with up-to-date, standard stellar evolution models). We note that the locally-extincted approximation used for the multi-band radiation transport is too coarse-grained in spectral resolution for the purposes of observational comparison in this chapter, hence we compute the detailed FIR properties in post-processing.

Major updates in these simulations from the FIRE-2 code version (Hopkins, Wetzel, Kereš, et al., 2018) include updated explicit cooling functions and stellar evolution tracks, resulting in a better-resolved cold ISM phase, as well as a "velocity-aware," more conservative coupling of the terminal SNe ejecta momentum (representing unresolved work in an unresolved phase of SNe evolution) to surrounding gas (see Hopkins, Wetzel, Wheeler, et al., 2023; Hopkins, 2024, for details and discussion). The primary change of interest here resulting from this feedback coupling is that galaxies with halo mass (M_{halo}) $\gtrsim 10^{11} M_\odot$ have lower stellar masses compared to FIRE-2. We do not anticipate this to significantly affect the results presented here,

[2]GIZMO is publicly available at http://www.tapir.caltech.edu/~phopkins/Site/GIZMO.html.

Model	AGN	$\epsilon_{\rm CR}^{BH}$	$\nu_{\rm CR}$ [s^{-1}]
noAGN+κ_{const}	×	×	$10^{-9}\,\beta_{\rm CR}\,{R_{GV}}^{-0.6}$
AGN+κ_{const}	✓	3×10^{-4}	$10^{-9}\,\beta_{\rm CR}\,{R_{GV}}^{-0.6}$
AGN+κ_{var}	✓	1×10^{-3}	$\propto S_{\pm}/\Gamma_{\pm} \sim v_A^3/\Gamma_{\pm}\ell_A$

Table 5.1: **Model properties** for the FIRE-3 simulations analyzed in this chapter, specifically the BH CR injection efficiency and the treatment of CR scattering. Two models include AGN feedback (with mass loading $\dot{M}_{\rm wind} = \dot{M}_{\rm BH}$, kinetic wind velocity $v_{\rm wind}$ = 3000 km s^{-1}, kinetic energy loading $5 \times 10^{-5}\ \dot{M}_{\rm BH}c^2$, radiative efficiency $\epsilon_{\rm r}^{\rm BH}$=0.1), but with two different models for the CR scattering rate (which determines the emergent 'streaming' or 'diffusion' speeds. One model does not include AGN feedback and uses the simple power-law scaling for the CR scattering rate.

tending to move galaxies *along* the FRC at a given M_*, but we caution that future work referring to FIRE-3 may incorporate a different terminal SNe momentum coupling.[3]

Our sample contains cosmological realizations of 22 unique halos whose halo, morphological, and merger histories are outlined in Hopkins, Wetzel, Kereš, et al. (2018), Hopkins, Chan, Garrison-Kimmel, et al. (2020), Wellons et al. (2023), and Byrne et al. (2024). These are analyzed for three different physics variations delineated in Table 5.1, and we discuss the relevant physics parameters varied and their implementations below.

We stress that our sample is not selected to be cosmologically representative, and so it is entirely possible that our results may under-/over-predict the true intrinsic scatter compared to the "true" FRC owing to under-/over-sampling regions of cosmological parameter space in halo merger/growth histories and larger-scale (L ≥ 10 Mpc, beyond the high-resolution Lagrangian volume) cosmological environments. However, our results robustly illustrate the effect of differing models for CR and AGN feedback physics in paths leading to and shaping the $z = 0$ FRC, which is the scope of this work.

Cosmic Ray Physics

In the simulations used in this study, we follow CR protons and electrons from MeV to TeV energies. The CR physics is directly coupled to the dynamics, with CRs propagating along magnetic field lines according to the fully general CR transport

[3] Which, our preliminary results show, could affect galaxy stellar mass, producing massive galaxy stellar masses similar to that of FIRE-2.

equations (see Hopkins, Squire, and Butsky, 2022; Hopkins, Butsky, Panopoulou, et al., 2022, for details of the methodology), and self-consistently includes adiabatic/convective/turbulent terms, diffusive re-acceleration, streaming/gyro-resonant loss, Coulomb, ionization, hadronic and other collisional, radioactive decay, annihilation, Bremstrahhlung, inverse Compton (IC), and synchrotron loss terms. Hadronic losses for CR protons are assumed to be dominated by the proton-proton interaction, with total pion loss rates following Mannheim and Schlickeiser (1994) and Guo and Oh (2008) and those of Evoli et al. (2017) for antimatter.

CRs are injected with a power-law spectrum in momentum at SNe (Types Ia & II) and stellar winds (OB/WR) to neighboring gas cells with fixed fractions $\epsilon_{\rm CR}^{\rm inj} = 0.1$ and $\epsilon_{\rm e}^{\rm inj} = 0.002$ of the initial ejecta kinetic energy going into CRs (protons) and leptons (electrons), motivated by theoretical and observational studies on the efficiency of diffusive-shock acceleration (Caprioli, 2012; Yuan, Liu, and Bi, 2012). For the CR modeling, all quantities needed to compute the fully non-equilibrium CR dynamics and losses are captured in-code, except for the microphysical CR scattering rate as a function of rigidity $\nu_{\rm CR}(\rm R_{GV})$, where $\rm R_{GV}$ is the rigidity in gigavolts of a given CR bin ($\rm E_{CR}/q$), which ultimately drives (non-linearly via the dynamical equations) the effective diffusion and/or streaming speeds of the CRs. We utilize 8 (11) bins for CR protons (electrons) from MeV - TeV energies. As noted in Appendix C.3.2 of Hopkins, Butsky, Panopoulou, et al. (2022, and references therein), for this range of energies, ∼10 bins are enough to both efficiently and robustly model the self-consistent integration of the CR spectra.

For $\nu_{\rm CR}(\rm R_{GV})$, we explore two model variations. One follows standard practice in CR-MHD galaxy simulations and assumes a spatially and temporally constant scaling for the scattering rate as a function of CR rigidity $\nu_{\rm CR} \sim 10^{-9} \beta_{\rm CR}\, (\rm R_{GV})^{-0.6}\ s^{-1}$ where $\beta_{\rm CR} = v_{\rm CR}/c$ as in (Hopkins, Butsky, Panopoulou, et al., 2022), calibrated explicitly therein to fit all of the observations of CRs in Milky-Way Solar-Circle like conditions from observations such as Voyager, AMS-02, and Fermi. This corresponds roughly in the diffusive limits to an anisotropic/parallel diffusivity $\kappa_{\parallel} \sim v_{\rm CR}^2/3\nu_{\rm CR} \sim 3\times10^{29}\, \beta_{\rm CR}\, R_{\rm GV}^{0.6}\ {\rm cm^2\ s^{-1}}$ (so e.g. the effective isotropic diffusivity or streaming speed of ∼ GeV CR(e)s is $D_{xx} \sim 7\times10^{28}\ {\rm cm^2\ s^{-1}}$ or $\sim 100\ {\rm km\ s^{-1}}$) with anisotropic streaming, advective transport and diffusive re-acceleration automatically included self-consistently via the full non-equilibrium CR flux and energy transport equations (as distinct from e.g. common pure-diffusion, pure-streaming, or Fokker-Planck type equations). We denote simulations which use this CR transport

model hereafter with $\kappa_{\rm const}$.

We also explore an alternative CR transport model which varies $\nu_{\rm CR}$ (and therefore the predicted diffusive and streaming speeds), motivated in principle by so-called "extrinsic turbulence" theory (Jokipii, 1966) as presented in Hopkins, Squire, Butsky, and Ji (2022) but with an additional modified driving term at gyroresonant scales in the sub-grid scattering prescription in order to produce reasonable $\nu_{\rm CR}(R_{\rm GV})$, resulting in observables in agreement with the constraints mentioned above for $z = 0$ Milky-Way Solar-Circle like conditions. These runs are labeled as $\kappa_{\rm var}$.

In our $\kappa_{\rm var}$ model, we utilize an empirically-motivated driving term[4] $S_{\pm}$, given by fitting CR observables such as different MeV-TeV primary and secondary spectra, B/C, proton-to-antiproton and positron-to-electron as well as radioactive isotope ratios. This driving term scales dimensionally with plasma properties proportional to the turbulent magnetic dissipation rate $\sim v_A^3/\ell_A$ in terms of the Alfven speed and turbulent Alfven scale ℓ_A, akin to classic "extrinsic turbulence" type models for CR scattering (Jokipii, 1966), though the normalization and wavelength/scale-dependence is quite different from those classic models as required by the observations (see discussion in Hopkins, Squire, Butsky, and Ji, 2022, Section 5.3.3).

Supermassive Black Hole/AGN Physics

Many of the simulations explored in this chapter include black holes (BHs), with seeding, dynamics, accretion, and feedback physics described extensively in Wellons et al. (2023) and Hopkins, Wetzel, Wheeler, et al. (2023). BHs are randomly seeded from star-forming gas preferentially at high surface densities and low metallicites, and are permitted to merge if sufficiently close and gravitationally bound. Accretion from the ISM into the BH accretion reservoir is continuous with an accretion efficiency parameter calibrated from much higher-resolution simulations on smaller scales than resolved here that represent the effects of 'gravitational torques' driving accretion (Anglés-Alcázar, Quataert, et al., 2021), and flows from the accretion reservoir onto the BH on a depletion timescale motivated by a Shakura and Sunyaev (1973) α-disk.

Feedback from BHs consistently follows radiative, mechanical (kinetic), and CRs in the form of relativistic jets coupled to the general CR-MHD solver beyond the BH accretion kernel scale.

[4] $S_{\pm,\,ext} = (v_{A,\,\rm ideal}/0.007\,c)\,(v_{A,\,\rm ideal}/\ell_A)\,(k_\parallel\,\ell_A)^{-1/6}\,u_{\rm B}$

Radiative feedback is given by the accretion disc emitting a bolometric luminosity of

$$\dot{E}_{\rm rad}^{\rm BH} \equiv L_{\rm bol} = \epsilon_r^{BH} \dot{M}_{\rm BH} c^2 \tag{5.1}$$

with $\epsilon_{\rm r}^{\rm BH} = 0.1$ and the total photon momentum flux given by $\dot{p}_{rad} = L_{\rm abs}/c$, where $L_{\rm abs}$ is the photon luminosity absorbed by a given gas element. This radiative feedback is injected at the BH kernel location and transported according to the same locally extincted RHD approximation as the radiative feedback from stars (Hopkins, Grudić, et al., 2020).

Non-relativistic mechanical feedback in the form of outflows from the accretion disc are modeled using a hyper-refinement particle-spawning scheme with particle resolution ~1000 times higher (lower mass) than the typical gas cell in the simulation in order to effectively capture reverse shocks, and are de-refined when fully mixed with the ambient surrounding gas. These outflows have initial positions and velocities aligned with the spin axis of the BH, with kinetic wind velocities $\rm v_{wind}$ = 3000 km $\rm s^{-1}$ and mass-loading $\dot{M}_{\rm wind,BH} = \dot{M}_{\rm BH}$ which yield a kinetic energy loading $\dot{E}_{\rm wind}^{\rm BH} \approx 5 \times 10^{-5}\ \dot{M}_{\rm BH} \rm c^2$.

Since all of the simulations including BHs here also consider CR feedback, we model relativistic mechanical feedback in the form of jets by injecting CRs to the hyper-refined mechanical feedback cells, with injection properties identical to stellar CRs up to the injection efficiency, which is given by

$$\dot{E}_{\rm CR}^{\rm BH} \equiv \epsilon_{\rm CR}^{\rm BH} \dot{M}_{\rm BH} c^2 \tag{5.2}$$

with fiducial $\epsilon_{\rm CR}^{\rm BH} = 3 \times 10^{-4}$ for $\kappa_{\rm const}$ runs and $\epsilon_{\rm CR}^{\rm BH} = 10^{-3}$ for $\kappa_{\rm var}$ runs.

For all three feedback channels, the equivalent rest mass energy is removed from the accretion reservoir of the BH particle, without the inclusion of a BH mass limit or further accretion dependence. The choices of accretion energy conversion efficiencies are motivated by extensive parameter studies in Wellons et al. (2023) for models capable of reproducing galaxies which are reasonable on various population-wide scaling relations, as well as more detailed observational constraints (Byrne et al., 2024). In particular, the accretion conversion efficiency to cosmic rays differs between the two cosmic ray transport models because the variable transport model required a slightly higher value (holding all other efficiencies the same) to produce

reasonably quenched massive galaxies ($M^{z=0}_{\rm halo} \gtrsim 10^{13} M_\odot$) within the allowed uncertainties of the M_{BH}-σ, M_*-M_{halo}, and star-forming main sequence relations.

Simulation Post-Processing

For our fiducial results, we center the galaxies on the stellar center-of-mass and orient the galaxies to be face-on with the angular momentum of the neutral gas as the $\hat{z}$ axis. All vector fields (**r**, **B**, **v**) are transformed accordingly.

The production of the subsequent images is done after selecting all star and gas particles with positions $|x|$, $|y| \leq 0.15$ R_{200} and $|z| \leq 200$ kpc, and all images are generated at a 50 pc/pixel resolution.

We heavily emphasize that for both our radio continuum and far-infrared images, we do not include any template spectrum for the emission arising from the AGN for simulations including BHs as these vary widely with BH mass, inclination angle, and accretion rate, and would be sensitive to radiative properties on scales far below our resolution limit here. All AGN feedback modes included in the simulations are described in the above sections, and any ensuing effects on the radiative properties arise solely from the physical coupling of the radiative, kinetic, and mechanical feedback to gas.

Thus, the influence of AGN feedback on our results is in a more *indirect* manner owing to its interplay with ISM/CGM cooling and dynamics and cosmological galaxy-formation physics from the deposition scale of the BH interaction kernel ($\sim$ 10 pc from the BH itself) on the surrounding gas, which is of $\gtrsim$ pc resolution rather than through "direct" contributions via disk-, cocoon-, or jet-dominated radio/FIR emission.

Radio Continuum Emission

For the computation of the optically thin, non-thermal radio emission from our simulations, we follow the same exact procedure as in Ponnada, Panopoulou, Butsky, Hopkins, Skalidis, et al. (2024), where for each gas cell in our simulations, synchrotron emissivities are calculated from the internally evolved CRe spectra, $j_e(E)$, and components of the magnetic field perpendicular to the line of sight for a given galactic orientation, $\mathbf{B}_\perp$.

Then, we compute the critical frequency of emission for each spectral bin of CRe,

$$\nu_c(B_\perp, E) = \frac{3eB_\perp}{4\pi m_e c} \left(\frac{E}{m_e c^2}\right)^2 \tag{5.3}$$

where m_e is the electron mass, and c is the speed of light. We then compute the specific emissivities of each gas cell by integrating over j_e to determine the contribution from each energy bin at a given frequency, and finally produce Stokes I by integrating these specific emissivities along the line of sight using a projection routine first described in Hopkins, Hernquist, et al. (2005). Synchrotron self-absorption is not modeled as it is unimportant for radio continuum emission from galaxies at low brightness temperatures, though may be important for AGN jet template spectra not included here (Condon, 1992).

Far-Infrared Images

The production of the far-infrared images follows the procedure of Cochrane, Hayward, Anglés-Alcázar, Lotz, et al. (2019), Cochrane, Hayward, Anglés-Alcázar, and Somerville (2023a), and Cochrane, Anglés-Alcázar, et al. (2023b), using the radiative transfer code SKIRT[5] Version 8 (Baes et al., 2011; Camps and Baes, 2015). Predictions for the rest-frame ultraviolet (UV) to far-infrared (FIR) wavelengths are generated from the particle cut specified above. We assume a constant dust-to-metals ratio (D/Z) of 0.4 (Dwek, 1998), with metallicity evolved for each gas cell self-consistently, and dust destruction at $T > 10^6$ K (Draine and Salpeter, 1979) for a graphite, silicate, and PAH dust mixture following the Weingartner and Draine (2001) Milky Way dust model. We caution that the assumption of constant D/Z may not hold for dwarfs (Rémy-Ruyer et al., 2014; Choban et al., 2024), which may move them to slightly lower FIR luminosities. The SEDs and IMFs of Bruzual and Charlot (2003) are adopted for star particles, depending on their ages and metallicities.

The radiative transfer calculation is done using 10^6 photon packets on an octree dust grid where cell sizes are adjusted by the dust density distribution, constrained such that no dust cell may contain great than 10^{-4} per cent of the galaxy's total dust mass, and outputs global galaxy spectral energy distributions (SEDs) and images at the same fiducial pixel resolution. For extensive convergence tests of these parameter choices for our simulations, we refer the reader to the appendices in Cochrane, Hayward, Anglés-Alcázar, and Somerville (2023a).

Synthetic-Observational Sample Selection

We select all snapshots with $L_{60\mu m} \geq 10^{7.5}$ $L_\odot$ and $L_{1.4GHz} \geq 10^{18.5}$ W m^{-2} as a synthetic-observable parameter space to correspond roughly to the luminosity

[5] http://www.skirt.ugent.be

limits of observational studies of the $z = 0$ FRC. As a result, the majority of of our mock-observed "detections" draws from snapshots of relatively more massive halos ($M_{halo}^{z=0} \gtrsim 5 \times 10^{11}$ $M_\odot$), though lower mass halos populate the mock-observed space at low-$L_{60\mu m}$($\lesssim 10^{9.5}$ $L_\odot$). Since some of our simulation suite has snapshots sampled at higher time resolution (typically for the higher-resolution, $m_b = 2 \times 10^3$ - 10^4 $M_\odot$, `m11's` classical to intermediate dwarf galaxy simulations), we down-sample those to the same time sampling as the more sparsely snapshot sampled simulations to avoid biasing our conclusions. In total, we analyze over 8750 simulation snapshots for this work, with ~3100 snapshots meeting the mock-observational selection criteria, which is reduced to 1375 after the down-sampling of high time-resolution runs.

Finally, we invoke an additional cut in order to exclude snapshots that might plausibly be overly-contaminated by AGN accretion activity for our runs including BHs: we remove those which have $\frac{L_{bol}^{AGN}}{30} > {L_{60\mu m}}^{stars}$, where $L_{AGN}^{bol} \equiv 0.1\, \dot{M}_{BH} c^2$ is the AGN bolometric luminosity used in-code, and ${L_{60\mu m}}^{stars}$ is the stellar luminosity at 60 μm predicted by our radiative transfer post-processing without including any AGN. The factor of 30 accounts for the typical bolometric correction for typical type I (broad-line) quasars at this same wavelength (Richards et al., 2006).

In other words, we remove any snapshot where we would expect the AGN to potentially dominate the FIR luminosities we will study, as they would be removed in observational samples. This amounts to just 53 snapshots in our synthetically-observed sample (~3.5% of the total), and this selection cleans our sample from AGN contamination in the regime where AGN are expected to dominate the FIR as well as the radio continuum, given the observed normalization of the FRC for AGN (Kruit, 1971; Jong et al., 1971; Delhaize et al., 2017). Our results are not particularly sensitive to this cut at all, let alone to the precise ratio of luminosities used for the cut above.

In Figure 5.1, we show an illustrative example of the multi-wavelength image generation done for all of the simulated galaxies in our sample from radio to optical/UV frequencies. The synthetically-observed SEDs are similar in shape and normalization to those observed (Smith et al., 2012; Tabatabaei et al., 2017).

5.4 The Far-Infrared Radio Correlation on FIRE

The FRC from $z = 5$ to $z = 0$ for the synthetic observations described in Section 5.3 is shown in Figure 5.2. Since there is qualitatively little evolution in the FRC across this redshift range for the sample selected, we plot all the synthetic observations

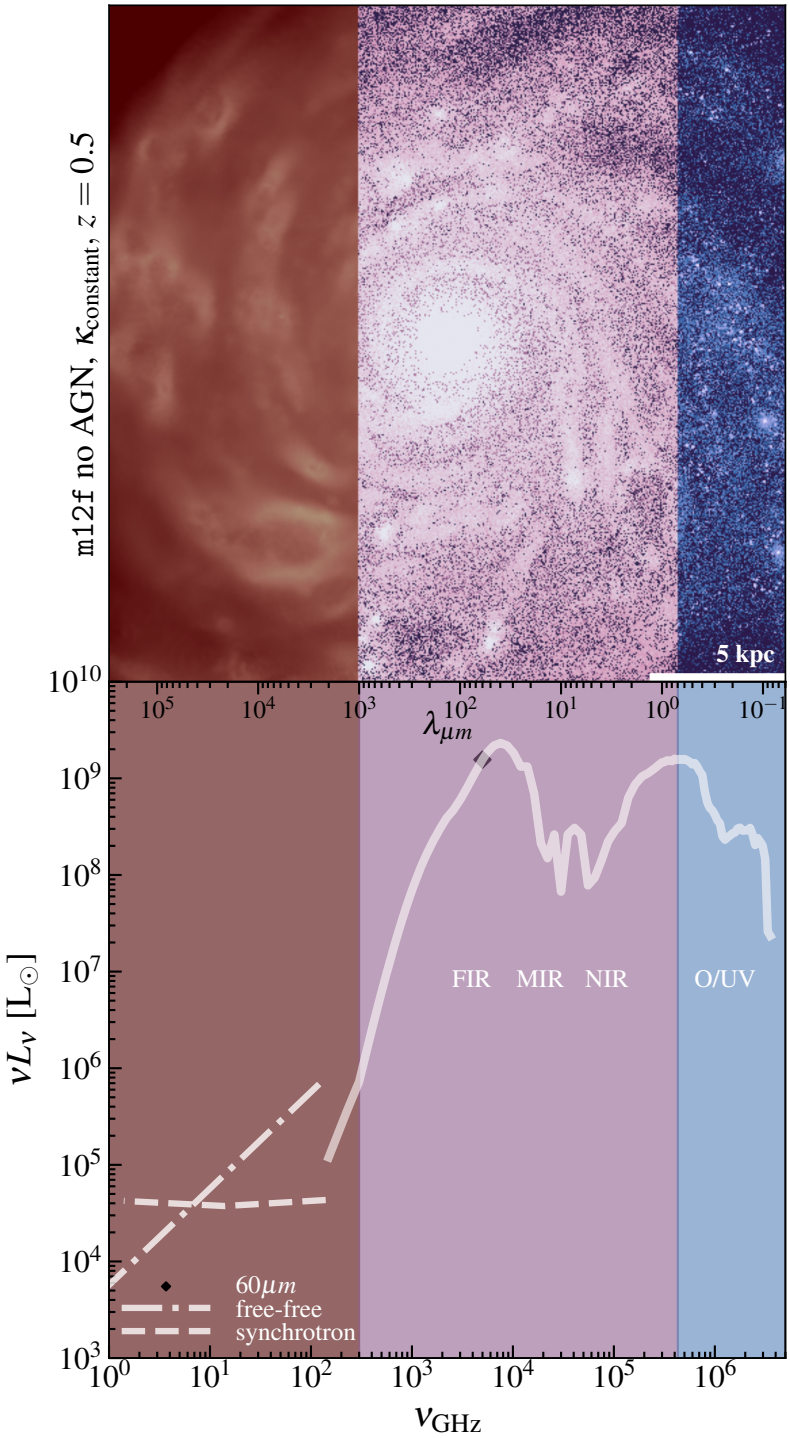

Figure 5.1: *Synthetic observations from radio to UV:* **Top**: radio continuum image at 140 MHz (**left**) generated from the procedure in Section 5.3, FIR image at $60\mu m$ (**center**), and FUV image at 150 nm (**right**), both generated using `SKIRT` (Camps and Baes, 2015) with procedure described in Section 5.3 for `m12f`, a Milky-Way-like simulated galaxy at $z = 0.5$. **Bottom**: Corresponding SED (νL_ν) in $L_\odot$ from 1.4 GHz to 85 nm, with optical/UV to FIR (solid), thermal free-free radio (dot-dashed), and non-thermal synchrotron (dashed) emission computed directly from self-consistently evolved magnetized gas, stellar, and CR properties. Our synthetic SEDs bear remarkable similarity to those observed across over six orders-of-magnitude in frequency/wavelength space.

together in the left panel, and show the redshift evolution of the FIR-radio flux ratios in the right panel.

Here, we compare the equivalent synthetic-observational quantities to those of Yun, Reddy, and Condon (2001) (hereafter Y01). Namely, we utilize the definition of the flux ratio of the 60-100μm FIR emission to 1.4 GHz radio emission, hereafter denoted as $q_{Y_{01}}$: $q_{\rm Y01} = \log_{10}(\frac{\rm FIR}{3.75\times10^{12}\,W\,m^{-2}}) - \log_{10}(\frac{S_{1.4\ \rm GHz}}{W\,m^{-2}\,Hz^{-1}})$, where FIR is defined as FIR $\equiv 1.26\times10^{-14}(2.58\,S_{60\,\mu m} + S_{100\,\mu m})$ W m^{-2}, and $S_{1.4\ \rm GHz}$ and $S_{60,100\mu m}$ are the flux densities in units of W m^{-2} and Jy, respectively.

We note that these frequencies/wavelengths are frequently studied in the literature in part as free-free contributions typically do not dominate the radio spectrum at 1.4 GHz, and 60-100 μm is typically close to the peak of dust emission, where K-corrections may not be as significant (see Figure 5.1). Though, the choice of K-correction may be important for the total FIR-radio correlation, which utilizes the integrated 8-1000μm emission. Those quantities may be more sensitive to dust temperature changes that may bias emission significantly at shorter wavelengths and be affected by limited observational constraints at higher z for the 'true' dust temperature (Liang et al., 2019), in addition to post-starburst effects (Hayward et al., 2014). We leave the exploration of those effects to future work.

From close inspection of Figure 5.2, a few important results are apparent:

1) The $z \approx 0$ snapshots, regardless of physics variation, approach the observed values of $q_{Y_{01}}$, though with larger scatter in the runs including AGN, particularly in AGN+κ_{const} runs.

2) The FIRE-3 simulations, at all redshifts sampled, regardless of physics variation (noAGN+κ_{const} , AGN+κ_{const} , AGN+κ_{var}) roughly lie along a linear FRC at high $L_{60\mu m}(\gtrsim 10^{9.5})$, and shift to a slightly super-linear relation at low $L_{60\mu m}(\lesssim 10^{9.5})$, particularly at higher redshifts ($z \gtrsim 1.5$).

3) There is little evolution in $q_{Y_{01}}$ with z, as galaxies approach the $z = 0$ FRC, with the mean value of $q_{Y_{01}}$ evolving by ~1 dex from the $z = 4$ value to the $z = 0$ value in the noAGN+κ_{const} , and by ~0.5 dex in the AGN+κ_{const} and AGN+κ_{var} runs.

The overall scatter in our FRC arises not solely from variation on short ($\lesssim$ 100 Myr) timescale variations in SFH near peak SF for the more massive `m12's and `m13's (Feldmann, Quataert, Hopkins, et al., 2017), or from late-time bursty star formation/'breathing modes" in the less-massive `m11's (Muratov et al., 2015; Sparre et al., 2017), but from a combination of such effects and significant galaxy-to-galaxy

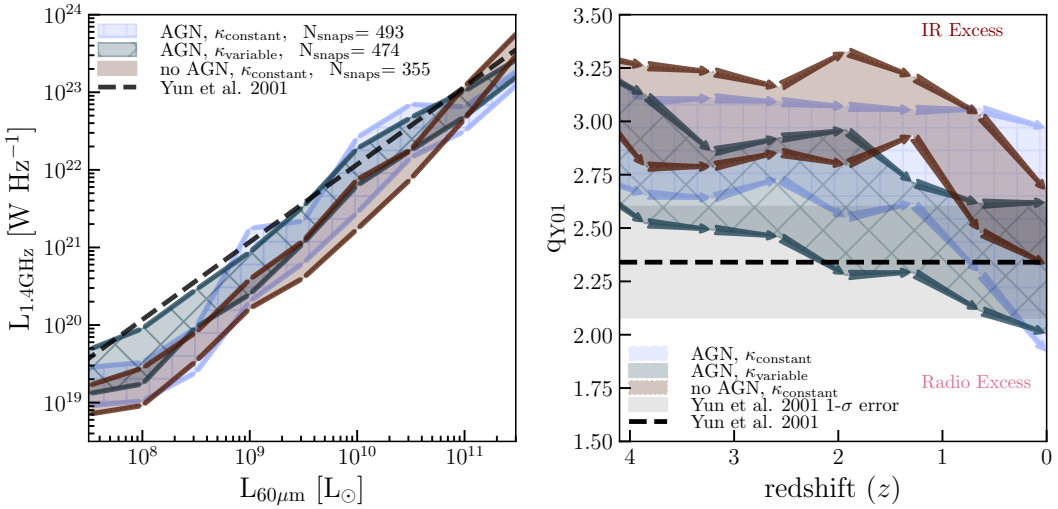

Figure 5.2: *The FRC for FIRE-3 simulations from z=0-5.* **Left:** $L_{1.4GHz}$ vs. $L_{60\mu m}$ for all snapshots analyzed in this study, with noAGN+κ_{const} , AGN+κ_{const} , AGN+κ_{var} in brown with no hatching, light blue with square hatching, and navy with diamond hatching, respectively, with the observed $z = 0$ relation of (Yun, Reddy, and Condon, 2001) for star-forming galaxies shown as the black dashed line. Hatched and shaded regions show the 32-68 percentile (approximate $\sim 1\sigma$) confidence intervals for equally spaced bins in $L_{60\mu m}$, with line segments demarcating bins. Regardless of physics variation (AGN vs. no AGN, $\kappa_{\rm const}$ vs. $\kappa_{\rm var}$), our simulations generally match the observed z=0 correlation at high $L_{60\mu m}$($L_{60\mu m} \geq 10^{9.5}$ $L_\odot$), with a weakly super-linear relation at low $L_{60\mu m}$($L_{60\mu m} \leq 10^{9.5}$ $L_\odot$) arising from a transition to super-linear $L_{\rm IR}$-SFR and $L_{1.4\ \rm GHz}$-SFR correlations. **Right:** $q_{Y_{01}}$ vs. redshift for the same snapshots as the left, here shown in equally-spaced redshift bins, with arrow segments demarcating bins. While all physics variations reach the observed $z = 0$ value of $q_{Y_{01}}$ on average, the evolution of $q_{Y_{01}}$ and its scatter varies with redshift owing to the interplay of AGN and CR transport physics, which is broken down further in Figure 5.4.

variation. We confirm this by examining each individual FRC for every simulated galaxy in our mock-observed sample.

The evolution of the scatter at low-z, however, is further modulated by an interplay of AGN and CR feedback, which we further detail in Figure 5.4, where we break down the total sample in $q_{Y_{01}}$ vs. z space by halo mass groupings and physics variation. Examining Figure 5.4 reveals that even without inserting a 'radio-loud' AGN spectrum by-hand, several of our snapshots for the `m12's` and `m13's` populate the 'radio excess' synthetic-observational parameter space, though not through the mechanism of a 'radio-loud' synchrotron jet beamed towards the observer at $z \lesssim 1.5$. This effect appears to be most pronounced for the `m12's`, with the systematic differ-

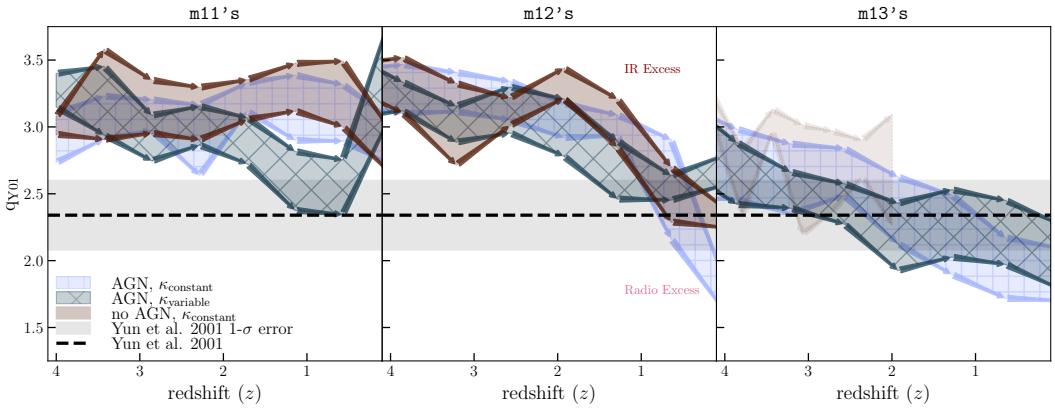

Figure 5.3: *FRC evolution with redshift by galaxy mass* shown by $q_{Y_{01}}$ vs. z with the same style as Figure 5.2, here grouped by $M_{\rm halo}^{z=0} \sim 3 \times 10^{10}$– 7×10^{11} $M_\odot$ (`m11's`, **left**), 7×10^{11} - 1.5×10^{12} $M_\odot$ (`m12's`, **middle**), and 5×10^{12} - 10^{13} $M_\odot$ (`m13's`, **right**). A slight systematic difference emerges in $q_{Y_{01}}$ vs. z between the AGN+κ_{const} and AGN+κ_{var} variants at moderate redshifts, and the AGN+κ_{const} sample exhibits a larger scatter at z=0 with a significant tail of "radio-excess" objects, particularly at the `m12` and `m13` mass scales, owing to longer-lived synchrotron halos arising from Type Ia SNe and BH accretion in quenching galaxies.

ence between the AGN+κ_{const} and AGN+κ_{var} model variants being most apparent at late times, however it also appears, albeit to a lesser extent, in the evolution of the `m13's`. The less massive `m11's`, on the other hand, populate the upper envelopes of the scatter in $q_{Y_{01}}$ vs. z at late times, although examination of individual galaxy FRCs for the more massive `m11` dwarf galaxies reveals similar behavior to the `m12's`.

These results reflect the first forward-modeled reproduction of the observed $z = 0$ FRC across a wide gamut of galaxy properties using cosmological zoom-in simulations of galaxies with on-the-fly, dynamically evolved CR spectra. Simultaneously, our results illustrate a diversity of paths leading to the $z = 0$ FRC across cosmic time owing to CR transport and AGN feedback physics, which we describe in detail below.

Calorimetry & Conspiracy Continue

The quasi-universality of $q_{Y_{01}}$ vs. z indicates a rough balance between the dominant synchrotron intensity-weighted CRe loss rate and UV escape for much of the evolutionary history of our simulated galaxy sample. This indicates a simple explanation for the evolution of the FRC from $z = 5 \rightarrow 0$: in the standard picture of star-formation-limited CRe and UV calorimetry (Voelk, 1989; Lacki, Thompson, and Quataert, 2010), in order to maintain a constant value of $q_{Y_{01}}$, the galaxies must

either be effective CRe and UV-calorimeters (where the synchrotron loss rate is far greater than other relevant loss rates and UV emission is effectively reprocessed) or the synchrotron cooling rate must fall at a similar rate to the UV optical depth (often called 'conspiracy' models in the literature).

We see calorimetry to be generally the case at high $L_{60\mu m} \geq 10^{9.5}\,L_\odot$ (or equivalently at higher galaxy-averaged SFRs, $\Sigma_{\rm gas}$, or $\Sigma_{\rm SFR}$ as often parameterized in one-zone models and other works), irrespective of redshift, with the galaxies with highest $L_{60\mu m}$corresponding to effective UV and CRe (and CR proton)[6] calorimeters (also called the 'high-$\Sigma_{\rm gas}$ conspiracy' Lacki, Thompson, and Quataert 2010).

However, despite this constancy of $q_{\gamma_{01}}$, a large fraction of our synthetic observations populates the 'IR-excess' parameter space, particularly for noAGN+κ_{const} runs at higher redshifts ($z \gtrsim 1.5$). This does not indicate excessive FIR emission, but rather a greater super-linear deviation from radio continuum-SFR calorimetry (Condon, 1992) than from FIR-SFR calorimetry (Kennicutt, 1998) for our sample between $z \sim 5 \rightarrow 1.5$, and so are better understood as 'radio-dim' objects at higher redshifts.

We confirm this by examining the 10 Myr-averaged SFRs at each snapshot in comparison to the literature calorimetric relations of Condon (1992) and Kennicutt (1998) for all of our synthetic observations in Figure 5.4. The larger relative loss of radio-emitting CRe compared to UV-emitting photons arises from a relatively ubiquitous prediction for our low-$L_{60\mu m}$ simulated galaxies across our physics model variations, which comprise a larger fraction of our sample with increasing redshift (as `m11's and `m12's have rising star-formation histories (SFHs) with time), wherein the dominant loss rate of synchrotron-emitting CRe increases faster than the dust opacity to UV radiation decreases.

This is not wholly unexpected from observations, as recent studies exploring the $L_{\rm IR}$-SFR (Bonato et al., 2024) have found a transition to increasingly super-linear $L_{\rm IR} \propto {\rm SFR}^{\alpha}$ at low total IR 8-1000μm luminosities ($L_{\rm TIR} \lesssim 10^{10} L_\odot$ or SFRs $\lesssim 1\,M_\odot\,{\rm yr}^{-1}$, with $\alpha \gtrsim 1.25$ and increasing with lower $L_{\rm TIR}$, as the obscured SFR fraction decreases at lower galaxy masses (Hayward et al., 2014; Whitaker et al.,

[6]For the simulations in this chapter, we do not separately evolve secondary-vs-primary electrons in snapshot outputs or include an explicit positron population as in (Hopkins, Butsky, Panopoulou, et al., 2022; Ponnada, Panopoulou, Butsky, Hopkins, Skalidis, et al., 2024). Instead secondary CRes (e.g. from pionic decay via CR proton hadronic losses) are directly added to the separately evolved CRe bins in-code. So we cannot directly comment on the secondary contribution, but this channel of CRe production is likely increasingly important at higher z as bremsstrahlung losses become important for CRe (Lacki, Thompson, and Quataert, 2010; Werhahn, Pfrommer, and Girichidis, 2021).

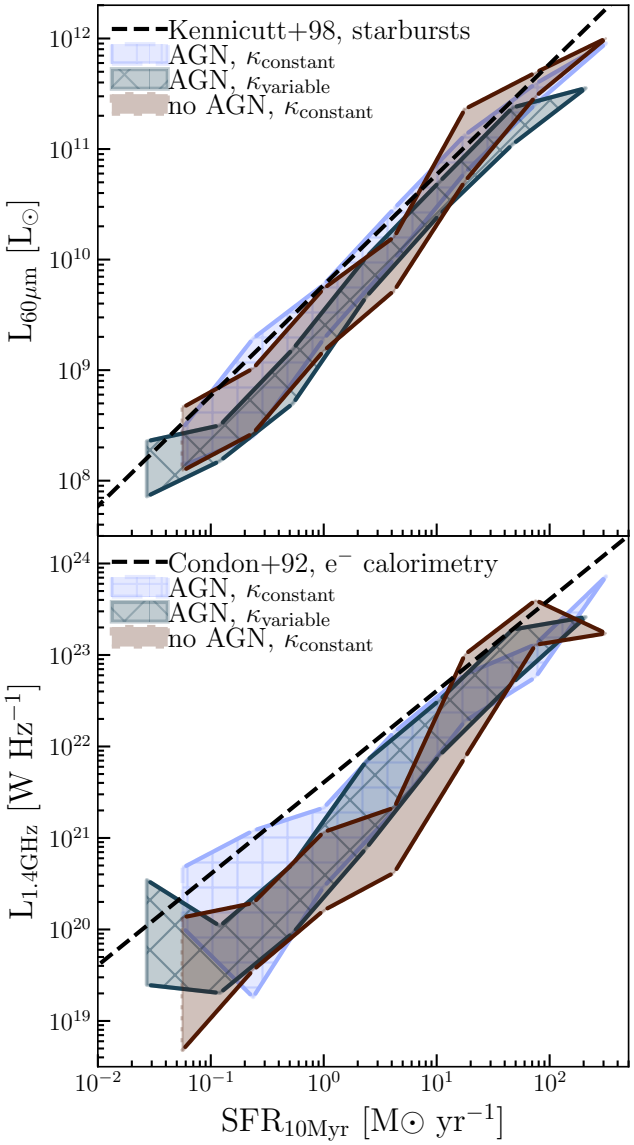

Figure 5.4: *Calorimetry & Conspiracy:* $L_{60\mu m}$ (**top**) and $L_{1.4GHz}$ (**bottom**) vs. 10-Myr averaged SFRs for snapshots from noAGN+κ_{const}, AGN+κ_{const}, and AGN+κ_{var} suites in brown with no hatching, light blue with square hatching, and navy with diamond hatching, respectively. Shaded regions show the 32-68 percentile (approximate $\sim 1\sigma$) confidence intervals and line segments demarcate bins. Expected calorimetric relations for the IR with SFR from starbursts (Kennicutt, 1998) and CRe calorimetry at 1.4 GHz (Condon, 1992) are shown in black dashed lines. Across all physics variations, our simulations generally approach calorimetric expectations at high $L_{60\mu m}$($L_{60\mu m} \geq 10^{9.5}$ $L_\odot$), with super-linear relations at low $L_{60\mu m}$($L_{60\mu m} \leq 10^{9.5}$ $L_\odot$) (or low $\Sigma_{\rm gas}$) owing to lower UV optical depths and high $\tau_{\rm diff}^{-1}/\tau_{\rm synch}^{-1}$ in weaker on average $\mathbf{B}_\perp$. At low SFRs (≤ 0.5 $M_\odot yr^{-1}$), our runs with AGN more often exhibit 'super-calorimetric' behavior in $L_{1.4GHz}$ with scatter extending beyond the 'calorimetric' relation, particularly at SFRs $\lesssim 0.1$ $M_\odot yr^{-1}$ owing to late-time contributions of CRs from Type Ia SNe and BH accretion in quenching galaxies.

2017). Similarly, stacking analyses of spiral galaxies have found even steeper best-fit 1.4 GHz radio-UV+TIR-estimated SFRs for galaxies with $M_* \leq 10^{10.5}$ $M_\odot$, where $L_{1.4\ GHz} \propto SFR^{\beta}$, where $\beta \sim 1.5$. Together, these trends naturally explain the modest hints of non-linearity in the FRC at low luminosities, with $q_{Y_{01}}$ increasing with decreasing $L_{60\mu m}$(Yun, Reddy, and Condon, 2001; Bell, 2003; Matthews, Condon, et al., 2021), and are in agreement with predictions from previous non-calorimetric one-zone steady-state models (Lisenfeld, Voelk, and Xu, 1996; Lacki, Thompson, and Quataert, 2010).

These trends are consistent with the behavior predicted by our simulations, and explained by examination of the relevant CRe cooling rates. The IC and synchrotron cooling rates are given by the following:

$$\tau^{-1}_{\rm IC,\ synch} = (4/3)\,\sigma_{\rm T}\,\gamma^2_{\rm CRe}\,c\,(u_{\rm rad}, u_{\rm B})/E_{\rm CRe}$$

(Rybicki and Lightman, 1986), where $\sigma_{\rm T}$ is the Thomson cross-section, $\gamma_{\rm CRe}$ is the CRe Lorentz factor, $E_{\rm CRe}$ is the characteristic energy of CRes emitting at the observing frequency[7] for a given gas cell's $\mathbf{B}_\perp$ (typically $\sim$ 0.5-30 GeV at 1.4 GHz), $u_{\rm rad}$ is the radiation energy density given self-consistently from summing all bands followed in our in-code radiation-hydrodynamics approximation in addition to the un-attenuated CMB, and $u_{\rm B}$ is the magnetic field energy density from our explicitly-evolved $\mathbf{B}$. The effective diffusive escape time can be computed as follows:

$$\tau^{-1}_{\rm diff} \sim v^{\rm iso}_{\rm stream}/\ell_{\rm CRe}$$

where $v^{\rm iso}_{\rm stream} \sim \kappa^{\rm iso}_{\rm eff}/\ell_{\rm CRe}$ is the isotropically-averaged effective CRe streaming speed (determined by the CR fluxes in-code, $v_{\rm stream} \sim \langle \mathbf{F}_{\rm CRe} \cdot \hat{g}/e_{\rm CRe}\rangle$ where $\hat{g}$ is the direction of $\nabla e_{\rm CRe}$), around the CRe energies which matter for the synchrotron losses of interest and $\ell_{\rm CRe} \equiv e_{\rm CRe}/\nabla_\parallel e_{\rm CRe}$ is the CRe pressure scale length. For simplicity, since this is order-of-magnitude anyways, we adopt a median $\ell_{\rm CRe} \sim$ kpc for our analysis, but using a variable number like the local disk scale length or galaxy size or median of different cell gradients in the galaxy gives similar results.

Comparing the synchrotron-intensity-weighted averages of the IC and diffusive loss rates for each of the synthetically-observed snapshots shows a general trend of IC

[7]Though note, in detail the emission at a given frequency arises from a *distribution* of energies at a given $\mathbf{B}_\perp$. However, this approximation is satisfactory for the order-of-magnitude comparisons here, despite the detailed forward-modeled emission utilizing multi-bin spectra.

loss rates being roughly similar to the synchrotron loss rates at all $z \lesssim 2$, with $\langle \tau_{\rm IC}^{-1} \rangle_{I_\nu}$ $\sim$ 0.1-3 $\langle \tau_{\rm synch}^{-1} \rangle_{I_\nu}$, rarely exceeding $\sim$ 10, broadly indicating equipartition between $u_{\rm rad}$ and $u_{\rm B}$ in synchrotron-emitting gas at lower redshifts, but $\langle \tau_{\rm IC}^{-1} \rangle_{I_\nu} \sim 10^{-0.5}$ - 10^2 $\langle \tau_{\rm synch}^{-1} \rangle_{I_\nu}$ at $z \gtrsim 2$. Surprisingly, even at higher redshifts where $u_{\rm rad,\,CMB} = 0.26\,(1+z)^4\,{\rm eV\,cm^{-3}}$ becomes large, the average IC loss rate can occasionally be comparable to that of synchrotron losses in dense, strongly magnetized, high synchrotron-emissivity gas! Meanwhile, $\langle \tau_{\rm diff}^{-1} \rangle_{I_\nu} \gtrsim$ 10-10^2 $\langle \tau_{\rm synch}^{-1} \rangle_{I_\nu}$ for low $L_{60\mu m}$ snapshots further off the FRC at all z, but with $\langle \tau_{\rm diff}^{-1} \rangle_{I_\nu} \sim$ 0.1-10 $\langle \tau_{\rm synch}^{-1} \rangle_{I_\nu}$ at high $L_{60\mu m}$, maintaining standard arguments of calorimetry and conspiracy at high and low $\Sigma_{\rm gas}$, respectively. In short, both IC losses and diffusive CRe escape play important roles at $z \gtrsim 2$ in shaping the FRC at the stellar masses/gas surface-densities sampled here, resulting in 'radio-dim' snapshots, whereas at $z \lesssim 2$, diffusive escape becomes the primary competing loss term to synchrotron losses.

Beyond Calorimetry & Conspiracy: 'Hooks', 'Lines', and 'Sinkers'

In Figure 5.5, we show the differing characteristic evolutionary paths of galaxies of the noAGN+κ_{const}, AGN+κ_{const}, and AGN+κ_{var} physics variations, with annotations indicating general behaviors characterizing all models shown in the noAGN+κ_{const} case (*middle panel, solid annotations*). Here, we average groups of galaxies by $z = 0$ halo mass corresponding to `m11's`, `m12's`, and `m13's` binning the synthetic observations meeting our selection criteria by redshift. Thus, the tracks detail temporal as well as galaxy-galaxy scatter.

Upon examining each individual FRC track and comparing to average trends shown here, we are able to characterize some general behaviors of each physics model. While there are some outlier galaxies within each physics variation of our sample, the general tracks of 'hooking' across the FRC to become relatively 'radio-excess' objects at late times in the AGN+κ_{const} case, gradually moving up to the observed FRC with late-time scatter primarily along 'lines' in the noAGN+κ_{const} case, and following similar early-time behavior before 'sinking' further down the FRC line in the AGN+κ_{var} case appear to be robust trends, and qualitatively explain the differences in the normalization and scatter of $q_{Y_{01}}$ presented in Figure 5.4 as a function of z. We expand upon and discuss the physical mechanisms driving these "tracks" and the late-time ($z \lesssim 1.5$) below.

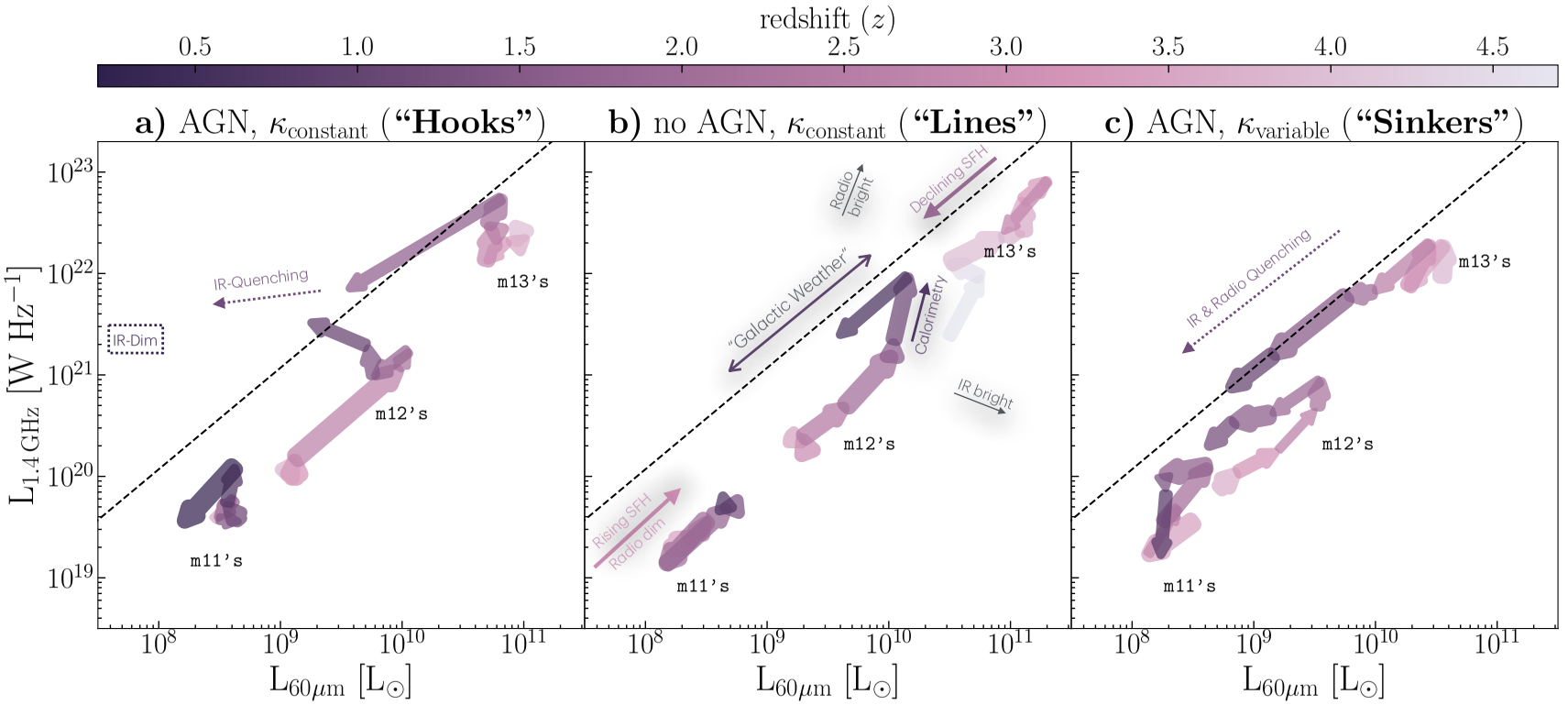

Figure 5.5: *FRC “tracks” on $L_{1.4GHz}$ vs. $L_{60\mu m}$ color coded by redshift* for **a)** AGN+κ_{const} (**left**), **b)** noAGN+κ_{const} (**center**), and **c)** AGN+κ_{var} physics variations (**right**), with the Yun, Reddy, and Condon (2001) $z = 0$ relation (black dashed line). The thickness of each arrow, colored by median redshift, qualitatively shows the relative 1σ scatter in a given redshift bin for the galaxies, which are mean averaged together by $\log_{10}(L_{60\mu m})$ and $\log_{10}(L_{1.4GHz})$ by mass groupings $M_{\rm halo}^{z=0} \sim 3\times10^{10}$– 7×10^{11}, 7×10^{11} - 1.5×10^{12}, and 5×10^{12} - 10^{13} $M_\odot$ (`m11's`, `m12's`, `m13's`). The different physics variations show different evolutionary paths with respect to z — **solid annotations** with shadowed tint in the middle panel highlight physics operating in all models while **dotted annotations** highlight the characteristic differences from the noAGN+κ_{const} scenario, driven by AGN feedback + CR transport physics. In AGN+κ_{const} models, `m12's` and `m13's` typically evolve parallel to the observed $z = 0$ FRC, tracking smoother, rising/constant SFHs before quenching at late times owing to AGN feedback, subsequently moving perpendicular to and ‘hooking’ the FRC, becoming ‘IR-dim’ objects with long-lived synchrotron contributions from Type Ia SNe and BH accretion. In noAGN+κ_{const} models, `m12's` and `m13's` typically rise up to the FRC ‘line’ tracking their SFHs, before exhibiting scatter slightly *along* the FRC owing to galaxy-to-galaxy scatter and late-time ‘galactic weather’ effects. AGN+κ_{var} models show a different here evolutionary track along the FRC, with `m12's` evolving up to and along the $z = 0$ FRC prior to ‘sinking’ ~1 dex in $L_{60\mu m}$, and `m13's` steadily ‘sinking’ by ~2 dex in $L_{60\mu m}$ from $z = 5$ to $z = 0$. For all three physics models, the averaged m11 tracks exhibit noisier variations due to burstier SFHs and larger galaxy-to-galaxy variations at this mass scale, though the more massive `m11's` exhibit qualitatively similar behavior to the `m12's` and `m13's`.

'Hooks': The FRC of AGN+κ_{const}

From Figures 5.2, 5.4, and 5.5, we see that the general behavior of the AGN+κ_{const} model variation is to maintain a roughly constant $q_{Y_{01}}$ with redshift but with increasing scatter at late times ($z \lesssim 1.5$), with the largest $\sim 1\sigma$ confidence interval, indicating a population of 'radio-excess' objects in our sample. Within each grouping of galaxies by halo mass, the average trend is to 'climb' up towards the FRC from early to late times as galaxies build up stellar mass with rising SFHs, often before 'hooking' across the observed $z = 0$ FRC with nearly perpendicular tracks, in many cases becoming 'radio-excess' objects at $z \sim 0$, ubiquitously for the `m12's` and `m13's`. While not as evident in Figures 5.4 and 5.5, we see similar behavior for the more massive `m11's` at the $\sim$ 3-5 $\times 10^{11}$ $M_\odot$ mass scale, which we show an example of in Figure 5.7.

This 'hook' pattern posits a somewhat obvious a posteriori, but previously unexplored progenitor scenario of 'radio-excess' objects across a broad range of $L_{60\mu m}$ (from $10^{7.5}$ - $10^{11.5}$ $L_\odot$): **'radio-excess' objects can in fact simply be 'IR-dim,' rather than intrinsically radio-bright**. Recall that in our synthetic observations here, we do not insert by hand any hard radio spectrum or template AGN spectrum, and remove from our sample snapshots with accretion rates which would noticeably pollute the $L_{60\mu m}$-$L_{100\mu m}$ luminosities. Thus, these are solely the *indirect* effects of AGN on the observables — meaning the evolution of $q_{Y_{01}}$ seen here is the end product of generic galaxy formation physics related to cosmological galaxy growth and quenching due to AGN+CR feedback, of which the exact sub-grid accretion disk physics (Hopkins, Grudic, et al., 2024) and jet-launching criteria (Su, Bryan, Hayward, et al., 2024) remain uncertain, and the emergent grid-scale transport rates of CRs from micro-physical, unresolved phenomena, of course, remains orders-of-magnitude uncertain in various phases of the ISM and CGM (Hopkins, Squire, Chan, et al., 2021; Hopkins, Squire, Butsky, and Ji, 2022; Hopkins, Squire, Butsky, and Ji, 2022; Kempski and Quataert, 2022; Butsky, Nakum, et al., 2023; Thomas, Pfrommer, and Pakmor, 2023; Butsky, Hopkins, et al., 2024).

Rather than tracing sparse star formation in any meaningful sense, $L_{1.4GHz}$ in these quenching objects at late times traces CR contributions from Type Ia SNe, which dominate at sSFRs $\lesssim 10^{-11}$, as well as injection from episodic BH accretion at late times. This is a strictly 'non-calorimetric' effect with regards to star-formation, which is pronounced in $q_{Y_{01}}$ owing to the cessation of young star formation, which $L_{60\mu m}$-$L_{100\mu m}$ is heavily sensitive to.

'Lines': The FRC of noAGN+κ_{const}

The behavior of the noAGN+κ_{const} physics variation in Figure 5.5 is largely summarized in Section 5.4. Our simulated galaxies run with this physics model, are most similar in approach to other galaxy simulations including CR-MHD in the literature (Werhahn, Pfrommer, and Girichidis, 2021; Werhahn, Pfrommer, Girichidis, Puchwein, et al., 2021; Werhahn, Pfrommer, Girichidis, and Winner, 2021; Pfrommer et al., 2022; Farcy et al., 2022; Thomas, Pfrommer, and Pakmor, 2023; Rodríguez Montero et al., 2024; Martin-Alvarez, Lopez-Rodriguez, et al., 2024), up to the difference of explicit, dynamic, on-the-fly evolution of CR(e) spectra here, and offer a useful point of comparison.

Across the mass range sampled here, our noAGN+κ_{const} galaxies largely rise up to the $z = 0$ FRC tracing their rising/constant SFHs with time, with lower-mass, low $L_{60\mu m}$ ($\leq 10^{9.5}$ $L_{\odot}$) galaxies having larger values of $q_{\gamma_{01}}$ associated with super-linear deviations from L_{IR}-SFR and $L_{1.4GHz}$-SFR correlations, and more-massive, higher $L_{60\mu m}$ snapshots approaching calorimetry and subsequently the FRC.

There is significant snapshot-snapshot scatter in our `m11's` and `m12's` at late times for a given galaxy, and considerable galaxy-to-galaxy variation contributing to the scatter, but it largely manifests *along* the relation, with 'galactic weather' of short-lived starbursts, outflow events, and late-time mergers tending to move galaxies parallel to the FRC rather than 'off' the relation. This is the primary cause of the 'downward' arrow pointing for the `m12's` "track" in Figure 5.5, which is of a qualitatively different nature than the 'sinking' described in the next subsection (c.f. Figure 5.6).

We note that the `m13's` included in this model variant sample are not run to low-z (typically halted at around $z \sim 2$, as indicated in Figure 5.4) as without AGN feedback, galaxies at this mass-scale fail to quench star formation and consequently over-/under-shoot low-z constraints by upwards of an order-of-magnitude, often becoming too dense in their centers to continue running the simulation forward in time (Byrne et al., 2024). However, the high-z `m13` snapshots represent an interesting sample of brighter, denser, and actively starbursting galaxies near cosmic noon, and so we include them here. Even in this more extremal end of Σ_{gas}, we find that the FRC holds, indicating that despite relatively higher bremsstrahlung, Coulomb and IC losses in this regime, secondary contributions from CR proton spallation 'save' the FRC at high-Σ_{gas}.

'Sinkers': The FRC of AGN+κ_{var}

The third pathological behavior we observe in our physics variation of AGN+κ_{var} is similar in many aspects to the AGN+κ_{const} evolutionary path described in 5.4, though with important qualitative differences. After entering our mock-observable parameter space from $z > 5$, the `m13's` appear to 'sink' down along the $z = 0$ FRC by $\gtrsim 2$ dex in $L_{60\mu m}$ and $L_{1.4GHz}$, with low-z snapshots contributing to the sample at low-$L_{60\mu m}$, filling in the upper envelope of the scatter in Figure 5.2. From examining the individual 'tracks' of each galaxy, we note that while there are some low SFR snapshots excursing into the 'radio-excess' parameter space, these occur less often than in the AGN+κ_{const} case, and often stabilize at later times back onto the $z = 0$ FRC as evinced by the pointings of the averaged arrows in Figure 5.5.

The `m12's` in this model variant exhibit similar behavior to the AGN+κ_{const} runs as well, but also 'sink' at late times owing to quenching, much alike the `m13's`, populating the low-$L_{60\mu m}$ parameter space at z ~ 0. Although the `m11's` exhibit qualitatively more scatter, it is primarily coherent along the FRC, indicating similar regulation of $L_{60\mu m}$ and $L_{1.4GHz}$ during sporadic burst-quench cycles via effective loss of dust opacity in addition to relatively faster diffusive escape of CRs, especially for the more massive `m11's` (see Figure 5.7). The averaged `m11's` track, however, becomes more 'radio-dim' at the latest times, indicating the balance of CRe diffusive loss vs. UV opacity is skewed at this mass scale, though this may be partly due to our use of a constant D/Z value of 0.4. For lower D/Z at the lowest masses, the 'sinking' behavior would then appear more similar to the `m12's` and `m13's`.

This explains the relatively smaller scatter of the AGN+κ_{var} model variation at late times in comparison to the AGN+κ_{const} runs; as the parallel diffusivity is allowed to vary with local plasma properties in the $\kappa_{\rm var}$ model, this allows for larger effective volume-averaged transport speeds, limiting the presence of longer-lived synchrotron emission in 'IR-dim' galaxies.

Recall that if we assume the dynamical equations for the CR flux and scattering rates have all reached steady-state in the diffusive limit, the amplitude of gyro-resonant scattering modes $\delta B^2(\lambda \sim r_g) \sim u_{\delta B}^{\rm gyro}$ is set by balance between some source terms $S_\pm$ and damping terms $\Gamma_\pm$, so $\dot{u}_{\delta B}^{\rm gyro} \sim +S_\pm - \Gamma_\pm u_{\delta B}^{\rm gyro} \rightarrow 0$, i.e. $\delta B^2/B^2 \rightarrow S_\pm/\Gamma_\pm u_{\rm B}$, with the emergent parallel diffusion coefficient being $\kappa_\parallel \sim v_{\rm cr}^2/3\bar{\nu}_{\rm s} \sim (v_{\rm cr}^2/\Omega_{\rm cr})\,(B^2/\delta B^2) \propto S_\pm^{-1}$ (with $\Omega_{\rm cr}$ the gyrofrequency; Zweibel 2013).

Taking this intuition and the source term used in the $\kappa_{\rm var}$ models (see Section 5.3), in

conjunction with standard scalings for “turbulent," Linear Landau, or collisionless damping for $\Gamma_{\pm}$ leads to an approximate scaling of $\kappa_{\parallel} \propto \mathbf{B}^{-\xi}$, where ξ is some weak power-law index ($\xi \sim 0.2$-0.5), of particular interest here for synchrotron calculations, notwithstanding weak dependencies on other plasma properties marginalized over. Essentially, denser, more strongly-magnetized regions of the galaxy tend to have higher turbulent dissipation rates, which drives stronger CR scattering (more CR confinement).

Despite this inverse scaling of $\kappa_{\parallel} \propto \mathbf{B}^{-\xi}$, these simulations tend to ‘sink’ down the FRC rather than becoming ‘radio-excess’ objects as they quench. This is somewhat non-intuitive — if CRes effectively spend more time in strongly magnetized gas, one might expect that these simulations would be more ‘radio-excess’ on average.

However, the scattering properties of CRs are better understood in the full context of the multi-phase ISM/CGM. If CRes primarily emit in dense, magnetized, neutral gas (Ponnada, Panopoulou, Butsky, Hopkins, Skalidis, et al., 2024; Martin-Alvarez, Lopez-Rodriguez, et al., 2024) as expected from the power-law relationship of $\mathbf{B} - \rho^{0.4-0.6}$ (Tritsis et al., 2015; Ponnada, Panopoulou, Butsky, Hopkins, Loebman, et al., 2022), and this gas is enveloped in a uniform bath of more diffuse phases where $\kappa_{\rm eff}$ is higher on average, the *global* synchrotron properties will be set simply by the ‘boundary’ condition of entering regions of approximate or total synchrotron calorimetry. So even if $\kappa_{\parallel} \rightarrow 0$ in strongly magnetized gas in the most extreme example, the rate limiting step for producing synchrotron emission is the scattering of CRes into such high-$\mathbf{B}$ regions, which on average is *lower* in this type of model, wherein $\kappa_{\rm eff}$ is higher outside these regions and CRs may more quickly escape the scattering halo of characteristic size ~ 10 kpc in which they have an order unity probability of re-entering the relatively synchrotron-bright gas disk/bulge (Hopkins, Squire, Chan, et al., 2021).

Morphological Variation Across ‘Tracks’

The different ‘tracks’ outlined above trace different stages of galaxy evolution, and thus different gas morphological properties. In particular, ‘IR-dim’ objects often display morphological disturbance in gas phase, with more lenticular-like synchrotron morphology and extended diffuse emission. We illustrate such characteristic morphological evolution in each track for one of our $\sim L^{*}$ halos, `m12f`, as a representative example in Figure 5.6.

The progression of simulations along each track becomes apparent from visual

examination of Figure 5.6: in each of our physics models, galaxies largely 'climb' up the FRC from irregular gas morphologies where they are 'radio-dim' on average due to stronger losses of CRes. The late-time morphological evolution, however, differs between the no AGN and AGN runs, with noAGN+κ_{const} runs at this mass scale maintaining star-formation and extended, structured gas distributions. The scatter subsequently manifests along the relation from late-time mergers and feedback episodes reflected by the more modest changes in gas morphology.

AGN+κ_{const} and AGN+κ_{var} runs contrast this with irregular, gas-deficient morphologies after quenching star formation, with $\kappa_{\rm const}$ runs more often becoming 'IR-dim' at late times by maintaining more extended, bright synchrotron emission from CRe produced by intermittent BH accretion and Type Ia SNe, while $\kappa_{\rm var}$ runs 'sink' down the correlation on average owing to faster CR diffusion.

5.5 Discussion and Conclusions

The globally-averaged properties of our synthetically observed sample here generally verify the predictions of non-calorimetric one-zone models (Lisenfeld, Voelk, and Xu, 1996; Lacki, Thompson, and Quataert, 2010) while evolving the details of stellar feedback, thermochemistry and ISM phase structure, magnetic fields, CR transport and its back-reaction on gas. This is all done in a cosmological context from relatively well-understood physics undergirding stellar evolution and gas cooling/heating with varied assumptions regarding far-less understood CR transport, here treated using a simple, constant in space and time model for the scattering rate $\nu_{\rm CR}$ as well as a model in which $\nu_{\rm CR}$ varies by orders of magnitude according to local plasma properties. This verification is particularly true of our noAGN+κ_{const} sample, which are most comparable to the aforementioned works when considering galaxy-averaged quantities in the context of the global FRC as we do here.

This simulation and synthetic observational effort illuminates physics driving the FRC in detail, which require this approach — the analysis of our noAGN+κ_{const} sample highlights how galaxies evolve with redshift to the $z = 0$ FRC and how relatively simple assumptions of constant power-law scalings for the $\kappa_{\parallel}$ motivated by empirical Milky-Way LISM constraints can reproduce the properties of the FRC reasonably well across a diversity of galaxy properties. Moreover, the detailed forward modeling of the emergent observables allows us to forego any implicit assumptions regarding dust optical depth to UV photons, which by construction constrains the predicted FIR luminosities, or resort to re-normalization schemes of spectra solved

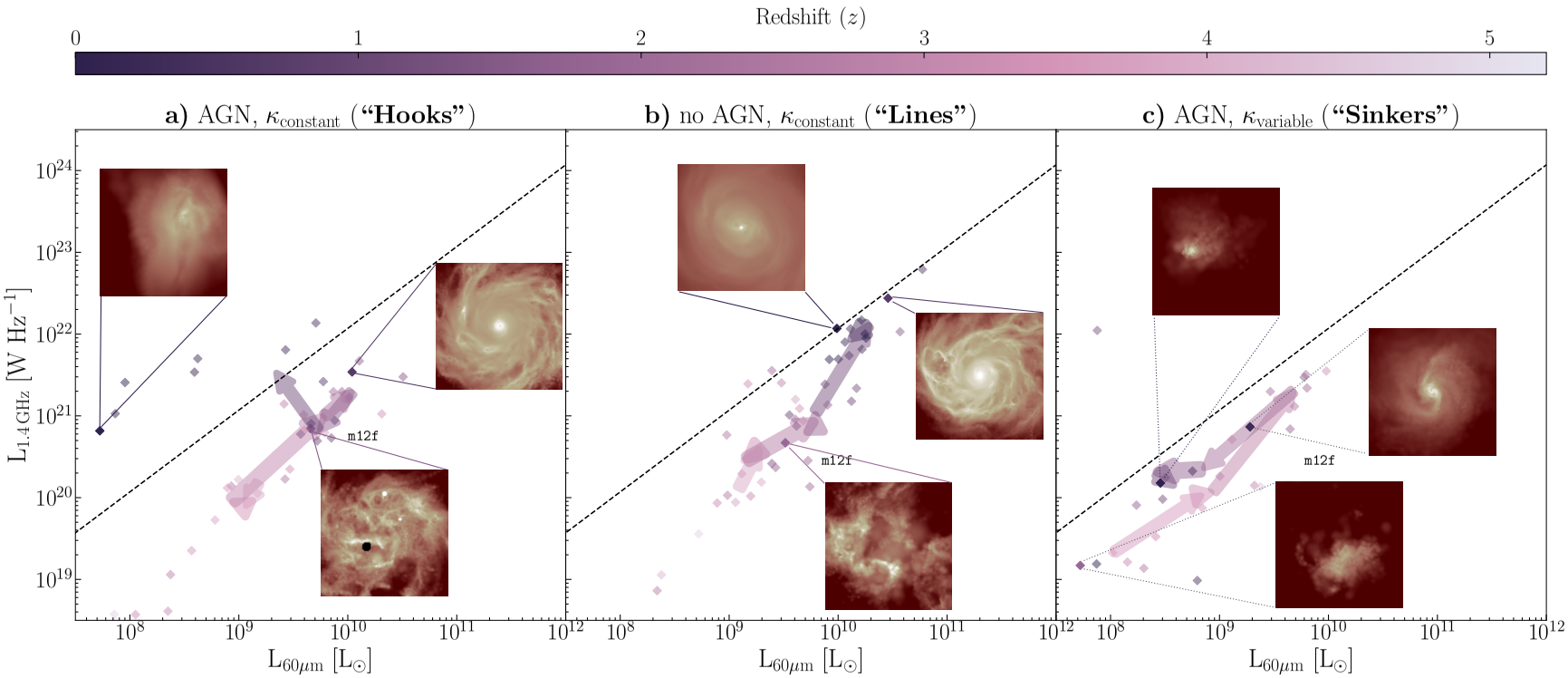

Figure 5.6: *Morphological evolution along FRC “tracks”*, here shown for an individual halo, `m12f`, as a representative case study for **a)** AGN+κ_{const} (**left**), **b)** noAGN+κ_{const} (**center**), and **c)** AGN+κ_{var} physics variations (**right**), with individual snapshots shown as points (pluses, circles, diamonds), along with the Yun, Reddy, and Condon (2001) $z = 0$ relation (black dashed line). Properties for the arrows are the same as in Figure 5.5. Insets show 1.4 GHz images in the central 25 kpc for three snapshots sampling early to late-time evolution in each case, highlighting characteristic underlying behavior for each model class’ “track" described in Section 5.4.

via steady-state assumptions in conjunction with a diffusion-loss treatment for CR transport, as has been invoked in other simulation works (Werhahn, Pfrommer, and Girichidis, 2021; Pfrommer et al., 2022). These assumptions which may significantly influence the predicted radio continuum synchrotron emission, particularly in galaxies with gas-dense central bulges or generally high gas surface densities (see Ponnada, Panopoulou, Butsky, Hopkins, Skalidis, et al., 2024, for a detailed discussion).

Beyond calorimetry and conspiracy, our AGN+κ_{const} and AGN+κ_{var} sample show how the FRC's scatter is shaped by galaxy evolution processes, in particular the role of quenching and the indirect effects of AGN on observables via feedback. Our finding that 'radio-excess' objects can instead simply be 'IR-dim' objects poses consequences for the 'small' scatter often quoted with regards to the FRC. If these objects are simply excluded from observational samples looking to characterize the FRC as 'radio-excess,' even if they have low-level star formation, the resulting scatter will by construction be smaller due to sampling bias.

In addition to this, studies aiming to infer AGN jet power from 'radio-excess' objects — especially if these are not high-accretion rate objects (as our selection criteria aim to exclude), the subsequent radio luminosity may have little to do with the intrinsic jet power of the AGN, and can even be dominated by Ia contributions in many cases! Indeed, lacking a better alternative observational metric, state-of-the-art observational studies utilize the excess from the FRC in order to constrain 'jet' power and its associated correlations with host galaxy properties (Jin et al., 2024). Curiously, taking these nominal constraints as informative regarding the 'jet' often leads to finding that the radio-AGN host galaxy quenching ages ($\gtrsim$ 3 Gyr) estimated from stellar mass assembly histories are often poorly correlated with even the oldest jet 'ages' from dynamical or spectral age estimations ($\sim$ 1 Gyr; Turner 2018). This serves as an additional point of support for these lower-luminosity 'radio-excess' objects more physically being 'IR-dim,' bearing similarity to some of our AGN+κ_{const} `m13's` at late times. This motivates further study of these types of simulations capable of evolving CR dynamics from AGN and stellar sources to aid in disambiguating the nature of observed 'radio-excesses' from the FRC in radio AGN studies.

Comparing the AGN+κ_{const} and AGN+κ_{var} physics variations, it is quite remarkable that the global properties of the FRC can be robustly reproduced despite $\kappa_{\rm eff}$ varying by *orders of magnitude* in the $\kappa_{\rm var}$ model. While there are notable differences

discussed prior regarding their scatter and evolution along diverging tracks, it appears that the global FRC may not precisely constrain the transport properties of CRs, at least for the empirically-motivated models explored here.

However, the differences in gas morphology and subsequent global FRC 'tracks' at late times hints at the possibility to constrain CR transport using the spatially-resolved FRC (Murphy, Braun, et al., 2006) as observational works have begun to attempt (Heesen, Buie, et al., 2019). Between our AGN+κ_{const} and AGN+κ_{var} models, even if bulk FRC properties are similar on aggregate, the exact distribution of synchrotron emission with respect to FIR emission will differ. We caution, however, that this may not immediately make clear how the diffusion properties in different gas phases translate to the radio properties, as we highlight in Section 5.4, due to the non-linear nature of CR transport (see also Ponnada, Butsky, et al., 2024, for further caveats of physically-motivated CR scattering models).

As CRs from BHs in our simulation are injected at large radii compared to the scales of the BH accretion disk, they are more analogous to stellar CRs in these models as their injection and diffusion properties are set by the ISM and CGM. This indicates that BH contributions may potentially explain some of the radio-excesses observed in the spatially resolved FRC at low FIR luminosities (Murphy, Braun, et al., 2006).

5.6 Summary and Future Work

In this chapter, we have presented end-to-end forward modeled synthetic observations of FIR and radio continuum emission from cosmological zoom-in simulations with "live" CR proton and electron spectra. We forward model the FRC for galaxies from the $M_{\rm halo}^{z=0}$ ~3×10^{10} - 1×10^{13} $M_\odot$ from z = 5 to z = 0 with three different physical models: one without AGN feedback and a constant-in-space and time treatment for the CR scattering rate, and two with multi-channel AGN feedback and two different models for the CR scattering rate.

Our results can be summarized as follows:

- All physics variations explored herein generally reproduce the z = 0 FRC, but with larger scatter in runs with AGN. Our forward-modeled FRC is linear at high $L_{60\mu m} \gtrsim 10^{9.5}$ $L_\odot$, but exhibits super-linearity at low $L_{60\mu m} \lesssim 10^{9.5}$ $L_\odot$.
- This FRC is maintained by standard arguments of 'calorimetry' and 'conspiracy' at high and low $\Sigma_{\rm gas}$, respectively, with diffusive escape being the

primary competing loss process to synchrotron-emitting gas at $z \lesssim 1.5$ and both IC and diffusive losses being important at higher z.

- How the late-time scatter of the FRC is shaped is sensitive to the *indirect* effects of AGN feedback as well as CR transport on the emergent observables. These effects create characteristic evolutionary "tracks" with galaxies evolving up to the $z = 0$ FRC before exhibiting differing behavior due to the physics variations, which aid in understanding the nature of 'outliers' to the FRC.

- Namely, galaxies run with our noAGN+κ_{const} model typically evolve up to and along 'lines' parallel to the $z = 0$ FRC at late times, with scatter owing to "galactic weather" effects.

- This differs from our AGN+κ_{const} model, more massive dwarf galaxies as well as $\sim L^*$ and massive elliptical galaxies evolve quasi-perpendicularly to the FRC as galaxies begin to quench, creating 'hook' patterns and becoming 'IR-dim' objects at late times, filling in the 'radio-excess' space with late-time contributions from BH accretion and Type Ia SNe. In our AGN+κ_{var} models, however, these same galaxies steadily 'sink' down along the FRC, exhibiting qualitatively less late-time scatter as a result, which owes to faster on average CRe escape which creates fewer 'IR-dim objects' in comparison the the AGN+κ_{const} model.

- Surprisingly, this modeling effort reveals a remarkable *insensitivity* of the global FRC to *orders-of-magnitude* variable CR scattering rates (and thus emergent diffusive/streaming transport rates), though morphological and spatially resolved constraints may prove fruitful to constrain these deeply uncertain physics.

In future work, we will utilize the types of synthetic observations produced here to constrain AGN feedback and CR transport across differing galaxy properties in concert with the latest spatially-resolved observational constraints. While in this chapter we explored how AGN and CR physics shapes the emergence and maintenance of the $z = 0$ FRC, with multi-wavelength synthetic observations in-hand, we will also explore the role observational K-corrections may play in determining the evolution of the global FRC with redshift (Sargent et al., 2010; Magnelli et al., 2015). Comparisons with these existing FRC constraints requires careful consideration of Malmquist bias effects in synthetic-observational sampling, as many of these

high-z constraints contain galaxies at equivalent halo masses to those explored here *at those redshifts*, rather than at $z = 0$, which will require re-simulations of massive galaxies at higher redshifts with FIRE-3 physics and CR-MHD, which is a considerable simulation effort with the zoom-in approach utilized here. For instance, while some of these flux-limited observational samples appear to infer a modestly *decreasing* ratio of $q \equiv L_{8-1000\mu m}/L_{1.4\,\mathrm{GHz}}$ with z, our theoretical predictions show a general trend of $q_{\gamma_{01}}$ modestly increasing with z, in line with analytic predictions (Murphy, 2009).

Indeed, we see hints towards this contradictory trend with z in our sample when limiting to only the brightest snapshots at a given redshift, as evinced by qualitatively weaker z-evolution in the rightmost panel of Figure 5.4, but requires larger (and more massive) simulation samples to make statistically meaningful predictions (see also Schober, Sargent, et al., 2023, for detailed discussion on disentangling mass and redshift trends in the FRC). Samples of this sort will enable comparisons to growing constraints at higher redshifts and detailed spatially-resolved comparisons at low redshifts in the ngVLA (Murphy, Bolatto, et al., 2018), SKA (Dewdney et al., 2009), & DSA-2000 (Hallinan et al., 2019) era which may further shed light on the complex, non-linear, and non-thermal physics of galaxies across cosmological time.

Acknowledgments

We wish to recognize and acknowledge the past and present Gabrielino-Tongva people and their unceded Indigenous lands upon which this research was conducted. Support for SP & PFH was provided by NSF Research Grants 20009234, 2108318, NASA grant 80NSSC18K0562, and a Simons Investigator Award. Numerical calculations were run on NSF/TACC allocation AST21010, TG-AST140023, TG-PHY240164, and NASA HEC SMD-16-7592. RKC was funded by support for program #02321, provided by NASA through a grant from the Space Telescope Science Institute, which is operated by the Association of Universities for Research in Astronomy, Inc., under NASA contract NAS 5-03127. RKC is grateful for support from the Leverhulme Trust via the Leverhulme Early Career Fellowship. ISB was supported by NASA through the Hubble Fellowship, grant HST-HF2-51525.001-A awarded by the Space Telescope Science Institute, which is operated by the Association of Universities for Research in Astronomy, Incorporated, under NASA contract NAS 5-26555. SW received support from the NASA RIA grant 80NSSC24K0838. DK was supported by NSF grant AST-2108324. The Flatiron institute is supported by the Simons Foundation.

5.7 Appendix: Auxiliary Figures

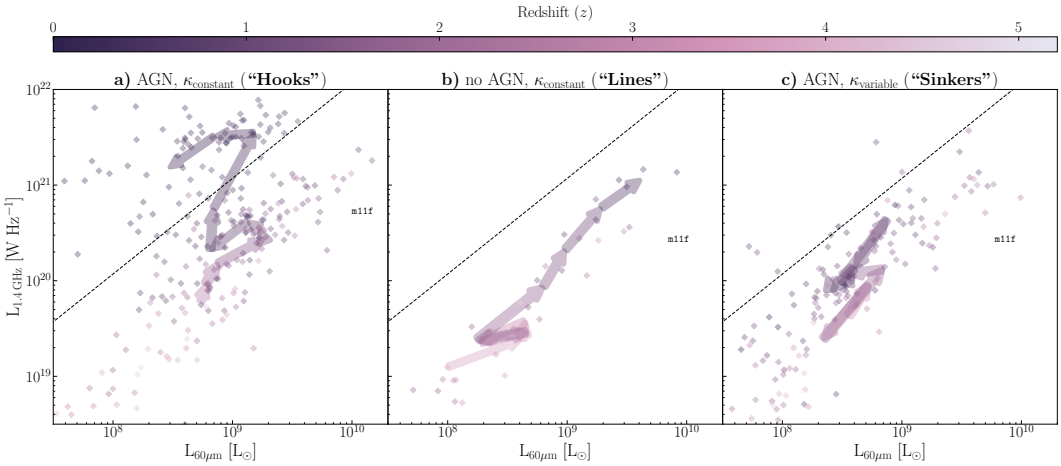

Figure 5.7: *Evolution along FRC "tracks,"* here shown for an individual massive dwarf, `m11f`, in the same style as Figure 5.6. The more massive dwarf galaxies in our simulation sample exhibit similar "tracks" as the `m12s` and `m13s` outlined in Figures 5.5 and 5.6.

Chapter 6

TIME-DEPENDENT COSMIC RAY WINDS FROM BURSTY STAR FORMATION AND ACTIVE GALACTIC NUCLEI

6.1 Chapter Abstract

Cosmic ray (CR) feedback in galaxy evolution has seen a theoretical resurgence in the past decade, but significant uncertainties remain in CR transport through the interstellar and circum-galactic media (ISM and CGM). While several works indicate CR effects may be notable in both star-forming and quenched massive galaxies, modeling the vast CR transport parameter space currently allowed by observations is computationally restrictive to survey. Analytic treatments of CR feedback have provided useful insights to potential ramifications in different regimes, but have relied on time-steady assumptions which may not well characterize CR effects at different cosmic epochs and galaxy mass scales. We present semi-analytic and numerical solutions describing the time-dependent evolution of CR pressure in the CGM under simplified assumptions, which allow for quick evaluation of the vast allowable CR transport parameter space. We demonstrate that time-dependent injection from bursty star formation and/or episodic black hole accretion can substantially alter CR pressure profiles, particularly in the outer halos of massive galaxies ($\gtrsim R_{vir}$). Our work further demonstrates that CR feedback may play a significant role in shaping the matter distribution around massive galaxies ($\gtrsim M_{\rm halo} \sim 10^{13} M_{\odot}$). Finally, we benchmark our analytic and numerical solutions against cosmic ray-magnetohydrodynamic (CR-MHD) cosmological zoom-in galaxy simulations directly modeling the CR scattering rate and emergent transport in full generality, demonstrating the surprisingly robust nature of our simplified approach. We conclude by motivating careful consideration of time-dependent "softening" effects in sub-grid routines for CR feedback, particularly for use in large cosmological volumes.

6.2 Introduction

In recent years, it has become clear that in order to advance our understanding of feedback in galaxy formation, the details of feedback "microphysics" must be modeled directly. Notably, there has been a resurgence of focus on one such "microphysical" source of feedback: cosmic rays (CRs) (see Ruszkowski and Pfrommer, 2023, for a recent review). Much work on CR feedback of late has focused on injection from supernovae (SNe) and resultant effects in galaxies at or below the break of the galaxy stellar mass function (Butsky and Quinn, 2018; Hopkins, Chan, Garrison-Kimmel, et al., 2020; Quataert, Thompson, and Jiang, 2022; Pfrommer et al., 2022; Thomas, Pfrommer, and Pakmor, 2023; Modak et al., 2023; Rodríguez Montero et al., 2024).

These works, in large part, have shown that for empirically-motivated CR transport parameters, CRs could have significant effects on galaxy growth and baryon cycling, influencing the bulk kinematics and phase structure of outflows and halo gas (Ji, Chan, et al., 2020; Butsky, Fielding, et al., 2020; Buck et al., 2020; Butsky, Werk, et al., 2022; Ponnada, Panopoulou, Butsky, Hopkins, Loebman, et al., 2022; Ponnada, Panopoulou, Butsky, Hopkins, Skalidis, et al., 2024).

Above the break in the galaxy mass function, active galactic nuclei (AGN) are crucial to regulating galaxy growth and evolution, particularly at high dark matter halo masses ($M_{\rm halo} \gtrsim 10^{13} M_{\odot}$; Harrison 2017). Despite long-standing knowledge of AGN feedback's role at these mass scales (Croton et al., 2006), *how* massive black holes' energy injection couples to the surrounding interstellar and circum-galactic medium (ISM and CGM) is largely unknown.

Many state-of-the-art simulations and semi-analytic models utilize variations on thermal and kinetic energy injection into AGN surroundings in order to effectively "quench" star formation in massive galaxies and reproduce observed galaxy properties (Schaye et al., 2015; Pillepich et al., 2018). While these approaches reify the importance of AGN, the physical nuances of feedback models remain a significant open question to be confronted with multi-wavelength observational constraints.

Indeed, radio emission arising from CR electrons tracing AGN activity has long been studied as an important clue towards AGN feedback and its coupling to galactic environments (see Heckman and Best, 2014; Hardcastle and Croston, 2020, for relevant reviews). Idealized simulations of massive galaxies (Su, Hopkins, Bryan, et al., 2021; Su, Bryan, Hayward, et al., 2024; Su, Bryan, Hopkins, et al., 2025) have begun to explore the vital role CRs from AGN may play in the cessation of star

formation and maintenance of quenching, in conjunction with other known feedback mechanisms.

Self-consistent, cosmological simulations of galaxy formation have also found that injecting a small, fixed fraction of the AGN accretion energy into CRs (marginalizing over the details of the injection physics on the much smaller accretion disk scales), produce reasonably quenched massive galaxies (Wellons et al., 2023), without obviously violating known observational constraints (Byrne et al., 2024; Ponnada, Cochrane, et al., 2025).

Although CR transport parameters, which depend on plasma microphysics on ~AU scales (Zweibel, 2013), are still unknown, a novel framework is emerging where for plausible transport prescriptions, CRs *could be important for maintaining quenching* on longer timescales. Recently, (Quataert and Hopkins, 2025, hereafter, QH25) demonstrated using order-of-magnitude analytic arguments for plausible “effective" CR diffusion/streaming speeds and fractional injection of AGN accretion energy into CRs, CRs may drive outflows on larger scales (beyond $\gtrsim R_{vir}$) from group-mass halos ($M_{halo} \sim 10^{13}\ M_{\odot}$).

Analytic work modeling CR feedback from galaxies have typically focused on spherically-symmetric, steady-state wind solutions (Ipavich, 1975; Quataert, Thompson, and Jiang, 2022; Quataert, Jiang, and Thompson, 2022; Modak et al., 2023; Butsky, Nakum, et al., 2023; Hopkins, Quataert, et al., 2025) for spatially and temporally constant transport parameters and time-steady CR injection and pressure evolution, which have also been implemented as sub-grid models (Hopkins, Butsky, Ji, et al., 2023). While these approaches are physically intuitive and are valid first approximations, star formation across galaxy mass scales can be highly time-variable (Muratov et al., 2015; Sparre et al., 2017), and AGN accretion is notoriously episodic (Ulrich, Maraschi, and Urry, 1997).

So, while steady-state approximations may well characterize the Milky Way and other low-z spiral galaxies which have been continuously forming stars and thus steadily injecting CRs into their halos for the past several Gyr, these approximations may not hold for galaxies with burstier star formation histories (SFHs), highly episodic AGN injection, and/or galactic halos at high z due to non-negligible source evolution and long CR travel times. Moreover, the plasma conditions giving rise to macroscopic CR transport parameters are not a priori expected to be uniform in the ISM (Hopkins, Squire, Butsky, and Ji, 2022; Thomas, Pfrommer, and Pakmor, 2023), let alone in the CGM, with observations hinting towards rising effective

transport speeds with galactocentric radius around $\sim L^*$ galaxies (e.g. Butsky, Nakum, et al., 2023).

Ultimately, the macroscopic physical quantity of interest for CR effects on galaxy formation are the CR pressure P_{CR} and its gradient. Numerical experiments and galaxy-scale simulations which explicitly evolve CRs, however, remain very computationally expensive. Much like the traditional radiative transfer problem, modeling physics with signal speeds $\sim O(c)$ in systems where characteristic speeds are several dex slower on average introduces additional overhead on simulations which already suffer from having to evolve large spatial and temporal dynamic ranges for end-to-end predictions, even with "reduced speed-of-light" methods. To ameliorate this issue, further analytic treatments and robust numerical routines are required to advance our physical intuition and expand the prediction space for CR physics in galaxy formation.

Towards this end, we analytically and numerically explore CR feedback from star-forming and massive galaxies. Specifically, we relax two common assumptions in the literature of time-steady CR injection and pressure evolution (§6.3), and spatially constant CR transport parameters (§6.4), to explore semi-analytic and numerical solutions to CR transport in halos for diffusion and streaming/advection-dominated regimes. We provide a generalizable framework for the evolution of CR pressure profiles in galaxy halos, independent of the choice of transport parameters or injection cadence. To benchmark our simple, yet surprisingly viable semi-analytic approach, we compare against "true" numerical solutions, as well as a fully cosmological, cosmic-ray-magnetohydrodynamic zoom-in simulation of a massive galaxy with galaxy formation physics evolved self-consistently (§6.5). (§6.6) summarizes our results and motivates improved sub-grid modeling of CR physics in large-volume cosmological simulations including AGN feedback, for which we will present open-source numerical tools in a separate paper (Ponnada et al. 2025c, in prep.).

6.3 Analytic Expectations for Constant Cosmic Ray Transport Parameters

The transport of CRs through the ISM and into the CGM of massive halos is fundamentally a multi-scale problem connecting the details of "micro-physical" scattering of CRs ($r_{gyro} \lesssim$ AU for ~GeV CRs in $\sim |B|/\mu G$), which at present remain physically unknown (Hopkins, Squire, Butsky, and Ji, 2022; Kempski and Quataert, 2022; Butsky, Nakum, et al., 2023; Fielding, Ripperda, and Philippov, 2023; Butsky, Hopkins, et al., 2024; Kempski, Li, et al., 2024) to large, ~kpc galactic scales.

These micro-physical uncertainties determine the pitch-angle scattering rate $\nu_{\rm CR}$, which gives rise to *effective* 'streaming' or 'diffusive' behavior in varied limits of $\nu_{\rm CR}$. Thus, we may parametrize the relevant transport through 'effective transport parameters' on large scales $\kappa_{\rm eff}$ and $v_{\rm eff}$, as done in previous works (Hopkins, Chan, Garrison-Kimmel, et al., 2020; Butsky, Nakum, et al., 2023; Hopkins, Butsky, Ji, et al., 2023; Hopkins, Quataert, et al., 2025). We then treat CR transport here in the relativistic fluid limit with the CR pressure given by $P_{\rm CR} = (\gamma_{\rm CR,\,ad} - 1)\, e_{\rm CR}$, where $e_{\rm CR}$ is the CR energy density, and $\gamma_{\rm CR,\,ad} = 4/3$ is the CR adiabatic index.

We then assume that a fixed fraction of AGN accretion energy $\epsilon_{\rm CR,\,BH}$, or of SNe shocks per unit star formation ($\sim 0.1 \times 10^{51}$ erg/100 $M_\odot/c^2$), $\epsilon_{\rm SF}$ (approximately 10% of the stellar population-averaged SNe ejecta kinetic energy Caprioli (2012)), is converted into CRs. The rate of CR energy injection is given by

$$\dot{E}_{\rm CR}(t) = \epsilon_{\rm CR,BH/SF}\, \dot{M}_{\rm BH/SF}(t)\, c^2 \tag{6.1}$$

The injection occurs as a "pulse", with infinitesimal width represented as a spatial and temporal δ-function initially, centered at the origin. Then, the CR pressure source term S becomes

$$S = \dot{P}_{\rm CR}(t) = (\gamma_{\rm CR,\,ad} - 1)\, \dot{E}_{\rm CR,BH/SF}(t)\, c^2 \delta(\vec{r}, t) \tag{6.2}$$

where $\vec{r}$ is the vector position from the central BH, and t represents the time the pulse was injected. If such a pulse of CRs experience post-injection losses due to hadronic collisions, ionization, Coulomb interactions, and so on, the "calorimetric fraction" can be written as $f_{\rm cal}$, where pure calorimetry means $f_{\rm cal} = 1$ (no CRs escape into the CGM).

We then assume spherical symmetry following Hopkins, Butsky, Ji, et al. (2023), and solve for the Green's function solutions to the 3D diffusion-advection equation of the following form, assuming magnetic fields are isotropically tangled on large spatial scales in the CGM (which simulations indicate is a reasonable approximation Ji, Chan, et al., 2020; Ponnada, Panopoulou, Butsky, Hopkins, Loebman, et al., 2022) [1]

[1] Note, in practice the CR transport equations are not formally a diffusion-advection equation, but implicit in our assumptions here is combining the 'streaming' and 'diffusive' limits of micro-physical scattering to *effective* transport speeds on scales >> the CR scattering mean free path, which give rise to the resulting pressure. Exact separation of 'streaming-like' vs. 'diffusive' behavior is only

$$\frac{\partial P_{\rm CR}(\vec{r},t)}{\partial t} = \nabla\cdot\left[\kappa_{\rm eff}(r)\nabla P_{\rm CR} - \frac{4}{3}v_{\rm eff}(r)P_{\rm CR}\right] + (1-f_{\rm cal})\,S(t) - \Lambda_{{\rm st}/ad}(r,t) \tag{6.3}$$

where $v_{\rm eff}$ is the magnitude of the effective advection/convection + streaming velocity $\mathbf{v}_{\rm eff} = \mathbf{u}_{\rm gas} + v_{\rm A}\hat{\nabla}P_{\rm CR}$, $\Lambda_{{\rm st}/ad}$ is the streaming+ adiabatic loss term ($P_{\rm CR}(\nabla\cdot\mathbf{v}_{\rm eff})$) with $v_{\rm A}$ the local Alfvén speed and $\kappa_{\rm eff}$ the *effective* local diffusive transport coefficient from microphysical scattering on gyro-resonant scales.

We then move the term in $\Lambda_{{\rm st}/ad}$ of the form $\frac{P_{\rm CR}}{3}\nabla\cdot\mathbf{v}_{\rm eff}$ into the bracketed transport term for simplicity, leaving = $\Lambda_{{\rm st}/ad} = \frac{2v_{\rm eff}P_{\rm CR}}{3r}$. This means we implicitly assume $\langle\mathbf{v}_{\rm A}\rangle$ averaged over large spatial scales sampled by CR travel paths along isotropically tangled field lines gives rise to approximately radial "streaming" motion, though the equations presented here remain agnostic to local non-radial components in $\hat{\nabla}P_{\rm CR}$.

In essence, this parameterization separates the scalar transport behavior into "diffusion-like" and "streaming + advection-like" regimes (though see footnote [1]). Below, we demonstrate how the normalization and shape of the CR pressure profile is sensitive to the episodic accretion history of the black hole and variations in $\kappa_{\rm eff}$ and/or $v_{\rm eff}$.

Case 1: Constant $\kappa_{\rm eff}$, No Advection

If $\kappa_{\rm eff}$ is a constant value due to an effectively constant $\nu_{\rm CR}$) throughout the ISM and CGM as is commonly assumed for simplicity in most state-of-the-art galaxy simulations including CR feedback (and when averaged over large spatial scales as we are assuming here) (Butsky and Quinn, 2018; Chan, Kereš, Hopkins, et al., 2019; Hopkins, Chan, Garrison-Kimmel, et al., 2020; Farcy et al., 2022; Hopkins, Butsky, Panopoulou, et al., 2022; Rodríguez Montero et al., 2024; Ponnada, Cochrane, et al., 2025), and $v_{\rm eff} \rightarrow 0$, Equation 6.3 reduces to a diffusion equation with a Green's function solution with a Gaussian form:

possible when these coefficients are constants, and otherwise become strictly degenerate once their true arbitrary scalings with various locally varying plasma properties are considered (see Hopkins, Squire, Chan, et al. 2021 Appendix B, and Hopkins, Butsky, Ji, et al. 2023 for more detailed discussions).

$$P_{\rm CR}(\vec{r},t) = \int_0^t \frac{\dot{E}_{\rm CR}(t')}{3\left(4\pi\kappa_{\rm eff}\,t'\right)^{3/2}} \exp\left(-\frac{r^2}{4\,\kappa_{\rm eff}\,t'}\right) dt' \tag{6.4}$$

Here, r is the scalar galactocentric distance in spherical coordinates, and t' is the time since injection of a given pulse, or the look-back time to the injection at time t_i ($t' = t - t_i$).

Now, if $\dot{M}_{\rm BH/SF}$ are dominated by a single injection event, this Gaussian expression is the exact closed-form solution. This is what is shown in Quataert and Hopkins (2025), where the authors consider constant-$\kappa_{\rm eff}$ models for CR energy injection from AGN, with a small, fixed fraction of accretion energy converted to CRs. There, the authors find that for isotropically-averaged $\kappa_{\rm eff} \sim 10^{30}$ cm^2 s^{-1}, $P_{\rm CR}$ can be approximately in equipartition or greater than the thermal pressure $P_{\rm th}$ around the virial radius of massive galaxies ($M_{\rm halo} \gtrsim 10^{13} M_\odot$) with similar assumptions as above, comparing to empirical thermal pressure profiles for galaxy groups and clusters from X-ray observations (Arnaud et al., 2010).

Otherwise, when $\dot{M}_{\rm BH/SF}$ are more complex, Equation 6.4 represents the convolution of the Green's function solution with the time dependent source term. In steady-state, for the same spherically symmetric assumptions here, a simple closed form solution of $P_{\rm CR} = \frac{\dot{E}_{\rm CR}}{12\pi\,\kappa_{\rm eff}\,r}$ can be found, as has been widely adopted in the literature (Hopkins, Chan, Garrison-Kimmel, et al., 2020; Hopkins, Squire, Chan, et al., 2021; Hopkins, Chan, Squire, et al., 2021; Quataert, Thompson, and Jiang, 2022; Butsky, Nakum, et al., 2023). This solution is valid out to the effective diffusive transport radius $\sim \sqrt{\kappa_{\rm eff}\tau}$, with a significant exponential tail extending out to $\sim \sqrt{4\kappa_{\rm eff}\tau}$, where τ represents the time over which CRs have been injected.

Case 2: $v_{\rm eff}$-dominated Transport

In the limit of $\kappa_{\rm eff} \rightarrow 0$, CR transport is dominated by advective outflow and/or by streaming, and Equation 6.3 reduces to the advection equation in spherical coordinates. In steady-state, this has a well-known solution of $P_{\rm CR} = \dot{E}_{\rm CR}/(12\pi v_{\rm eff} r^2)$ (Quataert, Jiang, and Thompson, 2022; Quataert, Thompson, and Jiang, 2022; Hopkins, Quataert, et al., 2025) out to some finite travel distance $\sim v_{\rm eff} t$.

We now explore time-dependence of injection — consider a strongly peaked injection history around z $\sim$ 2 – 3 as expected for peak star formation or z $\sim$ 1 – 2 for

peak massive black hole accretion, which then falls off with time as $\sim t^{-\xi}$, where ξ is some power-law fit the to falling (but bursty) low-redshift injection history.

Now, if $\dot{\mathrm{E}}_{\mathrm{CR}} \sim t^{-\xi}$, and the injected pulse propagates primarily at $\mathrm{v_{eff}}$, then $\dot{\mathrm{E}}_{\mathrm{CR}}$ increases with t', the look-back time to injection. Thus, the expected $\mathrm{P_{CR}}$ profile in this limit should be shallower than the r^{-2} behavior of the steady-state wind case, instead being $\propto r^{-2+\xi}$. This holds when $\dot{E}$ varies significantly on a timescale $\lesssim$ the transport time $\mathrm{r/v_{eff}}$.

Such a solution can be worked out via the method of characteristics for a constant $\mathrm{v_{eff}}$, where $\mathrm{r(t) = r_0 + v_{eff} * t}$. Explicitly including the time dependence within the boundary condition, for the characteristic where the radius of an expanding shell is directly related to $\mathrm{v_{eff}}$ and there is no shell mixing leads to

$$P_{\mathrm{CR}}(r,t) = \frac{\dot{\mathrm{E}}_{\mathrm{CR}}(t')}{(12\pi v_{\mathrm{eff}} r^2)} H(t') \tag{6.5}$$

where for this case $t' = t - \frac{r}{v_{\mathrm{eff}}}$ exactly and H is the Heaviside step function. Essentially, the pressure profile at a given radius will depend on the CR injection at t' , and truncate beyond the finite travel-time distance.

Case 3: Constant κ_{eff}, Constant $\mathbf{v_{eff}}$

When the transport of CRs is not solely in the diffusive limit, we must account for the effective streaming and/or advection speed. In this scenario, for uniform $\mathrm{v_{eff}}$ an exact solution to Eq. 6.3 in Cartesian coordinates can be found,

$$P_{\mathrm{CR}}(\vec{r},t) = \int_0^t \frac{\dot{E}_{\mathrm{CR}}(t')}{3\left(4\pi\kappa_{\mathrm{eff}}\, t'\right)^{3/2}} \exp\left(-\frac{\|\mathbf{r} - \mathbf{v_{eff}} t'\|^2}{4\,\kappa_{\mathrm{eff}}\, t'}\right) dt'$$

wherein $\mathbf{r}$ and $\mathbf{v_{eff}}$ represent the vector position and effective advection and/or streaming speed. However, proper treatment of Eq. 6.3 in spherical coordinates forgoes such an exact and simple solution via Galilean transformation of a Gaussian. This owes to the extra curvature terms of form $\frac{2}{r}\nabla P$ introduced by the divergence in spherical coordinates. The far-field regime (large r) is precisely where these curvature terms will be less significant for the shifted Gaussian solution, though it will strictly over-estimate the true total pressure at inner to intermediate radii and subsequently not conserve total energy as the exact solution should.

We can approximate the true form for constant $\kappa_{\rm eff}$ and $v_{\rm eff}$, by ignoring the curvature terms, finding

$$P_{\rm CR,BH}(\vec{r},t) = \int_0^t \frac{\dot{E}_{\rm CR}(t')}{3\left(4\pi\kappa_{\rm eff}\,t'\right)^{3/2}}\,\exp\left(-\frac{(r-v_{\rm eff}t')^2}{4\,\kappa_{\rm eff}\,t'}\right)dt' \tag{6.6}$$

While strictly approximate, this functional form provides intuition for the true diffusion and streaming/advection solution, wherein as shells expand and move outwards from the central source, they will mix owing to diffusion, with the shells associated with a single injection event being "smeared" out in radius as they propagate outwards.

However, it is possible to correct for this over-estimation to leading order by noting Eq. 6.6 simply represents the convolution of a time-dependent source function with a normalized spatial Green's function kernel. Thus, we can re-write Eq. 6.6 as $\int_0^t \dot{E}_{\rm CR}(t) g_0(r,t')dt'$, where $g_0(r,t') \equiv \frac{1}{3{\rm A(t)}\left(4\pi\kappa_{\rm eff}\right)}$, and ${\rm A(t)} \equiv \frac{\dot{E}_{\rm CR}(t')dt'}{\int_0^\infty 12\pi r^2 g_0(r,t')dr}$ is the kernel normalization function which ensures the shifted approximate Gaussian solution conserves total energy injected at any fixed time interval. We enforce this normalization condition in the proceeding results, and we discuss and show later how this simple approximate solution can be used as a semi-analytic model which matches the true numerical solution to Eq. 6.3 to a surprisingly high degree of accuracy.

Contrasting Constant CR Transport Parameter Behavior with Injection History

The evolution of the CR pressure in halo with an arbitrary injection history can be modeled using the approaches in the previous subsections, and in this section we explore the resulting variation in spatial distribution of CR energy at a given time snapshot for different injection histories.

We show different the different model injection histories we utilize for comparison in this work in Figure 6.1, and in Figure 6.2, we contrast the *qualitative* behaviors of Case 1 and Case 3 pressure profiles integrated over cosmic time up to $z \sim 0.8$ for single large delta function injection, the reference empirically-motivated time-dependent injection, and reference bursty, time-dependent injection histories.

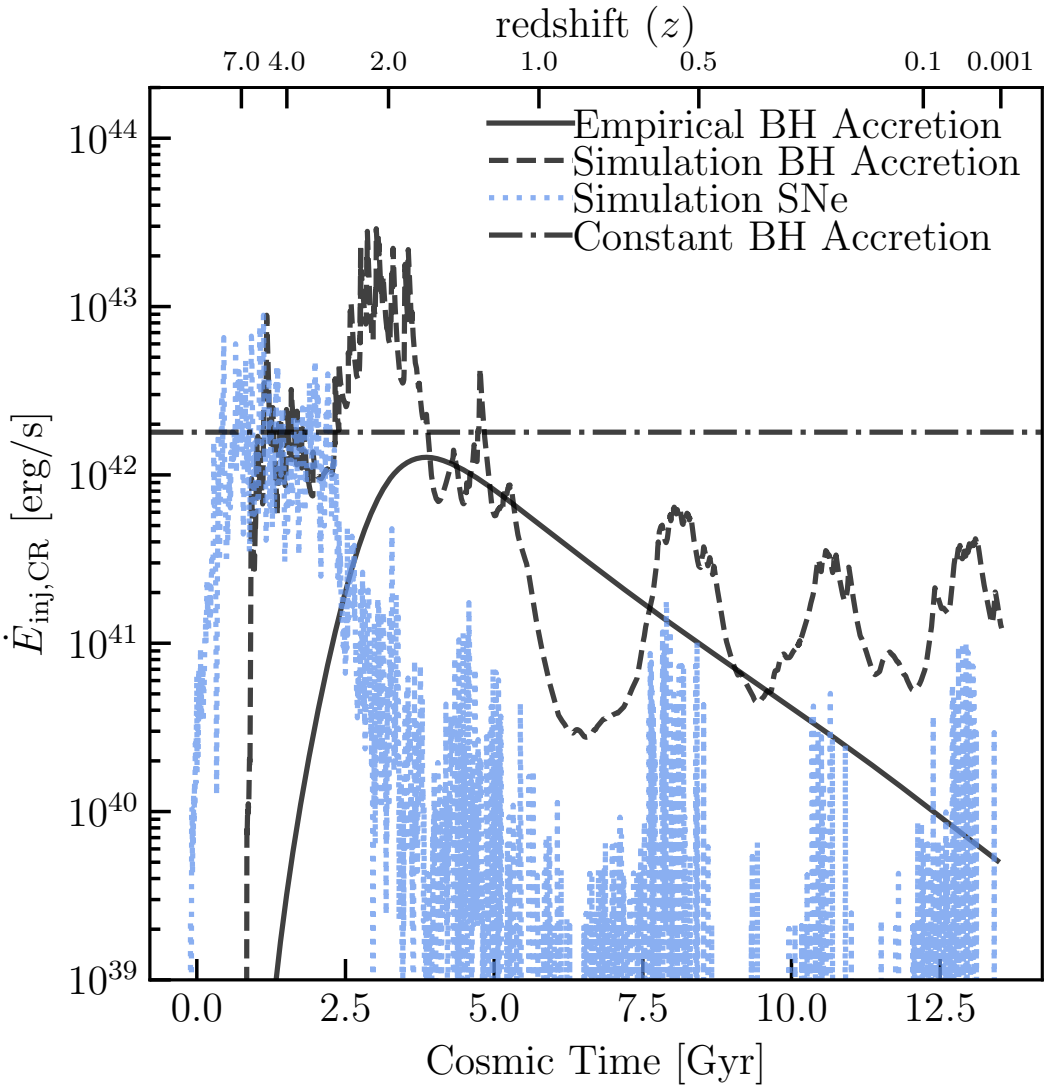

Figure 6.1: *Reference CR energy injection histories used for our model comparisons in this study.* The simulation injection histories from BH and stellar contributions (black dashed and blue dotted) are taken from a fully dynamical CR-MHD simulation of a massive halo from the FIRE-3 simulation suite (Hopkins, Wetzel, Wheeler, et al., 2023; Byrne et al., 2024). The empirically motivated injection history (solid line) follows the average black hole accretion rate for $M_{\rm halo}^{z=0} = 10^{13} M_{\odot}$ from the empirical model `Trinity` (Fig. 16 of Zhang, Behroozi, et al., 2023). The constant BH accretion model takes the total energy integrated over time for the simulation model history and averages over a Hubble time. For each BH accretion cases, we assume $\epsilon_{\rm CR,BH} = 3 \times 10^{-4}$.

To simplify the qualitative comparison here, we consider only injection from black hole accretion with the same $\epsilon_{\rm CR,BH} = 3 \times 10^{-4}$ for each case. The delta function approximation follows Quataert and Hopkins (2025), where we assume black hole growth peaked at z∼3, whereas the empirically motivated injection history follows the average black hole accretion rate for $M_{\rm halo}^{z=0} = 10^{13} M_{\odot}$ from the empirical model Trinity (Fig. 16 of Zhang, Behroozi, et al., 2023). This empirical injection history marginalizes over short time-scale variability that would be seen in individual halos, as it represents an ensemble average. To demonstrate how highly time-variable injection can affect the resulting pressure, we also take the black hole accretion rate directly evolved in a cosmological zoom-in FIRE-3[2] simulation of a $M_{\rm halo}^{z=0} = 10^{13} M_{\odot}$ halo, run with a spectrally-resolved treatment of CR dynamics, evolving a spatially and temporally constant power-law scattering rate $\nu_{\rm CR}$ with CR rigidity, which gives rise to a constant $\kappa_{\rm eff}$ (Hopkins, Wetzel, Wheeler, et al., 2023; Ponnada, Cochrane, et al., 2025). We compare these same time-dependent injection histories for Case 2 (constant advection/streaming-only solutions) in Figure 6.3.

When examining Figure 6.2 and Figure 6.3, two behaviors immediately become clear. First — effective streaming/advection (for plausible speeds) moves the bulk of the CR energy outwards relative to the pure diffusion case. This is clear not only from the translation of the pressure fronts outwards, but from the flattening of the profiles at larger radii. Comparing this to the delta function case, this implies that *CR pressure may not only be important at the virial radius of massive galaxies (Quataert and Hopkins, 2025), but even out to larger, cosmologically relevant scales* ($\geq R_{200} \sim 300$ kpc).

Secondly, *time dependent injection can significantly alter CR pressure profiles*. This is evinced by the changes apparent for the same toy model transport parameters between the panels of Figures 6.2 and 6.3. In particular, compared to a singular delta function source, time-dependent injection naturally elevates the pressure profiles in the inner halo ($r \lesssim 100$ kpc due to late-time injection beyond z ∼ 3, and also serves to flatten the profiles at large radii relative to steady-state scalings described in §6.3.

The isolated effect of time dependence is especially clear in Figure 6.3, where there is no diffusion to smooth out the pressure at large radii — any flattening relative to the analytic expectation of a $\sim r^{-2}$ profile owes solely to the time dependence of injection, as we discussed in Section 6.3. Such flattening of the profiles even in the empirical injection case, which by construction averages over short fluctuations

[2] https://fire.northwestern.edu/

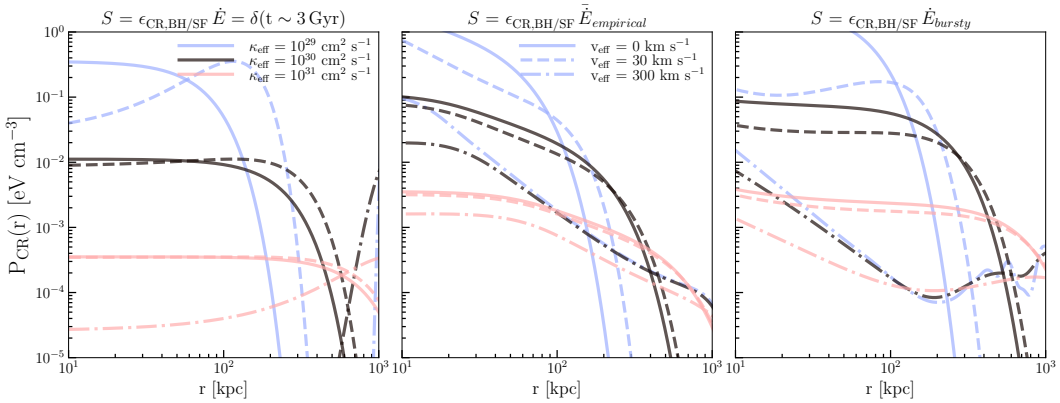

Figure 6.2: *Exact diffusion-only (Eq. 6.4) and approximate semi-analytic diffusion+streaming/advection (Eq. 6.6) solutions for P_{CR} in a massive galaxy halo ($M_{halo}^{z=0} = 10^{13} M_\odot$) at $z = 0.8$.* **Left:** Solutions for a single, strongly peaked δ-function injection at $z \sim 3$ with $\epsilon_{\rm CR,BH} = 3 \times 10^{-4}$. **Center:** Solutions for a peaked but slowly decaying CR injection history for a massive halo taken from an empirical model for the average black hole accretion rate (Zhang, Behroozi, et al., 2023), with $\epsilon_{\rm CR,BH} = 3 \times 10^{-4}$. The colors denote increasing $\kappa_{\rm eff}$ (10^{29}, 10^{30}, 10^{31}) cm^2 s^{-1} in order of blue, black, pink, with solid, dashed, and dot-dashed linestyles denoting rising $v_{\rm eff}$ (0, 100, 300) km s^{-1}. **Right:** The same solutions for a bursty, time-dependent CR injection history for a simulated halo of the same mass with the same injection efficiency. Diffusion + streaming/advection solutions here are *approximate,* and thus re-scaled to conserve the total energy injected following §6.3, whereas diffusion-only ($v_{\rm eff} = 0$) solutions are exact. Compared to a single δ-injection, time-dependent injection can shift the distribution of CR energy, increasing the pressure at inner radii for the same transport parameterization due to late-time injection, and flattening profiles at large radii relative to steady-state expectations.

in the injection rate, indicates that even the slow evolution of the *average* black-hole accretion rate (or cosmic star formation rate) can substantially influence the distribution of CR pressure in low-z halos. Of course, if the injection history features large variation with time, this will naturally appear in the pressure profiles as seen in the right panel of Fig 6.3 and seen (though less pronounced) in the "bumps" in the Case 3 (diffusion + advection/streaming) profiles in Figure 6.2. In the presence of diffusion, the individual injection 'bursts' get smeared across radial shells, though large amplitude fluctuations (depending on the effective diffusivity) may not get fully smeared into the flattened out bulk profile (see the structure of the lowest diffusivity line in Fig. 6.2, right panel).

In the following sections, we compare these analytic and approximate expectations

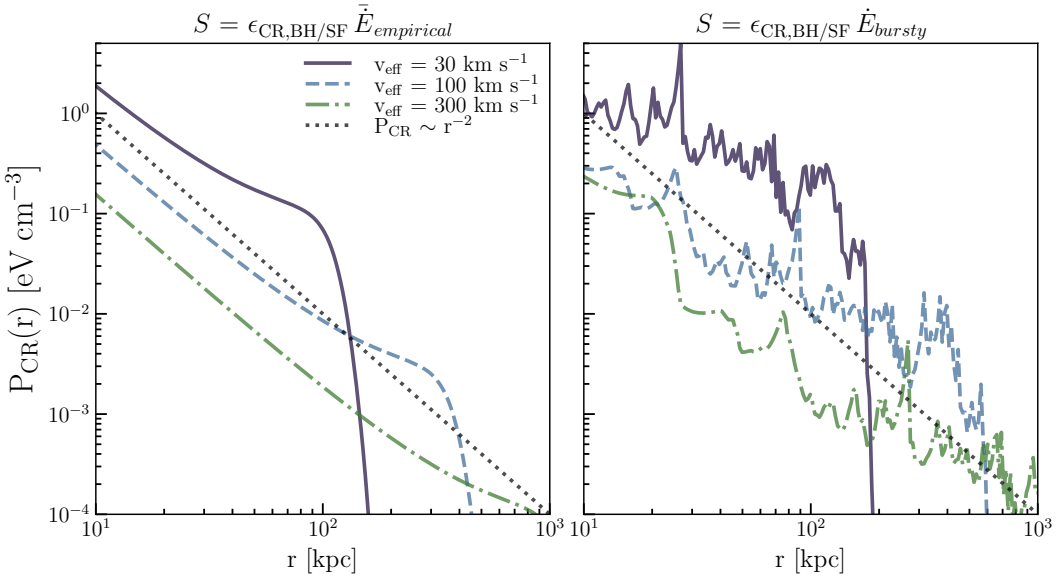

Figure 6.3: *Analytic streaming/advection-only solutions (Eq. 6.5) for P_{CR} in galactic halos at $z = 0.8$.* **Left:** Solutions for a peaked but slowly decaying CR injection history for a massive halo ($M_{\rm halo} = 10^{13} M_\odot$ taken from an empirical model for the average black hole accretion rate (Zhang, Behroozi, et al., 2023), with $\epsilon_{\rm CR,BH} = 3 \times 10^{-4}$. Purple solid, blue dashed, and green dot-dashed line represent different values of constant $v_{\rm eff}$. Black dotted guide lines show the $P_{\rm CR} \sim r^{-2}$ slope expected for steady-state solutions. **Right:** The same constant $v_{\rm eff}$ solutions for a bursty, time-dependent CR injection history for a simulated halo of the same mass with the same injection efficiency. In both cases, variation of $\dot{E}(t)$ leads to flattening of the average pressure profiles relative to the steady-state case, with the bursty injection history showing more episodic plateaus and bursts owing to large changes in accretion (injection) rates on timescales short compared to the effective travel times to a given radius.

to exact numerical solutions of Eq. 6.3 for arbitrarily variable $\kappa_{\rm eff}$ and $v_{\rm eff}$, and validate our simple numerical model for the evolution of CR pressure against full CR-MHD galaxy simulations.

6.4 Numerical Solutions to Time-Dependent CR Pressure Evolution

In this section, we present exact numerical solutions to Eq. 6.3 and compare our approximate solutions, which we show robustly describes the evolution of time-dependent CR pressure to leading order in galaxy halos. There is not a simple closed form analytic expression in this case, and so we now explore exact numerical solutions for the CR pressure given our aforementioned assumptions.

To solve Eq. 6.3, we utilize a finite volume approach on a logarithmic radial grid

of N_{grid} = 1500 cell centers evenly spaced between $\log_{10}$(r/kpc) = -2 to 3.5, with a zero Neumann and outflow boundary condition at the inner and outer boundaries, respectively. In this parameterization, the first grid cell implicitly contains r = 0, and P_{CR} is initialized to 0 in each grid cell. We model the delta function source term by injecting $(\gamma_{CR} - 1)\dot{E}_{CR}[t]$ in the first grid cell, normalized by the first cell's volume. The diffusive and effective streaming+advective fluxes are computed between cell faces (assuming spherical symmetry) in a strictly energy conserving manner, with the evolved property being $P_{CR,i} = (\gamma_{CR} - 1)E_{CR,i}/V_i$, the volumetrically-averaged CR pressure within each spherical cell. For time integration, we use an implicit Runge-Kutta method of order 5 from the Radau IIA family (Hairer and Wanner, 1996; Hairer and Wanner, 1999), implemented in `scipy` (Virtanen et al., 2020). This implicit method is suited for stiff problems like fast diffusion, and allows for larger time-stepping on high-resolution grids compared to explicit Runge-Kutte methods of the same order.

In Figure 6.4, we show the resulting numerical solutions to the Case 3 (diffusion + advection/streaming) CR transport for the same time-variable injection histories as in Figure 6.2, evaluated out to z = 0.8. Here, when we are working with the exact numerical solutions, we do not re-scale the corresponding profile in any manner — the curves are manifestly energy conserving and any loss of energy simply represents the transport of flux out of the domain (f_{cal} = 0 is assumed). We again assume $\epsilon_{CR,BH} = 3 \times 10^{-4}$ for each case, and again demonstrate only injection from BH accretion.

Like our approximate solutions in Figure 6.2 demonstrated, the true solution to the diffusion + advection/streaming equation in the presence of non-negligible time dependence and v_{eff} results in more CR energy being shifted out to large radii, with the P_{CR} profiles for bursty injection retaining some of the burst structure for large injection events and lower values of κ_{eff}, but increasingly 'losing memory' of the burst structures as diffusion becomes more important. Relative to the single δ injection approximation, CRs injected at later times boost the inner halo (r $\lesssim$ 100 kpc) profiles substantially.

In Figure 6.5, we compare a simple power-law scaling of $\kappa_{eff} \sim r^{-1}$ (subsuming 'streaming/advection-like' behavior into diffusion), motivated by the closed form solution to the diffusion-advection/streaming dynamics in flux steady state under spherical symmetry to the constant diffusion-advection/streaming solution with time dependence. In these types of solutions (as discussed in §6.3), for a given constant

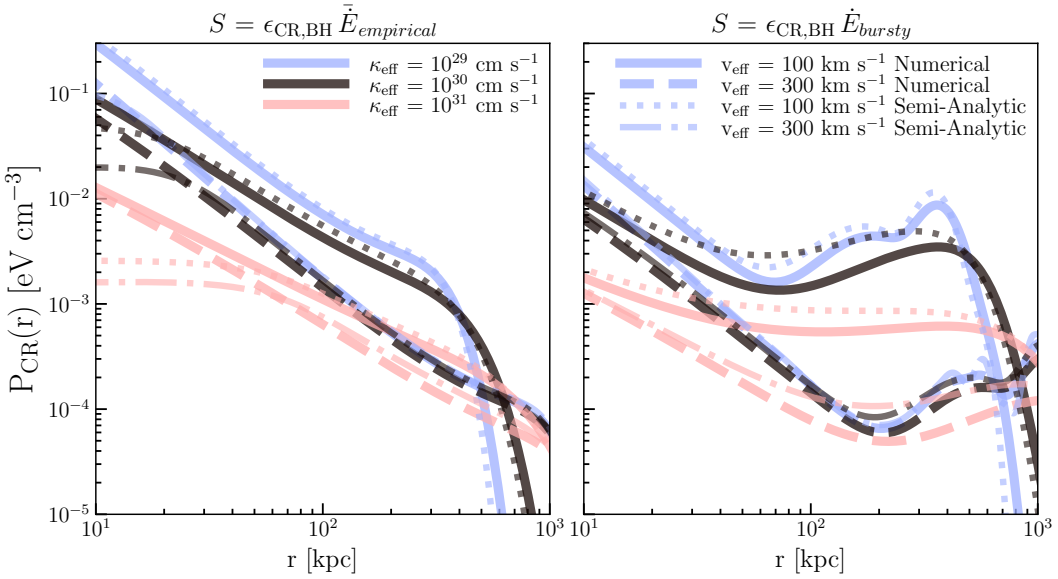

Figure 6.4: *Exact numerical and approximate semi-analytic solutions for P_{CR} (Eq. 6.3) in galactic halos at $z = 0.8$.* **Left:** Solutions for a peaked but slowly decaying CR injection history for a massive halo taken from an empirical model for the average black hole accretion rate (Zhang, Behroozi, et al., 2023), with $\epsilon_{\rm CR,BH} = 3 \times 10^{-4}$. **Right:** The same solutions for a bursty, time-dependent CR injection history for a simulated halo of the same mass with the same injection efficiency. In both panels, colors denote $\kappa_{\rm eff}(10^{29}, 10^{30}, 10^{31})$ cm^2 s^{-1} in order of blue, black, pink, with solid and dashed lines denoting different $v_{\rm eff}$ (100, 300) km s^{-1}, with the same shown for the approximate semi-analytic solutions in dotted and dot-dashed lines, respectively . The true numerical solutions verify that time-dependent injection shifts the distribution of CR energy out to larger radii, which is further enhanced due to non-negligible effective streaming/advection relative to diffusion-only cases (c.f. Fig. 6.2), and the approximate solutions show a high degree of validity, particularly at large radii, but with slight overestimation relative to the numerical solutions at intermediate radii.

$\kappa_{\parallel}$ and $v_{\rm st,eff}$, for radii $r \geq r_{\rm st} = \kappa_{\parallel}/v_{\rm eff}$, $\kappa_{\rm eff} = v_{\rm eff} * r$.

Hence, in steady-state, the solutions for the constant $v_{\rm eff}$ streaming/advection only case and a $\kappa_{\rm eff} \sim r^1$ 'diffusive' case become degenerate beyond the 'streaming-radius', out to some effective streaming/advection cut-off radius $r_{\rm cut,\,st/adv} = v_{\rm eff} * \tau_{\rm inj}$. Beyond this radius, the differing effects of "streaming/advection-like" and "diffusive" behavior may become significant. Furthermore, while this approximation holds quite well for steadily star-forming galaxies with relatively constant CR injection rates, it remains unclear how well this holds for time-variable injection, and if time-dependence can break this degeneracy between transport behavior.

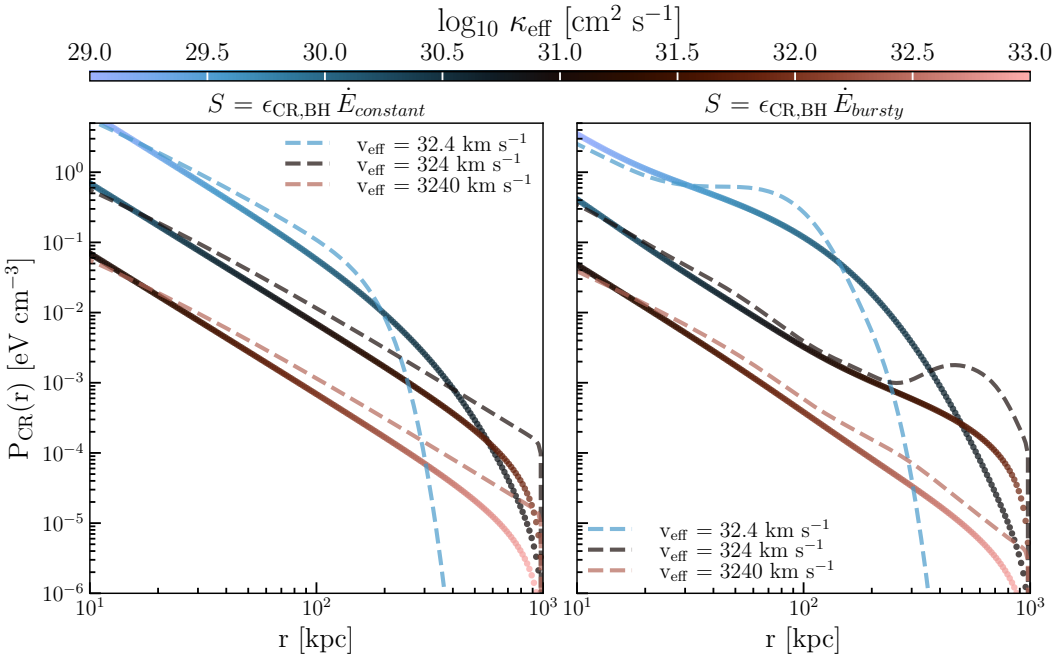

Figure 6.5: *Numerical solutions for P_{CR} (Eq. 6.3) in a massive galactic halo ($M_{halo}^{z=0} = 10^{13} M_{\odot}$) at $z = 1.299$.* Solid multi-color lines show the solutions assuming $\kappa_{\rm eff} = \kappa_{\parallel,\rm ISM} \frac{r}{10\ \rm kpc}$ (valid in steady-state for continuous injection) with 'advection/streaming-like' behavior subsumed into 'diffusion.' Dashed lines represent lower/higher constant $\kappa_{\parallel}$ + $v_{\rm eff}$ * r diffusion + advection/streaming solutions at fixed "streaming/advective" radius $r_{\rm st}$ = 10 kpc. In both panels, colors are scaled to $\kappa_{\rm eff}$ (increasing from blue to pink) used for each model solution. **Left:** Solutions for a constant CR injection history with $\epsilon_{\rm CR,BH} = 3 \times 10^{-4}$. **Right:** The same solutions for a bursty, time-dependent CR injection history for a simulated halo of the same mass with the same injection efficiency. While the flux-steady state approximation of $\kappa_{\rm eff} \sim r$ behavior holds out to the effective diffusive radius $\sim \sqrt{\kappa_{\rm eff} \tau}$, subsuming non-steady 'advection/streaming'-like behavior into $\kappa_{\rm eff}$ can over-/under-predict the "true" $P_{\rm CR}(r)$ at large radii due to finite travel-time effects and diffusive "softening", which can be very significant for $r \gtrsim R_{\rm vir}$ depending on non-trivial injection histories and the values of $\kappa_{\rm eff}$ and $v_{\rm eff}$.

From examining Figure 6.5, we see that even in the continuous injection case, subsuming a constant v_{eff} into purely 'diffusion-like' behavior as $\kappa_{eff} \sim r$ leads to significant differences at large radii due to finite travel time effects. This owes primarily due to the extended tail of a given 'diffusion-like' Green's function solution (§6.3), where despite the location of the 'diffusive' peak exactly localizing to $r_{cut,\ st/adv}$, the additional diffusive behavior at the boundary moves additional CR flux outwards. This means for $r \gtrsim r_{cut,\ st/adv}$, P_{CR} is strictly over-estimated whereas for $r \lesssim r_{cut,\ st/adv}$, P_{CR} is under-estimated. Assuming steady state and subsuming 'diffusion-like' behavior into a purely 'streaming/advection' solution with $v_{eff} \sim \kappa/r$ would result in vice-versa under-/over-estimation of P_{CR} in this case (i.e., one would miss extended tails of CR pressure where they ought to be).

In the case examined in Fig. 6.5, this over-estimation is evident for the lowest κ_{eff}, v_{eff}, parameterization in the constant injection case, and when $\tau_{inj} > t_{Adv}, t_{diff}$ as in the higher κ_{eff}, v_{eff}, parameterizations, the steady-state $\kappa_{eff} \sim r$ begins to under-predict the true P_{CR} at large radii. These time-dependent effects are further exacerbated for non-steady injection as evinced by the solutions for the bursty injection histories. Of course, the degree of under-/over-estimation here also depends on the time variability of CR injection (which for fixed transport parameterizations will affect the degree to which $P_{CR}(r)$ is in steady-state), radial variation of κ_{eff} and/or v_{eff}(which we stress can in principle arbitrarily vary with plasma conditions), and subsequently the exact value of r_{st}, and so we simply show a characteristic case of fixed r_{st} = 10 kpc for plausible values of constant κ_{eff} and v_{eff} as one example.

We again emphasize that the true behavior of CR transport at these large halo radii is essentially unknown. Direct simulations of CR pitch-angle scattering in turbulence in various regimes have rarely focused on the CGM (though see Reichherzer et al., 2025, for a relevant exploration of scattering conditions in the ICM). There are, however, observational hints towards rising κ_{eff} in the CGM of $\sim L^*$ galaxies (Butsky, Nakum, et al., 2023), and if κ_{eff} were sufficiently large and arising from the 'diffusive' limit of the CR scattering rate, these 'diffusive softening' effects relative to the "true" constant diffusion + streaming/advection solution may become less important as sharp gradients would be smoothed over and P_{CR} at a given radius would more quickly reach a steady-state. So in this regime, the "softened" solution may actually present the more physically "correct" representation of P_{CR} compared to the constant diffusion + advection/streaming transport parameterization.

Nonetheless, in Figure 6.6, we demonstrate how the different behaviors of the

solutions in Figure 6.4 lead to strongly varying gradients, particularly when finite travel time effects are significant. Here, we show the dimensionless gradient of P_{CR} at t = 5 Gyr (z = 1.25, closer in time to the peak variability in injection) for the same range of CR transport parameterizations as in Fig. 6.5. We stress that we intentionally choose higher-z snapshots for this model injection to emphasize the regime in which time-dependent effects would be significant, but where time-dependent effects are important depends upon the exact nature of a given source i.e., for rising star-formation histories at late times as seen in dwarf galaxies, these effects may be more important at low-z, though we discuss the context of satellite galaxies in more detail below.

In Figure 6.6, for fixed r_{st}, the spatial scale at which strong CR pressure gradients emerge due to finite travel time effects is strongly dependent upon how the transport is modeled i.e., using the degenerate steady-state solution vs. evolving 'diffusive' and 'advection/streaming-like' terms separately. Again, while we neglect adiabatic effects here, we caution that not accounting for varying source injection times will artificially modulate the physical scale at which CRs dynamically drive winds, as well as the magnitude of this effect. The significance of this time-dependent effect depends on the ratio of the ∇P_{CR} to the virial pressure gradient at a given radius — here we have presented the gradients in dimensionless form as the relevance of this effect will depend on the exact energetics of the system being modeled. But we stress that in any sub-grid assuming steady-state, these important effects may compound for non-trivial time-variable source injection and/or source spatial distribution non-linearly in the emergent dynamical effects of CRs on the background gas.

Notwithstanding a clear understanding of the CR transport, we stress that the most common assumptions in the literature thus far have invoked constant transport parameterizations as we have exemplified here, and so we caution careful consideration of these time-dependent effects in sub-resolution or analytic modeling of CR feedback around galaxies, particularly for complex source distributions or in large cosmological volumes.

Another important consequence of this is that *time dependence of P_{CR} can break the degeneracy between effective 'diffusion-like' and 'streaming-like' behaviors,* as we aimed to discern. We discuss the observational implications of this further below, and in the next section, we explore how variation in transport parameters may further compound with time-dependent effects.

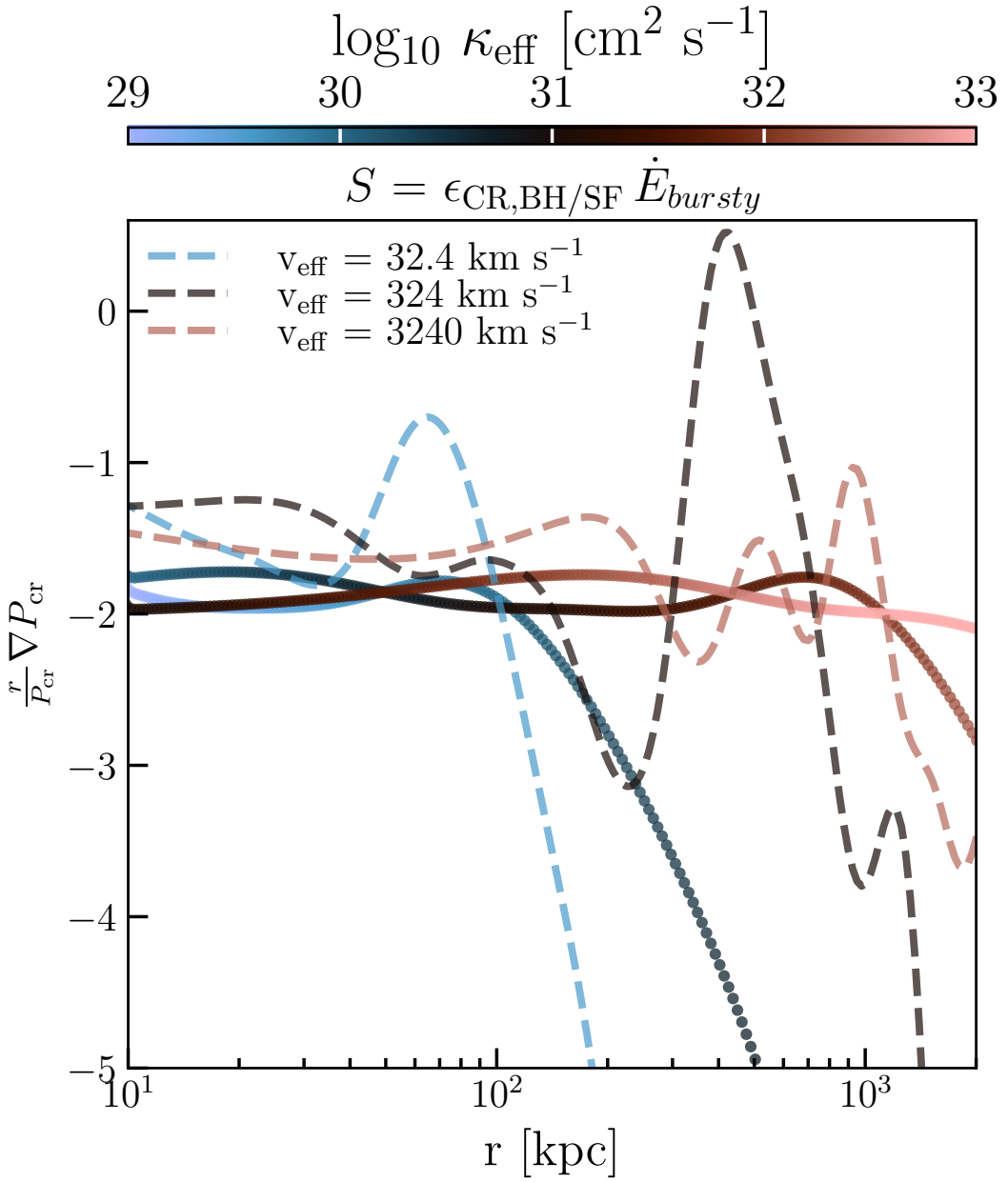

Figure 6.6: *Dimensionless CR Pressure Gradient in a massive galactic halo* ($M_{halo}^{z=0} = 10^{13} M_{\odot}$) *at* $z = 1.25$. Solid multi-color lines show the solutions assuming $\kappa_{\rm eff} = \kappa_{\parallel,\rm ISM} \frac{r}{10\ \rm kpc}$ (valid in steady-state for continuous injection) with 'advection/streaming-like' behavior subsumed into 'diffusion.' Dashed lines represent lower/higher constant $\kappa_{\parallel}$ + $v_{\rm eff}$ * r diffusion + advection/streaming solutions at fixed streaming radius $r_{\rm st}$ = 10 kpc. In both panels, colors are scaled to $\kappa_{\rm eff}$ (increasing from blue to pink) used for each model solution. Use of steady-state approximations can shift strong gradients relative to the diffusion + advection/streaming solutions and smooth over features which may appear in advection/streaming-dominated transport regimes.

6.5 Validation of Our Simplified Approach Against full CR-MHD Simulations

In Figure 6.7, we demonstrate the validity of our simplified assumptions and numerical modeling here by comparing our time-dependent semi-analytic and numerical solutions against a cosmological zoom-in simulation of a massive galaxy halo with explicit CR-MHD. We emphasize that it is not our goal in this chapter to exactly one-to-one match the reference simulation profile, as we have neglected inter alia collisional and adiabatic loss terms in our modeling for simplicity, but to demonstrate robustly capturing time-dependent effects which would otherwise be missed in a steady-state formulation. As such, we again choose a high-z snapshot time of the same massive galaxy simulation as this is the regime where these effects would be most significant, and contribution from in-spiraling satellite galaxies is relatively lower.

We see that solving for P_{CR} utilizing the star formation history, black hole accretion rate, and emergent value of κ_{eff} [3] evolved directly by the simulation from the scattering rate, we are able to well reproduce the shape of the full simulation P_{CR} profiles at large radii, which would be missed utilizing the steady-state 'effective diffusion' approximation.

In Figure 6.7, we have assumed only streaming losses at fixed $v_A = 30$ km s^{-1}, while in the full simulation, all relevant loss terms are evolved. While we assume $f_{cal} = 0$ for simplicity, we note that some non-zero fraction of the CR energy in the full simulation has to be lost to hadronic collisions as the central region around the BH is above the calorimetric surface density limit (Lacki, Thompson, and Quataert, 2010; Hopkins, Chan, Garrison-Kimmel, et al., 2020; Hopkins, Squire, Chan, et al., 2021; Ponnada, Cochrane, et al., 2025) at $z \sim 2-3$, but comparison of the total energy in the simulation volume to the total energy injected at the presented snapshot indicates that this is merely an order-unity correction (i.e., a large fraction of the CRs indeed escape into the halo).

Our simplified model predictions agree quite well with the true simulation for $v_{eff} = 650$ km s^{-1}, with streaming losses having negligible effect for large v_{eff} (c.f. the semi-analytic line of Eq. 6.6 and the numerical solution lines). As we discussed before, the local Alfvén speed and bulk gas motions can vary arbitrarily —

[3] Here, we take κ_{eff} for the $\sim$ GeV proton energy bin — as the comparison simulations are spectrally-resolved, the "true" κ_{eff} would be $\kappa_{iso} \sim c^2/(9\,\langle \nu_{CR}(r)\rangle_{E_{CR}})$, where $\langle \nu_{CR}(r)\rangle_{E_{CR}}$ is the CR energy averaged scattering rate across energy bins for gas cells at a given radius r, to account for possible shifting of the CR energy peak away from the canonical ~GeV (Hopkins, Butsky, Panopoulou, et al., 2022; Girichidis, Pfrommer, Pakmor, et al., 2022). For our proof-of-concept here, we choose the strictly constant, unweighted value.

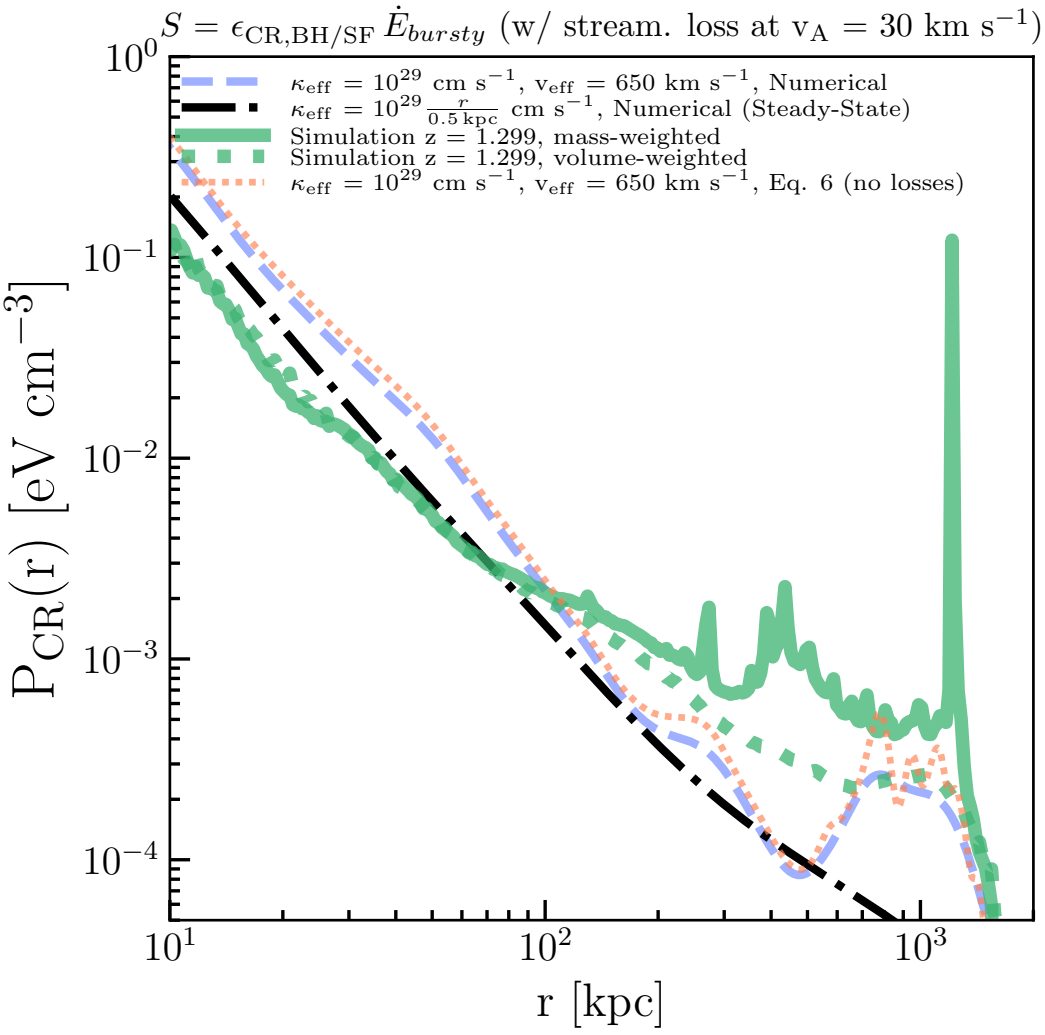

Figure 6.7: *Validation of our simplified modeling of P_{CR} against a fully dynamic, cosmological zoom-in simulation of a massive galactic halo ($M_{halo}^{z=0} = 10^{13} M_\odot$) at* $z = 1.299$. The line for a well-fit constant $\kappa_{\rm eff}$ and $v_{\rm eff}$ model is shown in dashed blue, and the full simulation result, mass and volume weighted medians in each radial bin, are shown by the green solid and dotted lines, respectively. The black dot-dashed line shows the same source injection evolved with the steady-state $\kappa_{\rm eff}$ formulation ($\kappa_{\rm eff} \sim r$), and the orange densely dotted line shows our simplified semi-analytic approach. Accounting for time-dependence of injection, our simplified approach can reasonably match the true result at large $r \gtrsim R_{\rm vir}$ to within a factor of a few, compared to the order-of-magnitude difference of the steady-state assumption at large radii. The mass-weighted simulation profile highlights the increasingly important contribution of in-spiraling satellite galaxies at large radii for modest z, with large 'spikes' of CR pressure.

nonetheless, we find that even profiles that significantly differ from the steady-state solutions can be well 'fit' (to within a factor of a few) particularly at large radii by our approximations, for some constant value of $v_{\rm eff}$ within the range we have sampled, particularly at large radii $r \gtrsim R_{\rm vir}$ where the bulk of the CR energy resides in this example case, and indeed capture features owing to extended periods of enhanced injection at higher z transported to the outer halo via "streaming/advection-like" behavior. Such features around r $\sim$ 1000 kpc ($\sim$ 3 $R_{\rm vir}$) are notably missed by the steady-state $\kappa_{\rm eff}$ formulation, and as we stress in the earlier section, these can be quite significant for the dynamical effects of CRs on the background gas and subsequent evolution of the galaxy.

We note also the mass weighted profile of the "true" simulation shows significant 'bursts', several of which are coincident with the locales of in-spiraling satellite galaxies. While we compare against the volume-weighted median to avoid biasing our validation (particularly as we do not include those satellite galaxies as sources in our modeling), we emphasize that the CR contributions from these satellites as they similarly diffuse and stream/advect outwards may contribute to the volume-weighted lines, hence explaining why we predict coincident 'dips' in our model lines evolving solely the central galaxy contributions. We stress that at lower redshifts, as these satellite galaxies of massive halos will have rising or approximately constant star formation histories relative to the massive central, which is expected in a population-averaged sense (Zhang, Behroozi, et al., 2023), these contributions may become increasingly important for massive groups and clusters at large halo radii from the central massive galaxy.

6.6 Discussion and Conclusions

In this work, we have analytically and semi-analytically detailed the effects of arbitrarily time-variable CR injection and spatially constant 'effective' transport parameters on the bulk CR pressure/energy distribution in galaxy halos. We demonstrate that bursty and time-dependent sources can have substantial effects on the distribution and evolution of CR pressure, particularly on large scales which may not be in pressure steady-state, and for which finite travel-time effects and/or source evolution can modify solutions significantly from steady-state expectations. Below, we summarize our results and discuss their relevant implications.

Implications for sub-grid models of CR feedback

We stress that these time-dependent effects are particularly of concern when utilizing sub-grid models for CR feedback in large volume simulations. For instance, if we were to utilize the steady-state formalism of Hopkins, Butsky, Ji, et al. (2023), Figures 6.5 and 6.6 make clear how at fixed simulation time, one may over-predict the true P_{CR} at a given radius if not accounting for finite travel-time effects of a given source (by implicitly using a larger than physical r_{max} or equivalently t_{max} in the sub-grid model proposed there), while simultaneously missing or shifting strong gradients owing to this same truncation due to diffusive 'softening' effects if the transport is in the 'streaming/advection-like' regime.

In this chapter we have only exemplified how these behaviors manifest at fixed time intervals, but we emphasize that these effects would compound non-linearly in any sub-grid implementation of CR feedback coupled to hydrodynamics, and it is not trivial to understand exactly how. Even in the example above, if one were to over-predict P_{CR} but miss large ∇P_{CR}, it is unclear whether one would still find the "true" dynamical outflow/inflow condition for the same conditions at a given time (thermal/magnetic pressure at a given radius etc.) but for the wrong reasons, or simply find the wrong answer entirely. This is particularly of importance as the non-linear, dynamical interaction of CRs in galactic halos via large-scale pressure gradients is the *principal* method by which several studies in the literature find CRs impact galaxy formation (Butsky and Quinn, 2018; Hopkins, Chan, Garrison-Kimmel, et al., 2020; Buck et al., 2020; Hopkins, Chan, Squire, et al., 2021; Huang and Davis, 2022; Quataert, Thompson, and Jiang, 2022; Armillotta, Ostriker, Kim, et al., 2024). Missing these effects across large time intervals would thus compound non-linearly with other generic galaxy formation physics of gas dynamics, star formation, and stellar/black-hole feedback via thermal and mechanical channels.

So, we recommend that 'best practice' for sub-grid implementations carefully consider the finite time-travel effects of each independent source, evaluating the contributions from each source at $\tau_{\rm inj,\,\it i}$, the time since injection from each source. As Hopkins, Butsky, Ji, et al. (2023) note, this presents inherent challenges for implementation in tree-based codes, and so we leave development of fast numerical schemes for updates to such sub-grid models to future work. The proof-of-concept of the semi-analytic, time-dependent approach presented here also presents an interesting new avenue to create a new subgrid model for CR feedback. While we leave presentation of a comprehensive numerical recipe and validation across different

galaxy mass regimes to future work, we briefly outline the approach here. For each source, $P_{CR}(\vec{r},t)$ can be estimated via Eq. 6.6 at a given timestep and appropriately normalized following the time-dependent kernel in Section 6.3, for a given choice of κ_{eff} and/or v_{eff} (which can be arbitrarily variable). To minimize the overhead cost of tracking each individual source, one could group sources (star forming particles or black hole sink particles) within each node to avoid tree-recomputation and compute the contribution to $P_{CR}(\vec{r},t)$ from each tree node. For each gas cell, the relevant tree nodes can be flagged to avoid unnecessary computation. For example, in large volumes containing massive galaxies or clusters, the contribution to P_{CR} at very large radii ($\gtrsim R_{vir}$) can become dominated by satellite galaxies at late times owing to quenching of centrals in contrast to rising SFHs in satellites. Every few time-steps (which requires calibration), the source tagging can be re-identified to avoid artificially missing source contributions owing to the prior grouping. Then, the relevant "shielding" terms to account for losses can be computed post-hoc, akin to the LEBRON methods outlined in other subgrid models (Hopkins, Butsky, Ji, et al., 2023) and the relevant CR thermochemical, pressure, and radiative contributions can be computed and conjoined with the hydrodynamics.

Implications for determining 'streaming/advection-like' vs. 'diffusive' transport in galaxy halos

In §6.4, we discussed how for constant CR transport parameters, the 'diffusion-like' and 'streaming-like' solutions become degenerate in pressure steady-state, for constant source injection. We find that for non-trivial source injection, deviation from the steady-state formulation can break this degeneracy. As we have noted above, in this work we are agnostic to whether the behavior in galaxy halos, particularly in the outer halos where there are few constraints, is 'streaming-like' vs. 'diffusion-like.' However, the predictions diverging presents a potentially interesting avenue to constrain the effective transport behavior in halos. We find that for non-trivial source injection, deviation from the steady-state formulation can break this degeneracy. As we have noted above, in this work we are agnostic to whether the behavior in galaxy halos, particularly in the outer halos where there are few constraints, is 'streaming-like' vs. 'diffusion-like.' However, the predictions diverging presents a potentially interesting avenue to constrain the effective transport behavior in halos.

In Figure 6.7, we show how the steady-state formulation of subsuming 'advection/streaming' into 'diffusion' with $\kappa_{eff} \sim r$ can lead to flattening out features associated with elevated injection over finite time intervals at higher redshifts (as is

expected for virtually any massive galaxy with strongly peaked BH accretion/star formation at $z \sim 2-3$) which otherwise are modestly smoothed and transported via advective/streaming-like behavior out to large radii.

We speculate that such transport features may be related to observable phenomena around massive galaxies and clusters, and are potentially of significance for constraining CR transport. For instance, 'Odd Radio Circles,' or ORCs, (Norris, Intema, et al., 2021; Norris, Crawford, and Macgregor, 2021) which are edge-brightened discs of diffuse radio continuum emission have been detected in recent $\sim$ GHz surveys. Follow-up observations have spatially associated these objects on-sky with massive galaxies $M_{\rm halo} \sim 10^{13} M_{\odot}$ at $z \sim 0.2-0.6$. While some studies have proposed these to be associated with virial shocks around such galaxies, (Yamasaki, Sarkar, and Li, 2023), there have also been idealized simulations demonstrating that CR-laden AGN jets can reproduce similar morphological features (Lin and Yang, 2024) — indeed the features we see naturally emerge from bursty SF/AGN injection transported out via streaming/advection in Figure 6.7 qualitatively bear resemblance to such structures at large radii, albeit at different redshift.

We leave an extensive survey of injection + transport conditions to future work (Butsky & Ponnada et al. in prep.), but we note that for plausible injection efficiencies, accretion/SF histories, and bulk CGM CR transport speeds, such features may represent transient periods in the bulk propagation of CRs out to large radii, which may inform us about the nature of CR transport in the outer CGM of massive galaxies. Therefore, the observed rarity of ORCs may be related to balance of diffusive vs. streaming-like transport with losses (and possible re-acceleration) out to a given galactocentric radius convolved with a time-dependent source injection history.

Motivation for exploring CR feedback across galaxy mass scales

In Figure 6.3, we demonstrated how even modest 'advection/streaming-like' behavior and time-dependent injection shifts $\rm P_{CR}$ out to larger radii (and therefore significantly shifts the distribution of $\rm E_{CR} \sim r^2 P_{CR}$ outward relative to steady-state approximations. This further corroborates the findings of Quataert and Hopkins (2025), who demonstrate for single δ-injection at $z \sim 2-3$ and plausible $\kappa_{\rm eff}$, $P_{\rm CR}$ can be dynamically significant in the outskirts of galaxy groups and clusters and potentially resolve the σ_8 tension between weak-lensing and cluster SZ measurements. We emphasize that not only may this be the case, but time-dependent effects may considerably compound, subsequently affecting how CR feedback influences

both the matter power spectrum and regulation of galaxy growth via 'preventative' feedback on large-scales ($k^{-1} \sim$ Mpc).

Idealized simulations of CR jets (Su, Hopkins, Bryan, et al., 2021; Su, Bryan, Hayward, et al., 2024; Lin and Yang, 2024; Su, Bryan, Hopkins, et al., 2025) and cosmological zoom-in simulations with BH-generated CRs and explicit CR-MHD (Wellons et al., 2023; Byrne et al., 2024; Ponnada, Cochrane, et al., 2025) are limited in their predictive power at these large-scales, therefore implementation of CR feedback in large volume cosmological simulations of galaxy formation à la IllustrisTNG (Pillepich et al., 2018), Simba (Davé et al., 2019), Astrid (Ni et al., 2022), FABLE (Henden et al., 2018), and FIREbox (Feldmann, Quataert, Faucher-Giguère, et al., 2023) (among others) is necessary.

Towards this end, Ramesh, Nelson, and Girichidis (2024) implement the steady-state sub-grid formulation of Hopkins, Butsky, Ji, et al. (2023) in a (25 Mpc h^{-1})^3 cosmological volume utilizing TNG physics, incorporating CR contributions from stellar sources. The implementation therein utilizes $t_{max} = t_{sim}$, which as we caution in §6.6 would over-estimate the true pressure contribution from all sources of finite age due to finite travel-time effects and potentially miss or shift strong pressure gradients, in addition to the other limitations described in Hopkins, Butsky, Ji, et al. (2023) regarding neglecting adiabatic losses. Notwithstanding these caveats, Ramesh, Nelson, and Girichidis find qualitatively similar conclusions regarding CR effects to the literature results from zoom-in and idealized simulations of $\lesssim L^*$ galaxies, warranting further study.

We propose further exploration of CR effects in large volumes akin to Ramesh, Nelson, and Girichidis (2024), particularly even larger volumes (which would more statistically sample galaxy groups and clusters) including treatments of CR injection from AGN (e.g., including small fixed-fractions of accretion energy in the form of a CR fluid as per (Wellons et al., 2023; Byrne et al., 2024; Ponnada, Cochrane, et al., 2025) and this work) as this would potentially expand the prediction space for CR effects via additional observables probing more massive systems like galaxy groups and clusters, e.g. weak-lensing and other matter clustering constraints (Sharma et al., 2025), X-ray emission stacks (Zhang, Comparat, et al., 2024), and radio continuum observations (Weeren et al., 2019).

And of course, comparisons of such observations with crudely parameterized theoretical predictions will only net an understanding of 'effective' bulk CR transport parameters averaged over large spatial scales, but these present a way to empirically

constrain the resurging theoretical study of CR scattering in MHD turbulence from first-principles (Kempski, Fielding, et al., 2023; Lemoine, 2023; Kempski, Li, et al., 2024; Butsky, Hopkins, et al., 2024) and thus the emergent effects on galaxy formation across cosmic epochs and mass scales, towards a clear physical theory of CR transport in galactic environments.

Acknowledgements

We wish to recognize and acknowledge the past and present Gabrielino-Tongva people and their unceded Indigenous lands upon which this research was conducted. Support for SP & PFH was provided by NSF Research Grants 20009234, 2108318, NASA grant 80NSSC18K0562, and a Simons Investigator Award. Numerical calculations were run on NSF/TACC allocation AST21010, TG-AST140023, and TG-PHY240164. ISB was supported by NASA through the Hubble Fellowship, grant HST-HF2-51525.001-A awarded by the Space Telescope Science Institute, which is operated by the Association of Universities for Research in Astronomy, Incorporated, under NASA contract NAS 5-26555. The Flatiron institute is supported by the Simons Foundation.

Chapter 7

SUMMARY AND FUTURE PROSPECTS

In this thesis, I charted a two pronged approach of testing observational methodologies of measuring quantities related to galactic magnetic fields and cosmic rays marred by dubious assumptions, and constraining highly uncertain cosmic ray transport parameters through emergent macroscopic observables. To do so, I extensively used cosmic-ray-magnetohydrodynamic, cosmological zoom-in simulations from the FIRE-2 and FIRE-3 suites (Hopkins, Wetzel, Kereš, et al., 2018; Hopkins, Wetzel, Wheeler, et al., 2023). These simulations, which explicitly evolve known physics pertaining to stellar evolution and their feedback result in galaxies with realistic multi-phase structure in the interstellar and circumgalactic media, and so serve as powerful testbeds for understanding the non-thermal physics of galaxies.

Towards my research directions, I developed numerical tools to generate end-to-end synthetic observations across the entire electromagnetic spectrum to expand the interpretive and predictive power of modern simulations of galaxy formation. Building on intuition gained from these full-physics simulations, I also developed new analytic and semi-analytic formalisms to better constrain and physically understand relevant parameters of these non-thermal components of galaxies from existing observations, and to more generally and accurately sample the vast allowable cosmic-ray parameter space in the under-explored context of massive galaxies as well as systems at high redshift.

Summary of Conclusions

The main results of this thesis are summarized below.

Chapter 2: Magnetic Fields on FIRE

1. In addition to reproducing detailed bulk properties and spatially resolved constraints on Milky-Way-like galaxies, FIRE-2 simulations with and without CRs reasonably reproduce observed magnetic field strengths and geometries in different phases of the ISM of the Milky Way and nearby spiral galaxies, and are in agreement with upper limits on the existing (but expanding) constraints on **B** in the CGM. Moreover, these constraints can be met with a power-law **B**-ρ

relation expected from adiabatic flux-freezing in ideal MHD, with "flattened" relations found in observational explained by noisy density-estimators with fraught underlying assumptions of thermal pressure equilibrium in the CNM, which we show is a poor assumption in the dynamic ISM.

2. Simulated galaxies with CR-dominated halos show slightly weaker **B** on average in tenuous gas associated with the disk-halo interface owing to prevention of recycling "fountain flows" by CR pressure gradients.

3. Rotation-/dispersion-measure inferences for **B** may under-predict "true" dynamical field trength by a factor of a few in the ISM and by factors of 15-20x in the CGM owing primarily to field reversals integrated along the lines of sight.

4. Simulated CR-pressure dominated halos around L^* galaxies exhibit factors of $\sim$ 2-3 higher dispersion measures in the inner CGM owing to additional support of "cool" CGM gas, consistent with predictions of other tracers.

Chapter 3: Synchrotron Emission on FIRE

1. Using CR-MHD simulations with "live" CR(e) spectra injected with a universal power-law in rigidity from SNe motivated by diffusive shock acceleration and an empirically-motivated power-law scaling for the CR scattering rate (Hopkins, Butsky, Panopoulou, et al., 2022), we can self-consistently reproduce realistic synchrotron emission from low-z L^* galaxies. The resulting emission characteristics are consistent with the as of yet most high-resolution view of radio continuum emission from spiral galaxies.

2. This self consistent computation of the emergent emission reveals that most of the synchrotron emission arises from relatively denser phases of the ISM and inner-CGM, rather than the volume-filling phases, contrary to common assumptions in classic equipartition models (Beck and Krause, 2005).

3. Due to the emission arising from denser phases, traditional equipartition estimates may under-predict the "true" **B** in the gas which dominates the emission by factors of a few in normal galaxies, and potentially much more significantly in starburst-like environments where CRe losses are strong.

4. We develop a non-equipartition analytic framework which can more accurately map onto **B** and e_{CR} in different phases of the ISM and inner CGM.

5. Furthermore, evolving CR(e) spectra is crucial to producing robust synchrotron predictions, particularly when loss terms are large as they can be in some L* galactic centers as well as starburst galaxies at high-z, and would not be captured utilizing simplified "single-bin" or steady-state treatments.

Chapter 4: Synchrotron Signatures of Cosmic Ray Transport

1. Using "single-bin" CR-MHD FIRE-2 simulations, we explore the emergent synchrotron emission from L* galaxy and massive dwarf simulations with constant, extrinsic turbulence-motivated, and self-confinement-motivated CR transport.

2. We find that extrinsic turbulence-motivated CR transport results in bulk and spatially resolved synchrotron properties similar to the phenomenological constant transport model at $z = 0$, but that emission emerging from galaxies with from self-confinement-motivated CR transport can significantly diverge.

3. The qualitative difference of the self-confinement-motivated CR transport owe to the fundamental scaling of self-confinement transport scalings, wherein the scattering rate is directly proportional to e_{CR}, which can quickly runaway to building up large e_{CR} and driving significant 'blowouts.'

4. These 'blowouts' fundamentally alter the gas phase structure and morphology of the simulated L* galaxies with self-confinement CR transport, resulting in morphologies and emission properties uncharacteristic of observed L* spirals at $z = 0$.

Chapter 5: 'Hooks,' 'Lines,' and 'Sinkers,': The Far-Infrared-Radio Correlation on FIRE

1. We demonstrate the surprising insensitivity of the global $z \approx 0$ far-infrared-radio correlation of galaxies to orders-of-magnitude locally variable CR transport parameters using fully cosmological zoom-in, spectrally-resolved CR-MHD simulations from the FIRE-3 simulation suite, for three distinct models of CR transport and multi-channel AGN feedback across three orders of magnitude in $z = 0$ galaxy halo mass.

2. We perform full Monte-Carlo radiative transfer postprocessing to produce UV-IR multi-band images along with synthetic synchrotron emission using

pipelines developed in Chapter 3, allowing for self-consistent evaluation of emergent observables.

3. We qualitatively confirm analytic predictions of UV photon and CRe "calorimetry" at high $L_{60\mu m}$ and "conspiracy" of CRe & UV photon escape at low $L_{60\mu m}$, with important contributions of secondary CRes from CRp calorimetry at very high $L_{60\mu m}$.

4. Notably, the different models chart different evolutionary tracks with z leading up to the $z = 0$ FRC (dubbed 'hooks,' 'lines,' and 'sinkers') due to *indirect* effects of AGN feedback as well as varied CR transport with the spatially resolved emission showing pathological behaviors between models, which can potentially explain the nature of so-called "radio-excess" outliers to the $z = 0$ FRC as instead being "IR-dim" owing to late-time quenching. These varied spatially resolved properties offer a potential avenue to constrain CR transport, even if the galaxy-integrated emission properties are insensitive to the model variations.

Chapter 6: Time Dependent Cosmic Ray Winds from AGN and Bursty Star Formation

1. We derive analytic solutions to CR pressure evolution in galaxy halos under spherical symmetry for CR transport on large scales parameterized with constant $\kappa_{\rm eff}$ and $v_{\rm eff}$ for arbitrarily time-dependent sources, and demonstrate that time-dependence can significantly alter CR pressure profiles. Notably, non-negligibly decreasing injection histories as expected for massive galaxies ($M_{\rm halo} \gtrsim 10^{13} M_{\odot}$) and even modest large-scale effective advection/streaming can lead to a larger share of CR energy being transported to large radii, motivating further exploration of CRs feedback from massive galaxies.

2. Our semi-analytic approximate solutions show a surprising degree of validity when compared to true numerical solutions to the diffusion-advection problem in spherical coordinates.

3. We demonstrate how certain artefacts in predicted sub-grid pressure profiles at high to modest z may arise from assuming the CR pressure around galaxies is in steady-state, leading to diffusive 'softening' of sharp gradients which may be preserved by 'streaming-like' behavior for reasonable CR transport parameterizations. These time-dependent features may also break the degeneracy

between large-scale 'streaming-' and 'diffusion-like' behaviors in steady state, and so motivate exploration of potentially related observable phenomena like Odd Radio Circles in this context.

4. We demonstrate the validity of our semi-analytic approach in the regime where time-dependent effects ought to matter, and outline implementation into a novel sub-grid model for CR feedback which we will develop in future work for use in large volume cosmological simulations, where time-dependent effects may compound significantly and CR contributions around massive halos can be explored in detail.

Future Outlook: Towards a physical picture of CR scattering

There still remain many questions regarding galactic magnetic fields and CR transport in galaxy formation. In my view, the most pressing is the lack of a first-principles theory for CR propagation. As discussed in Chapters 3 and 6, evidence has emerged in recent years that the quasi-linear theory models of old have fundamental problems in reproducing the limited observable constraints on CR spectra in our Galaxy from Voyager, AMS-02, and Fermi, in addition to synchrotron spectral slopes of observed systems (Hopkins, Squire, Butsky, and Ji, 2022; Kempski and Quataert, 2022). This has led to a return to the "drawing board," where *foundationally different, 'intermittent' models of CR scattering have been proposed* (Butsky, Hopkins, et al., 2024). Namely, it is possible for power-law distributions of scattering structures of gyro-resonant scales to reproduce known spectral shapes, which is of growing interest in connection to magnetic complexes which naturally form via MHD intermittency and instabilities (Kempski, Fielding, et al., 2023; Fielding, Ripperda, and Philippov, 2023).

I will run state-of-the-art CR-MHD ISM 'box' simulations to distinguish between quasi-linear scattering and otherwise plausible intermittent scattering models via additional observables. These simulations will be tailored specifically to answer this novel open question, utilizing numerical advances in the `GIZMO` code (Hopkins, Squire, and Butsky, 2022) I have gained expertise with, which allow for the evolution of CR(e) spectra in order to create multi-wavelength observables at γ-ray and radio frequencies with my existing pipelines. These can then be compared against the highest resolution Galactic observations.

These simulations may also be used to forward-model other ISM phenomena which may potentially relate to CR scattering, such as radio-wave 'extreme scattering

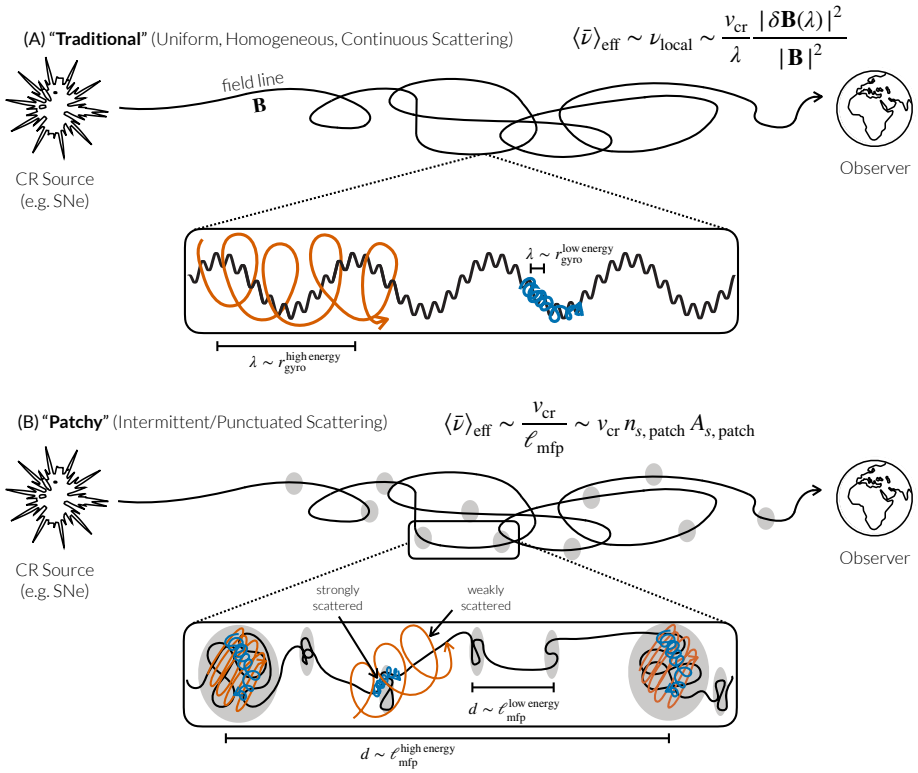

Figure 7.1: *Quasi-linear ('traditional') vs. intermittent ('patchy') CR scattering; Figure taken from Butsky, Hopkins, et al. (2024) with permission from the author.*

events' (Coles, Kerr, et al., 2015; Kempski, Li, et al., 2024), detected through scintillation and dispersion in sightlines towards point sources like pulsars and quasars and tiny-scale atomic structures (Heiles, 1997), detected in HI 21-cm absorption towards similar objects. The plasma structures giving rise to these refringent and absorptive effects are remarkably similar in size to the CR gyroresonant scales of interest, motivating exploration of their plausible physical connections. I will to do so by leveraging existing frameworks for radio-wave propagation through a set of defined properties for turbulent, ionized media as has been performed in the ISM pulsar literature (e.g., Coles, Rickett, et al., 2010, for example methodology), as well as my own tools for mock HI observations. Following these examples, I will develop radio-wave propagation tools to work with modern CR-MHD simulations which evolve the relevant plasma properties self-consistently, to lend insights connecting these fields of study.

Future Outlook: Synthetic Observations to constrain B and CRs on galactic scales, across redshift and galaxy mass

While zooming in on these smaller scale questions with tailored simulations, I will also continue following my synthetic observational approach to constrain galactic-scale quantities — I will make comprehensive multi-wavelength predictions connecting non-thermal physics to observables from radio to γ-ray frequencies at an opportune time for observatories like the Deep Synoptic Array, CHIME/FRB, next generation Very Large Array, PRIMA, AXIS, and legacy NASA missions like Spitzer and SOFIA. These predictions will further aid observational interpretation, and explore the potential Chapters 2-6 have identified for spatially-resolved observables of galaxies to constrain the elusive nature of CR transport as well as the role of **B** on galactic scales. These sorts of observational comparisons will inform our understanding of these physics not only in $\sim L^*_{z=0}$ systems, but also in more massive systems and across z as highlighted in Chapters 5 and 6.

On the $\sim L^*$ galaxy front, very recent observations of CR-driven outflows around spiral galaxies in the radio continuum (Matthews, Cotton, et al., 2025) along with upcoming high-resolution radio interferometric observations pushing to lower surface brightnesses ((Hallinan et al., 2019), to name one example) provide promising avenues for like-for-like comparisons to inform us regarding the non-thermal properties of galaxies on spatially resolved $\lesssim$ kpc scales. Revisiting the inventory of existing archival observations of spatially resolved spiral galaxies and applying the intuition and formalism developed in Chapter 3 may also provide a more physical understanding of the role **B** may play in regulating the cold and warm neutral ISM and tenuous disk-halo interface, building further on the heuristic comparison I performed to the observational fits edge-on spiral galaxies in that Chapter. In Chapter 6, we also emphasize the variation of spatially resolved properties across different wavelengths with CR transport physics — this leads to an interesting avenue of determining whether cross-correlations of spatially resolved emission properties pertaining to CRs and star-formation (like the radio synchrotron and FIR emission) can lend insights into the effective CR transport properties in different ISM phases. While this has been explored in the literature using steady-state diffusion-loss models (Heesen, Buie, et al., 2019), we emphasized in Chapter 5 how due to the non-linear nature of CR transport, the exact mapping between radio emission and CRe diffusion may not be obvious a priori, and requires dynamical modeling. Initial results testing these methodologies using explicit the CR-MHD simulations in Chapter 3 have already raised questions regarding these estimators (Knutas, Ponnada, & Panopoulou

in prep.), and utilizing these simulations to generate more careful, physically-robust estimators akin to our modeling in Chapter 3 may be fruitful for expanding our observational constraints on CR transport.

Beyond $\sim L^*$ at $z = 0$, a wealth of radio observations of both radio "mini-halos" at the galaxy group mass scale and extended "giant-halos" at the cluster mass scale exists and is quickly expanding (Gitti et al., 2018; Rajpurohit et al., 2025), which could lend insights into the role CR feedback plays in regulating massive galaxy growth, and the role CRs from AGN in particular may play in quenching, as we touch on in Chapters 5 and 6. These of course, will require new simulations evolving CRs, of which large-volume boxes may require improved sub-grid approaches as we outline in Chapter 6. By running and utilizing modern simulations explicitly resolving kinetic, radiative, thermal, and CR-feedback modes from AGN, I will generate novel constraints on the feedback modes of AGN, including CRs, via emergent observables which will elucidate the role of CR feedback in massive galaxy ecosystems at high- and low-z. These multi-wavelength predictions and detailed comparisons will not only utilize radio-frequency observations, but leverage observational constraints on massive galaxy and cluster halo environments at low-z in the UV and X-ray, for which massive galaxy constraints from stacks are more robust (Shreeram et al., 2024). Indeed, preliminary work (Goyal, Ponnada et al. in prep.) has shown that massive galaxy simulations run with identical CR transport but varied AGN CR injection efficiencies can produce reasonable low-z massive galaxies with notably differing CGM temperatures + densities, which when forward modeled to observables, may place novel constraints on the the role of CRs in the physical admixture of AGN feedback, at a time ripe for predictions for NASA missions like the Advanced X-ray Imaging Satellite (AXIS), which will probe massive galaxy halos and clusters in emission, and novel X-ray stacks from eROSITA (Zhang, Comparat, et al., 2024).

Of particular interest now are *the most massive galaxies at high-z, where the CR-feedback paradigm remains largely unexplored* and observational constraints on galaxy formation are abuzz in the James Webb Space Telescope (JWST) era. New simulations which evolve massive galaxy populations *at high-z* may prove similarly fruitful in conjunction with these growing high-z observables from JWST. To this end, I will run a new suite of FIRE-3 simulations of massive galaxies at high-z with spectrally-resolved CR-MHD and multi-channel AGN feedback, which I have established the required expertise in to fill this critical gap. This considerable computational effort will not only enable detailed exploration of non-thermal physics,

but be of general use for exploring the drivers of massive galaxy + black hole growth and evolution in the early Universe, and will be utilized for a host of collaborative works, leveraging my multi-wavelength synthetic-observational pipelines to investigate primordial galactic ecosystems observed via JWST and with sensitive radio/millimeter arrays like LOFAR and ALMA.

Furthermore, the expected explosion of matter distribution constraints from FRB sightlines in the next decade (Hallinan et al., 2019; Connor, Ravi, et al., 2024) in conjunction with improved foreground subtraction of the Galactic dispersion measure component may lend insights to the nature of feedback from galaxies on large scales as alluded to in Chapter 6 via constraints on the matter power spectrum (which is more sensitive to massive systems; Sharma et al. 2025), as well as the degree of non-thermal pressure support in our own Galaxy's halo, as mock-observations for CR-dominated halos show enhanced $\mathrm{DM_{halo}}$ as we demonstrated in Chapter 2 and I will show in future work can be constraining with existing and future upper-limits (Ponnada & Hummels in prep., Cook et al. 2023).

In summary, synthetic observations and careful observational comparisons are *essential* to uncovering some of the *most fundamental* questions regarding **B** and CRs in galaxy formation. Some of these questions for which better physically constrained measurements and observational predictions are required but not heretofore mentioned (though this list is not exhaustive) include disentangling the dynamo mechanisms by which galactic magnetic fields are amplified over cosmological time through turbulence and ordered differential rotation (Schober, Schleicher, et al., 2015; Beck, Chamandy, et al., 2020) via comparisons state-of-the-art observable indicators of **B** geometries through dust and synchrotron polarization (Lopez-Rodriguez et al., 2022; Martin-Alvarez, Lopez-Rodriguez, et al., 2024), and understanding the role of galaxy mergers on **B** (and vice-versa (Lopez-Rodriguez, 2021; Whittingham et al., 2021; Whittingham et al., 2023). And, of course, this multi-wavelength, multi-tracer approach is designed to answer perhaps the most pressing question about non-thermal physics in galaxy formation in broad strokes: the degree to which they sculpt galaxies and their halos over time.

BIBLIOGRAPHY

Anglés-Alcázar, Daniel, Claude-André Faucher-Giguère, et al. (Oct. 2017). "The cosmic baryon cycle and galaxy mass assembly in the FIRE simulations." In: *Monthly Notices of the Royal Astronomical Society* 470.4, pp. 4698–4719. DOI: 10.1093/mnras/stx1517.

Anglés-Alcázar, Daniel, Eliot Quataert, et al. (Aug. 2021). "Cosmological simulations of quasar fueling to subparsec scales using Lagrangian hyper-refinement." In: *The Astrophysical Journal* 917. Publisher: IOP ADS Bibcode: 2021ApJ...917...53A, p. 53. ISSN: 0004-637X. DOI: 10.3847/1538-4357/ac09e8.

Armillotta, Lucia, Eve C. Ostriker, Chang-Goo Kim, et al. (Mar. 2024). "Cosmic-ray acceleration of galactic outflows in multiphase gas." In: *The Astrophysical Journal* 964. Publisher: IOP ADS Bibcode: 2024ApJ...964...99A, p. 99. ISSN: 0004-637X. DOI: 10.3847/1538-4357/ad1e5c.

Armillotta, Lucia et al. (Apr. 2022). "Cosmic-ray transport in varying galactic environments." In: *The Astrophysical Journal* 929. ADS Bibcode: 2022ApJ...929..170A, p. 170. ISSN: 0004-637X. DOI: 10.3847/1538-4357/ac5fa9.

Arnaud, M. et al. (July 2010). "The universal galaxy cluster pressure profile from a representative sample of nearby systems (REXCESS) and the YSZ – M500 relation." en. In: *Astronomy & Astrophysics* 517. Publisher: EDP Sciences, A92. ISSN: 0004-6361, 1432-0746. DOI: 10.1051/0004-6361/200913416.

Baes, Maarten et al. (Sept. 2011). "Efficient three-dimensional NLTE dust radiative transfer with SKIRT." en. In: *The Astrophysical Journal Supplement Series* 196.2. Publisher: The American Astronomical Society, p. 22. ISSN: 0067-0049. DOI: 10.1088/0067-0049/196/2/22.

Basu, Aritra et al. (Aug. 2013). "Magnetic fields in nearby normal galaxies: Energy equipartition." In: *Monthly Notices of the Royal Astronomical Society* 433.2. arXiv: 1305.2746 Publisher: Oxford University Press, pp. 1675–1686. ISSN: 13652966. DOI: 10.1093/mnras/stt845.

Beattie, James R. et al. (Dec. 2022). "The density distribution and physical origins of intermittency in supersonic, highly magnetized turbulence with diverse modes of driving." In: *Monthly Notices of the Royal Astronomical Society* 517. ADS Bibcode: 2022MNRAS.517.5003B, pp. 5003–5031. ISSN: 0035-8711. DOI: 10.1093/mnras/stac3005.

Beck, R., A. Shukurov, et al. (Nov. 2003). "Systematic bias in interstellar magnetic field estimates." In: *Astronomy & Astrophysics* 411, pp. 99–107. DOI: 10.1051/0004-6361:20031101.

Beck, R. et al. (July 2005). "Revised equipartition and minimum energy formula for magnetic field strength estimates from radio synchrotron observations." In: *Astronomische Nachrichten* 326.6, pp. 414–427. DOI: 10.1002/asna.200510366.

Beck, Rainer (Oct. 2001). "Galactic and extragalactic magnetic fields." In: *Space Science Reviews* 99, pp. 243–260. DOI: 10.1023/A:1013805401252.

– (Dec. 2015a). "Magnetic fields in spiral galaxies." In: *The Astronomy and Astrophysics Review* 24, 4, p. 4. DOI: 10.1007/s00159-015-0084-4.

– (June 2015b). "Magnetic fields in the nearby spiral galaxy IC 342: A multi-frequency radio polarization study." In: *Astronomy and Astrophysics* 578. arXiv: 1502.05439 Publisher: EDP Sciences, A93. ISSN: 14320746. DOI: 10.1051/0004-6361/201425572.

Beck, Rainer, Luke Chamandy, et al. (Mar. 2020). "Synthesizing observations and theory to understand galactic magnetic fields: Progress and challenges." In: *Galaxies* 8.1. arXiv: 1912.08962 Publisher: MDPI AG, p. 4. ISSN: 20754434. DOI: 10.3390/GALAXIES8010004.

Beck, Rainer et al. (2000). "Magnetic fields in normal galaxies." In: *RSPTA* 358.1767. Publisher: Royal Society, pp. 777–796. ISSN: 1364-503X. DOI: 10.1098/RSTA.2000.0558.

Bell, A. R. (Jan. 1978). "The acceleration of cosmic rays in shock fronts - I." In: *Monthly Notices of the Royal Astronomical Society* 182, pp. 147–156. DOI: 10.1093/mnras/182.2.147.

– (Sept. 2004). "Turbulent amplification of magnetic field and diffusive shock acceleration of cosmic rays." In: *Monthly Notices of the Royal Astronomical Society* 353.2, pp. 550–558. DOI: 10.1111/j.1365-2966.2004.08097.x.

Bell, Eric F. (Apr. 2003). "Estimating star formation rates from infrared and radio luminosities: The origin of the radio-infrared correlation." In: *The Astrophysical Journal* 586. ADS Bibcode: 2003ApJ...586..794B, pp. 794–813. ISSN: 0004-637X. DOI: 10.1086/367829.

Bellardini, Matthew A. et al. (Aug. 2021). "3D gas-phase elemental abundances across the formation histories of Milky Way-mass galaxies in the FIRE simulations: initial conditions for chemical tagging." In: *Monthly Notices of the Royal Astronomical Society* 505.3, pp. 4586–4607. DOI: 10.1093/mnras/stab1606.

Biermann, L. (Jan. 1950). "Über den Ursprung der Magnetfelder auf Sternen und im interstellaren Raum (miteinem Anhang von A. Schlüter)." In: *Zeitschrift Naturforschung Teil A* 5, p. 65.

Bisschoff, D. et al. (June 2019). "New very local interstellar spectra for electrons, positrons, protons, and light cosmic ray nuclei." In: *The Astrophysical Journal* 878. ADS Bibcode: 2019ApJ...878...59B, p. 59. ISSN: 0004-637X. DOI: 10.3847/1538-4357/ab1e4a.

Bonato, Matteo et al. (July 2024). *Correlations between IR luminosity, star formation rate, and CO luminosity in the local Universe*. arXiv:2407.10801 [astro-ph].

Booth, C. M. et al. (Nov. 2013). "Simulations of disk galaxies with cosmic ray driven galactic winds." In: *The Astrophysical Journal Letters* 777.1, L16, p. L16. DOI: 10.1088/2041-8205/777/1/L16.

Borlaff, Alejandro S. et al. (Nov. 2021). "Extragalactic magnetism with SOFIA (Legacy Program). I. The magnetic field in the multiphase interstellar medium of M51." In: *The Astrophysical Journal* 921.2, 128, p. 128. DOI: 10.3847/1538-4357/ac16d7.

Boulares, Ahmed et al. (Dec. 1990). "Galactic Hydrostatic Equilibrium with Magnetic Tension and Cosmic-Ray Diffusion." In: *The Astrophysical Journal* 365, p. 544. DOI: 10.1086/169509.

Bracco, Andrea et al. (Aug. 2023). "The Orion-Taurus ridge: a synchrotron radio loop at the edge of the Orion-Eridanus superbubble." In: *arXiv e-prints*, arXiv:2308.16663, arXiv:2308.16663. DOI: 10.48550/arXiv.2308.16663.

Bruzual, G. et al. (Oct. 2003). "Stellar population synthesis at the resolution of 2003." In: *Monthly Notices of the Royal Astronomical Society* 344.4, pp. 1000–1028. DOI: 10.1046/j.1365-8711.2003.06897.x.

Bryan, Greg L. et al. (Mar. 1998). "Statistical properties of X-Ray clusters: analytic and numerical comparisons." In: *The Astrophysical Journal* 495.1, pp. 80–99. DOI: 10.1086/305262.

Buck, Tobias et al. (Sept. 2020). "The effects of cosmic rays on the formation of Milky Way-mass galaxies in a cosmological context." In: *Monthly Notices of the Royal Astronomical Society* 497.2, pp. 1712–1737. DOI: 10.1093/mnras/staa1960.

Burbidge, G. R. (Sept. 1956). "On Synchrotron Radiation from Messier 87." In: *The Astrophysical Journal* 124, p. 416. DOI: 10.1086/146237.

Bustard, Chad et al. (Apr. 2020). "Cosmic-ray-driven outflows from the Large Magellanic Cloud: Contributions to the LMC filament." In: *The Astrophysical Journal* 893. ADS Bibcode: 2020ApJ...893...29B, p. 29. ISSN: 0004-637X. DOI: 10.3847/1538-4357/ab7fa3.

Butsky, Iryna, Jonathan Zrake, et al. (July 2017). "Ab initio simulations of a supernova-driven galactic dynamo in an isolated disk galaxy." In: *The Astrophysical Journal* 843.2, p. 113. ISSN: 0004-637X. DOI: 10.3847/1538-4357/AA799F.

Butsky, Iryna S., Drummond B. Fielding, et al. (Nov. 2020). "The impact of cosmic rays on thermal instability in the circumgalactic medium." In: *The Astrophysical Journal* 903.2. arXiv: 2008.04915 Publisher: American Astronomical Society, p. 77. ISSN: 15384357. DOI: 10.3847/1538-4357/abbad2.

Butsky, Iryna S., Philip F. Hopkins, et al. (Mar. 2024). "Galactic cosmic-ray scattering due to intermittent structures." In: *Monthly Notices of the Royal Astronomical Society* 528. ADS Bibcode: 2024MNRAS.528.4245B, pp. 4245–4254. ISSN: 0035-8711. DOI: 10.1093/mnras/stae276.

Butsky, Iryna S., Shreya Nakum, et al. (May 2023). "Constraining cosmic ray transport with observations of the circumgalactic medium." In: *Monthly Notices of the Royal Astronomical Society* 521. ADS Bibcode: 2023MNRAS.521.2477B, pp. 2477–2483. ISSN: 0035-8711. DOI: 10.1093/mnras/stad671.

Butsky, Iryna S., Jessica K. Werk, et al. (Aug. 2022). "The impact of cosmic rays on the kinematics of the circumgalactic medium." In: *The Astrophysical Journal* 935.2, 69, p. 69. DOI: 10.3847/1538-4357/ac7ebd.

Butsky, Iryna S. et al. (Dec. 2018). "The role of cosmic-ray transport in shaping the simulated circumgalactic medium." In: *The Astrophysical Journal* 868.2, 108, p. 108. DOI: 10.3847/1538-4357/aaeac2.

Byrne, Lindsey et al. (Oct. 2024). "Effects of multichannel active galactic nuclei feedback in FIRE cosmological simulations of massive galaxies." In: *The Astrophysical Journal* 973. Publisher: IOP ADS Bibcode: 2024ApJ...973..149B, p. 149. ISSN: 0004-637X. DOI: 10.3847/1538-4357/ad67ca.

Camps, P. et al. (Mar. 2015). "SKIRT: An advanced dust radiative transfer code with a user-friendly architecture." In: *Astronomy and Computing* 9, pp. 20–33. ISSN: 2213-1337. DOI: 10.1016/j.ascom.2014.10.004.

Caprioli, Damiano (July 2012). "Cosmic-ray acceleration in supernova remnants: non-linear theory revised." en. In: *Journal of Cosmology and Astroparticle Physics* 2012.07, p. 038. ISSN: 1475-7516. DOI: 10.1088/1475-7516/2012/07/038.

Casasola, V. et al. (Sept. 2017). "Radial distribution of dust, stars, gas, and star-formation rate in DustPedia face-on galaxies." In: *Astronomy & Astrophysics* 605. arXiv: 1706.05351 Publisher: EDP Sciences, A18. ISSN: 0004-6361. DOI: 10.1051/0004-6361/201731020.

Chan, T. K., D. Kereš, P. F. Hopkins, et al. (Sept. 2019). "Cosmic ray feedback in the FIRE simulations: constraining cosmic ray propagation with GeV γ-ray emission." In: *Monthly Notices of the Royal Astronomical Society* 488.3, pp. 3716–3744. DOI: 10.1093/mnras/stz1895.

Chan, T. K., Dušan Kereš, Alexander B. Gurvich, et al. (Aug. 2022). "The impact of cosmic rays on dynamical balance and disk-halo interaction in L$\star$ disk galaxies." In: *Monthly Notices of the Royal Astronomical Society*. DOI: 10.1093/mnras/stac2236.

CHIME/FRB Collaboration et al. (Aug. 2018). "The CHIME fast radio burst project: system overview." In: *The Astrophysical Journal* 863.1, 48, p. 48. DOI: 10.3847/1538-4357/aad188.

Choban, Caleb R. et al. (Apr. 2024). "A Dusty Locale: evolution of galactic dust populations from Milky Way to dwarf-mass galaxies." In: *Monthly Notices of the Royal Astronomical Society* 529.3, pp. 2356–2378. DOI: 10.1093/mnras/stae716.

Chyzy, K. T. et al. (2011). "Magnetic fields in Local Group dwarf irregulars." In: *Astronomy and Astrophysics* 529, p. 94. ISSN: 00046361. DOI: 10.1051/0004-6361/201015393.

Cochrane, R. K., D. Anglés-Alcázar, et al. (Aug. 2023b). "The impact of AGN-driven winds on physical and observable galaxy sizes." In: *Monthly Notices of the Royal Astronomical Society* 523. ADS Bibcode: 2023MNRAS.523.2409C, pp. 2409–2421. ISSN: 0035-8711. DOI: 10.1093/mnras/stad1528.

Cochrane, R. K., C. C. Hayward, D. Anglés-Alcázar, J. Lotz, et al. (Sept. 2019). "Predictions for the spatial distribution of the dust continuum emission in 1 < z < 5 star-forming galaxies." In: *Monthly Notices of the Royal Astronomical Society* 488. Publisher: OUP ADS Bibcode: 2019MNRAS.488.1779C, pp. 1779–1789. ISSN: 0035-8711. DOI: 10.1093/mnras/stz1736.

Cochrane, R. K., C. C. Hayward, D. Anglés-Alcázar, and R. S. Somerville (Feb. 2023a). "Predicting sub-millimetre flux densities from global galaxy properties." In: *Monthly Notices of the Royal Astronomical Society* 518.4, pp. 5522–5535. DOI: 10.1093/mnras/stac3451.

Coles, W. A., M. Kerr, et al. (Aug. 2015). "Pulsar observations of extreme scattering events." In: *The Astrophysical Journal* 808.2, 113, p. 113. DOI: 10.1088/0004-637X/808/2/113.

Coles, W. A., B. J. Rickett, et al. (July 2010). "Scattering of pulsar radio emission by the interstellar plasma." In: *The Astrophysical Journal* 717.2, pp. 1206–1221. DOI: 10.1088/0004-637X/717/2/1206.

Condon, J. J. (1992). "Radio emission from normal galaxies." en. In: *Annual Rev. Astron. Astrophys., Vol. 30, p. 575-611 (1992)* 30, p. 575. ISSN: 0066-4146. DOI: 10.1146/annurev.aa.30.090192.003043.

Condon, J. J. et al. (July 1991). "Correlations between Far-Infrared, Radio, and Blue Luminosities of Spiral Galaxies." In: *The Astrophysical Journal* 376. ADS Bibcode: 1991ApJ...376...95C, p. 95. ISSN: 0004-637X. DOI: 10.1086/170258.

Connor, Liam, Vikram Ravi, et al. (Sept. 2024). *A gas rich cosmic web revealed by partitioning the missing baryons*. arXiv:2409.16952. DOI: 10.48550/arXiv.2409.16952.

Connor, Liam et al. (Sept. 2022). "The observed impact of galaxy halo gas on fast radio bursts." en. In: *Nature Astronomy* 6.9. Publisher: Nature Publishing Group, pp. 1035–1042. ISSN: 2397-3366. DOI: 10.1038/s41550-022-01719-7.

Cook, Amanda M. et al. (Feb. 2023). *An FRB Sent Me a DM: Constraining the Electron Column of the Milky Way Halo with Fast Radio Burst Dispersion Measures from CHIME/FRB*. arXiv:2301.03502 [astro-ph]. DOI: 10.48550/arXiv.2301.03502.

Croton, Darren J. et al. (Jan. 2006). "The many lives of active galactic nuclei: cooling flows, black holes and the luminosities and colours of galaxies." In: *Monthly Notices of the Royal Astronomical Society* 365. ADS Bibcode: 2006MNRAS.365...11C, pp. 11–28. ISSN: 0035-8711. DOI: 10.1111/j.1365-2966.2005.09675.x.

Crutcher, Richard M. (Sept. 2012). "Magnetic fields in molecular clouds." In: *Annual Review of Astronomy and Astrophysics* 50, pp. 29–63. ISSN: 00664146. DOI: 10.1146/annurev-astro-081811-125514.

Crutcher, Richard M. et al. (Nov. 2010). "Magnetic fields in interstellar clouds from zeeman observations: Inference of total field strengths by bayesian analysis." In: *Astrophysical Journal* 725.1, pp. 466–479. ISSN: 15384357. DOI: 10.1088/0004-637X/725/1/466.

Cummings, A. C. et al. (Nov. 2016). "Galactic Cosmic Rays in the Local Interstellar Medium: Voyager 1 Observations and Model Results." In: *The Astrophysical Journal* 831. ADS Bibcode: 2016ApJ...831...18C, p. 18. ISSN: 0004-637X. DOI: 10.3847/0004-637X/831/1/18.

Davé, Romeel et al. (June 2019). "SIMBA: Cosmological simulations with black hole growth and feedback." In: *Monthly Notices of the Royal Astronomical Society* 486. ADS Bibcode: 2019MNRAS.486.2827D, pp. 2827–2849. ISSN: 0035-8711. DOI: 10.1093/mnras/stz937.

Delhaize, J. et al. (June 2017). "The VLA-COSMOS 3 GHz large project: The infrared-radio correlation of star-forming galaxies and AGN to $z \lesssim 6$." en. In: *Astronomy and Astrophysics* 602, A4. ISSN: 0004-6361. DOI: 10.1051/0004-6361/201629430.

Desiati, Paolo et al. (Aug. 2014). "The transport of cosmic rays across magnetic fieldlines." In: *The Astrophysical Journal* 791.1, 51, p. 51. DOI: 10.1088/0004-637X/791/1/51.

Dewdney, P. E. et al. (Aug. 2009). "The Square Kilometre Array." In: *IEEE Proceedings* 97.8, pp. 1482–1496. DOI: 10.1109/JPROC.2009.2021005.

Di Mauro, Mattia et al. (June 2024). "Data-driven constraints on cosmic-ray diffusion: Probing self-generated turbulence in the Milky Way." In: *Physical Review D* 109.12. Publisher: American Physical Society, p. 123003. DOI: 10.1103/PhysRevD.109.123003.

Draine, B. T. et al. (July 1979). "On the physics of dust grains in hot gas." In: *The Astrophysical Journal* 231, pp. 77–94. DOI: 10.1086/157165.

Draine, Bruce T. (2011). *Physics of the Interstellar and Intergalactic Medium*.

Dwek, Eli (July 1998). "The evolution of the elemental abundances in the gas and dust phases of the Galaxy." In: *The Astrophysical Journal* 501, p. 643. DOI: 10.1086/305829.

Evans II, Neal J. (1999). "Physical conditions in regions of star formation." In: *Annual Review of Astronomy and Astrophysics* 37.1, pp. 311–362. DOI: 10.1146/annurev.astro.37.1.311.

Evoli, Carmelo et al. (Feb. 2017). "Cosmic-ray propagation with DRAGON2: I. numerical solver and astrophysical ingredients." In: *Journal of Cosmology and Astroparticle Physics* 2017.2, 015, p. 015. DOI: 10.1088/1475-7516/2017/02/015.

Farcy, Marion et al. (July 2022). "Radiation-magnetohydrodynamics simulations of cosmic ray feedback in disc galaxies." In: *Monthly Notices of the Royal Astronomical Society* 513. ADS Bibcode: 2022MNRAS.513.5000F, pp. 5000–5019. ISSN: 0035-8711. DOI: 10.1093/mnras/stac1196.

Federrath, C. et al. (Mar. 2010). "Comparing the statistics of interstellar turbulence in simulations and observations. Solenoidal versus compressive turbulence forcing." In: *Astronomy & Astrophysics* 512, A81, A81. DOI: 10.1051/0004-6361/200912437.

Feldmann, Robert, Eliot Quataert, Claude-André Faucher-Giguère, et al. (July 2023). "FIREbox: simulating galaxies at high dynamic range in a cosmological volume." In: *Monthly Notices of the Royal Astronomical Society* 522. Publisher: OUP ADS Bibcode: 2023MNRAS.522.3831F, pp. 3831–3860. ISSN: 0035-8711. DOI: 10.1093/mnras/stad1205.

Feldmann, Robert, Eliot Quataert, Philip F. Hopkins, et al. (Sept. 2017). "Colours, star formation rates and environments of star-forming and quiescent galaxies at the cosmic noon." In: *Monthly Notices of the Royal Astronomical Society* 470. Publisher: OUP ADS Bibcode: 2017MNRAS.470.1050F, pp. 1050–1072. ISSN: 0035-8711. DOI: 10.1093/mnras/stx1120.

Fermi, Enrico (Apr. 1949). "On the origin of the cosmic radiation." In: *Physical Review* 75.8, pp. 1169–1174. DOI: 10.1103/PhysRev.75.1169.

Fielding, Drummond B. et al. (May 2023). "Plasmoid Instability in the Multiphase Interstellar Medium." In: *The Astrophysical Journal Letters* 949.1, L5, p. L5. DOI: 10.3847/2041-8213/accf1f.

Fitt, A. J. et al. (Mar. 1993). "Magnetic fields in late-type galaxies." In: *Monthly Notices of the Royal Astronomical Society* 261.2, pp. 445–452. ISSN: 0035-8711. DOI: 10.1093/mnras/261.2.445.

Fletcher, A. et al. (Apr. 2011). "Magnetic fields and spiral arms in the galaxy M51." In: *Monthly Notices of the Royal Astronomical Society* 412.4, pp. 2396–2416. ISSN: 00358711. DOI: 10.1111/j.1365-2966.2010.18065.x.

Gaensler, B. M. et al. (Mar. 2005). "The magnetic field of the Large Magellanic Cloud revealed through Faraday rotation." In: *Science* 307.5715, pp. 1610–1612. DOI: 10.1126/science.1108832.

Gensior, Jindra et al. (Jan. 2023). "Realistic H I scale heights of Milky Way-mass galaxies in the FIREbox cosmological volume." In: *Monthly Notices of the Royal Astronomical Society* 518.1, pp. L63–L68. DOI: 10.1093/mnrasl/slac138.

Ginzburg, V. L. et al. (Jan. 1965). "Cosmic magnetobremsstrahlung (synchrotron radiation)." In: *Annual Review of Astronomy and Astrophysics* 3, p. 297. DOI: 10.1146/annurev.aa.03.090165.001501.

Girichidis, Philipp, Thorsten Naab, Michał Hanasz, et al. (Sept. 2018). "Cooler and smoother - the impact of cosmic rays on the phase structure of galactic outflows." In: *Monthly Notices of the Royal Astronomical Society* 479.3, pp. 3042–3067. DOI: 10.1093/mnras/sty1653.

Girichidis, Philipp, Thorsten Naab, Stefanie Walch, et al. (Jan. 2016). "Launching cosmic-ray-driven outflows from the magnetized interstellar medium." In: *The Astrophysical Journal* 816. ADS Bibcode: 2016ApJ...816L..19G, p. L19. ISSN: 0004-637X. DOI: 10.3847/2041-8205/816/2/L19.

Girichidis, Philipp, Christoph Pfrommer, Michał Hanasz, et al. (Jan. 2020). "Spectrally resolved cosmic ray hydrodynamics – I. Spectral scheme." In: *Monthly Notices of the Royal Astronomical Society* 491.1, pp. 993–1007. ISSN: 0035-8711. DOI: 10.1093/mnras/stz2961.

Girichidis, Philipp, Christoph Pfrommer, Rüdiger Pakmor, et al. (Mar. 2022). "Spectrally resolved cosmic rays - II. Momentum-dependent cosmic ray diffusion drives powerful galactic winds." In: *Monthly Notices of the Royal Astronomical Society* 510. Publisher: OUP ADS Bibcode: 2022MNRAS.510.3917G, pp. 3917–3938. ISSN: 0035-8711. DOI: 10.1093/mnras/stab3462.

Gitti, M. et al. (Sept. 2018). "Radio-continuum surveys with SKA and LOFAR: a first look at the perspectives for radio mini-halos." In: *Astronomy & Astrophysics* 617, A11, A11. DOI: 10.1051/0004-6361/201832749.

Grudić, Michael Y. et al. (Sept. 2021). "STARFORGE: Towards a comprehensive numerical model of star cluster formation and feedback." In: *Monthly Notices of the Royal Astronomical Society* 506.2, pp. 2199–2231. DOI: 10.1093/mnras/stab1347.

Guo, Fulai et al. (Feb. 2008). "Feedback heating by cosmic rays in clusters of galaxies." In: *Monthly Notices of the Royal Astronomical Society* 384.1, pp. 251–266. DOI: 10.1111/j.1365-2966.2007.12692.x.

Gurnett, D. A. et al. (Sept. 2013). "In situ observations of interstellar plasma with Voyager 1." In: *Science* 341.6153. Publisher: American Association for the Advancement of Science, pp. 1489–1492. DOI: 10.1126/science.1241681.

Gurvich, Alexander B. et al. (Nov. 2020). "Pressure balance in the multiphase ISM of cosmologically simulated disc galaxies." In: *Monthly Notices of the Royal Astronomical Society* 498.3, pp. 3664–3683. DOI: 10.1093/mnras/staa2578.

Guszejnov, Dávid et al. (Feb. 2020). "Evolution of giant molecular clouds across cosmic time." In: *Monthly Notices of the Royal Astronomical Society* 492.1, pp. 488–502. ISSN: 13652966. DOI: 10.1093/mnras/stz3527.

Hafen, Zachary et al. (Aug. 2022). "Hot-mode accretion and the physics of thin-disc galaxy formation." In: *Monthly Notices of the Royal Astronomical Society* 514.4, pp. 5056–5073. DOI: 10.1093/mnras/stac1603.

Hairer, Ernst et al. (1996). "Stability function of implicit RK-methods." en. In: *Solving Ordinary Differential Equations II: Stiff and Differential-Algebraic Problems*. Ed. by Ernst Hairer et al. Berlin, Heidelberg: Springer, pp. 40–50. ISBN: 978-3-642-05221-7. DOI: 10.1007/978-3-642-05221-7_3.

– (Nov. 1999). "Stiff differential equations solved by Radau methods." In: *Journal of Computational and Applied Mathematics* 111.1, pp. 93–111. ISSN: 0377-0427. DOI: 10.1016/S0377-0427(99)00134-X.

Hallinan, Gregg et al. (Sept. 2019). "The DSA-2000 — A Radio Survey Camera." In: *Bulletin of the American Astronomical Society*. Vol. 51, 255, p. 255. DOI: 10.48550/arXiv.1907.07648.

Han, J. L., R. N. Manchester, A. G. Lyne, et al. (May 2006). "Pulsar rotation measures and the large-scale structure of the Galactic magnetic field." In: *The Astrophysical Journal* 642.2, pp. 868–881. DOI: 10.1086/501444.

Han, J. L. et al. (June 1999). "Pulsar rotation measures and the magnetic structure of our Galaxy." In: *Monthly Notices of the Royal Astronomical Society* 306.2, pp. 371–380. ISSN: 00358711. DOI: 10.1046/j.1365-8711.1999.02544.x.

Han, J. L. et al. (Aug. 2017). "Observing Interstellar and Intergalactic Magnetic Fields." In: *ARA&A* 55.1. Publisher: Annual Reviews Inc., pp. 111–157. ISSN: 0066-4146. DOI: 10.1146/ANNUREV-ASTRO-091916-055221.

Hanasz, M. et al. (Dec. 2021). "Simulations of cosmic ray propagation." en. In: *Living Reviews in Computational Astrophysics* 7.1. arXiv:2106.08426 [astro-ph], p. 2. ISSN: 2367-3621, 2365-0524. DOI: 10.1007/s41115-021-00011-1.

Hardcastle, M. J. et al. (June 2020). "Radio galaxies and feedback from AGN jets." en. In: *New Astronomy Reviews* 88. arXiv:2003.06137 [astro-ph], p. 101539. ISSN: 13876473. DOI: 10.1016/j.newar.2020.101539.

Harrison, C. M. (July 2017). "Impact of supermassive black hole growth on star formation." en. In: *Nature Astronomy* 1.7. Number: 7 Publisher: Nature Publishing Group, pp. 1–8. ISSN: 2397-3366. DOI: 10.1038/s41550-017-0165.

Haverkorn, Marijke (Jan. 2015). "Magnetic fields in the Milky Way." In: *Magnetic Fields in Diffuse Media*. Ed. by Alexander Lazarian et al. Vol. 407. Astrophysics and Space Science Library, p. 483. DOI: 10.1007/978-3-662-44625-6_17.

Hayward, Christopher C. et al. (Dec. 2014). "The total infrared luminosity may significantly overestimate the star formation rate of quenching and recently quenched galaxies." In: *Monthly Notices of the Royal Astronomical Society* 445.2, pp. 1598–1604. DOI: 10.1093/mnras/stu1843.

Heckman, Timothy M. et al. (Aug. 2014). "The coevolution of galaxies and supermassive black holes: insights from surveys of the contemporary universe." In: *Annual Review of Astronomy and Astrophysics* 52. ADS Bibcode: 2014ARA&A..52..589H, pp. 589–660. ISSN: 0066-4146. DOI: 10.1146/annurev-astro-081913-035722.

Heesen, V., II Buie E., et al. (Feb. 2019). "Calibrating the relation of low-frequency radio continuum to star formation rate at 1 kpc scale with LOFAR." In: *Astronomy & Astrophysics* 622, A8, A8. DOI: 10.1051/0004-6361/201833905.

Heesen, V., F. De Gasperin, et al. (Apr. 2023). "Diffusion of cosmic-ray electrons in M 51 observed with LOFAR at 54 MHz." en. In: *Astronomy & Astrophysics* 672, A21. ISSN: 0004-6361, 1432-0746. DOI: 10.1051/0004-6361/202245223.

Heesen, V., M. Krause, et al. (May 2018). "Radio haloes in nearby galaxies modelled with 1D cosmic ray transport using SPINNAKER." In: *Monthly Notices of the Royal Astronomical Society* 476. ADS Bibcode: 2018MNRAS.476..158H, pp. 158–183. ISSN: 0035-8711. DOI: 10.1093/mnras/sty105.

Heesen, Volker (Dec. 2021). "The radio continuum perspective on cosmic-ray transport in external galaxies." In: *Astrophysics and Space Science* 366. ADS Bibcode: 2021Ap&SS.366..117H, p. 117. ISSN: 0004-640X. DOI: 10.1007/s10509-021-04026-1.

Heiles, Carl (May 1997). "Tiny-scale atomic structure and the cold neutral medium." en. In: *The Astrophysical Journal* 481.1. Publisher: IOP Publishing, p. 193. ISSN: 0004-637X. DOI: 10.1086/304033.

Helou, G. et al. (Nov. 1985). "Thermal infrared and nonthermal radio : remarkable correlation in disks of galaxies." In: *The Astrophysical Journal* 298. ADS Bibcode: 1985ApJ...298L...7H, pp. L7–L11. ISSN: 0004-637X. DOI: 10.1086/184556.

Helou, G. et al. (Sept. 1993). "A Physical Model of the Infrared-to-Radio Correlation in Galaxies." In: *The Astrophysical Journal* 415. ADS Bibcode: 1993ApJ...415...93H, p. 93. ISSN: 0004-637X. DOI: 10.1086/173146.

Henden, Nicholas A. et al. (Oct. 2018). "The FABLE simulations: A feedback model for galaxies, groups and clusters." In: *Monthly Notices of the Royal Astronomical Society* 479.4. arXiv:1804.05064 [astro-ph], pp. 5385–5412. ISSN: 0035-8711, 1365-2966. DOI: 10.1093/mnras/sty1780.

Hopkins, Philip F, Iryna S Butsky, Suoqing Ji, et al. (June 2023). "A simple subgrid model for cosmic ray effects on galactic scales." In: *Monthly Notices of the Royal Astronomical Society* 522.2, pp. 2936–2950. ISSN: 0035-8711. DOI: 10.1093/mnras/stad976.

Hopkins, Philip F, Michael Y Grudić, et al. (Jan. 2020). "Radiative stellar feedback in galaxy formation: Methods and physics." In: *Monthly Notices of the Royal Astronomical Society* 491.3, pp. 3702–3729. ISSN: 0035-8711. DOI: 10.1093/mnras/stz3129.

Hopkins, Philip F, Andrew Wetzel, Coral Wheeler, et al. (Feb. 2023). "FIRE-3: updated stellar evolution models, yields,and microphysics and fitting functions for applications in galaxy simulations." In: *Monthly Notices of the Royal Astronomical Society* 519.2, pp. 3154–3181. ISSN: 0035-8711. DOI: 10.1093/mnras/stac3489.

Hopkins, Philip F. (Apr. 2013). "A model for (non-lognormal) density distributions in isothermal turbulence." In: *Monthly Notices of the Royal Astronomical Society* 430. ADS Bibcode: 2013MNRAS.430.1880H, pp. 1880–1891. ISSN: 0035-8711. DOI: 10.1093/mnras/stt010.

– (June 2015). "A new class of accurate, mesh-free hydrodynamic simulation methods." In: *Monthly Notices of the Royal Astronomical Society* 450.1, pp. 53–110. DOI: 10.1093/mnras/stv195.

– (Oct. 2016). "A constrained-gradient method to control divergence errors in numerical MHD." In: *Monthly Notices of the Royal Astronomical Society* 462.1, pp. 576–587. ISSN: 0035-8711. DOI: 10.1093/mnras/stw1578.

– (Apr. 2017). "Anisotropic diffusion in mesh-free numerical magnetohydrodynamics." In: *Monthly Notices of the Royal Astronomical Society* 466. ADS Bibcode: 2017MNRAS.466.3387H, pp. 3387–3405. ISSN: 0035-8711. DOI: 10.1093/mnras/stw3306.

– (Apr. 2024). *The Importance of Subtleties in the Scaling of the 'Terminal Momentum' For Galaxy Formation Simulations*. Publication Title: arXiv e-prints ADS Bibcode: 2024arXiv240416987H. DOI: 10.48550/arXiv.2404.16987.

Hopkins, Philip F., Iryna S. Butsky, Georgia V. Panopoulou, et al. (July 2022). "First predicted cosmic ray spectra, primary-to-secondary ratios, and ionization rates from MHD galaxy formation simulations." In: *Monthly Notices of the Royal Astronomical Society* 000.0000. arXiv: 2109.09762, pp. 0–000. ISSN: 0035-8711. DOI: 10.1093/MNRAS/STAC1791.

Hopkins, Philip F., T. K. Chan, Shea Garrison-Kimmel, et al. (Mar. 2020). "But what about.: Cosmic rays, magnetic fields, conduction, and viscosity in galaxy formation." In: *Monthly Notices of the Royal Astronomical Society* 3, pp. 3465–3498. ISSN: 13652966. DOI: 10.1093/mnras/stz3321.

Hopkins, Philip F., T. K. Chan, Suoqing Ji, et al. (Mar. 2021). "Cosmic ray driven outflows to Mpc scales from L_* galaxies." In: *Monthly Notices of the Royal Astronomical Society* 501.3, pp. 3640–3662. DOI: 10.1093/mnras/staa3690.

Hopkins, Philip F., T. K. Chan, Jonathan Squire, et al. (Mar. 2021). "Effects of different cosmic ray transport models on galaxy formation." In: *Monthly Notices of the Royal Astronomical Society* 501. ADS Bibcode: 2021MNRAS.501.3663H, pp. 3663–3669. ISSN: 0035-8711. DOI: 10.1093/mnras/staa3692.

Hopkins, Philip F., Michael Y. Grudic, et al. (Mar. 2024). "FORGE'd in FIRE: Resolving the End of Star Formation and Structure of AGN Accretion Disks from Cosmological Initial Conditions." In: *The Open Journal of Astrophysics* 7, 18, p. 18. DOI: 10.21105/astro.2309.13115.

Hopkins, Philip F., Lars Hernquist, et al. (June 2005). "A physical model for the origin of quasar lifetimes." In: *The Astrophysical Journal Letters* 625.2, pp. L71–L74. DOI: 10.1086/431146.

Hopkins, Philip F., Eliot Quataert, et al. (Jan. 2025). *Cosmic rays masquerading as hot CGM gas: An inverse-Compton origin for diffuse X-ray emission in the circumgalactic Medium*. arXiv:2501.18696 [astro-ph]. DOI: 10.48550/arXiv.2501.18696.

Hopkins, Philip F., Jonathan Squire, Iryna S. Butsky, and Suoqing Ji (Oct. 2022). "Standard self-confinement and extrinsic turbulence models for cosmic ray transport are fundamentally incompatible with observations." In: *Monthly Notices of the Royal Astronomical Society*. ADS Bibcode: 2022MNRAS.tmp.2710H. ISSN: 0035-8711. DOI: 10.1093/mnras/stac2909.

Hopkins, Philip F., Jonathan Squire, T. K. Chan, et al. (Mar. 2021). "Testing physical models for cosmic ray transport coefficients on galactic scales: self-confinement and extrinsic turbulence at ~GeV energies." In: *Monthly Notices of the Royal Astronomical Society* 501. ADS Bibcode: 2021MNRAS.501.4184H, pp. 4184–4213. ISSN: 0035-8711. DOI: 10.1093/mnras/staa3691.

Hopkins, Philip F., Andrew Wetzel, Dušan Kereš, et al. (Oct. 2018). "FIRE-2 simulations: Physics versus numerics in galaxy formation." In: *Monthly Notices of the Royal Astronomical Society* 480.1, pp. 800–863. ISSN: 13652966. DOI: 10.1093/mnras/sty1690.

Hopkins, Philip F. et al. (Jan. 2016). "Accurate, meshless methods for magnetohydrodynamics." In: *Monthly Notices of the Royal Astronomical Society* 455.1, pp. 51–88. ISSN: 0035-8711. DOI: 10.1093/mnras/stv2180.

Hopkins, Philip F. et al. (Jan. 2022). "A consistent reduced-speed-of-light formulation of cosmic ray transport valid in weak- and strong-scattering regimes." In: *Monthly Notices of the Royal Astronomical Society* 509. ADS Bibcode: 2022MNRAS.509.3779H, pp. 3779–3797. ISSN: 0035-8711. DOI: 10.1093/mnras/stab2635.

Huang, Xiaoshan et al. (June 2022). "Cosmic-Ray-driven Multiphase Gas Formed via Thermal Instability." In: *The Astrophysical Journal* 931. ADS Bibcode: 2022ApJ...931..140H, p. 140. ISSN: 0004-637X. DOI: 10.3847/1538-4357/ac69dc.

Huang, Xiaoshan et al. (Apr. 2022). "The launching of cosmic ray-driven outflows." In: *Monthly Notices of the Royal Astronomical Society* 511. ADS Bibcode: 2022MNRAS.511.5125H, pp. 5125–5141. ISSN: 0035-8711. DOI: 10.1093/mnras/stac059.

Ipavich, F. M. (Feb. 1975). "Galactic winds driven by cosmic rays." In: *The Astrophysical Journal* 196. Publisher: IOP ADS Bibcode: 1975ApJ...196..107I, pp. 107–120. ISSN: 0004-637X. DOI: 10.1086/153397.

Ivison, R. J. et al. (June 1985). "Radio continuum and far-infrared emission from spiral galaxies : a close correlation." en. In: *Astronomy and Astrophysics* 147, pp. L6–L9. ISSN: 0004-6361. DOI: 10.1051/0004-6361/201014552.

Jansson, Ronnie et al. (Sept. 2012). "A new model of the Galactic magnetic field." In: *The Astrophysical Journal* 757.1, 14, p. 14. DOI: 10.1088/0004-637X/757/1/14.

Ji, Suoqing, T. K. Chan, et al. (Aug. 2020). "Properties of the circumgalactic medium in cosmic ray-dominated galaxy haloes." In: *Monthly Notices of the Royal Astronomical Society* 496.4, pp. 4221–4238. ISSN: 13652966. DOI: 10.1093/mnras/staa1849.

Ji, Suoqing, Dušan Kereš, et al. (July 2021). "Virial shocks are suppressed in cosmic ray-dominated galaxy haloes." In: *Monthly Notices of the Royal Astronomical Society* 505.1, pp. 259–273. DOI: 10.1093/mnras/stab1264.

Ji, Suoqing et al. (May 2018). "The impact of magnetic fields on thermal instability." In: *Monthly Notices of the Royal Astronomical Society* 476.1, pp. 852–867. DOI: 10.1093/mnras/sty293.

Jin, Gaoxiang et al. (Sept. 2024). *The host galaxies of radio AGN: new views from combining LoTSS and MaNGA observations*. arXiv:2409.01279 [astro-ph]. DOI: 10.48550/arXiv.2409.01279.

Jokipii, J. R. (Nov. 1966). "Cosmic-Ray Propagation. I. Charged Particles in a Random Magnetic Field." In: *The Astrophysical Journal* 146. ADS Bibcode: 1966ApJ...146..480J, p. 480. ISSN: 0004-637X. DOI: 10.1086/148912.

Jong, T. de et al. (Nov. 1971). "Observations of core sources in Seyfert and normal galaxies with the Westerbork synthesis radio telescope at 1415 MHz." en. In: *Astronomy and Astrophysics* 15, pp. 110–122. ISSN: 0004-6361.

– (June 1985). "Radio continuum and far-infrared emission from spiral galaxies : a close correlation." en. In: *Astronomy and Astrophysics* 147, pp. L6–L9. ISSN: 0004-6361.

Kalberla, Peter M. W. et al. (Sept. 2009). "The Hi Distribution of the Milky Way." In: *Annual Review of Astronomy and Astrophysics* 47.1, pp. 27–61. DOI: 10.1146/annurev-astro-082708-101823.

Kempski, Philipp, Drummond B. Fielding, et al. (Nov. 2023). "Cosmic ray transport in large-amplitude turbulence with small-scale field reversals." In: *Monthly Notices of the Royal Astronomical Society* 525.4, pp. 4985–4998. DOI: 10.1093/mnras/stad2609.

Kempski, Philipp, Dongzi Li, et al. (Dec. 2024). *A unified model of cosmic ray propagation and radio extreme scattering events from intermittent interstellar structures*. Publication Title: arXiv e-prints ADS Bibcode: 2024arXiv241203649K. DOI: 10.48550/arXiv.2412.03649.

Kempski, Philipp et al. (July 2022). "Reconciling cosmic ray transport theory with phenomenological models motivated by Milky-Way data." In: *Monthly Notices of the Royal Astronomical Society* 514. ADS Bibcode: 2022MNRAS.514..657K, pp. 657–674. ISSN: 0035-8711. DOI: 10.1093/mnras/stac1240.

Kennicutt, Robert C. (1998). "Star Formation in Galaxies Along the Hubble Sequence." In: *Annual Review of Astronomy and Astrophysics* 36.1, pp. 189–231. DOI: 10.1146/annurev.astro.36.1.189.

Kocz, J. et al. (Oct. 2019). "DSA-10: a prototype array for localizing fast radio bursts." In: *Monthly Notices of the Royal Astronomical Society* 489.1, pp. 919–927. DOI: 10.1093/mnras/stz2219.

Krause, Marita et al. (Mar. 2018). "CHANG-ES IX: Radio scale heights and scale lengths of a consistent sample of 13 spiral galaxies seen edge-on and their correlations." en. In: *Astronomy & Astrophysics* 611. arXiv:1712.03780 [astro-ph], A72. ISSN: 0004-6361, 1432-0746. DOI: 10.1051/0004-6361/201731991.

Kruit, P. C. van der (Nov. 1971). "Observations of core sources in Seyfert and normal galaxies with the Westerbork synthesis radio telescope at 1415 MHz." In: *Astronomy and Astrophysics* 15. ADS Bibcode: 1971A&A....15..110V, pp. 110–122. ISSN: 0004-6361.

Krumholz, Mark R. et al. (Feb. 2019). "The Role of Magnetic Fields in Setting the Star Formation Rate and the Initial Mass Function." In: *Frontiers in Astronomy and Space Sciences* 6, 7, p. 7. DOI: 10.3389/fspas.2019.00007.

Kulsrud, Russell et al. (May 1969). "The effect of wave-particle interactions on the propagation of cosmic rays." In: *The Astrophysical Journal* 156, p. 445. DOI: 10.1086/149981.

Lacki, Brian C., Todd A. Thompson, Eliot Quataert, et al. (June 2011). "On the GeV and TeV detections of the starburst galaxies M82 and NGC 253." en. In: *The Astrophysical Journal* 734.2. Publisher: The American Astronomical Society, p. 107. ISSN: 0004-637X. DOI: 10.1088/0004-637X/734/2/107.

Lacki, Brian C. et al. (July 2010). "The Physics of the Far-infrared-Radio Correlation. I. Calorimetry, Conspiracy, and Implications." In: *The Astrophysical Journal* 717. ADS Bibcode: 2010ApJ...717....1L, pp. 1–28. ISSN: 0004-637X. DOI: 10.1088/0004-637X/717/1/1.

Lacki, Brian C. et al. (Apr. 2013). "The equipartition magnetic field formula in starburst galaxies: accounting for pionic secondaries and strong energy losses." In: *Monthly Notices of the Royal Astronomical Society* 430.4, pp. 3171–3186. ISSN: 0035-8711. DOI: 10.1093/mnras/stt122.

Lan, Ting Wen et al. (2020). "Constraining magnetic fields in the circumgalactic medium." In: *Monthly Notices of the Royal Astronomical Society* 496.3, pp. 3142–3151. ISSN: 13652966. DOI: 10.1093/MNRAS/STAA1750.

Lemoine, Martin (Sept. 2023). "Particle transport through localized interactions with sharp magnetic field bends in MHD turbulence." In: *Journal of Plasma Physics* 89. ADS Bibcode: 2023JPlPh..89e1701L, p. 175890501. ISSN: 0022-3778. DOI: 10.1017/S0022377823000946.

Liang, Lichen et al. (Oct. 2019). "On the dust temperatures of high-redshift galaxies." In: *Monthly Notices of the Royal Astronomical Society* 489.1, pp. 1397–1422. ISSN: 0035-8711. DOI: 10.1093/mnras/stz2134.

Lin, Yen-Hsing et al. (Jan. 2024). *AGN jet-inflated bubbles as possible origin of odd radio circles*. Publication Title: arXiv e-prints ADS Bibcode: 2024arXiv240108207L. DOI: 10.48550/arXiv.2401.08207.

Lisenfeld, U. et al. (Feb. 1996). "A quantitative model of the FIR/radio correlation for normal late-type galaxies." In: *Astronomy and Astrophysics* 306. ADS Bibcode: 1996A&A...306..677L, p. 677. ISSN: 0004-6361. DOI: 10.48550/arXiv.astro-ph/9603130.

Lopez-Rodriguez, Enrique (June 2021). "The magnetic field across the molecular warped disk of Centaurus A." In: *Nature Astronomy* 5, pp. 604–614. DOI: 10.1038/s41550-021-01329-9.

Lopez-Rodriguez, Enrique et al. (Sept. 2022). "Extragalactic magnetism with SOFIA (SALSA Legacy Program). IV. Program overview and first results on the polarization fraction." In: *The Astrophysical Journal* 936.1, 92, p. 92. DOI: 10.3847/1538-4357/ac7f9d.

Magnelli, B. et al. (Jan. 2015). "The far-infrared/radio correlation and radio spectral index of galaxies in the SFR-M_∗ plane up to z~2." en. In: *Astronomy & Astrophysics, Volume 573, id.A45, <NUMPAGES>18</NUMPAGES> pp.* 573, A45. ISSN: 0004-6361. DOI: 10.1051/0004-6361/201424937.

Manchester, R. N. et al. (Apr. 2005). "The Australia Telescope National Facility pulsar catalogue." In: *The Astronomical Journal* 129.4, pp. 1993–2006. DOI: 10.1086/428488.

Mannheim, K. et al. (June 1994). "Interactions of cosmic ray nuclei." In: *Astronomy & Astrophysics* 286, pp. 983–996. DOI: 10.48550/arXiv.astro-ph/9402042.

Marinacci, Federico et al. (2014). "The formation of disc galaxies in high-resolution moving-mesh cosmological simulations." In: *Monthly Notices of the Royal Astronomical Society* 437.2, pp. 1750–1775. ISSN: 13652966. DOI: 10.1093/mnras/stt2003.

Martin-Alvarez, Sergio, Julien Devriendt, et al. (Sept. 2018). "A three-phase amplification of the cosmic magnetic field in galaxies." In: *Monthly Notices of the Royal Astronomical Society* 479.3, pp. 3343–3365. ISSN: 13652966. DOI: 10.1093/mnras/sty1623.

Martin-Alvarez, Sergio, Enrique Lopez-Rodriguez, et al. (May 2024). "Extragalactic magnetism with SOFIA (SALSA Legacy Program). VII. A tomographic view of far-infrared and radio polarimetric observations through MHD simulations of galaxies." In: *The Astrophysical Journal* 966.1, 43, p. 43. DOI: 10.3847/1538-4357/ad2e9e.

Matthews, A. M., J. J. Condon, et al. (June 2021). "Cosmic star formation history measured at 1.4 GHz." In: *The Astrophysical Journal* 914. Publisher: IOP ADS Bibcode: 2021ApJ...914..126M, p. 126. ISSN: 0004-637X. DOI: 10.3847/1538-4357/abfaf6.

Matthews, A. M., W. D. Cotton, et al. (Jan. 2025). "A Galactic-scale Magnetized Wind around a Normal Star-forming Galaxy." In: *The Astrophysical Journal Letters* 978.2, L25, p. L25. DOI: 10.3847/2041-8213/ada252.

Modak, Shaunak et al. (Oct. 2023). "Cosmic-ray driven galactic winds from the warm interstellar medium." In: *Monthly Notices of the Royal Astronomical Society* 524. ADS Bibcode: 2023MNRAS.524.6374M, pp. 6374–6391. ISSN: 0035-8711. DOI: 10.1093/mnras/stad2257.

Muratov, Alexander L. et al. (Dec. 2015). "Gusty, gaseous flows of FIRE: galactic winds in cosmological simulations with explicit stellar feedback." In: *Monthly Notices of the Royal Astronomical Society* 454. Publisher: OUP ADS Bibcode: 2015MNRAS.454.2691M, pp. 2691–2713. ISSN: 0035-8711. DOI: 10.1093/mnras/stv2126.

Murphy, E. J., A. Bolatto, et al. (Dec. 2018). "The ngVLA Science Case and Associated Science Requirements." In: *Science with a Next Generation Very Large Array*. Ed. by Eric Murphy. Vol. 517. Astronomical Society of the Pacific Conference Series, p. 3. DOI: 10.48550/arXiv.1810.07524.

Murphy, E. J., R. Braun, et al. (Feb. 2006). "An Initial Look at the Far-Infrared-Radio Correlation within Nearby Star-forming Galaxies Using the Spitzer Space Telescope." In: *The Astrophysical Journal* 638. ADS Bibcode: 2006ApJ...638..157M, pp. 157–175. ISSN: 0004-637X. DOI: 10.1086/498636.

Murphy, Eric J. (Nov. 2009). "The Far-Infrared-Radio Correlation at High Redshifts: Physical Considerations and Prospects for the Square Kilometer Array." In: *The Astrophysical Journal* 706. ADS Bibcode: 2009ApJ...706..482M, pp. 482–496. ISSN: 0004-637X. DOI: 10.1088/0004-637X/706/1/482.

National Academies of Sciences, Engineering, and Medicine (2023). *Pathways to discovery in astronomy and astrophysics for the 2020s*. Washington, DC: The National Academies Press. DOI: 10.17226/26141.

Ni, Yueying et al. (June 2022). "The ASTRID simulation: the evolution of supermassive black holes." In: *Monthly Notices of the Royal Astronomical Society* 513.1, pp. 670–692. ISSN: 0035-8711. DOI: 10.1093/mnras/stac351.

Norris, Ray P., Huib T. Intema, et al. (Jan. 2021). "Unexpected circular radio objects at high Galactic latitude." In: *Publications of the Astronomical Society of Australia* 38, e003, e003. DOI: 10.1017/pasa.2020.52.

Norris, Ray P. et al. (Oct. 2021). "Odd radio circles and their environment." In: *Galaxies* 9.4, 83, p. 83. DOI: 10.3390/galaxies9040083.

Ntormousi, Evangelia et al. (Sept. 2020). "A dynamo amplifying the magnetic field of a Milky-Way-like galaxy." In: *Astronomy & Astrophysics* 641, A165, A165. DOI: 10.1051/0004-6361/202037835.

O'Sullivan, S. P. et al. (July 2020). "New constraints on the magnetization of the cosmic web using LOFAR Faraday rotation observations." In: *Monthly Notices of the Royal Astronomical Society* 495.3, pp. 2607–2619. DOI: 10.1093/mnras/staa1395.

Ogrodnik, Mateusz A. et al. (Mar. 2021). "Implementation of cosmic ray energy spectrum (CRESP) algorithm in PIERNIK MHD code. I. Spectrally resolved propagation of cosmic ray electrons on Eulerian grids." In: *The Astrophysical JournalSupplement Series* 253. ADS Bibcode: 2021ApJS..253...18O, p. 18. ISSN: 0067-0049. DOI: 10.3847/1538-4365/abd16f.

Owen, Ellis R. et al. (July 2023). "Cosmic Ray Processes in Galactic Ecosystems." In: *Galaxies* 11. ADS Bibcode: 2023Galax..11...86O, p. 86. DOI: 10.3390/galaxies11040086.

Padovani, Marco et al. (June 2021). "Spectral index of synchrotron emission: insights from the diffuse and magnetised interstellar medium." In: *Astronomy & Astrophysics* 651, A116, A116. DOI: 10.1051/0004-6361/202140799.

Pakmor, R., C. Pfrommer, et al. (June 2016). "GALACTIC WINDS DRIVEN BY ISOTROPIC AND ANISOTROPIC COSMIC-RAY DIFFUSION IN DISK GALAXIES." In: *The Astrophysical Journal Letters* 824.2. arXiv: 1605.00643 Publisher: IOP Publishing, p. L30. ISSN: 2041-8205. DOI: 10.3847/2041-8205/824/2/L30.

Pakmor, Rüdiger, Rebekka Bieri, et al. (Feb. 2024). "Magnetic field amplification in cosmological zoom simulations from dwarf galaxies to galaxy groups." In: *Monthly Notices of the Royal Astronomical Society* 528. ADS Bibcode: 2024MNRAS.528.2308P, pp. 2308–2325. ISSN: 0035-8711. DOI: 10.1093/mnras/stae112.

Pakmor, Rüdiger, Thomas Guillet, et al. (2018). "Faraday rotation maps of disc galaxies." In: *Monthly Notices of the Royal Astronomical Society* 481.4, pp. 4410–4418. ISSN: 13652966. DOI: 10.1093/mnras/sty2601.

Pakmor, Rüdiger, Freeke Van De Voort, et al. (2020). "Magnetizing the circumgalactic medium of disc galaxies." In: *Monthly Notices of the Royal Astronomical Society* 498.3, pp. 3125–3137. ISSN: 13652966. DOI: 10.1093/mnras/staa2530.

Pakmor, Rüdiger et al. (June 2013). "Simulations of magnetic fields in isolated disc galaxies." In: *Monthly Notices of the Royal Astronomical Society* 432.1, pp. 176–193. DOI: 10.1093/mnras/stt428.

Pakmor, Rüdiger et al. (Mar. 2014). "Magnetic fields in cosmological simulations of disk galaxies." In: *Astrophysical Journal Letters* 783.1. arXiv: 1312.2620, p. L20. ISSN: 20418205. DOI: 10.1088/2041-8205/783/1/L20.

Parker, E. N. (Nov. 1958). "Dynamics of the interplanetary gas and magnetic fields." In: *The Astrophysical Journal* 128, p. 664. DOI: 10.1086/146579.

Patra, Narendra Nath (Dec. 2020). "H I scale height in spiral galaxies." In: *Monthly Notices of the Royal Astronomical Society* 499.2, pp. 2063–2075. DOI: 10.1093/mnras/staa2959.

Peng, Wang et al. (May 2009). "Magnetohydrodynamic Simulations of Disk Galaxy Formation: The Magnetization of the Cold and Warm Medium." In: *The Astrophysical Journal, Volume 696, Issue 1, pp. 96-109 (2009).* 696.1. Publisher: Institute of Physics Publishing, p. 96. ISSN: 0004-637X. DOI: 10.1088/0004-637X/696/1/96.

Pfrommer, Christoph et al. (Sept. 2022). "Simulating radio synchrotron emission in star-forming galaxies: small-scale magnetic dynamo and the origin of the far-infrared–radio correlation." In: *Monthly Notices of the Royal Astronomical Society* 515.3, pp. 4229–4264. ISSN: 0035-8711. DOI: 10.1093/mnras/stac1808.

Pillepich, Annalisa et al. (Jan. 2018). "Simulating galaxy formation with the IllustrisTNG model." In: *Monthly Notices of the Royal Astronomical Society* 473. ADS Bibcode: 2018MNRAS.473.4077P, pp. 4077–4106. ISSN: 0035-8711. DOI: 10.1093/mnras/stx2656.

Ponnada, Sam B., Iryna S. Butsky, et al. (May 2024). "Synchrotron signatures of cosmic ray transport physics in galaxies." In: *Monthly Notices of the Royal Astronomical Society* 530. Publisher: OUP ADS Bibcode: 2024MNRAS.530L...1P, pp. L1–L6. ISSN: 0035-8711. DOI: 10.1093/mnrasl/slae017.

Ponnada, Sam B., Rachel K. Cochrane, et al. (Feb. 2025). "Hooks, lines, and sinkers: How active galactic nucleus feedback and cosmic-ray transport shape the far-infrared–radio correlation of galaxies." en. In: *The Astrophysical Journal* 980.1. Publisher: The American Astronomical Society, p. 135. ISSN: 0004-637X. DOI: 10.3847/1538-4357/ada280.

Ponnada, Sam B., Georgia V. Panopoulou, Iryna S. Butsky, Philip F. Hopkins, Sarah R. Loebman, et al. (Nov. 2022). "Magnetic fields on FIRE: Comparing B-fields in the multiphase ISM and CGM of simulated L* galaxies to observations." In: *Monthly Notices of the Royal Astronomical Society* 516. ADS Bibcode: 2022MNRAS.516.4417P, pp. 4417–4431. ISSN: 0035-8711. DOI: 10.1093/mnras/stac2448.

Ponnada, Sam B., Georgia V. Panopoulou, Iryna S. Butsky, Philip F. Hopkins, Raphael Skalidis, et al. (Feb. 2024). "Synchrotron emission on FIRE: equipartition estimators of magnetic fields in simulated galaxies with spectrally resolved cosmic rays." In: *Monthly Notices of the Royal Astronomical Society* 527.4, pp. 11707–11718. DOI: 10.1093/mnras/stad3978.

Prochaska, J. Xavier et al. (Oct. 2019). "The low density and magnetization of a massive galaxy halo exposed by a fast radio burst." In: *Science* 366.6462, pp. 231–234. ISSN: 10959203. DOI: 10.1126/science.aay0073.

Quataert, Eliot et al. (Feb. 2022). "The physics of galactic winds driven by cosmic rays - II. Isothermal streaming solutions." In: *Monthly Notices of the Royal Astronomical Society* 510. Publisher: OUP ADS Bibcode: 2022MNRAS.510..920Q, pp. 920–945. ISSN: 0035-8711. DOI: 10.1093/mnras/stab3274.

Quataert, Eliot et al. (Feb. 2022). "The physics of galactic winds driven by cosmic rays I: Diffusion." In: *Monthly Notices of the Royal Astronomical Society* 510. ADS Bibcode: 2022MNRAS.510.1184Q, pp. 1184–1203. ISSN: 0035-8711. DOI: 10.1093/mnras/stab3273.

Quataert, Eliot et al. (Feb. 2025). *Cosmic ray feedback in massive halos: implications for the distribution of baryons*. Publication Title: arXiv e-prints ADS Bibcode: 2025arXiv250201753Q. DOI: 10.48550/arXiv.2502.01753.

Rajpurohit, K. et al. (May 2025). *Radial profiles of radio halos in massive galaxy clusters: Diffuse giants over 2 Mpc*. arXiv:2505.05415 [astro-ph]. DOI: 10.48550/arXiv.2505.05415.

Ramesh, Rahul et al. (Sept. 2024). *IllustrisTNG + Cosmic Rays with a Simple Transport Model: From Dwarfs to L* Galaxies*. ADS Bibcode: 2024arXiv240918238R. DOI: 10.48550/arXiv.2409.18238.

Rand, Richard J. et al. (Aug. 1989). "The local Galactic magnetic field." In: *The Astrophysical Journal* 343, p. 760. DOI: 10.1086/167747.

Rappaz, Yoan et al. (May 2022). "Rotation measure and synchrotron emission signatures in simulations of magnetized galactic discs." In: *Monthly Notices of the Royal Astronomical Society* 512.1, pp. 1450–1468. DOI: 10.1093/mnras/stac516.

Ravi, V. et al. (Dec. 2016). "The magnetic field and turbulence of the cosmic web measured using a brilliant fast radio burst." In: *Science* 354.6317, pp. 1249–1252. DOI: 10.1126/science.aaf6807.

Reichherzer, Patrick et al. (Mar. 2025). "Efficient micromirror confinement of subteraelectronvolt cosmic rays in galaxy clusters." In: *Nature Astronomy* 9. ADS Bibcode: 2025NatAs...9..438R, pp. 438–448. ISSN: 2397-3366. DOI: 10.1038/s41550-024-02442-1.

Reissl, S. et al. (Sept. 2016). "Radiative transfer with POLARIS: I. Analysis of magnetic fields through synthetic dust continuum polarization measurements." In: *Astronomy and Astrophysics* 593, A87. ISSN: 14320746. DOI: 10.1051/0004-6361/201424930.

Rémy-Ruyer, A. et al. (Mar. 2014). "Gas-to-dust mass ratios in local galaxies over a 2 dex metallicity range." In: *Astronomy & Astrophysics* 563, A31, A31. DOI: 10.1051/0004-6361/201322803.

Richards, Gordon T. et al. (Oct. 2006). "Spectral Energy Distributions and Multiwavelength Selection of Type 1 Quasars." In: *The Astrophysical Journal Supplement Series* 166. Publisher: IOP ADS Bibcode: 2006ApJS..166..470R, pp. 470–497. ISSN: 0067-0049. DOI: 10.1086/506525.

Rieder, Michael et al. (Dec. 2017). "A small-scale dynamo in feedback-dominated galaxies - III. Cosmological simulations." In: *Monthly Notices of the Royal Astronomical Society* 472.4, pp. 4368–4373. DOI: 10.1093/mnras/stx2276.

Robinson, Hector et al. (Oct. 2023). *Regulating star formation in a magnetized disk galaxy*. Tech. rep. Publication Title: arXiv e-prints ADS Bibcode: 2023arXiv231015244R Type: article.

Rodrigues, L. F.S. et al. (Feb. 2019). "Evolution of galactic magnetic fields." In: *Monthly Notices of the Royal Astronomical Society* 483.2, pp. 2424–2440. ISSN: 0035-8711. DOI: 10.1093/MNRAS/STY3270.

Rodríguez Montero, Francisco et al. (June 2024). "The impact of cosmic rays on the interstellar medium and galactic outflows of Milky Way analogues." In: *Monthly Notices of the Royal Astronomical Society* 530. Publisher: OUP ADS Bibcode: 2024MNRAS.530.3617R, pp. 3617–3640. ISSN: 0035-8711. DOI: 10.1093/mnras/stae1083.

Ruszkowski, Mateusz et al. (June 2023). *Cosmic ray feedback in galaxies and galaxy clusters – A pedagogical introduction and a topical review of the acceleration, transport, observables, and dynamical impact of cosmic rays*. Publication Title: arXiv e-prints ADS Bibcode: 2023arXiv230603141R. DOI: 10.48550/arXiv.2306.03141.

Rybicki, George B. et al. (1986). *Radiative Processes in Astrophysics*.

Salem, Munier et al. (Feb. 2014). "Cosmic ray driven outflows in global galaxy disc models." In: *Monthly Notices of the Royal Astronomical Society* 437. ADS Bibcode: 2014MNRAS.437.3312S, pp. 3312–3330. ISSN: 0035-8711. DOI: 10.1093/mnras/stt2121.

Salem, Munier et al. (Feb. 2016). "Role of cosmic rays in the circumgalactic medium." In: *Monthly Notices of the Royal Astronomical Society* 456. ADS Bibcode: 2016MNRAS.456..582S, pp. 582–601. ISSN: 0035-8711. DOI: 10.1093/mnras/stv2641.

Sargent, M. T. et al. (May 2010). "No Evolution in the IR-Radio Relation for IR-luminous Galaxies at z < 2 in the COSMOS Field." In: *The Astrophysical Journal* 714. ADS Bibcode: 2010ApJ...714L.190S, pp. L190–L195. ISSN: 0004-637X. DOI: 10.1088/2041-8205/714/2/L190.

Schaye, Joop et al. (Jan. 2015). "The EAGLE project: simulating the evolution and assembly of galaxies and their environments." In: *Monthly Notices of the Royal Astronomical Society* 446. ADS Bibcode: 2015MNRAS.446..521S, pp. 521–554. ISSN: 0035-8711. DOI: 10.1093/mnras/stu2058.

Schechter, P. (Jan. 1976). "An analytic expression for the luminosity function for galaxies." In: *The Astrophysical Journal* 203, pp. 297–306. DOI: 10.1086/154079.

Schmidt, Maarten (Mar. 1959). "The rate of star formation." In: *The Astrophysical Journal* 129. Publisher: IOP ADS Bibcode: 1959ApJ...129..243S, p. 243. ISSN: 0004-637X. DOI: 10.1086/146614.

Schober, J., M. T. Sargent, et al. (Nov. 2023). "A model for the infrared-radio correlation of main sequence galaxies at gigahertz frequencies and its variation with redshift and stellar mass." en. In: *Astronomy & Astrophysics* 679. Publisher: EDP Sciences, A47. ISSN: 0004-6361, 1432-0746. DOI: 10.1051/0004-6361/202245218.

Schober, J., D. R. G. Schleicher, et al. (Aug. 2015). "Saturation of the turbulent dynamo." en. In: *Physical Review E* 92.2, p. 023010. ISSN: 1539-3755, 1550-2376. DOI: 10.1103/PhysRevE.92.023010.

Seta, Amit et al. (2019). "Revisiting the equipartition assumption in star-forming galaxies." In: *Galaxies* 7.2. arXiv: 1903.11856 Publisher: MDPI AG. ISSN: 20754434. DOI: 10.3390/GALAXIES7020045.

Seta, Amit et al. (2021). "Magnetic fields in the Milky Way from pulsar observations: effect of the correlation between thermal electrons and magnetic fields." In: *Monthly Notices of the Royal Astronomical Society* 502.2, pp. 2220–2237. ISSN: 0035-8711. DOI: 10.1093/mnras/stab128.

Shakura, N. I. et al. (Jan. 1973). "Black holes in binary systems. Observational appearance." In: *Astronomy & Astrophysics* 24, pp. 337–355.

Sharma, Kritti et al. (Apr. 2025). *A hydrodynamical simulations-based model that connects the FRB DM–redshift relation to suppression of the matter power spectrum via feedback*. en. arXiv:2504.18745 [astro-ph]. DOI: 10.48550/arXiv.2504.18745.

Shreeram, Soumya et al. (2024). *Quantifying observational projection effects with a simulation-based hot CGM model*.

Shukurov, Anvar et al. (Apr. 2017). "Cosmic rays in intermittent magnetic fields." In: *The Astrophysical Journal Letters* 839.1, L16, p. L16. DOI: 10.3847/2041-8213/aa6aa6.

Simard-Normandin, M. et al. (Nov. 1980). "Rotation measures and the galactic magnetic field." In: *The Astrophysical Journal* 242, pp. 74–94. DOI: 10.1086/158445.

Simpson, Christine M. et al. (Aug. 2016). "The role of cosmic-ray pressure in accelerating galactic outflows." In: *The Astrophysical Journal Letters* 827.2. arXiv: 1606.02324 Publisher: American Astronomical Society, p. L29. ISSN: 0004-637X. DOI: 10.3847/2041-8205/827/2/L29.

Skilling, J. (Sept. 1975). "Cosmic Ray Streaming—I Effect of Alfvén Waves on Particles." In: *Monthly Notices of the Royal Astronomical Society* 172.3, pp. 557–566. ISSN: 0035-8711. DOI: 10.1093/mnras/172.3.557.

Smith, D. J. B. et al. (Nov. 2012). "Herschel-ATLAS: multi-wavelength SEDs and physical properties of 250 μm selected galaxies at z < 0.5." In: *Monthly Notices of the Royal Astronomical Society* 427.1, pp. 703–727. DOI: 10.1111/j.1365-2966.2012.21930.x.

Sobey, C. et al. (Apr. 2019). "Low-frequency Faraday rotation measures towards pulsars using LOFAR: probing the 3D Galactic halo magnetic field." In: *Monthly Notices of the Royal Astronomical Society* 484.3, pp. 3646–3664. DOI: 10.1093/mnras/stz214.

Soliman, Nadine H. et al. (May 2025). "Dust battery: A novel mechanism for seed magnetic field Ggneration in the early Universe." In: *The Astrophysical Journal* 985.1, 55, p. 55. DOI: 10.3847/1538-4357/adcb39.

Sparre, Martin et al. (Apr. 2017). "(Star)bursts of FIRE: observational signatures of bursty star formation in galaxies." In: *Monthly Notices of the Royal Astronomical Society* 466. Publisher: OUP ADS Bibcode: 2017MNRAS.466...88S, pp. 88–104. ISSN: 0035-8711. DOI: 10.1093/mnras/stw3011.

Springel, Volker et al. (Feb. 2003). "Cosmological smoothed particle hydrodynamics simulations: a hybrid multiphase model for star formation." In: *Monthly Notices of the Royal Astronomical Society* 339.2, pp. 289–311. DOI: 10.1046/j.1365-8711.2003.06206.x.

Steinwandel, U. P., M. C. Beck, et al. (Feb. 2019). "Magnetic buoyancy in simulated galactic discs with a realistic circumgalactic medium." In: *Monthly Notices of the Royal Astronomical Society* 483.1, pp. 1008–1028. DOI: 10.1093/mnras/sty3083.

Steinwandel, Ulrich P., Klaus Dolag, Harald Lesch, and Andreas Burkert (Jan. 2022). "Driving Galactic Outflows with Magnetic Fields at Low and High Redshift." In: *The Astrophysical Journal* 924.1, 26, p. 26. DOI: 10.3847/1538-4357/ac2ffd.

Steinwandel, Ulrich P., Klaus Dolag, Harald Lesch, Benjamin P. Moster, et al. (May 2020). "On the origin of magnetic driven winds and the structure of the galactic dynamo in isolated galaxies." In: *Monthly Notices of the Royal Astronomical Society* 494. ADS Bibcode: 2020MNRAS.494.4393S, pp. 4393–4412. ISSN: 0035-8711. DOI: 10.1093/mnras/staa817.

Stepanov, Rodion et al. (Jan. 2014). "An observational test for correlations between cosmic rays and magnetic fields." In: *Monthly Notices of the Royal Astronomical Society* 437.3. arXiv: 1205.0578, pp. 2201–2216. ISSN: 00358711. DOI: 10.1093/mnras/stt2044.

Stern, Jonathan et al. (Apr. 2021). "Virialization of the Inner CGM in the FIRE simulations and implications for galaxy disks, star formation, and feedback." In: *The Astrophysical Journal* 911.2, 88, p. 88. DOI: 10.3847/1538-4357/abd776.

Strong, A. W., T. A. Porter, et al. (Oct. 2010). "Global cosmic-ray-related luminosity and energy budget of the Milky Way." In: *The Astrophysical Journal Letters* 722.1, pp. L58–L63. DOI: 10.1088/2041-8205/722/1/L58.

Strong, Andrew W. et al. (Dec. 1998). "Propagation of Cosmic-Ray Nucleons in the Galaxy." In: *The Astrophysical Journal* 509.1, pp. 212–228. DOI: 10.1086/306470.

Strong, Andrew W. et al. (July 2000). "Diffuse continuum gamma rays from the Galaxy." In: *The Astrophysical Journal* 537.2, pp. 763–784. DOI: 10.1086/309038.

Su, Kung Yi, Philip F. Hopkins, Christopher C. Hayward, et al. (Oct. 2017). "Feedback first: The surprisingly weak effects of magnetic fields, viscosity, conduction and metal diffusion on sub-L* galaxy formation." In: *Monthly Notices of the Royal Astronomical Society* 471.1, pp. 144–166. ISSN: 13652966. DOI: 10.1093/MNRAS/STX1463.

Su, Kung-Yi, Greg L. Bryan, Christopher C. Hayward, et al. (Aug. 2024). "Unravelling jet quenching criteria across L* galaxies and massive cluster ellipticals." In: *Monthly Notices of the Royal Astronomical Society* 532. Publisher: OUP ADS Bibcode: 2024MNRAS.532.2724S, pp. 2724–2740. ISSN: 0035-8711. DOI: 10.1093/mnras/stae1629.

Su, Kung-Yi, Greg L. Bryan, Philip F. Hopkins, et al. (Feb. 2025). *Modeling cosmic rays at AGN jet-driven shock fronts*. arXiv:2502.00927 [astro-ph]. DOI: 10.48550/arXiv.2502.00927.

Su, Kung-Yi, Christopher C Hayward, et al. (2018). "Stellar feedback strongly alters the amplification and morphology of galactic magnetic fields." In: *Monthly Notices of the Royal Astronomical Society: Letters* 473.1, pp. L111–L115. ISSN: 1745-3925. DOI: 10.1093/mnrasl/slx172.

Su, Kung-Yi, Philip F. Hopkins, Greg L. Bryan, et al. (Oct. 2021). "Which AGN jets quench star formation in massive galaxies?" In: *Monthly Notices of the Royal Astronomical Society* 507. ADS Bibcode: 2021MNRAS.507..175S, pp. 175–204. ISSN: 0035-8711. DOI: 10.1093/mnras/stab2021.

Tabatabaei, F. S. et al. (Feb. 2017). "The Radio Spectral Energy Distribution and Star-formation Rate Calibration in Galaxies." In: *The Astrophysical Journal* 836.2, 185, p. 185. DOI: 10.3847/1538-4357/836/2/185.

Tang, Qing-Wen et al. (Sept. 2014). "Discovery of GeV emission from the direction of the luminous infrared galaxy NGC 2146." en. In: *The Astrophysical Journal* 794.1. Publisher: The American Astronomical Society, p. 26. ISSN: 0004-637X. DOI: 10.1088/0004-637X/794/1/26.

Thomas, T. et al. (May 2023). "Cosmic-ray-driven galactic winds: transport modes of cosmic rays and Alfvén-wave dark regions." In: *Monthly Notices of the Royal Astronomical Society* 521. ADS Bibcode: 2023MNRAS.521.3023T, pp. 3023–3042. ISSN: 0035-8711. DOI: 10.1093/mnras/stad472.

Tritsis, A. et al. (Aug. 2015). "Magnetic field-gas density relation and observational implications revisited." In: *Monthly Notices of the Royal Astronomical Society* 451.4, pp. 4384–4396. DOI: 10.1093/mnras/stv1133.

Tsung, Tsun Hin Navin et al. (May 2023). *The Impact of Cosmic Rays on Thermal and Hydrostatic Stability in Galactic Halos*. Publication Title: arXiv e-prints ADS Bibcode: 2023arXiv230514432T. DOI: 10.48550/arXiv.2305.14432.

Tumlinson, Jason et al. (2017). "The circumgalactic medium." In: DOI: 10.1146/annurev-astro-091916.

Turner, Ross J. (May 2018). "Duty-cycle and energetics of remnant radio-loud AGN." In: *Monthly Notices of the Royal Astronomical Society* 476.2, pp. 2522–2529. DOI: 10.1093/mnras/sty433.

Ulrich, Marie-Helene et al. (Jan. 1997). "Variability of active galactic nuclei." In: *Annual Review of Astronomy and Astrophysics* 35. ADS Bibcode: 1997ARA&A..35..445U, pp. 445–502. ISSN: 0066-4146. DOI: 10.1146/annurev.astro.35.1.445.

Vallée, J. P. et al. (1995). "Magnetic field versus gas density, in different physical conditions." In: *Ap&SS* 234.1. Publisher: Kluwer Academic Publishers, pp. 1–10. ISSN: 0004-640X. DOI: 10.1007/BF00627277.

van de Voort, Freeke et al. (Mar. 2021). "The effect of magnetic fields on properties of the circumgalactic medium." In: *Monthly Notices of the Royal Astronomical Society* 501.4, pp. 4888–4902. DOI: 10.1093/mnras/staa3938.

Vanderlinde, Keith et al. (Oct. 2019). "The Canadian Hydrogen Observatory and Radio-transient Detector (CHORD)." In: *Canadian Long Range Plan for Astronomy and Astrophysics White Papers*. Vol. 2020, 28, p. 28. DOI: 10.5281/zenodo.3765414.

Virtanen, Pauli et al. (2020). "SciPy 1.0: Fundamental algorithms for scientific computing in Python." In: *Nature Methods* 17, pp. 261–272. DOI: 10.1038/s41592-019-0686-2.

Voelk, H. J. (June 1985). "Radio continuum and far-infrared emission from spiral galaxies : a close correlation." en. In: *Astronomy and Astrophysics* 147, pp. L6–L9. ISSN: 0004-6361.

– (July 1989). "The correlation between radio and far-infrared emission for disk galaxies : a calorimeter theory." In: *Astronomy and Astrophysics* 218. ADS Bibcode: 1989A&A...218...67V, pp. 67–70. ISSN: 0004-6361.

Walter, Fabian et al. (Dec. 2008). "THINGS: The H I nearby galaxy survey." In: *The Astronomical Journal* 136.6, pp. 2563–2647. DOI: 10.1088/0004-6256/136/6/2563.

Wang, Peng et al. (May 2009). "Magnetohydrodynamic simulations of disk galaxy formation: The magnetization of the cold and warm medium." In: *The Astrophysical Journal* 696.1, pp. 96–109. DOI: 10.1088/0004-637X/696/1/96.

Weeren, R. J. van et al. (Feb. 2019). "Diffuse radio emission from galaxy clusters." en. In: *Space Science Reviews* 215.1, p. 16. ISSN: 1572-9672. DOI: 10.1007/s11214-019-0584-z.

Weingartner, Joseph C. et al. (Feb. 2001). "Dust grain-size distributions and extinction in the Milky Way, Large Magellanic Cloud, and Small Magellanic Cloud." In: *The Astrophysical Journal* 548.1, pp. 296–309. DOI: 10.1086/318651.

Wellons, Sarah et al. (Apr. 2023). "Exploring supermassive black hole physics and galaxy quenching across halo mass in FIRE cosmological zoom simulations." In: *Monthly Notices of the Royal Astronomical Society* 520.4, pp. 5394–5412. ISSN: 0035-8711. DOI: 10.1093/mnras/stad511.

Werhahn, Maria, Christoph Pfrommer, Philipp Girichidis, Ewald Puchwein, et al. (Aug. 2021). "Cosmic rays and non-thermal emission in simulated galaxies - I. Electron and proton spectra compared to Voyager-1 data." In: *Monthly Notices of the Royal Astronomical Society* 505.3, pp. 3273–3294. ISSN: 0035-8711. DOI: 10.1093/mnras/stab1324.

Werhahn, Maria, Christoph Pfrommer, Philipp Girichidis, and Georg Winner (Aug. 2021). "Cosmic rays and non-thermal emission in simulated galaxies - II. γ-ray maps, spectra, and the far-infrared-γ-ray relation." In: *Monthly Notices of the Royal Astronomical Society* 505. ADS Bibcode: 2021MNRAS.505.3295W, pp. 3295–3313. ISSN: 0035-8711. DOI: 10.1093/mnras/stab1325.

Werhahn, Maria et al. (Dec. 2021). "Cosmic rays and non-thermal emission in simulated galaxies - III. Probing cosmic-ray calorimetry with radio spectra and the FIR-radio correlation." In: *Monthly Notices of the Royal Astronomical Society* 508.3, pp. 4072–4095. DOI: 10.1093/mnras/stab2535.

Werk, Jessica K. et al. (Sept. 2014). "The COS-Halos survey: Physical conditions and baryonic mass in the low-redshift circumgalactic medium." In: *The Astrophysical Journal* 792. Publisher: IOP ADS Bibcode: 2014ApJ...792....8W, p. 8. ISSN: 0004-637X. DOI: 10.1088/0004-637X/792/1/8.

Wetzel, Andrew et al. (Feb. 2022). "Public data release of the FIRE-2 cosmological zoom-in simulations of galaxy formation." In: *arXiv e-prints*, arXiv:2202.06969, arXiv:2202.06969.

Whitaker, Katherine E. et al. (Dec. 2017). "The constant average relationship between dust-obscured star formation and stellar mass from z = 0 to z = 2.5." en. In: *The Astrophysical Journal* 850.2. Publisher: The American Astronomical Society, p. 208. ISSN: 0004-637X. DOI: 10.3847/1538-4357/aa94ce.

Whittingham, Joseph et al. (Sept. 2021). "The impact of magnetic fields on cosmological galaxy mergers - I. Reshaping gas and stellar discs." In: *Monthly Notices of the Royal Astronomical Society* 506.1, pp. 229–255. DOI: 10.1093/mnras/stab1425.

– (Nov. 2023). "The impact of magnetic fields on cosmological galaxy mergers - II. Modified angular momentum transport and feedback." In: *Monthly Notices of the Royal Astronomical Society* 526.1, pp. 224–245. DOI: 10.1093/mnras/stad2680.

Wibking, Benjamin D. et al. (2021). "The global structure of magnetic fields and gas in simulated Milky Way-analogue galaxies." In: *Monthly Notices of the Royal Astronomical Society* 000, pp. 1–13.

Wolfire, M. G. et al. (Apr. 1995). "The neutral atomic phases of the interstellar medium." In: *The Astrophysical Journal* 443. ADS Bibcode: 1995ApJ...443..152W, p. 152. ISSN: 0004-637X. DOI: 10.1086/175510.

Wunderlich, E. et al. (June 1987). "A further study of the relation of the radio-far-infrared in galaxies. I. Observations and data processing." en. In: *Astronomy and Astrophysics, Suppl. Ser., Vol. 69, p. 487-504 (1987)* 69, p. 487. ISSN: 0365-0138.

Yamasaki, Shotaro et al. (Sept. 2023). *Are Odd Radio Circles virial shocks around massive galaxies? Implications for cosmic-ray diffusion in the circumgalactic medium*. arXiv:2309.17451 [astro-ph]. DOI: 10.48550/arXiv.2309.17451.

Yang, H. -Y. K. et al. (Nov. 2017). "The spatially uniform spectrum of the Fermi Bubbles: The leptonic active galactic nucleus jet scenario." In: *The Astrophysical Journal* 850. ADS Bibcode: 2017ApJ...850....2Y, p. 2. ISSN: 0004-637X. DOI: 10.3847/1538-4357/aa9434.

Yim, Kijeong et al. (Dec. 2014). "The interstellar medium and star formation in edge-on galaxies. II. NGC 4157, 4565, and 5907." In: *The Astronomical Journal* 148.6, 127, p. 127. DOI: 10.1088/0004-6256/148/6/127.

Yuan, Qiang et al. (Dec. 2012). "An Attempt at a Unified Model for the Gamma-Ray Emission of Supernova Remnants." In: *The Astrophysical Journal* 761.2, 133, p. 133. DOI: 10.1088/0004-637X/761/2/133.

Yun, Min S. et al. (June 2001). "Radio properties of infrared-selected galaxies in the IRAS 2 Jy sample." In: *The Astrophysical Journal* 554. ADS Bibcode: 2001ApJ...554..803Y, pp. 803–822. ISSN: 0004-637X. DOI: 10.1086/323145.

Zhang, Dong (Nov. 2018). "A review of the theory of galactic winds driven by stellar feedback." In: *Galaxies* 6. ADS Bibcode: 2018Galax...6..114Z, p. 114. DOI: 10.3390/galaxies6040114.

Zhang, Haowen, Peter Behroozi, et al. (Jan. 2023). "TRINITY I: self-consistently modelling the dark matter halo-galaxy-supermassive black hole connection from z = 0-10." In: *Monthly Notices of the Royal Astronomical Society* 518. Publisher: OUP ADS Bibcode: 2023MNRAS.518.2123Z, pp. 2123–2163. ISSN: 0035-8711. DOI: 10.1093/mnras/stac2633.

Zhang, Yi, Johan Comparat, et al. (Jan. 2024). *The hot circum-galactic medium in the eROSITA all sky survey I. X-ray surface brightness profiles*. arXiv:2401.17308 [astro-ph]. DOI: 10.48550/arXiv.2401.17308.

Zweibel, Ellen G. (May 2013). "The microphysics and macrophysics of cosmic rays." In: *Physics of Plasmas* 20. ADS Bibcode: 2013PhPl...20e5501Z, p. 055501. ISSN: 1070-664X. DOI: 10.1063/1.4807033.